Computational and experimental studies on stabilities, reactions and reaction rates of cations and ion-dipole complexes

Colofon

ISBN-13	978-90-393-4847-5
Printer	Ponsen en Looijen B.V. Wageningen
Copyright	2008, H. K. Ervasti
Cover	H. K. Ervasti

Computational and experimental studies on stabilities, reactions and reaction rates of cations and ion-dipole complexes

Computationele en experimentele studies aan de stabiliteit, reacties en reactiesnelheid van ionen en ion-dipool complexen

(met een samenvatting in het nederlands)

Proefschrift

ter verkrijging van de graad van doctor aan de Universiteit Utrecht op gezag van de rector magnificus, prof.dr. J.C. Stoof, ingevolge het besluit van het college voor promoties in het openbaar te verdedigen op maandag 25 augustus 2008 des middags te 2.30 uur

door

Henri Kristian Ervasti

geboren op *23 november 1978 te Kuusamo, Finland*

Promotor: Prof.dr. L. W. Jenneskens

Co-promotor: Dr. P. J. A. Ruttink

Contents

Chapter 1
General introduction

Henri Ervasti (2008): Computational and experimental studies on stabilities, reactions and reaction rates of cations and ion-dipole complexes

This thesis is about positively charged ionized molecules and their complexes. The focus is especially on ion and complex stabilities, ion-molecule interactions, and the reactions and the rates of the reactions, in gas-phase, low-pressure conditions. The stabilities, interactions, and reactions have been probed through theoretical methods, mainly involving computer simulations, as well as through mass spectrometric experimental methods.

We can study computationally properties of the molecules, such as the dipole moment and stability. We can also look at the energetics and the kinetics of reactions. A reaction can be a spontaneous one, or it might need some energy input to make it happen. A molecular ion can go through several possible reactions, which need varying amounts of energy to occur. From computations, these individual energies can be identified to see which reactions are the most favourable. The reactions can involve breaking of the molecules (dissociation) as well as forming new ones (association), isomerisation, catalysis, and so on. As the reactions that we study involve dissociation and association - a phenomenon not explainable by the classical theory of mechanics - a computer program, which uses the quantum-mechanical theory as its basis, is necessary to model these reactions.

Mass spectrometric experimental methods are based on creating molecular ions in low-pressure and rather low-temperature conditions. It is originally an analytical method and was created to identify different compounds in samples, which would be separated according to their mass-to-charge ratio after the ionisation. As ionising is energy demanding and can lead to dissociation of molecules, often the identification has to be done according to what fragments of the original molecule are present. The appearing fragmentation patterns are nearly always unique to a certain ionised molecule in certain conditions, making an accurate identification possible. As the conditions, namely high vacuum and low temperatures, in a mass spectrometer are similar to those one would encounter in the upper layers of atmosphere, or in interstellar molecular dust clouds, it is often used to study reactions relevant in these circumstances.

In this introduction I will go through what are ions, how they are formed, how stabile they are, and what reactions can they go through. The various effects on the stability will be introduced here, and gone through in more detail in Chapters 2 and 3 of this thesis. Also introduced will be computational methods used throughout this thesis, as well as mass spectrometry which is used alongside computations in the studies displayed in Chapters 4 and 5 of this thesis. Chapters 6 and 7 are fully computational studies, of which Chapter 6 focuses on reaction path studies and Chapter 7 on reaction kinetics. A brief introduction to reaction kinetics is therefore also present in the introduction.

1. Ions

An ion is a particle that has an electrical charge upon it. Ions have properties that electrically neutral particles do not; they are strongly affected by electric and magnetic fields, which can accelerate or change the direction of the ions. They find attractive forces among oppositely charged particles, while repulsive forces appear against similarly charged particles. When we talk about ionised molecules, we talk about molecules which have an unequal number of protons and electrons in it. A molecule with an electron in excess is called an anion and an atom or a molecule missing an electron is called a cation. In this

thesis I have focused on cations. Cations can be formed by "knocking off" electrons from molecules by focusing a source of energy to the molecules. In this case the ionised molecule is often not only a cation, but might be also a radical, since it might end up having an unpaired electron in one of its molecular orbitals. These are called "radical cations".

Another way to form a molecular cation is that the molecule snatches a proton (thus, a hydrogen atom that has lost its only electron, H^+) from another (already ionised) molecule, resulting in excess of protons. Here, the number of electrons in the protonated molecule stays the same and no radical is formed. The ability of a molecule to snatch a proton is called Proton Affinity (abbreviation PA is commonly used) and a molecule with a larger value of proton affinity can take a proton from another protonated molecule with a smaller proton affinity value [1]. Ionised molecules are not usually as stable as their neutral counterparts, though they can be stabilised in diverse ways.

2. Ion stability and complex formation

The stability of an ion is dependent on the energy needed for it to undergo a reaction. There are several factors affecting the stability of an ion. An ion can be stabilised or destabilised by inductive and resonance effects. Here, an addition of an atom or a functional group (such as hydroxyl or amine group, or a fluorine atom) to an ion affects the stability against the possible reactions. Inductive effects affect the energy level of the ion directly, while resonance effects have influence on the energy levels of the reactions. These effects will be discussed in more detail in Chapter 2.

Ion stabilisation can occur also via a complex formation between an ion and a neutral molecule. Now, a proton can serve as the bonding element. The bonding strengths in ionized systems are typically stronger than in the neutral counterparts and the structures formed are more stable [2]. For example, if a protonated water molecule approaches a neutral water molecule from the correct direction, it can find attractive forces with the electrons in a non-bonding orbital, and from the multipoles (mainly dipole and quadrupole moments) of the neutral water molecule (Figure 1). A 'proton-bound dimer' is formed, which is a metastable structure. The Stabilisation Energy, SE, for a protonated water dimer, $(H_2O)_2H^+$, has been measured in an experiment to be 31.6 kcal mol^{-1} [3a], while computations give from 33.6 - 35.0 kcal mol^{-1} [3b-d)]. Similar binding occurs with radical cations. Now, the stabilisation energy in a water dimer radical cation, $(H_2O)_2^{\bullet+}$, has been computed to be 22 kcal mol^{-1} against the most

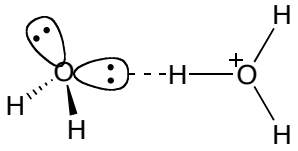

Figure 1. Protonated water molecule, H_3O^+, experiencing stabilisation by coordinating into a non-bonding orbital and multipoles of a neutral water molecule, H_2O.

favourable dissociation into H_3O^+ and $HO^{\bullet}$ [4]. This kind of complex is called 'hydrogen bridged radical cation'. As in proton bound dimers, the bridging atom is a proton. Thus, a common name for the proton bound dimers and hydrogen bridged radical cations can be formulated: 'proton bound complexes'. The stabilisation energies in proton bound complexes are a magnitude stronger than in neutrals; for the water example, several studies

have estimated the hydrogen bonding strength in neutral water to be in range of 3.6-5.0 kcal mol^{-1} [2,5].

2.1 Stability estimation using the Meot-Ner relation

Could we somehow estimate this kind of stabilization already before entering into experiments or computations to study the reaction? Certainly, a tool to investigate the stability of various proton-bound dimers and hydrogen-bridged radical cation complexes without experimental or demanding computational effort would be useful. It has been found [6] that the stabilisation energy is related linearly to the proton affinity difference (ΔPA) between the monomers forming the complex. This is called the Meot-Ner relation.

Meot-Ner [6d] studied proton-bound dimers with ΔPA of the monomers varying from 9 to 70 kcal mol^{-1}. He stated that the stabilisation energy, SE, of the complex can be estimated using the following equation:

$$SE = a - b \cdot \Delta PA, \qquad (1)$$

where *a* and *b* are parameters depending on the connecting atoms (*e.g.* R_1-N•••H^+•••O-R_2 or R_1-O•••H^+•••O-R_2) of the monomers, regardless of the bulk of the monomers. *a* and ΔPA have units of kcal mol^{-1} and *b* is unitless.

Nevertheless, some proton bridged dimers failed to fall into the category described with the linear correlation scheme in Meot-Ner's study. Usually, these were complexes of small monomers with low polarizability and small dipole moment, or a monomer with larger polarizability and a significant dipole moment. The dipole moment effect on the SE estimation and on the geometry of proton-bound dimers and hydrogen-bridged radical cations will be discussed in Chapter 3.

3. Reaction mechanisms

As mentioned earlier, ions and their complexes with neutral molecules are prone to go through various reactions. Common reaction mechanisms in the gas-phase ion-molecule complexes, besides the dissociation, involve (a) protonation - de-protonation, (b) Proton Transport Catalysis (PTC), and (c) Quid-pro-Quo (QpQ) mechanisms.

(a) Protonation - de-protonation reaction

A protonation reaction is rather straightforward: Here at the encounter of two monomers a proton goes from one monomer to the other one. The monomer losing the proton has lower proton affinity at the atom losing the proton than the atom receiving the proton in the other monomer [7]. After the protonation, the ion can have attractive ion-dipole (or any higher-order ion-multipole) interactions with the neutral species and form a complex.

(b) Proton transport catalysis

In proton transport catalysis a proton is transferred from one atom in a molecule to another with the help of a catalysing neutral molecule. As in any catalysis, introduction of a

catalyzing agent lowers the isomerisation barrier. In addition, in PTC, due to the proton-bound complex formation, there is more energy available for the isomerisation since the complex is more stabile than the separated monomers. In Scheme 1 is depicted how such a reaction in principle works. It applies both to cations [8a] and radical cations [8b]. Molecule AB, consisting of parts A and B has been protonated. Isomerisation from BAH^+ to ABH^+ is energy demanding and does not happen easily. When introducing a catalyzing agent (molecule C), it makes a proton-bound complex, lowers the reaction barrier, and makes the isomerisation possible. Usually, the PTC requires the proton affinities to be in the order B > C > A, although this is not necessarily always the case.

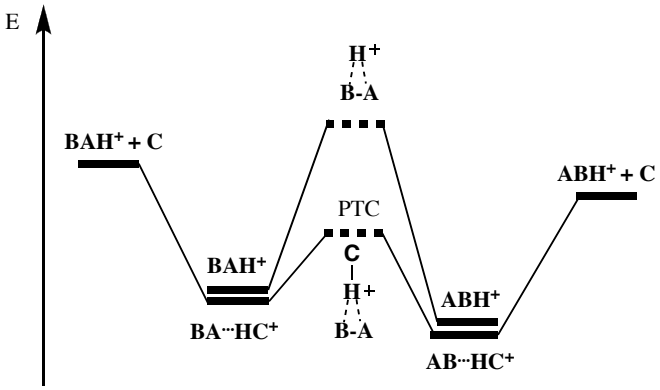

Scheme 1. A schematic view on unassisted isomerisation reaction and on a Proton Transport Catalysis (PTC) isomerisation reaction.

An example of PTC is from the article by Gauld *et al.* [9], where the interconversion of two isomers, $CH_3OH^{\bullet+}$ and $CH_2OH_2^{\bullet+}$, was studied. A large barrier of 25.9 kcal mol^{-1} separates the $CH_3OH^{\bullet+}$ from interconverting into its distonic isomer, $CH_2OH_2^{\bullet+}$, and they are individually observable. With introduction of a polar solvent, e.g. water, the two isomers become easily interconversible. Using the water molecule as a proton transport catalyst, the interconversion barrier was computed to decline to mere 2.9 kcal mol^{-1}.

(c) Quid-pro-Quo mechanism

In the 'Quid-pro-Quo' (QpQ) mechanism a pair of protons are exchanged between two monomers. In Scheme 2 a general mechanism has been illustrated.

A neutral molecule, CH, assists a proton exchange from A to C and C to B in protonated BAH+*. First, a proton-bound complex is formed via the proton of BA. Then, a QpQ transition state is reached, where the catalyzing agent makes two proton bridges to the AB molecule: The proton H^+ is bridging A and C, and the proton H^+* is now bridging B and C. The reaction proceeds so that the C takes the proton H^+ from A, while C stays bridged to the B via proton H^+*. Thus, C took a proton from A of AB and gave the other one to the B of AB. The QpQ works also the other way – a protonated molecule CH^{*+} can isomerise neutral BAH, yielding ABH* and CH^+. Usually the QpQ works only if the proton affinities follow the order B > C > A, as in proton transport catalysis. It is possible that proton transport catalysis and Quid-pro-Quo mechanisms both cause the same isomerisation in

certain complexes. In experiments, the QpQ mechanism can be differentiated from a PTC mechanism by using partially deuterated compounds.

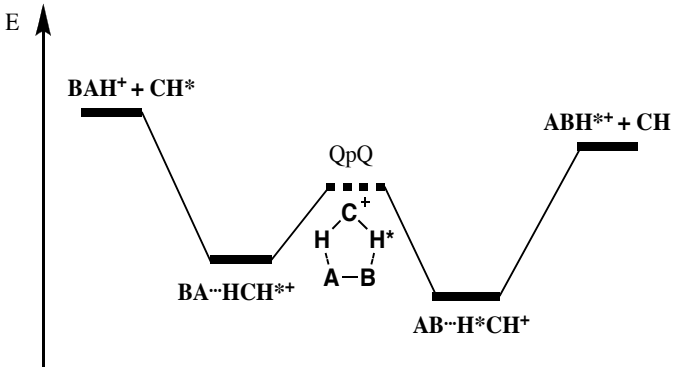

Scheme 2. A schematic view on Quid-pro-Quo (QpQ) isomerisation reaction. An asterisk (*) is used to label one of the hydrogen atoms to separate between the exchanging hydrogen atoms.

A QpQ example is the interconversion between $CH_3O^{\bullet}$ and $CH_2OH^{\bullet}$. The unassisted interconversion has a barrier of 29.7 kcal mol^{-1} [10]. This barrier can lowered by catalysis, namely using protonated methanol. Here we see that the catalyzed interconversion has activation energy of 15.8 kcal mol^{-1}. The protonated methanol gives one of its two protons located at the oxygen atom to the oxygen atom of the $CH_3O^{\bullet}$ moiety, and receives another back from the carbon atom's hydrogen atoms.

4. Mass spectrometry

Reactions that need a lot of energy are slower than the reactions with small energy requirements. I have divided the stability of an ionized molecule in three classes: "Stable", "metastable" and "unstable" ions. A "stable" ion has long lifetime (> millisecond). A "metastable" ion is considered to have lifetimes from microsecond to millisecond timeframe. This name is commonly used in the field of mass spectrometry, since this is the usual time-of-flight for an ion from the source to the detector [1]. An "unstable" ion dissociates in less than a microsecond.

A basic mass spectrometer consists of an ion source, a magnet, and a detector. This gives weak fragmentation peaks for the metastable ions and is used for studying small organic compounds. To study fragmentation more selectively, electrostatic analysers (ESA), collision cells, and deflectors can be added to the mass spectrometer (see Figure 2 for one example setup for such a mass spectrometer). This setup is already enough to study a range of organic molecules and other samples. The studied sample is introduced in the ion source, where it is then ionised using electron impact ionisation or chemical ionisation. The ion source has low-pressure conditions and is also filled with carrier gas, like carbon monoxide, CO. There is an electric field in the ion source (usually 5-10kV) to accelerate the ions towards the magnet. On the way the ions pass through a field-free region (ffr). The ions then enter the magnet, where ions with a certain mass per charge ratio (*m/z*) are chosen to enter the second ffr. The chosen ions fly through the second ffr, possibly fragmenting, and along the possible fragments, arrive at an electrostatic analyser. In the ESA the ions are

separated according to their respective *m/z* ratios by static electric field, and flown to the detector plate. Alternatively, a further selection of the fragments can be made at the second ESA and this selection can be flown to the second detector plate. The ion detection is then analysed using computer programs to produce a graphical figure in various amplitudes and peak widths (see Figure 3 for an example).

Figure 2. A layout of a VG ZAB-R Analytical Mass Spectrometer. The magnet is first used to select the mass/charge ration of interest and electrostatic analyzers (ESA) are used to further focus on certain fragments of the metastable ion dissociation products. There are three field-free regions (ffr) and 5 collision cells.

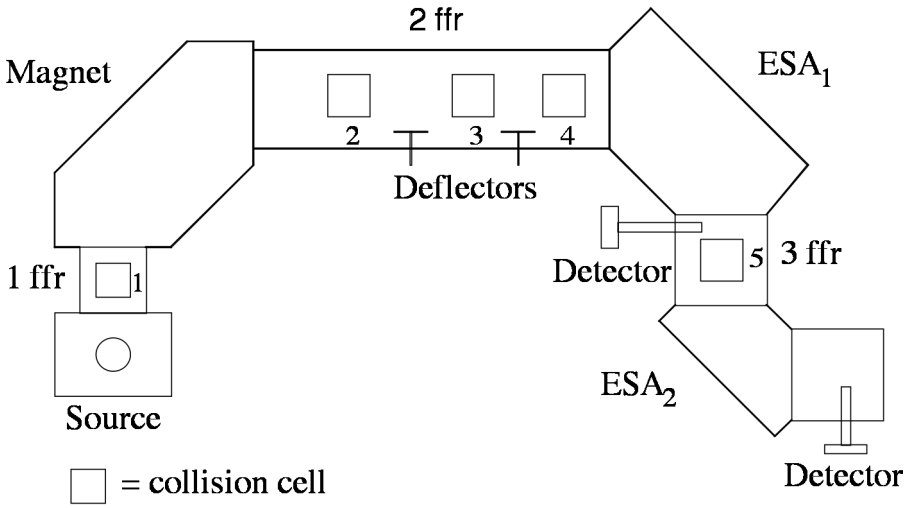

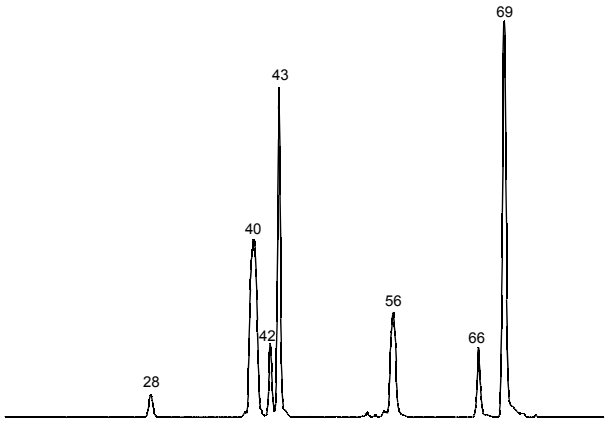

Figure 3: An example of a mass spectrum. Here, the Metastable Ion (MI) spectrum of ionized methylpropioliate [$HCCC(=O)OCH_3$] shows fragmentation into particles with mass per charge (*m/z*) ratios of 69, 66, 56, 43, 42, 40 and 28.

Fragmentations that need more energy to occur can be achieved by colliding the ions against neutral inert molecules. The collision cells (Figure 2) can be filled with some inert gas (like nitrogen or argon) so that the ions collide with the gas. In the collisions kinetic energy is transformed to internal energy of the molecules, causing even stable ions to fragment. In this case, unfortunately, the identification is often more difficult as a large number of fragmentations can become energetically possible, obscuring the mass spectrum.

A further possibility to study the fragments is to use neutralization - re-ionisation mass spectrometry [1]. In neutralization - re-ionisation mass spectrometry, the arriving ions are first neutralised in the first collision cell, which is filled with a neutralising agent. Here, ion-molecule complexes get separated from the covalently bound ions, since the neutral fragments fly apart without the binding electrostatic interaction. The deflector plates now carry a small positive charge and are used to dispose of the ions that failed to neutralise. The surviving covalently bound molecules are then re-ionised at the next collision cell with an ionizing agent, and in the ESA the fragments are separated.

The neutral fragments produced during the fragmentation can be studied similarly by using the reflector plates to deflect away all the ions, after which the neutral fragments are ionised in a collision cell.

As the fragmentation patterns are different for different molecules, the studied sample can be identified if reference data are available. A usual way to achieve more information about specific reaction patterns occurring during the fragmentation is to replace some of the atoms of the studied molecule with their isotopes. By determining into which dissociated fragment the isotopes end up, some conclusions can be drawn about the reactions occurring and even the precise formula of the ion might be found. Still, in many cases there are still various possibilities, which cannot be separated using mass spectrometry. Either other types of experiments are needed, or the reactions paths have to be determined with the help of computations.

5. Computations in studying ions and ion-molecule complexes

Frequently the intermediate complexes in fragmentations are short-lived and are not easy to identify experimentally, but they are crucial in determining the outcome of a reaction. Thus, they are often studied computationally. There are a large variety of different methods and different basis sets to choose from in the computational field. Usually, the prospective modeller must make a choice of sometimes very similar, but still distinct possibilities. Sometimes this might feel like entering teashop as a coffee drinker – how to know what is good and fits your purpose the best? It is also the question of quantity vs. quality. Does one take a big amount of tea for its cheap price and loose quality or buy a little bit of high-grade leaves with expense? We can understand this as the computational limitation – more accurate methods take more time and might become unfeasible to use, while the less accurate methods take less time and are used to give more qualitative answers. As an alternative, we can select different varieties of tea to make a blend that would retain as much of the quality as possible with reasonable price. In computations, we can use so-called "composite" methods to achieve more accuracy with less computational demand. Here, a series of computations with different levels of theory and basis sets in a chosen optimised geometry are performed. The results from these calculations are then used to estimate the

"exact" energy of the molecule in the chosen geometry. These methods have proven to be a good alternative to the use of only a single calculation.

The reader of this thesis will find that certain composite methods, namely CBS-QB3 and CBS-APNO, have been used as the principal methods in determining the properties of neutral and ionized molecules and complexes. The computations in Chapters 2 and 3 use CBS-QB3 calculations to achieve accurate energies. In Chapters 4, 5 and 6 CBS-QB3 and CBS-APNO have been used to achieve energy values used in energy level diagrams for metastable ion-molecule reactions occurring in three different ionised systems.

5.1 The basis of quantum mechanical methods

Quantum mechanics was created to explain phenomena not explainable by classical mechanics. In these phenomena are included the wave-particle duality of light (photons), the structure of atoms, and quantisation of energy [11]. Quantum mechanics has also the capability of explaining classical mechanics: As the system size becomes macroscopic, quantum mechanics results in the same conclusions as classical mechanics. Thus, quantum mechanics is not a theory that cancels classical mechanics, but adds to it.

We can use quantum mechanics to calculate properties of atoms and molecules. The most important property for us is the energy, since it determines the stability. The calculation of energy in quantum mechanical methods is based on solving the Schrödinger equation [12],

$$\hat{H}\Psi = E\Psi \quad , \tag{2}$$

where $\hat{H}$ is the Hamiltonian operator, Ψ is the wave function and E is the energy. Without going into further details, the reader needs only to know that the Schrödinger equation can be solved *approximately* for any molecular system (and exactly only for a very few exceptional cases), yielding the energy E of the system.

5.2 Zero-point (vibrational) energy

Every molecule has in its ground state some energy caused by the vibrations around their equilibrium positions. This energy is called the Zero-Point Vibrational Energy (ZPVE). Formally, the ZPVE contains only the vibrational energy, while Zero-Point Energy (ZPE) is assumed to contain also the zero-point energies caused by translational and rotational motion. In computations, the ZPVE and ZPE can be taken to have the same value, since in a (single-point) calculation the molecule does not move or rotate. The name zero-point energy (ZPE) is used in this thesis.

In the determination of absolute heats of formation of molecules, the ZPE contribution must be taken into account. The harmonic approximation of ZPE constitutes half of the sum of the vibrational frequencies ω_i,

$$ZPE = \tfrac{1}{2}\sum_i \omega_i \quad . \tag{3}$$

The vibrational frequencies can be obtained from experiments or computations. Unfortunately, computations in practise produce always systematically erroneous vibrational frequencies, and they are scaled to match experimental results better. In addition, the vibrations are not harmonic, but anharmonic. The permitted energy levels for anharmonic vibrations, $E_i(\upsilon)$, $\upsilon = 0,1,2,\ldots, \upsilon_{max}$, can be determined at each vibrational quantum number, υ, from the series

$$E_i(\upsilon) = \omega_i(\upsilon + ½) - \omega_i x_i(\upsilon + ½)^2 + \omega_i y_i(\upsilon + ½)^3 + \ldots , \quad (4)$$

where x_i and y_i are anharmonicity constants [13**]**. As the contribution of the terms rapidly decrease with the increasing power, the series is normally truncated to include only the two first terms. Now, the anharmonic zero-point energy, ZPE_{anh}, for the lowest state with $\upsilon = 0$ is

$$ZPE_{anh} = \sum_i E_i(0) = \sum_i \left[½\omega_i - ¼\omega_i x_i \right] . \quad (5)$$

As the ZPE in quantum chemical programs is usually computed using the harmonic approximation of vibrational frequencies, we end up with an error of ZPE_{anh} – ZPE = $-¼\sum\omega_i x_i$. This difference means that ZPE_{anh} is not linearly dependent on the harmonic frequencies. Therefore, a different scaling factor is needed for the ZPE estimation, than for the frequencies [14]. The scaling factors are also method and basis set dependent, which means that in different computations different scaling factors must be used to achieve the correct ZPE.

5.3 Heats-of-formation calculation

A quantity of interest in the modelling of molecules is the heat-of-formation, $\Delta_f H$, at 0 K and 298 K, as the thermochemistry largely dictates which reactions are possible. To know the heat-of-formation for a molecule A_iB_j, at 298 K, we first have to calculate the reaction enthalpy ($\Delta_r H_{0K}$) for reaction $A_iB_j \rightarrow iA + jB$:

$$\Delta_r H_{0K} = iH_{0K}(A) + jH_{0K}(B) - H_{0K}(A_iB_j) , \quad (6)$$

where $H_{0K}(X)$ is the enthalpy of species X at 0 K. Then the heat of formation at 0 K ($\Delta_f H_{0K}$) of molecule A_iB_j can be calculated as follows:

$$\Delta_f H_{0K}(A_iB_j) = i\Delta_f H_{0K}(A) + j\Delta_f H_{0K}(B) - \Delta_r H_{0K} . \quad (7)$$

From this, the $\Delta_f H(A_iB_j)$ at 298 K can be estimated from computed temperature corrections for the molecule, and empirical temperature corrections for all the atoms in the atomised molecule. Temperature correction parameters for the atoms come from experimental values [**15**]. Thus, $\Delta_f H_{298K}(A_iB_j)$ comes from equation

$$\Delta_f H_{298K}(A_iB_j) = \Delta_f H_{0K}(A_iB_j) + [H_{298K}(A_iB_j) - H_{0K}(A_iB_j)] - i\cdot[H_{298K}(A) - H_{0K}(A)] - j\cdot[H_{298K}(B) - H_{0K}(B)]\,. \quad (8)$$

The atomic enthalpies and heats-of-formation values can be obtained from experiments or separate computations using the same method [16]. The latter one is commonly used in conjunction with composite methods. The $[H_{298K}(X)-H_{0K}(X)]$ term is the enthalpy correction of the molecule, obtained from computations.

6. Non-composite methods

A variety of methods exist for predicting geometries, heats-of-formation and other properties out of computations, and these should give answers in par with experiments. For heat-of-formation estimates, one approach is to use relative energy calculations, where an anchor point is used (typically an experimental, or a very extensive computational result) and the energetics of the other species are then determined by comparing them to this anchor value. This is typical when using a single-step method in the computations. I will go through the methods, which have been used in this thesis.

6.1. Hartree-Fock theory

The most common approximation used to describe molecular wave functions is the Hartree-Fock (HF) approximation. It is based on minimizing the electronic energy of a single-determinant wave function using the variational principle, where the spin orbitals are varied until an energy minimum is found. The initial orbitals have to be guessed. To obtain *exact* Hartree-Fock orbitals, one would need to use an infinite amount of basis functions. In practise different limited size basis sets are used [17]. The cost of HF calculation increases as N^4 with the number of basis functions N, but in practise this can be lowered to $\sim N^3$ and less by pre-screening of small integrals and performing Coulomb and exchange evaluation separately with more efficient algorithms [18]. The HF theory is also *size-consistent*. With size consistency is meant that the calculated energy of a system, where two fragments are so far apart that they have no interaction, will be equal to the sum of energies of the two separately calculated fragments [17].

There are various approaches to the HF theory to make it more efficient in computations. An approach, where all the paired α and β spin orbitals are restricted to have the same spatial orbital, is called the Restricted Hartree-Fock theory (RHF). RHF treats all molecules as closed-shell molecules. It can be used to simulate a dissociation of a closed-shell molecule into two closed-shell fragments, but it cannot describe dissociation of a neutral molecule into two radicals, as the potential energy shows in this case an unphysical steep rise with increasing distance.

Also an open-shell restricted formalism has been introduced, where the spin value is restricted to the correct value: The restricted open-shell Hartree-Fock (ROHF) [19]. Here, certain orbitals are allowed to have only the α-spin electrons, while the rest of the orbitals are constrained the same way as in the RHF. In this case the constraints can prohibit

lowering of the variational energy, which would appear due to the fact that the α and β electrons can have different potentials, even though they are in the same spatial orbitals.

Another treatment of open-shell molecules was introduced by Pople and Nesbet [20], and is named Unrestricted Hartree-Fock (UHF). Now, the α and β electrons are in their respective spin orbitals. The clear advantage of this method over RHF is that the UHF can model a dissociation of a molecule into two radicals. Unfortunately, the UHF wave function does not change smoothly with increasing distance between the fragments, and either changes character or is heavily spin contaminated. When modelling radicals or excited states, in many cases the UHF computation can incorporate spin contamination in the wave function and lead to poor geometry and energy estimates [21].

6.2. Møller-Plesset perturbation theory

Hartree-Fock theory uses the average electric field caused by the other electrons to calculate the electron-electron repulsion energy in the system. In this way all the information concerning paired and higher-order electron correlation energies are not accounted for. As one way to add the electron correlation energies to the HF wave function, the Møller-Plesset (MP) theory with different orders of perturbation was introduced [22]. In the MP perturbation theory approach, the sum of zeroth and first order energies give the HF energy and the higher order terms are the correlation parts. The exact energy can be achieved, when convergent, from adding the zeroth-order Hamiltonian together with the sum of the 1^{st}, 2^{nd}, 3^{rd}, *et cetera*, to the n^{th} order perturbation (with $n \rightarrow \infty$ and with an infinitely large basis set). The computational demand increases as N^{2n}, with n being the order of the perturbation. As adding an infinite number of terms is impractical, the perturbation series is truncated to include only the first few perturbations. In practise, only the second and fourth order (which include also the lower orders) perturbation, *viz.* MP2 and MP4 methods, are used widely. The MP perturbation theory is always size-consistent, regardless of the order of the perturbation [17]. As the MP wave function is based on the HF wave function and the correlation is treated only perturbatively, it also has problems in treating many open-shell molecules. As for HF, the MP theory also has an unrestricted formalism. Together with spin projection methods for treating the spin-contaminated cases this often produces better results than the restricted formalism [23]. Nevertheless, it has been noted that in spin-contaminated cases the MP theory often gives slow convergence [24,25].

6.3. Coupled-Cluster theory and Quadratic Configuration Interaction

The Coupled-Cluster (CC) theory [26] was developed to account for the size-consistency problem in the Configuration Interaction (CI) theory, while Quadratic Configuration Interaction (QCI) theory was introduced as an alternative to the CC method [27]. Both the CC and QCI methods give very accurate results, when they include single and double excitations (SD), and they are also size consistent. Unfortunately, the CC and QCI methods are computationally very demanding; CCSD and QCISD scale to the sixth power with the increasing amount of basis functions. To improve the achieved energies, CC or QCI with perturbative triples, CCSD(T) and QCISD(T), respectively, can be used. The

perturbative triples term scales to the seventh power, but it is non-iterative and added in one-step calculation to the energy after the SD iterations [28].

For the treatment of radicals, the use of perturbative triples is needed to achieve reliable energies [29,30]. Accurate geometries can be achieved already at the SD level. The advantage of the CC theory over the QCI is that it is generally more reliable [31]. The need of demanding computations involved in these methods prohibits their use for larger molecules.

6.4 Density Functional Theory

Density Functional Theory (DFT) is based on, instead of multiple electron wave functions, the electron density [32] and single-particle wave functions in the Kohn-Sham formulation [32b]. Its main advantages are that the computational requirements do not increase as sharply as with most *ab initio* methods when the size of the system increases (the increase is similar to Hartree-Fock methods) [33], and that it is not so susceptible to spin contamination [34]. Many DFT-based functionals perform accurately in predicting geometries and are good choices to calculate radical species.

The DFT methods tend to delocalise spin and charge evenly even over large distances in symmetric systems. Bally and Sastry [35] studied two model systems; the dissociation of $H_2^{\bullet+} \rightarrow H^{\bullet} + H^+$ and $He_2^{\bullet+} \rightarrow He + He^{\bullet+}$, where in both cases aforementioned behaviour was apparent. This behaviour was not noticed, though, in asymmetric diatomic dissociations such as $LiH^{\bullet+}$, HeH^+, and $BeH^{\bullet}$ dissociations, and also not in $CH_3OH^{\bullet+} \rightarrow OH^{\bullet} + CH_3^+$ dissociation reaction. This is not to say that the spin and charge delocalisation effects are not present in the asymmetric systems, but that these effects are most apparent in the symmetric cases. The reaction barriers for dissociation in radicals are often estimated to be too low in DFT, which apparently results from the tendency to overestimate the lengths of the weak C-C and C-H bonds [36a]. It has been shown for the BLYP and B3LYP functionals of DFT that in some cases this has led to a miss of a TS [36]. Despite of these problems, they are not as common as the problems caused by spin contamination in HF and MP2.

7. Composite methods

The development of the composite methods took place mainly since the 1980's. The most used methods are in the Gaussian-n family [37] and CBS-n family [38], but other methods also exist, such as the Martin extrapolation (W-n) methods [39]. To outline the methods used in this thesis, we go through the computational steps and procedures used in CBS-APNO [38a] and CBS-QB3 [38c,d] to achieve the extrapolated energy.

7.1. The CBS-QB3 method

The CBS-QB3 method [38c,d], was introduced in 1998. The steps and procedures used in this method are outlined in Table 1. Following the work of Bauschlicher and Partridge [40] the geometry optimization uses the B3LYP functional with a large basis set. This gives reliable geometries even when dealing with spin-contaminated radicals. The

higher-order electron correlation estimate is obtained with CCSD(T), since it behaves better with spin contaminated radicals. The SCF energy is calculated in the MP2/CBSB3 step. The higher-order correlation energy correction to the SCF energy is obtained as the difference between UCCSD(T) and UMP4(SDQ) energies in the UCCSD(T)/6-31+G(d') step. The corrections towards larger basis set are acquired from the difference between UMP4(SDQ) and UMP2 energies in the MP4(SDQ)/CBSB4 and MP2/CBSB3 steps. To this is added the extrapolated correlation energy, extrapolated to infinite basis set in the MP2/CBSB3 step of the calculation. In the extrapolation the electrons are first localized into Paired Natural Orbitals (PNOs), using the same basis set. A PNO expansion is done for the second-order pair energies, which are then used to extrapolate to infinite-order pair energies [41a]. The localization into the PNOs can cause interorbital spin-orbit overlap, thus the extrapolation is then corrected with empirical spin-orbit overlap interference correction. Finally, a spin contamination correction is added for open-shell species.

Table 1. The computational steps in CBS-QB3 and CBS-APNO methods.

steps	method **CBS-QB3**	**CBS-APNO**
geometry optimization	B3LYP/CBSB7	UHF/6-311G**[a] QCISD/6-311G**[b]
ZPE	B3LYP/CBSB7	UHF/6-311G**
scaling factor	0.99	0.9251
SCF energy	UHF/CBSB3	UHF/CBSB5
correlation energy	UCCSD(T)/6-31+G(d') MP4SDQ/CBSB4	QCISD(T)/6-311+D(2df,p)[c] MP2(Full)/CBSB6[d]
basis set correction	MP2/CBSB3	MP2/CBSB5
empirical corrections	CBS-correlation spin-orbit overlap interference spin contamination	CBS-correlation spin-orbit overlap interference

[a] for ZPE estimation
[b] for the energy calculation
[c] for valence correlation
[d] for core correlation

In general, CBS-QB3 has shown improvement in comparison to composite methods using MP2 in their geometry optimisation, especially in the handling of spin-contaminated radicals, because of the use of the B3LYP method. B3LYP performs well in the geometry optimisation and also for frequency calculations to obtain the ZPE, compared to methods using MP2 and UHF in frequencies calculation [28,40,42]. CBS-QB3 performs reasonably

well also for triplet state biradical molecules, but singlet state biradical molecules have shown to give large errors [43]. The CBS-QB3 method was tested with 299 molecules, giving a mean absolute deviation (MAD) of 1.10 kcal mol^{-1} [38d]. The aforementioned problem of extended bond lengths in TS structures when using B3LYP has been noted to cause somewhat larger deviations in the estimation of heats-of-formation, than the aforementioned MAD [36a].

7.2. CBS-APNO method

Roughly speaking, using more robust methods and larger basis sets in the extrapolation scheme improves the results, giving smaller deviations from the experiments, but possibly limiting the use of the method to small molecules. Also the approach to the problem has some effect on the speed and accuracy. For example the use of (Atomic) Paired Natural Orbitals ((A)PNO), instead of the usual Hartree-Fock atomic and molecular orbitals, in the extrapolation has shown promising results [41].

In CBS-APNO the initial geometry is optimized and the ZPE estimated at the UHF/6-311G** level of theory. As the UHF is not necessarily reliable in estimating geometries for spin-contaminated cases, a second geometry optimisation is done at QCISD/6-311G(d,p) level, after which the correlation energy is determined at QCISD/6-311G+G(2df,p) level. The SCF energy is then calculated in the HF/CBSB5 step. To the combined QCISD(T) correlation energy and SCF energy then first a core correlation is added from a MP2(Full)/CBSB6 step. Following this, the last step of the computation involves a second order correlation energy correction, correlation correction between the second order correlation and the extrapolated Full CI correlation, and finally the spin-orbital overlap correction. Both the SCF and correlation energy are extrapolated. The SCF extrapolation scheme to the CBS limit is based on l^{-6} asymptotic convergence [41b] with increasing angular momentum l. This extrapolation replaces the calculations with high-order basis functions. The correlation energy extrapolation is done as in the CBS-QB3 method.

The mean absolute deviation for CBS-APNO in the energy estimation has been estimated to be only 0.53 kcal mol^{-1} [38a,b]. Despite of its accuracy, due to its demanding computations, such as the QCISD/6-311G(d,p) geometry optimisation step, it is not so convenient to use for larger systems with many first-row atoms. Another problem is that the CBS-APNO is initiated by a UHF geometry optimisation, which may result in a poor geometry to start the QCISD geometry optimisation in the next step. This can lead to a situation that the QCISD geometry optimisation fails to converge. This problem also gets worse when moving into larger molecules. In these cases it might be necessary to do a separate QCISD geometry optimisation from a better starting point and use these coordinates to do the CBS-APNO calculation without geometry optimisation in the initial UHF step.

8. Reaction rates and dynamics in proton-bound complexes

The usual time frame for metastable ion/molecule complex low-energy dissociation reactions is from microseconds to milliseconds. There are several methods to measure the

reaction rates of ions experimentally, although only a few can or have been used to measure ion-molecule complexes. Therefore, the reaction rates of ion-molecule complex dissociation are usually estimated using either statistical calculations, such as Rice-Ramsperger-Kassel-Marcus (RRKM) [44] theory, or trajectory calculations [44a].

8.1. Reaction rate estimation using RRKM

Reaction rates have been studied in many formulations already since the 1850's [45]. The first suggestion that the reaction rate of a reaction with an excited reactant depended on its internal energy *E,* was made by Hinshelwood (1926) [46]. This idea was further developed by Rice and Ramsperger in 1927 [47] and Kassel in 1928 [48]. Their formulation is generally called the classical RRK theory. In 1952, Marcus [49] extended the RRK theory to include a proper treatment of pressure, quantized vibrations and rotations, in a rigorous mathematical framework.

Nevertheless, the implementation of the RRKM theory was still somewhat tedious with the calculation of the sum-of-states of the activated complex using the integration over the density-of-states in the TS with respect to energy. This was greatly simplified by the Beyer-Swinehart direct-count algorithm [50], applied by Stein and Rabinovitch [51] to the RRKM theory to calculate the sums and densities of states. The RRKM theory in its simple form is written as

$$k(E,J) = \frac{W^{\#}(E,J)}{h\rho(E,J)} \quad , \tag{9}$$

where the reaction rate constant $k(E,J)$ is a function of total energy of the system, E, and total angular momentum, J. The result is dependent on the sum of states of the transition state (TS), $W^{\#}(E,J)$, which is obtained as the sum of possible vibrational modes between the TS and the total energy of the system, E, and the density of states, $\rho(E,J)$, of the ground state (GS) at given E and J. In our calculations we are interested only in the direct dissociation with $J = 0$.

One important aspect of the statistical reaction rate estimation methods is that they are based on the ergodicity condition. The ergodicity condition means that the energy of the activated complex, which will initially be only in certain degrees of freedom of the complex, must be rapidly randomized over all the degrees of freedom of the activated reactant. Another important aspect is that most statistical methods consider the reactions to be one-way only. They do not account for reactions re-crossing back to the reactants, after passing the transition state. Therefore, the reaction rates computed are always upper bounds to the true reaction rates.

A final note on the RRKM theory is that it works best on "tight" transition states (see Figure 4(a)), where a clear TS precedes the dissociation. It can be modified to a situation where the dissociation proceeds without a potential energy barrier. In this case the TS is called "loose" (Figure 4(b)). The reaction rate is now determined by a centrifugal barrier and can be determined by finding the smallest reaction rate constant $k(E)$ along the potential energy curve towards the dissociation. Nevertheless, finding an exact position of

the TS for this kind of situation is difficult. This leads to a situation where it is reasonable to study the dissociation using trajectory calculations.

The RRKM theory is used in Chapters 6 and 7 of this thesis.

8.2. Trajectory calculations in studying reaction dynamics

Bunker and Hase [52] demonstrated how the exact 'classical' reaction rate constant *k(E)* could be obtained from classical trajectory calculations. With classical is meant that the trajectories are based on classical mechanics. It was shown that, at a certain total energy *E*, a microcanonical ensemble of classical trajectories which were randomly excited, decayed exponentially according to equation

$$N(t) = N(0)e^{-k(E)t}, \tag{10}$$

where $N(0)$ is the number of trajectories in the starting ensemble, *k(E)* is the rate constant, and *N(t)* is the number of trajectories, which have not reached the products by the time *t*. The rate constant obtained from the trajectory calculations equal the exact RRKM rate constant if there are no trajectories re-crossing the transition state and the ergodicity condition is followed [44,52]. Nevertheless, there are cases when this does not hold. For example, some of the molecule's vibrational states might be weakly coupled, disallowing the ergodicity condition, leading to situation where the molecule's microcanonical ensemble is not maintained during the reaction. This situation often occurs in weakly bound complexes, where the intermolecular vibrational energy redistribution (IVR) does not occur efficiently [53]. In any case, it is necessary to include quantum effects to the trajectory calculations by performing ab initio (or DFT) potential surface calculations between the classical steps. This naturally increases the computational demand for the study of the system. Fortunately, with the ongoing development of computers and computational capacity has allowed computations of larger and more complex systems.

Figure 4. Two types of transition states in chemical reactions: (a) a "tight" TS that is relatively easy to place about at the top of the potential energy barrier, and (b) a "loose" TS whose position must be located by finding the centrifugal barrier.

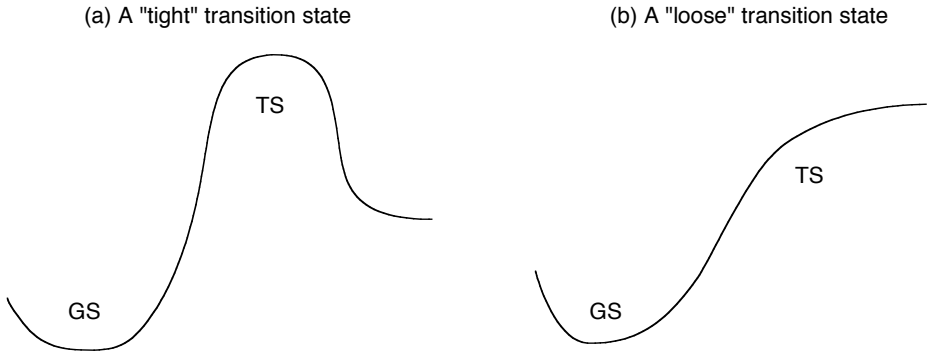

The number of trajectories needed for a proper microcanonical ensemble depends on the size, symmetry and linearity of the system, and can be thousands already for a small organic molecule. This number of trajectories is tedious to compute. There is need to somehow limit the number, and also the length, of the trajectories. This problem is approached in Chapter 7 of this thesis. One solution is to use a cut-off distance for the trajectories. The trajectory is run until the two separating fragments reach a certain distance from each other. At this point, the trajectory is cut off and further behaviour of the trajectory is predicted using inverse square fitting of the potential and kinetic energy terms as a function of distance. This is first done for all 'pure' modes, which is to say that only one vibrational mode is excited at a time to start up the trajectory. The behaviour of trajectories started by exciting more than one vibrational mode are then predicted from the fitting parameters obtained for the 'pure' modes, by mixing the parameters of the 'pure' modes. This might be a rather simple but powerful way to create a microcanonical ensemble by running only a limited number of trajectories, and then predicting the rest of the needed trajectories.

References

[1] J.L. Holmes, C. Aubry, P.M. Mayer, Assigning Structures to Ions in Mass Spectrometry, CRC Press, Boca Raton, 2007.

[2] For selected reviews, see (a) P.A. Kollman, L.C. Allen, Chem. Rev. 72(3) (1972) 283; (b) C. Laurence, M. Berthelot, Perspect. Drug Discovery Des. 18 (2000) 39-60; (c) M. Meot-Ner, Chem. Rev. 105 (2005) 213.

[3] (a) A.J. Cunningham, J.D. Payzant, P. Kebarle, J. Am. Chem. Soc. 94(22) (1972) 7627; (b) K. Hiraoka, H. Takimoto, S. Yamabe, J. Phys. Chem. 90 (1986) 5910; (c) M.J. Frisch, J.E. Del Bene, J.S. Binkley, H.F. Schaefer III, J. Chem. Phys. 84(4) (1986) 2279; (d) F.C. Pickard IV, E.K. Pokon, M.D. Liptak, G.C. Shields, J. Chem. Phys. 122 (2005) 024302.

[4] P.M.W. Gill and L. Radom, J. Am. Chem. Soc. 110 (2005) 4931.

[5] (a) M.W. Feyereisen, D. Feller, D.A. Dixon, J. Phys. Chem. 100(8) (1996) 2993; (b) J.G C.M. van Duijneveldt-van de Rijdt, F.B. van Duijneveldt, J. Chem. Phys. 111(9) (1999) 3812.

[6] (a) R. Yamdagni, P. Kebarle, J. Am. Chem. Soc. 93(26) (1971) 7139; (b) R. Yamdagni and P. Kebarle, J. Am. Chem. Soc. 95(11) (1973) 3504; (c) J.W. Larson, T.B. McMahon, J. Am. Chem. Soc. 104 (1982) 6255; (d) M. Meot-Ner, J. Am. Chem. Soc. 106 (1984) 1257.

[7] see, for example: E.W. Godbole, P. Kebarle, Trans. Faraday Soc. 58 (1962) 1897.

[8] (a) D.K. Bohme, Int. J. Mass Spec. Ion Processes 115 (1992) 95; (b) J.W. Gauld, L. Radom, J. Am. Chem. Soc. 119 (1997) 9831.

[9] J.W. Gauld, H. Audier, J. Fossey, L. Radom, J. Am. Chem. Soc. 118 (1996) 6299.

[10] P.C. Burgers, P.J.A. Ruttink, Int. J. Mass Spec. 242 (2005) 49.

[11] M. Planck, Verh. Deutsch. Physik. Ges. 2(17) (1900) 237.

[12] E. Schrödinger, Ann. Physik 79 (1926) 361.

[13] P.W. Atkins, Physical Chemistry, 3rd ed., Oxford University Press, 1986.

[14] R.S. Grev, C.L. Janssen, and H.F. Schäfer, J. Chem. Phys. 95(7) (1991) 5128.

[15] D.D. Wagman, W.H. Evans, V.B. Parker, R.H. Schumm, I. Halows, S.M. Bailey, K.L. Churney, R.N. Nuttall, J. Phys. Chem. Ref. Data 11, Suppl. 2., 1982.
[16] A. Nicolaides, A. Rauk, M.N. Glukhovtsev, and L. Radom, J. Phys. Chem. 100 (1996) 17460.
[17] A. Szabo, N.S. Ostlund, Modern Quantum Chemistry: Introduction to Advanced Electronic Structure Theory, Dover Publications Inc., 1996.
[18] P.-O. Widmark, B. Roos, European Summerschool in Quantum Chemistry 2005, Book I, Lund University, 2005.
[19] (a) H.C. Longuet-Higgins, J.A. Pople, Proc. Phys. Soc. Lond. A, 68 (1955) 591; (b) C.C.J. Roothaan, Rev. Mod. Phys. 32 (1960) 179; (c) R. McWeeny, Mol. Phys., 28(5) (1974) 1273.
[20] J.A. Pople and R.K. Nesbet, J. Chem. Phys. 22 (1954) 571.
[21] (a) L. Farnell, J.A. Pople, L. Radom, J. Phys. Chem., 87 (1983) 79; (b) J.C. Schug, D.H. Phillips, J. Chem. Phys. 59(4) (1973) 1616.
[22] C. Møller, M.S. Plesset, Phys. Rev. 46 (1934) 618.
[23] (a) P.O. Löwdin, Phys. Rev., 97 (1955) 1509; (b) K. Yamaguchi, F. Jensen, A. Dorigo, K.N. Houk, Chem. Phys. Letters, 149(5,6) (1988) 537; (c) J.S. Andrews, D. Jayatilaka, R.G.A. Bone, N.C. Handy, R.D. Amos, Chem. Phys. Letters, 183(5) (1991) 423.
[24] N.C. Handy, P.J. Knowles, K. Somasundram, Theor. Chim. Acta, 68 (1985) 87.
[25] M. Alcamí, O. Mó, M. Yáñez, Mass Spectrometry Reviews, 20 (2001) 195.
[26] (a) J. Čížek, J. Chem. Phys. 45 (1966) 4256; (b) J. Čížek, J. Paldus, Int. J. Quantum Chem. 5 (1971) 539.
[27] J.A. Pople, M. Head-Gordon, K. Raghavachari, J. Chem. Phys. 87(10) (1987) 5968.
[28] K. Raghavachari, J.A. Pople, E.S. Replogle, M. Head-Gordon, J. Phys. Chem. 94 (1990) 5579.
[29] P.M. Mayer, C.J. Parkinson, D.M. Smith, L. Radom, J. Chem. Phys., 108(2) (1998) 604.
[30] Y.-Y. Chuang, E.L. Coitiño, D.G. Truhlar, J. Phys. Chem. A, 104 (2000) 446.
[31] L. A. Curtiss, P. C. Redfern, K. Raghavachari, J. A. Pople, Chem. Phys. Lett. 359 (2002) 390.
[32] (a) P. Hohenberg, W. Kohn, Phys. Rev. B 136(3) (1964) 864; (b) W. Kohn, L. J. Sham, Phys. Rev. A 140(4) (1965) 1133.
[33] P.-O. Widmark, B. Roos in European Summerschool in Quantum Chemistry 2005, Book II, Lund University, 2005.
[34] J. Baker, A. Scheiner, J. Andzelm, Chem. Phys. Lett. 216 (1993) 380.
[35] T. Bally and G. Narahari Sastry, J. Phys. Chem. A Letters, 101(43) (1997) 7923.
[36] (a) M. Saeys, M.-F. Reyniers, G.B. Marin, V. van Speybroeck, M. Waroquier, J. Phys. Chem. A 107 (2003) 9147; (b) J. Baker, M. Muir, J. Andzelm, J. Chem. Phys. 102(5) (1994) 2063.
[37] (a) L.A. Curtiss, K. Raghavachari, G.W. Trucks, J.A. Pople, J. Chem. Phys. 94 (1991) 7221, (b) L.A. Curtiss, K. Raghavachari, P.C. Redfern, V. Rassolov and J.A. Pople, J. Chem. Phys. 109(18) (1998) 7764; (c) L.A. Curtiss, K. Raghavachari, P.C. Redfern, J.A. Pople, J. Chem. Phys. 114 (2001) 108; (d) L.A. Curtiss, P.C. Redfern, K. Raghavachari, J. Chem. Phys. 126 (2007) 084108.

[38] (a) J.A. Montgomery, Jr., J.W. Ochterski, G.A. Petersson, J. Chem. Phys., 101 (1994) 5900; (b) J.W. Ochterski, G.A. Petersson, J.A. Montgomery, Jr., J. Chem. Phys. 104 (1996) 2598; (c) J.A. Montgomery, Jr., M.J. Frisch, J.W. Ochterski, G.A. Petersson, J. Chem. Phys. 110(6) (1999) 2822; (d) J.A. Montgomery, Jr., M.J. Frisch, J.W. Ochterski, G.A. Petersson, J. Chem. Phys. 112(15) (2000) 6532.
[39] (a) J.M.L. Martin, G. de Oliveira, J. Chem. Phys. 111 (1999) 1843; (b) J.M.L. Martin, Chem. Phys. Lett. 310 (1999) 271; (c) S. Parthiban, G. de Oliveira, J.M.L. Martin, J. Phys. Chem. A 105 (2001) 895; (d) S. Parthiban, J.M.L. Martin, J. Chem. Phys. 114 (2001) 6014.
[40] C.W. Bauschlicher, jr., H. Partridge, J. Chem. Phys. 103(5) (1995) 1788.
[41] (a) G.A. Petersson, A. Bennett, T.G. Tensfeldt, M.A. Al-Laham, W.A. Shirley, J. Mantzaris, J. Chem. Phys. 89(4) (1988) 2193; (b) G.A. Petersson, A. Al-Laham, J. Chem. Phys. 94(9) (1991) 6081.
[42] D.J. Henry, C.J. Parkinson, L. Radom, J. Phys. Chem. A 106 (2002) 7927.
[43] G.P.F. Wood, L. Radom, G.A. Petersson, E.C. Barnes, M.J. Frisch, J.A. Montgomery, Jr, J. Chem. Phys. 125 (2006) 094106.
[44] (a) R.G. Gilbert, S.C. Smith, Theory of Unimolecular and Recombination Reactions, Blackwell Scientific Publications, 1990; (b) W. Hase, T. Baer, Unimolecular Reaction Dynamics: Theory and Experiments, Oxford University Press, 1996.
[45] K.J. Laidler, M.C. King, J. Phys. Chem. 87 (1983) 2657.
[46] C.N. Hinshelwood, Proc. Roy. Soc. (London) A113 (1926) 230.
[47] O.K. Rice, H.C. Ramsperger, J. Am. Chem. Soc. 49 (1927) 1617.
[48] L.S. Kassel, J. Phys. Chem. 32 (1928) 225.
[49] R.A. Marcus, J. Chem. Phys. 20(3) (1952) 359.
[50] T. Beyer, D.F. Swinehart, Comm. ACM 16(6) (1973) 379.
[51] S.E. Stein, B.S. Rabinovitch, J. Chem. Phys. 58 (1973) 2438.
[52] D.L. Bunker, W.L. Hase, J. Chem. Phys. 59 (1973) 4621
[53] (a) Z.S. Huang, R.E. Miller, J. Chem. Phys. 90 (1989) 1478; (b) P.A. Block, K.W. Jucks, L.G. Pedersen, R.E. Miller, Chem. Phys. 139 (1989) 15.

Chapter 2

Energy and stability of protonated ketenes: Inductive and resonance effects

Abstract

The proton affinities (PA) of electronegatively substituted ketenes RCH=C=O (R = H, CH_3, NH_2, OH and F) at various sites have been assessed by CBS-QB3 calculations. The most favorable protonation site was found to be the CH carbon atom to produce the acylium ions RCH_2C^+=O. The PA values, relative to that of CH_2=C=O, can be interpreted in terms of destabilizing effects of the R group in RCH=C=O [J. Am. Chem. Soc. 113, 6021 (1991)] and by positive or negative inductive effects of R in RCH_2C^+=O. For HOCH=C=O the two destabilizing effects are of similar magnitude and this rationalizes that its PA (823 kJ mol^{-1})* is virtually the same as that for CH_2=C=O (820 kJ mol^{-1}). For all ketenes (except for R = H), protonation leads to significant activation of the C=C bond. In the extreme case, protonation of H_2NCH=C=O at CH (PA = 917 kJ mol^{-1}) leads to the weakly bonded complex $H_2NCH_2^+$•••C=O with a C–C length of 2.92 Å and which only needs 15 kJ mol^{-1} to dissociate to $H_2NCH_2^+$ + CO. In fact, the covalently bonded species, $H_2NCH_2C^+$=O, does not exist, the most stable configuration being CH_2=N(H)–H^+•••C=O. When NH_4^+ (PA[NH_3] = 854 kJ mol^{-1}) approaches the NH_2 group of H_2NCH=C=O (PA at N = 845 kJ mol^{-1}), the stable hydrogen-bridged cation H_3N–H^+•••NH_2–CH=C=O is produced. The NH_4^+ group can move over to the CH group or it can attack the CH group directly. After passing a transition state, dissociation follows to NH_3 + $CH_2NH_2^+$ + CO. For neutral methylketene, CBS-QB3 calculates a heat of formation of –63 kJ mol^{-1}, in good agreement with an experimental value (–67 ± 5 kJ mol^{-1}) but not with another experimental number (–95 ± 5 kJ mol^{-1}) and these matters are discussed. Suggestions for further experimental work are proposed to address this discrepancy.

Henri K. Ervasti, Peter C. Burgers and Paul J.A. Ruttink, Eur. J. Mass Spectrom. 10, 791–799 (2004)

* In this Chapter unit kJ mol^{-1} are used. Conversion factor to kcal mol^{-1} is 4.184^{-1}.

Henri Ervasti (2008): Computational and experimental studies on stabilities, reactions and reaction rates of cations and ion-dipole complexes

Introduction

Ketenes have been the subject of considerable attention [1]. Electronegatively substituted ketenes are important intermediates in organic chemistry. Thus, HOCH=C=O was proposed as a reactive intermediate in the photolysis of CH_2=O in an Ar matrix [2] while FCH=C=O was prepared by the dehydrochloronation of fluoroacetyl chloride with triethylamine at –78°C [3]. H_2NCH=C=O has not yet been observed but substituted aminoketenes are highly reactive and important intermediates in organic synthesis [4].

In an interesting theoretical study on the stability of neutral ketenes, Tidwell and co-workers [2] found that in substituted ketenes, RCH=C=O, an electropositive R group (such as lithium) leads to stabilization, whereas electronegative subsituents (such as NH_2) lead to destabilization, as indicated by the energy difference (= stabilization energy, SE) for the isodesmic reaction

$$RCH{=}C{=}O + CH_3CH{=}CH_2 \rightarrow CH_3CH{=}C{=}O + RCH{=}CH_2 + SE \qquad (1)$$

From that study, a correlation between SE and group electronegativity of R clearly emerged. For example, aminoketene, H_2NCH=C=O, hydroxyketene, HOCH=C=O and fluoroketene, FCH=C=O, are destabilized with respect to ketene by 44, 73 and 86 kJ mol^{-1}, respectively. In contrast to formaldehyde, which protonates at oxygen to produce the resonance stabilized carbenium ion $^+CH_2$–OH ↔ CH_2=O^+H [5], protonation of ketene occurs at carbon to produce the stable acetylium ion CH_3C^+=O; protonation at the oxygen atom would generate CH_2=C^+OH which lies 175 kJ mol^{-1} above CH_3C^+=O [6]. Protonation at =C= is even less favorable: the resulting ion $^+CH_2CH$=O, a destabilized carbenium ion [7], collapses into the three-member ring structure lying 232 kJ mol^{-1} above CH_3C^+=O [6]. Also, the proton affinity (PA) of ketene is much larger than that of formaldehyde (820 vs. 718 kJ mol^{-1}) [8].

It appears from the literature [9] that for RCH=C=O the most favorable site for protonation, too, may be at the CH carbon to produce RCH_2C^+=O, as is the case for the parent ketene. In the gas phase, ions RCH_2C^+=O may undergo heterolytic C–C cleavage to produce R–CH_2^+ + CO as, for example, is the case for $HOCH_2C^+$=O [10]. The stability of RCH_2^+ heavily depends on the electron releasing capability of R [5] leading to resonance stabilization (+M effect). In fact, it appears that for R=NH_2 the product ion $NH_2CH_2^+$ is so stable from the +M effect that the covalently bonded precursor ion, $NH_2CH_2C^+$=O, may not even exist [11] and this may explain the absence of B_1-type ions in the mass spectra of underivatized peptides [12].

The purpose of this paper is to establish the structure, energy and stability of protonated ketenes using the model chemistry CBS-QB3. In particular, we wish to establish what effect R has on the PA of RCH=C=O and what effect it has on the stability of RCH_2C^+=O, that is to say, what effect the substituent has on the C–C bond dissociation energy of RCH_2C^+=O. We will show that protonation of electronegatively substituted ketenes leads to activation of the C=C bond to the extent that protonation may even become dissociative. We also comment here on the vexing discrepancy that exists for the different experimental heats of formation of neutral methylketene and we offer suggestions for further experiments.

Theoretical methods

The calculations were performed using GAMESS-UK [13] and Gaussian 98 Revision A9. [14] For the geometry optimizations, GAMESS-UK was used since, in our experience, this program is more reliable in finding stationary points on the potential energy surface, particularly for transition states. The standard CBS-QB3 [15a] and CBS-APNO [15b] model chemistries were used to calculate the heats of formation using the automatic options in Gaussian 98 in all cases. Of these methods, the CBS-APNO method is the most reliable, yielding a mean absolute deviation (MAD) of 2.2 kJ mol^{-1} for the G2 [15c] test set of molecules and ions. The MADs for the G2, G3 [15d] and CBS-QB3 methods are 6.2, 4.3 and 3.6 kJ mol^{-1}, respectively.

The energies and proton affinities of the molecules and ions studied are given in Tables 1, 2, 3 and 4. Supplementary information is available upon request.

Results and discussion

Protonation site of RCH=C=O

The following compounds were investigated: R = H, CH_3, NH_2, OH and F with the following numbering of the protonation sites: $R^1–C^2H=C^3=O^4$. In all cases, the most favorable site for protonation was found to be at the CH carbon (atom 2) to produce $RCH_2C^+=O$, see Table 2. For $R=NH_2$ protonation at this site led to a weakly bonded complex, $H_2NCH_2^+•••C=O$, with a C–C bond length of 2.92 Å, which only needs 15 kJ mol^{-1} to dissociate to $H_2NCH_2^+ + CO$. This complex can rearrange, via a barrier of 4 kJ mol^{-1} to the hydrogen-bridged ion, $CH_2N(H)–H^+•••C=O$, which lies 13 kJ mol^{-1} below $H_2NCH_2^+•••C=O$. Our result that the ion of putative structure, $H_2NCH_2C^+=O$, is, in fact, a complex between $CH_2NH_2^+$ and CO, is in agreement with earlier findings [11].

Proton affinities of RCH=C=O and heats of formation of $RCH_2C^+=O$

As we go from H to F, we see that the PA at atom 2 first rises and then falls again. A qualitative interpretation of this observation is given below. The Δ_fH values obtained by CBS-QB3 for the various $RCH_2C^+=O$ ions are listed in Table 3. As mentioned above, the covalently bonded ion, $H_2NCH_2C^+=O$, does not exist and so no CBS value for its heat of formation can be computed. For ion $OCH_2C^+=O$, an estimate from the literature is available [10], 502 kJ mol^{-1}, much smaller than our CBS-QB3 value (551 kJ mol^{-1}). This estimate was obtained by substitution of an H atom in $CH_3C^+=O$ by an OH group on a non-charge baring site, that is to say the effect of OH substitution on the heats of formation of alkanes (–21 kJ mol^{-1}, for example $CH_3CH_3 \rightarrow CH_3CH_2OH$) was used to obtain $\Delta_fH[HOCH_2C^+=O]$. We have used this procedure to estimate $\Delta_fH[RCH_2C^+=O]$ using the CBS-QB3 $\Delta_fH[CH_3C^+=O]$ = 661 kJ mol^{-1} as reference, see Table 3.

In effect, this procedure can be represented by the isodesmic reaction:

$$CH_3CH_2R + CH_3C^+=O \rightarrow CH_3CH_3 + RCH_2C^+=O + SE \qquad (2)$$

Table 1. Energies (Hartree) and CBS–QB3 heats of formation (kJ mol^{-1}) for ketene, substituted ketenes and their protonation products.

Species	E(B3LYP / CBSB7)	E_{TOTAL}(0 K)	E(ZPE)	$\Delta_f H$ (298 K)
CH_2=C=O	–152.64775	–152.37580	82	–49
CH_3C^+=O	–152.96858	–152.68600	116	661
CH_2=C^+OH	–152.90565	–152.61950	112	836
$[CH_2CHO]^+$	–152.87788	–152.59710	116	893
CH_3CH=C=O	–191.97175	–191.59920	158	–63
$CH_3CH_2C^+$=O	–192.30155	–191.91830	191	623
$C_2H_5^+$•••C=O	–192.23652	–191.85980	173	782
CH_3CH=C^+OH	–192.24521	–191.85690	188	785
CH_3CH^+CH=O	–192.22839	–191.84460	185	818
HOCH=C=O	–227.86355	–227.49730	97	–156
$HOCH_2C^+$=O	–228.18578	–227.80870	129	551
$HOCH_2C$=O^+ TS1[a]	–228.18016	–227.80100	128	571
$HOCH_2^+$•••C=O	–228.18192	–227.80300	126	569
$HOCH_2C$=O^+ TS2[a]	–228.17631	–227.80120	121	574
$^+CH_2OH$•••C=O	–228.19053	–227.81400	122	540
$HOCH^+CH$=O	–228.16149	–227.78020	129	626
H_2O^+CH=C=O	–228.14928	–227.76310	130	671
HOCH=C^+OH	–228.13448	–227.74810	129	710
H_2NCH=C=O	–208.00099	–207.63250	130	12
O=C•••H_2N^+=CH2	–208.36366	–207.98600	158	611
H_2N^+=CH_2•••C=O	–208.35865	–207.98110	158	625
H_2NCH^+CH=O	–208.34016	–207.95770	164	682
H_3N^+CH=C=O	–208.33933	–207.95210	168	697
H_2NCH=C^+OH	–208.27765	–207.89650	163	842
H_3NH^+•••NH_2CH=C=O	–264.96174	–264.45010	259	552
H_3N–H^+–$CH(NH_2)$C=O TS1[b]	–264.93821	–264.42900	250	606
H_3N–$HCH(NH_2)C^+$=O	–264.94084	–264.43270	257	598
H_3N•••$H_2NCH_2C^+$=O TS2b	–264.93793	–264.43362	255	596
H_2N^+=$CH_2(NH_3)$•••C=O	–264.96298	–264.46140	254	528
FCH=C=O	–251.87904	–251.51060	65	–164
FCH_2C^+=O	–252.18764	–251.81050	98	573
$FCHCH^+$=O	–252.13097	–251.75090	95	729
FCH=C^+OH	–252.12735	–251.74220	96	753
HF^+CHC=O	–252.09743	–251.71270	90	831
CH_2=CH_2	–78.61398	–78.41663	132	55
CH_3CH=CH_2	–117.94406	–117.64620	206	25

Table 1, continued

CH_3CH_3	–79.85626	–79.63055	193	–83
$CH_3CH_2CH_3$	–119.18069	–118.85586	268	–102

[a] The structures of the transition states are shown in Figure 1

[b] The structures of the transition states are shown in Figure 2

where SE is taken as zero. From Table 3, it can be seen that agreement between the estimated and CBS-QB3 values is poor, especially for FCH=C=O, where the difference is as much as 100 kJ mol^{-1}. These differences can be interpreted in terms of positive and negative inductive effects of the R group. Thus, CH_3 has a positive inductive (+I) effect because it donates electrons through sigma bonds. Thus, in the ion $CH_3CH_2C^+=O$, electrons are pushed towards the charge making the ion more stable, 623 vs. 640 kJ mol^{-1}, that is to say, SE for Equation (2) is +17 kJ mol^{-1}. In contrast, OH and especially F have relatively strong negative inductive (–I) effects as these electronegative groups pull electrons through sigma bonds, making the ions $HOCH_2C^+=O$ and $FCH_2C^+=O$ less stable. The most recent experimental value for $\Delta_fH[CH_3CH_2C^+=O]$, 618 ± 1 kJ mol^{-1} [21b], is in excellent agreement with theory (see Table 3), but the experimental value for $\Delta_fH[HOCH_2C^+=O]$ is 43 kJ mol^{-1} higher than our ab initio value, see Table 3. This discrepancy will be discussed later.

A qualitative interpretation of the ordering of the PA values of RCH=C=O (at atom 2) now emerges. According to the calculations [Equation (1)] by Tidwell and co-workers [2], $CH_3CH=C=O$ is slightly destabilized (by 14 kJ mol^{-1}) by n-π donation relative to $CH_2=C=O$. This raises the PA. We now find that the protonated species $CH_3CH_2C^+=O$ is slightly stabilized relative to $CH_3C^+=O$, see Table 2. This too raises the PA and indeed the PA of $CH_3CH=C=O$ is higher than that of $CH_2=C=O$, see Table 2. Neutral hydroxyketene too is destabilized [2] relative to $CH_2=C=O$ but we now find that the protonated species, $HOCH_2C^+=O$, is also destabilized and these two destabilizing effects, we argue, compensate each other and the result is that HOCH=C=O and $CH_2=C=O$ have the same PA. For FCH=C=O, destabilization by the –I effect in the protonated

Table 2. CBS-QB3 proton affinities (kJ mol^{-1}) of substituted ketenes $R^1–C^2H=C^3=O^4$.

R	1	2	3	4
H	—	820 820[a] 823[b]	588[c]	645
CH_3	—	844 845[d] 842[e] 840[f]	649	681
NH_2	845	917[g]	860	699
OH	703	823	748	664
F	534	793	636	613

[a] Experimental value (± 8) from Reference 16

[b] Experimental value (± 3) from Reference 17

[c] Collapses to three-member ring

[d] Experimental value (± 3) from Reference 18

[e] Experimental value (± 3) from Reference 19

[f] Experimental value (± 4) from Reference 17

[g] Forms complex $H_2NCH_2^+$•••C=O

species, $FCH_2C^+=O$, is so large, see Table 3, that it overcompensates for the destabilizing effect in the neutral and so the PA of FCH=C=O is substantially smaller than that of $CH_2=C=O$.

Table 3. Heats of formation, dissociation limits (DL)[a] and bond dissociation energies (BDE)[b] (kJ mol^{-1}) of $RCH_2C^+=O$.

R	Δ_fH(Est)[c]	Δ_fH		DL		BDE	
		CBS	Exp	CBS	Exp	CBS	Exp
H	661[e]	661	657[f]	981	979	320	322
CH_3	640	623	618[g]	795	791	172	173
NH_2	699	625[h]		640	632		15
OH	508	551	594[i]	594	590	43	0
F	473		573		720		147

[a] $DL = \Delta_fH[RCH_2^+] + \Delta_fH[C=O]$

[b] $BDE = \{\Delta_fH[RCH_2^+] + \Delta_fH[C=O]\} - \Delta_fH[RCH_2C^+=O]$

[c] Estimate from Equation (2) with SE = 0

[d] Experimental values (± 4) from Reference 8

[e] Reference value

[f] Value (± 2) from Reference 20

[g] Value (± 1) from Reference 21(b)

[h] Complex $H_2NCH_2^+$•••C=O

[i] Value from Reference 10

Bond dissociation energies of $RCH_2C^+=O$

The quantity $\{\Delta_fH[RCH_2^+] + \Delta_fH[C=O]\} - \Delta_fH[RCH_2C^+=O]$ equals the C–C bond dissociation energy (BDE) of $RCH_2C^+=O$, see Table 3. It can be seen that the BDE decreases rapidly in the order H > F > CH_3 > OH > NH_2. This represents (except for R = CH_3) the order of resonance stabilization [the positive "mesomeric" (+M) effect] caused by electron donation of the R group in the product ion RCH_2^+. The SE of the substituent in RCH_2^+ can be assessed from the isodesmic reaction [5]

$$CH_3^+ + CH_3R \rightarrow CH_4 + CH_2R^+ + SE \qquad (3)$$

leading to the following SEs (kJ mol^{-1}): H(0), F(88), CH_3(180), OH(259), NH_2(397) (experimental heats of formation were taken from Reference 8). The SE values for F, OH and NH_2 represent a trade-off between destabilizing –I and stabilizing +M effects, where the +M effect outweighs the –I effect. For CH_3, the SE originates from the +I effect. For NH_2, the SE of $CH_2NH_2^+$ is so large that the ion $H_2NCH_2C^+=O$ is not capable of existence, fragmenting immediately into $H_2NCH_2^+$ + CO. Indeed, the estimate of $H_2NCH_2C^+=O$ [699 kJ mol^{-1}, from Equation (2)] lies well above the dissociation limit (632 – 640 kJ mol^{-1}) for $H_2NCH_2^+$ + CO, see Table 3.

The ion $HOCH_2C^+=O$ can be made by simple bond cleavage of ionized 1,3-

dihydroxyacetone [10]. The measured AE led to $\Delta_fH[HOCH_2C^+{=}O]$ = 594 kJ mol^{-1}, which is much higher than our CBS-QB3 result (551 kJ mol^{-1}). The observation that the measured Δ_fH is so high has been addressed but no satisfactory explanation could be given [10]. We note that *m/z* 59 in the mass spectrum of 1,3-dihydroxyacetone is only 1% of the base peak (*m/z* 31) and so the AE measurement may not be very reliable. In addition, the measured AE value for $HOCH_2C^+{=}O$ is at the ion's experimental and theoretical dissociation limit to CH_2OH^+ + CO (see Table 3) and so we conclude that the measured AE is indeed too high.

The ion undergoes one fragmentation in the metastable time frame, viz. to $HOCH_2^+$ + CO with a small kinetic energy release ($T_{0.5}$ = 6 meV or 0.6 kJ mol^{-1}). It is possible that this small $T_{0.5}$ value results from fragmentation of an ion–molecule complex [27]. To test this hypothesis we have calculated the barrier for the transformation $HOCH_2C^+{=}O \rightarrow CH_2O\text{-}H^+{\bullet\bullet\bullet}C{=}O$, see Figure 1. Upon elongation of the C–C bond a transition state is reached which leads to the species $HOCH_2^+{\bullet\bullet\bullet}C{=}O$. Next the CO molecule is transferred to the O–H hydrogen atom to yield the hydrogen-bridged ion–molecule complex $^+CH_2O\text{-}H{\bullet\bullet\bullet}C{=}O$ which can then dissociate. The ion $^+CH_2O{-}H{\bullet\bullet\bullet}C{=}O$ lies lower in energy than the starting ion $HOCH_2C^+{=}O$, see Figure 1. Thus, the small $T_{0.5}$ value results, we propose, from dissociation of the complex ion $^+CH_2O{-}H{\bullet\bullet\bullet}C{=}O$.

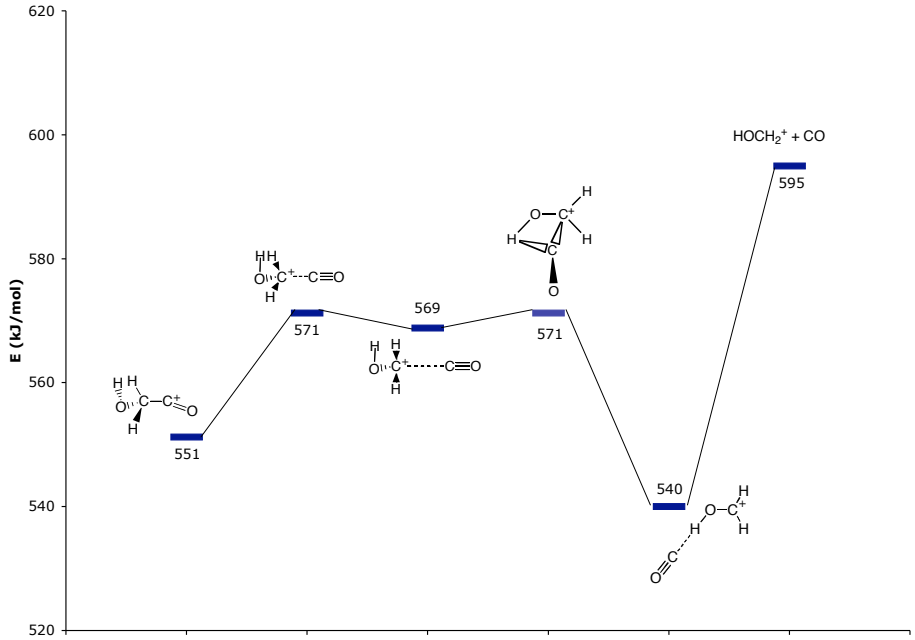

Figure 1. Energy level diagram (CBS-QB3, 298 K) for the dissociation of $HOCH_2C^+{=}O$ into $^+CH_2OH$ + CO.

The captodative carbenium ions $RCH^+CH{=}O$

Protonation at atom 3 leads to the captodative carbenium ions $RCH^+CH{=}O$, which are

stabilized by the +M or +I (for R = CH_3) effect of R, but destabilized by the –M effect of CH = O. In fact, when R = H the ion is not capable of existence, it either collapses to CH_3C^+=O or to a three-member ring. The differences in PA at atoms 2 and 3 decreases in the order H > CH_3 > F > OH > NH_2, see Table 2, and this shows that the heat of formation of RCH^+CH=O, relative to RCH_2C^+=O decreases in that order, showing the effect of increasing resonance stabilization in RCH^+CH=O in that order. Our calculations show that, although the RCH^+CH=O ions lie above the lowest lying dissociation products, viz. RCH_2^+ + CO, they do lie (except for $^+CH_2CH$=O) in wells.

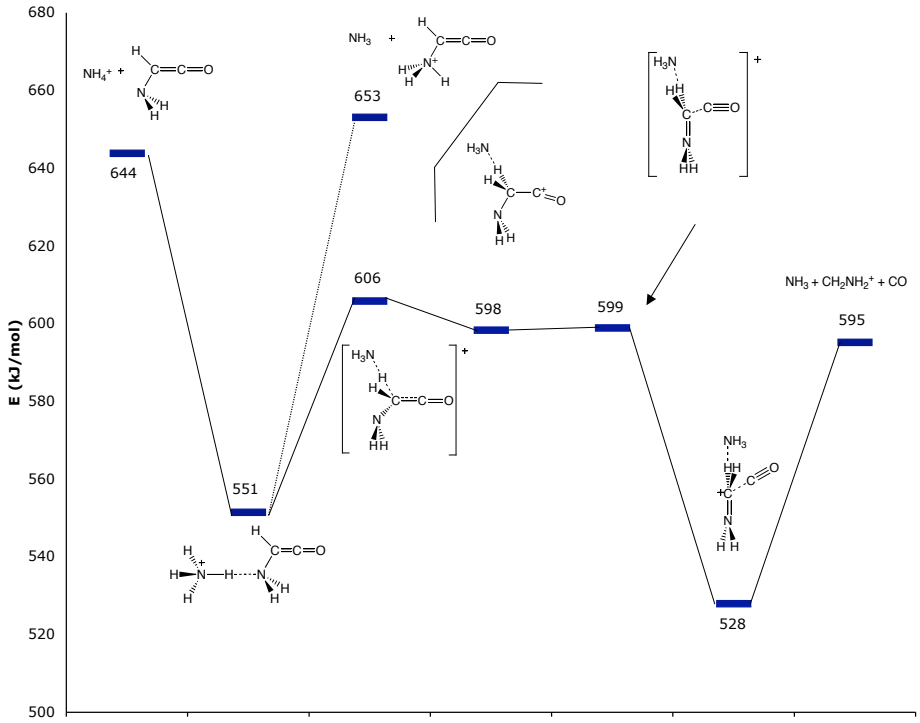

Figure 2. Energy level diagram (CBS-QB3, 298 K) for the protonation of H_2NCH=C=O by NH_4^+.

Protonation of H_2NCH=C=O by NH_4^+

As stated above, the most favorable protonation site of H_2NCH=C=O is at the CH group, PA = 917 kJ mol^{-1} and this protonation leads to the complex $H_2NCH_2^+$•••C=O. NH_4^+ should be a good protonation agent, as the PA of NH_3 is only 854 kJ mol^{-1}. The calculated energy diagram for protonation of aminoketene with NH_4^+ is given in Figure 2. When NH_4^+ moves towards aminoketene, the hydrogen-bridged species NH_3–H^+•••NH_2CH=C=O is formed. The CBS-QB3 Δ_fH of this ion is 552 kJ mol^{-1} which is close to the estimate using Mautner's correlation equations [28] from which Δ_fH = 548 kJ mol^{-1}. This ion can

dissociate back to the starting ions or, following proton transfer, to $NH_3 + H_3N^+–CH=C=O$ which lie 9 kJ mol^{-1} higher in energy than the starting ions. However, substantially below these levels, the NH_4^+ ion can move over to the CH group. The transition state (at 606 kJ mol^{-1}) for proton transfer to the C–H group lies above the dissociation limit for $NH_3 + H_2NCH_2^+ + CO$ but below the energy for the starting ions. Next the C–C bond stretches to produce $CH_2NH_2^+$ co-ordinated with CO and NH_3, after which dissociation to $CH_2NH_2^+ + CO + NH_3$ follows.

Heats of formation of ketene, methylketene and $CH_3CH_2C^+=O$: an appraisal

There has been a lively discussion in the literature as to what the heats of formation of methylketene and its protonated form should be and a summary and discussion is given here. An overview of the relevant experimental and theoretical heats of formation of ketene, methylketene and their protonated forms is given in Table 4.

The appearance energies (AEs) for the reactions

$$RCH_2C(=O)OC_6H_5 \rightarrow RCH=C=O + C_6H_5OH^{\bullet+} + e^-, \qquad (4)$$

where R = H, CH_3 have been measured using monochromatic electrons [23] and by photoionization [24], see Table 4. Since $\Delta_{f,298}H^o[C_6H_5OH^{\bullet+}]$ is accurately known (722 [23] or 725 ± 1 [2] kJ mol^{-1}) and $\Delta_{f,298}H^o[RCH_2C(=O)OC_6H_5]$ can be estimated by additivity [-280 [23,24] kJ mol^{-1} (R = H) and –297 [23] or –300 [24] kJ mol^{-1} (R = CH_3)]; such measurements yield $\Delta_{f,298}H^o[RCH=C=O]$ provided that the reactions have no reverse barriers. It can be seen from Table 4 that the AEs for Reaction (4) for formation of ketene (R = H) are very different, 948 ± 5 kJ mol^{-1} (monochromatic electrons [23]) and 928 ± 1 kJ mol^{-1} (photoionization [24]), but no reasons for these different values were given. It can also be seen that the heats of formation for ketene derived from these different AE values are the same, –54 kJ mol^{-1} (and similar to an earlier experimental value, –48 kJ mol^{-1} [22] and the CBS-QB3 and CBS-APNO values, –49 and –51 kJ mol^{-1} [25], respectively). How can different AE values yield the same Δ_fH^o? It appears that opinions differ as to how AE data should be interpreted. Traeger has argued [29] that in the mass spectrometer the product ions are not formed at any well-defined equilibrium thermodynamic temperature, but rather close to 0 K. To account for this, Traeger has introduced a correction term [29] which for the formation of ketene from Equation (4) is:

$$H_{corr} = \{H^o_{298} - H^o_0\}[CH_2=C=O] + \{H^o_{298} - H^o_0\}C_6H_5OH^{\bullet+} - (5/2)RT$$

which, in effect, is added to the measured AE [29]. Auxiliary data are then necessary to evaluate $H^o_{298} - H^o_0$ and, when this is done, for formation of ketene from phenyl acetate, H_{corr} is found to be 24 kJ mol^{-1}. This leads to an "effective" AE of 952 kJ mol^{-1}, which is very close, by coincidence we argue, to the value of Holmes et al. [23] (948 kJ mol^{-1}), who do not use a temperature correction. We note that the absolute PAs, derived from the experimental ΔH^o_fs for ketene and $CH_3C^+=O$, 825 ± 4 or 819 ± 6 kJ mol^{-1} are in good agreement with the measured PAs, 820 ± 816 and 823 ±317 kJ mol^{-1}, see Table 4.

The reversed situation is found for methylketene. Here, the measured AEs are almost the same (see Table 4) but the derived Δ_fH^os for methylketene are very different, –95 ± 523

and −67 ± 524 kJ mol^{-1}. Again, Traeger [24] uses a correction term that, in this case, is 27 kJ mol^{-1}, whereas Holmes and co-workers [23] do not; since the two AEs are very similar this correction term corresponds to the difference in the derived Δ_fH^os. Which value for Δ_fH^o [$CH_3CH=C=O$] is the correct one? Holmes et al. argue that a value of –67 kJ mol^{-1} would result in an unusual energy change from $CH_2=C=O$ to $CH_3CH=C=O$ of about −16 kJ mol^{-1}, much lower than, for instance, found for methyl substitution in ethene, –32 kJ mol^{-1} or in formaldehyde, -57 kJ mol^{-1}, whereas their value for Δ_fH^o [$CH_3CH=C=O$] (–95 kJ mol^{-1}) would lead to a more reasonable energy change of about –40 kJ mol^{-1}. In addition, Holmes et al. [23] find that vinyl substitution in ketene ($CH_2=C=O \rightarrow CH_2=CH–CH=C=O$) does not lead to an anomalous energy change: Δ_fH^o[$CH_2=CH–CH=C=O$] was assessed as 9 ± 4 kJ mol^{-1}, from the measured Δ_fH^o of the radical cation and the IE of $CH_2=CH-CH=C=O$. They argue that this finding lends further support for their experimentally derived Δ_fH^o[$CH_3CH=C=O$]. However, we find by CBS-QB3 that Δ_fH^o[$CH_2=CH-CH=C=O$] is 29 kJ mol^{-1}, 20 kJ mol^{-1} higher than the indirectly assessed value, illustrating that substitution of ketene may indeed be anomalous.

Table 4. Heats of formation (Δ_fH) of ketene and methylketene and their protonated forms. PA = proton affinity, AE = appearance energy for the reaction $CH_2C(=O)OC_6H_5 \rightarrow C_6H_5OH^{\bullet+} + RCH=C=O + e^-$ (R = H, CH_3). All values in kJ mol^{-1}.

Ketene	AE	$\Delta_fH[CH_2=C=O]$	$\Delta_fH[CH_3C=O^+]$	PA
Experimental	948 ± 5[d]	–48 ± 2[a]	657 ± 2[b]	820 ± 8[c]
	928 ± 1[f]	–54 ± 5[d]		823 ± 3[e]
		–54 ± 2[f]		
Theory		–49[g]	661[h]	820[i]
		–51[j]	656[k]	823[i]
Methylketene	AE	$\Delta_fH[CH_3CH=C=O]$	$\Delta_fH[CH_3CH_2C=O^+]$	PA
Experimental	924 ± 3[d]	–95 ± 5[d]	618 ± 1[m]	817 ± 6[i]
	931 ± 2[f]	–67 ± 5[f]	618 ± 1[m]	843 ± 6[i]
				840 ± 4[e]
				845 ± 3[l]
				842 ± 3[n]
Theory		–63[g]	623[h]	844[i]
		–68[o]	618[o]	844[i]
		–69[j]	615[k]	846[i]

[a] Reference 22; [b] Reference 20; [c] Reference 16; [d] Reference 23; [e] Reference 17; [f] Reference 24; [g] This work, CBS-QB3, see also Reference 25; [h] This work, CBS-QB3; [i] Derived value from PA = Δ_fH [RCHCO] + Δ_fH [H^+] – Δ_fH [RCH_2CO^+], R = H, CH_3, Δ_fH [H^+] = 1530 kJ mol^{-1} (for example, –49 + 1530 – 661 = 820); [j] Reference 25, CBS-APNO; [k] This work, CBS-APNO; [l] Reference 18; [m] Reference 21(b); [n] Reference 19; [o] Reference 26

Apart from the different AE values for formation of ketene (which is an experimental problem) a more fundamental question appears to be whether a temperature correction is

necessary (which is an interpretation issue) and agreement on this topic should be reached.

On the other hand, the value obtained by Traeger (–67 kJ mol^{-1}) is very close to previous theoretical values of –69 [25] and –68 kJ mol^{-1} [26]. Our CBS-QB3 value (-63 kJ mol^{-1}) too is in good agreement with Traeger's value. (We note that CBS-APNO calculations give a slightly lower value (–69 kJ mol^{-1} [25]) than the CBS-QB3 method). It is of interest to note that from the results of Tidwell and co-workers [2] (at the HF/6-31G*//HF/6-31G** level of theory) for the isodesmic reaction (1) for R = H, a value of –66 kJ mol^{-1} is calculated for $\Delta_f H^o[CH_3CH=C=O]$ (SE = –14 kJ mol^{-1}). Thus all levels of theory give consistent results.

In addition, the heat of formation of the propanoyl cation $H_3CH_2C^+=O$ has recently been obtained by photoionization mass spectrometry [21b] by measurement of the AE for the reaction $CH_3CH_2C(CH_3)=O \rightarrow CH_3CH_2C^+=O + CH_3^{\bullet}$, $\Delta_{f,298}H^o[CH_3CH_2C^+=O] = 618 \pm 1$ kJ mol^{-1}, with temperature correction. This represents a significant revision upwards of the previous value of 591 ± 2 kJ mol^{-1} [21a], and possible sources of error for the earlier lower value were identified [21b]. The value of 618 kJ mol^{-1} is in excellent agreement with theoretical calculations, see Table 4. From $\Delta_{f,298}H^o[CH_3CH_2C^+=O]$ and $\Delta_{f,298}H^o[CH_3CH=C=O]$ we can calculate the absolute PA of $CH_3CH=C=O$ as 817 kJ mol^{-1} (using $\Delta_{f,298}H^o[CH_3CH=C=O]$ = –95 kJ mol^{-1} [23]) or 843 kJ mol^{-1} (using $\Delta_{f,298}H^o[CH_3CH=C=O]$ = –67 kJ mol^{-1} [24]). It can be seen that the calculated PA value based on $\Delta_{f,298}H^o[CH_3CH=C=O]$ = –67 kJ mol^{-1} closely matches the experimental values of 840 ± 4 [17], 845 ± 3 [18] and 842 ± 3 [19] kJ mol^{-1}, see Table 4. We therefore conclude that $\Delta_{f,298}H^o[CH_3CH=C=O]$ = –67 kJ mol^{-1} is, in fact, the correct value.

To further address the above discrepancy, we offer the following suggestions for additional experimental work.

Substitution of an H by OH in $CH_2=CH_2$ ($\Delta_{f,298}H^o$ = 52 kJ mol^{-1} [8]) to form $CH_2=CHOH$ ($\Delta_{f,298}H^o$ = –125 kJ mol^{-1} [8]) lowers the heat of formation by 177 kJ mol^{-1} [8]. Using $\Delta_{f,298}H^o[CH_2=C=O]$ = –48 kJ mol^{-1}, we estimate by this additivity scheme $\Delta_{f,298}H^o[HOCH=C=O]$ = –225 kJ mol^{-1}. The CBS-QB3 value is –156 kJ mol^{-1}, see Table 1, resulting in a discrepancy of 69 kJ mol^{-1}, much larger than the discrepancy found for methylketene (28 kJ mol^{-1}). Similarly, the difference between the estimated and CBS-QB3 $\Delta_{f,298}H^o[H_2NCH=C=O]$ is as much as 83 kJ mol^{-1}, and the discrepancy for FCH=C=O is 75 kJ mol^{-1} (heats of formation from Reference 8 and Table 1). Again, these observations indicate that for reasons yet unknown, substitution of ketene is anomalous in terms of additivity. All these discrepancies lie far outside the experimental uncertainties of AE measurements (and the interpretation thereof, i.e. with or without temperature correction [29]) and so we suggest AE measurements of the reactions in Equation (4) where R = OH, NH_2, F.

Acknowledgments

PJAR thanks the Netherlands Organization for Scientific Research (NWO) for making available the TERAS supercomputer of SARA in Amsterdam. The authors thank Professor J.L. Holmes for stimulating discussions.

References

[1] T.T. Tidwell, Ketenes, John Wiley & Sons Inc., New York, USA, 1995.
[2] L. Gong, M.A. McAllister, T.T. Tidwell, J. Am. Chem. Soc. 113 (1991) 6021.
[3] W.T. Brady, E.F. Hoff, Jr, J. Am. Chem. Soc. 90 (1968) 6256.
[4] L.S. Hegedus, R. Imwinkelried, M. Alarid-Sargent, D. Dvorak, Y. Satoh, J. Am. Chem. Soc. 112 (1990) 1109.
[5] S. Hoz, J.Wolk, Tetrahedron Lett. 31 (1990) 4085.
[6] CBS-QB3 calculations, this work.
[7] A.-M. Dömmrose, H.-F. Grützmacher, Int. J. Mass Spectrom. Ion Proc. 76 (1987) 95.
[8] (a) S. Lias, J.E. Bartmess, J.F. Liebman, J.L. Holmes, R.D. Levin, W.G. Mallard, J. Phys. Chem. Ref. Data 17, Supplement 1, 1988; (b) NIST Chemistry WebBook, http://webbook.nist. gov/chemistry/
[9] See for example, R. Leung-Toung, M.R. Peterson, T.T. Tidwell, I.M. Czizmadia, J. Mol. Structure (Theochem.) 183 (1989) 319, and references cited therein.
[10] M.C. Blanchette, J.L. Holmes, C.E.C.A. Hop, F.P. Lossing, R. Postma, P.J.A. Ruttink, J.K. Terlouw, J. Am. Chem. Soc. 108 (1986) 7589.
[11] (a) C.W. Tsang, A.G. Harrison, J. Am. Chem. Soc. 98 (1976) 1301; (b) W.D. van Dongen, W. Heerma, J. Haverkamp, C.G. de Koster, Rapid Commun. Mass Spectrom. 10 (1996) 1237.
[12] M.M. Cordero, J.J. Houser, C. Wesdemiotis, Anal. Chem. 65 (1993) 1594.
[13] (a) M. Dupuis, D. Spanger, J. Wendolowski, NRCC Software Catalogue 1, Program No. QG01, GAMESS, 1980; (b) M. Guest and J. Kendrick, GAMESS User Manual, An Introductory Guide, CCP/86/1. Daresbury Laboratories, UK, 1986.
[14] M.J. Frisch, G.W. Trucks, H.B. Schlegel, G.E. Scuseria, M.A. Robb, J.R. Cheeseman, V.G. Zakrzewski, J.A. Montgomery, R.E. Stratmann, Jr, J.C. Burant, S. Dapprich, J.M. Millam, A.D. Daniels, K.N. Kudin, M.C. Strain, O. Farkas, J. Tomasi, V. Barone, M. Cossi, R. Cammi, B. Mennucci, C. Pomelli, C. Adamo, S. Clifford, J. Ochterski, G.A. Petersson, P.Y. Ayala, Q. Morokuma, K. Cui, D.K. Malick, A.D. Rabuck, K. Raghavachari, J.B. Foresman, J. Cioslowski, J.V. Ortiz, B.B. Stefanov, G. Liu, A. Liashenko, P. Piskorz, I. Komaromi, R. Gomperts, R.L. Martin, D.J. Fox, T. Keith, M.A. Al-Laham, C.Y. Peng, A. Nanayakkara, C. Gonzalez, M. Challacombe, P.M.W. Gill, B. Johnson, W. Chen, M.W. Wong, J.L. Andres, C. Gonzalez, M. Head-Gordon, E.S. Replogle, J.A. Pople, Gaussian 98 Revision A.7. Gaussian Inc., Pittsburgh PA, USA, 1998.
[15] (a) J.A. Montgomery Jr, M.J. Frish, J.W. Ochterski, G.A. Petersson, J. Chem. Phys. 110 (1999) 2822; (b) J.A. Montgomery, Jr., J.W. Ochterski, G.A. Petersson, J. Chem. Phys. 101 (1994) 5900; (c) L.A. Curtiss, K. Raghavachari, G.W. Trucks, J.A. Pople, J. Chem. Phys. 94 (1991) 7221; (d) L.A. Curtiss, K. Raghavachari, P.C. Redfern, V. Rassolov, J.A. Pople, J. Chem. Phys. 109 (1998) 7764.
[16] G.B. Debrou, J.E. Fulford, E.G. Lewars, R.E. March, Int. J. Mass Spectrom. Ion Phys. 26 (1978) 345.
[17] G. Bouchoux, J.Y. Salpin, Rapid Commun. Mass Spectrom. 13 (1999) 932.
[18] M.A. Armitage, M.J. Higgins, E.G. Lewars, R.E. March, J. Am. Chem. Soc. 102 (1980) 5064.

[19] G. Bouchoux, J.Y. Salpin, J. Phys. Chem. 100 (1996) 16555.
[20] J.C. Traeger, R.G. McLoughlin, J.C. Nicholson, J. Am. Chem. Soc. 104 (1982) 5318.
[21] (a) J.C. Traeger, Org. Mass Spectrom. 20 (1985) 223; (b) Z.A. Harvey, J.C. Traeger, J. Mass Spectrom. 39 (2004) 802.
[22] J.B. Pedley, R.D. Naylor, Thermochemical data of organic compounds, 2nd Edn. Chapman and Hall, London, UK, 1986.
[23] C. Aubry, J.L. Holmes, J.K. Terlouw, J. Phys. Chem. A 101 (1997) 5958.
[24] J.C. Traeger, Int. J. Mass Spectrom. 194 (2000) 261.
[25] A.P. Scott, L. Radom, Int. J. Mass Spectrom. Ion Proc. 160 (1997) 73.
[26] M.T. Nguyen, H.M.T. Nguyen, Chem. Phys. Lett. 300 (1999) 346.
[27] P.J.A. Ruttink, J. Phys. Chem, 91 (1987) 703.
[28] M. Meot-Ner (Mautner), J. Am. Chem. Soc. 106 (1984) 1257.
[29] J.C. Traeger, R.G. McLoughlin, J. Am. Chem. Soc. 103 (1981) 3647.

Chapter 3

Dipole moment effect on stabilisation energy of proton-bound complexes

Abstract

Stabilisation Energies (SE) of proton-bound complexes of the type $M_1 \bullet\bullet\bullet H \bullet\bullet\bullet M_2^+$ can be estimated using the Meot-Ner relation $SE = a + b \cdot \Delta PA$. The constants a and b are acquired from a least-squares fit of the data for known proton-bound dimers. The SE is thus linearly related to the proton affinity difference (ΔPA) of the two monomers M_1 and M_2. The original fit focused on proton-bound dimers, but this relation has also been applied to estimate SEs for hydrogen-bridged radical cations. This provided an incentive to investigate, by computational chemistry, if Proton-Bound Dimers and Hydrogen-Bridged Radical Cations can be described by common parameters.

From a survey of the reported SEs it appears that there are several problematic dimers that do not comply with the general trend. It has been suggested that significant deviations may be caused by a large dipole moment and/or polarizability of the neutral component of the complex.

In this Chapter we have studied the effect of the dipole moment on the SE using an extended Meot-Ner relation, $SE = a + b \cdot \Delta PA + c \cdot \mu$, in which μ represents the dipole moment of the neutral moiety of the complex. This generally leads to an improved estimate of the SE. A few problematic cases remain. For most of these the use of a 'functional' dipole moment of the neutral moiety provides a better estimate.

1. Introduction

Proton-bound complexes (PBCs), where monomer 1 (M_1) and monomer 2 (M_2) are bound together by a proton M_1•••H•••$M_2^{(\bullet)+}$, are usually more stable than the separated ion and neutral (e.g. $M_1H^{(\bullet)+} + M_2$). This allows longer lifetimes for these complexes, making them metastable, and the complexation can also have a catalyzing effect for example in isomerisation reactions, which would have far too large barriers to occur in solitary monomers [1]. This effect has been noticed to be important in areas such as atmospheric [2] and interstellar chemistry [3], and has been studied broadly using e.g. mass spectrometry [3c,4].

For asymmetric proton-bound complexes ($M_1 \neq M_2$) Larson and McMahon [5] and Meot-Ner [6a] found a linear correlation between the proton affinity difference (ΔPA) and the stabilisation energy (SE), which can be put in the form of the following equation:

$$SE = a + b \cdot \Delta PA, \qquad (1)$$

where a and b are correlation parameters, where a has the unit of kcal mol^{-1} and b is unitless. These parameters depend on the nature of the connecting atoms in the proton bridge. For example, the parameters are different for R_1-O•••H•••O-R_2^+ and R_1-O•••H•••N-R_2^+ PBDs. The parameters for O•••H•••O, N•••H•••O, and N•••H•••N PBDs, which are studied also in this Chapter, have been collected in Table 1.

Some authors [8] have used the Meot-Ner scheme to estimate SEs of hydrogen-bridged complexes successfully. This raises the question if treating the closed-shell proton-bound dimers (PBDs) and open-shell complexes, which are usually called 'hydrogen-bridged radical cations' (HBRCs), can be done using the same parameters in the Meot-Ner relation. This has not been studied before. In the literature usually these two types of complexes are studied separately. The reasoning came from the thought that in open-shell species the bridging moiety would not be a proton, but a hydrogen atom. This is not actually the case and this suggests that the same parameters could be used for both. We have created a common name to help discussing the two types of complexes in one: we call them proton-bound complexes (PBCs).

Table 1. Parameters a and b, and their correlation coefficients for O•••H•••O, N•••H•••O, and N•••H•••N PBDs.

Bond type	a	b[a]	coefficient[b]	N	ref.
O•••H•••O[c]	30.4	-0.30	0.999	20	[6,7]
N•••H•••N	23.2	-0.25	0.897	8	[6,7]
N•••H•••O	28.3	-0.23	0.979	48	[6,7]

[a] Note that in the references [6,7] these are positive values due to different choice for sign for the $b \cdot \Delta PA$ part of Eq. (1).
[b] Correlation coefficient
[c] Only complexes with water

The linear correlation scheme by Meot-Ner unfortunately does not perform very well at all times. Some proton-bound dimers in Meot-Ner's study [6a] failed to fall into the category described with the linear correlation scheme. It was noticed that these complexes were either small monomers with a low

polarizability and a small dipole moment, or complexes with monomers, which have a larger polarizability and a significant dipole moment. For example, the cyanide ligands showed more robust bonding than estimated. Also dimers containing acids, such as CH_3COOH, and three small dimers, O_2•••H•••O_2^+, OCO•••H•••CO_2^+ and H_2O•••H•••OCO^+, showed deviation from the correlation [6a].

We will concentrate in this article on the dipole moment (μ) effect, a suggested factor creating the abnormalities. Some recent publications refer to the dipole moment effect in complex formation [9,10]. In an article by Fridgen [10] it was shown that monomers with a large dipole moment could have anomalous proton positions in PBDs. The proton stays in certain cases closer to the monomer with the lower PA due to the strong stabilising ion-dipole interaction, whereas in the usual case the monomer with the higher PA would have the proton closer. This has prompted us to look into the dipole moment effect on the stability of proton bound complexes.

The simplest way to include the dipole moment effect in the Meot-Ner relation would be by adding an extra term multiplied with a new parameter to it. Only the dipole moment of the monomer further away from the proton will be significant, as the monomer closer to the proton will have (at least the greater part of) the positive charge, and thus the ion character is dominant. This means that we are not interested in the *difference* between the dipole moments of the monomers, as with the ΔPA, but just the *individual* dipole moment of the non-covalently bound species (the monomer further away from the proton). In certain cases, a further refinement to this could be to use the local dipole moment of the functional group of the monomer involved in the proton bridge.

We thus add another dimension, dipole moment (μ), to the linear correlation scheme of Meot-Ner, and give it a multiplication factor c. The extended Meot-Ner relation will now be simply

$$SE = a + b \cdot \Delta PA + c \cdot \mu \ . \qquad (2)$$

The parameter c has the dimension of kcal mol^{-1} D^{-1}. We have used this equation (2) to produce correlation schemes for several types of proton-bound complexes using the least squares fit procedure.

2. Computational methods

In this work we have studied computationally 120 complexes, including sets of 67 O•••H•••O, 12 N•••H•••N, 31 N•••H•••O and 10 C•••H•••O PBCs. Accurate energy estimates were obtained using CBS-QB3 complete basis set extrapolation methods as implemented in Gaussian 98 [10]. Some of the CBS-QB3 results were checked using the more accurate CBS-APNO method. All the computational results with information about the difference of the connecting atom distances to the proton, $\Delta_f H$, SE and the PA difference of the PBCs, and the individual dipole moments of the monomers, can be found in Table I of Appendix I.

3. Results and discussion

First we will discuss the possibility of using the same parameters to include both the proton-bound dimers and hydrogen-bridged radical cations in the Meot-Ner scheme. After this, we will introduce the dipole moment parameter in all four complex sets to improve the Meot-Ner correlation. Some problematic cases remain and these will be discussed in more detail.

Finally, we divide all four complex sets into two subsets, where the first subset has complexes where the molecule with the dipole moment has only one functional group, and where the second subset is for complexes with two functional groups for the molecule with the dipole moment. The latter is then used to see how much the use of a 'functional' dipole moment actually improves the results in comparison to the results obtained by using the total dipole moment of the neutral molecule.

3.1. Combining the PBDs and HBRCs in one group

First we shall look into the feasibility of combining the hydrogen-bridged radical cations (HBRCs) and proton-bound dimers (PBDs) into one set; the proton bound complexes (PBCs) set. We have calculated the parameters *a* and *b*, the standard deviation **σ** and the maximum deviation from the correlation for O•••H•••O, N•••H•••N, N•••H•••O, and C•••H•••O HBRC, PBD, and PBC data sets, using Equation (1). These are presented in Table 2.

Table 2. Parameters *a* and *b*, standard deviation (**s**), maximum deviation (maxdev), and the number of reference points (N), obtained using the Meot-Ner relation, Eq. (*1*). On the HBRC rows are the parameters for hydrogen-bridged radical cations, on the PBD rows are the parameters for the proton-bound dimers, and on the PBC are the combined results for the proton bound complexes.

O•••H•••O	**a**	**b**	**σ**	**maxdev**	**N**
HBRC	29.8	-0.37	2.0	5.1	47
PBD	28.5	-0.30	4.5	11.1	20
PBC	29.3	-0.34	3.0	11.8	67
N•••H•••N	**a**	**b**	**σ**	**maxdev**	**N**
HBRC	29.0	-0.40	2.7	4.7	5
PBD	27.1	-0.16	2.6	3.8	7
PBC	27.9	-0.26	3.0	4.3	12
N•••H•••O	**a**	**b**	**σ**	**maxdev**	**N**
HBRC	24.9	-0.21	3.8	7.5	14
PBD	28.0	-0.24	3.5	7.4	17
PBC	26.6	-0.23	3.9	9.2	31
C•••H•••O	**a**	**b**	**σ**	**maxdev**	**N**
HBRC	23.9	-0.30	2.6	3.8	5
PBD	30.7	-0.60	1.5	2.4	5
PBC	25.5	-0.42	2.5	4.1	10

If we look at the results of Table 2, we see that (with exception of C•••H•••O complexes) the parameters *a* and *b* of HBRCs and PBDs are relatively close to each other, indicating that these two sets could be combined. For the O•••H•••O complexes the

combining of the parameters leads to small changes: the standard deviation (σ) of the PBC fit falls between the σ of the HBRC and PBD fits. On the other hand, the maximum deviation increases to 11.8 kcal mol^{-1} from 5.1 and 11.1 kcal mol^{-1} for the HBRC and PBD fits, respectively. A closer look at the data set reveals that a proton-bound dimer with triplets as its ground state, CO--H-$O_2^{\bullet+}$, causes the largest deviation in both the PBD and PBC sets. On the contrary, the triplet ground state complex OC-H--O2$^{\bullet+}$ does not seem to be a problem in the C•••H•••O PBD and PBC sets; the maximum deviations are only 2.4 and 4.1 kcal mol^{-1}, respectively. In addition, the quintet species, O_2-H-$O_2^{\bullet\bullet\bullet+}$ does not give any problems, either. The feasibility of having the triplets in the data sets will be discussed in section 3.3.

The σ for the N•••H•••N and N•••H•••O PBC sets are only slightly worse than for the HBRC and PBD sets, and the maximum deviation in the N•••H•••N set even improves for the HBRC set. In the N•••H•••O PBC set the maximum deviation increases to 9.2 kcal mol^{-1}, with HNCO--H-NCO$^{\bullet+}$ being the problematic case. This will also be discussed in section 3.3 in more detail.

We have thus shown that the combination of the HBRC and PBD sets into a PBC set is reasonable and that the same parameters can be used for both. Further support for this comes from the fact that the obtained parameters for the PBC sets are close to those obtained by Meot-Ner [6,7] (Table 1) for O•••H•••O and N•••H•••O complexes. The N•••H•••N PBC set parameters are a bit different from the ones obtained by Meot-Ner, but this might come from the fact that the Meot-Ner set included only 8 dimers, while our set is slightly larger with 12 complexes.

The large standard deviations (σ > 2.9 kcal mol^{-1}) and large deviations from the linear correlation, especially with the triplet species and with some other problematic cases, show that there is room to improve the linear correlation. We shall first look into improving the linear correlation by including the dipole moment parameter in the Meot-Ner equation. After that we will have a look at the problematic cases.

3.2. Extending the Meot-Ner relation with the dipole moment parameter

The results obtained from including the dipole moment parameter, as depicted in Equation (2), for the four types of proton-bound complexes are collected in Table 3. Table 3 also re-lists the parameters obtained from the least squares fit for Equation (1). For the entire studied complex types the standard deviation and the maximum deviation from the least squares fits are improved by the inclusion of the dipole moment parameter. These results are encouraging, but the large maximum deviations do suggest that the accuracy of the correlation can still be poor in some cases, and a closer look into the results is needed.

3.3. Problematic cases

A number of problematic cases producing large deviations from the linear correlation fits are still left, of which we consider (a) complexes with a triplet state as the ground state, (b) symmetric complexes, (c) problematic cases with two functional groups, where we shall introduce 'functional' dipole moments to tackle most of these cases, and (d) the remaining persistent problematic cases, where we look closely in the electronic structure and orbitals

of these cases.

Table 3. The re-listed two-parameter fit results and the three-parameter fit results obtained using Eqs. (1) and (2) for O•••H•••O, N•••H•••N, N•••H•••O, and C•••H•••O proton-bound complexes.

O•••H•••O	**a**	**b**	**c**	**σ**	**maxdev**	**N**
2-param.	29.3	-0.34		3.0	11.8	67
3-param.	24.0	-0.27	2.18	2.2	6.9	"
N•••H•••N	**a**	**b**	**c**	**σ**	**maxdev**	**N**
2-param.	27.9	-0.26		3.0	4.3	12
3-param.	20.5	-0.21	2.41	2.1	3.7	"
N•••H•••O	**a**	**b**	**c**	**σ**	**maxdev**	**N**
2-param.	26.6	-0.23		3.9	9.2	31
3-param.	22.8	-0.19	1.24	3.7	8.4	"
C•••H•••O	**a**	**b**	**c**	**σ**	**maxdev**	**N**
2-param.	25.5	-0.42		2.5	4.1	10
3-param.	21.8	-0.35	3.10	1.1	2.5	"

(a) Triplets

The most problematic case involved is the CO--H-$O_2^{\bullet+}$ triplet species (entry 54 in Table I, Appendix I). It is not clear if a complex with a triplet as a ground state should be included in the sets with other PBCs, since especially the large polarizabilities of triplet state molecules can cause strong ion-molecule interactions [12]. It has been also suggested that B3LYP geometries do not perform equally well for triplet state molecules as for singlet and doublet state molecules [13]. Even though the OC-H--O2$^{\bullet+}$ complex gave no problem, we decided to omit the triplet entries from our further studies. It is then also not reasonable to include the quintet state species, O_2-H-$O_2^{::+}$, if the triplets are not present, and it has also been removed from the consideration form now on. The effect of removal of the triplets and the quintet on the O•••H•••O and C•••H•••O two and three parameter fits are shown in Table 4. Clearly, the removal has a large impact on the accuracy, and also on the reliability of the O•••H•••O set, supporting the removal, but no changes in the C•••H•••O are apparent.

(b) Symmetric Dimers

The achieved accuracy of about ±2 kcal mol^{-1} for the O•••H•••O and N•••H•••N three-parameter fits is reasonable. Nevertheless, especially the maximum deviation of 4.9 kcal mol^{-1} for the O•••H•••O set is rather large. Let us look what seems to be the most problematic species after the triplet removal. The symmetric dimers (entries 48-52 in Table I) show deviations between 2.6 and 5.0 kcal mol^{-1}, with the H_2O--H--OH_2^+ and CO--H--OC^+ dimers having the largest deviations of the series. For the N•••H•••N set the symmetric dimer HCN--H--NCH^+ gives the second-largest deviation from the series, 3.3 kcal mol^{-1}. These might be caused by the charge delocalization resulting from the use of the B3LYP functional, or otherwise inclusion of symmetric dimers with the

proton in the exact middle point is not feasible, since the ΔPA is zero (no use for the *b* parameter) and it is not clear how to implement the dipole moment parameter in this case. Should we consider the symmetric dimer having the proton in the middle, with two neutrals on both sides with a dipole moment factor, or just ignore this term as well? This is discussed below.

Table 4. The two and three-parameter fit results for O•••H•••O, and C•••H•••O proton-bound complexes after removal of the complexes with the triplets and the quintet.

O•••H•••O	**a**	**b**	**c**	**σ**	**maxdev**	**N**
2-param.	29.8	-0.36		2.5	8.8	65
3-param.	25.2	-0.29	1.77	2.0	4.9	"
C•••H•••O	**a**	**b**	**c**	**σ**	**maxdev**	**N**
2-param.	25.0	-0.39		2.5	4.1	9
3-param.	21.6	-0.34	3.01	1.1	2.5	"

CBS-APNO studies on the symmetric dimers (except for O_2--H--$O_2^{\cdot+}$) show that the CO--H--OC^+ and H_2O--H--OH_2^+ structures and energies agree with the CBS-QB3 scheme. On the other hand, the CO_2--H--O_2C^+ and CH_2O--H--OCH_2^+ structures from the QCISD(T) geometry optimisation in the APNO scheme produce dimers, where the proton is localized close to one of the monomers. In the CH_2O--H--OCH_2^+ case the resulting energy difference to the CBS-QB3 result is 1.8 kcal mol^{-1} (Δ_fH(APNO) = 111.8 kcal mol^{-1}), while in the CO_2--H--O_2C^+ case it is even larger, nearly 3 kcal mol^{-1} (Δ_fH(APNO) = 27.2 kcal mol^{-1}).

The reason for the asymmetry in the CO_2--H--O_2C^+ and CH_2O--H--OCH_2^+ dimers lies probably in the HF method used for the initial geometry optimisation, which tends to strongly localize the charge into one of the monomers. This biases the starting point strongly also for the QCISD optimisation step in CBS-APNO, and this step does not reach a symmetric dimer, either. This indicates that there is a potential barrier between the biased case and the symmetric case. If we force the symmetry by describing the O•••H distances with the same variable, we get a HF geometry with one negative frequency. For these results we used the zero-point energy from the HF frequency calculation. With these geometries we obtain Δ_fH values for CH_2O--H--OCH_2^+ and CO_2--H--O_2C^+ of 111.8 and 26.8 kcal mol^{-1}, respectively. The correspondence with the CBS-QB3 values, 110.0 and 24.3 kcal mol^{-1}, is not improved for CH_2O--H--OCH_2^+, but it improves by 0.4 kcal mol^{-1} for CO_2--H--O_2C^+. Therefore we conclude that the CBS-QB3 values are somewhat too low.

It is not clear what is the reason for the larger deviations for the symmetric O•••H•••O dimers, and for the HCN-H-NCH^+ dimer. Possibly, symmetric dimers should be treated as separate class of complexes. We decided to omit the symmetric dimers from the further least-squares fits. By omitting all of the symmetric dimers we can improve the results for the asymmetric O•••H•••O and N•••H•••N complexes. Removing the symmetric dimers from the O•••H•••O three-parameter fit, the standard deviation σ,

improves slightly from 2.0 (Table 4) to 1.7 kcal mol^{-1} (Table 5). For N•••H•••N three-parameter fit, omitting the symmetric dimers improves the σ from 2.1 (Table 3) to 1.7 kcal mol^{-1} (Table 5). Improvements for the maximum deviations are also noticed.

Table 5. Parameters *a*, *b*, and *c*, standard deviation (σ), maximum deviation (maxdev), and the number of reference points (N) for the O•••H•••O and N•••H•••N proton-bound complexes without symmetric dimers and triplets.

O•••H•••O	**a**	**b**	**c**	**σ**	**maxdev**	**N**
PBC	26.5	-0.31	1.31	1.7	4.4	61
N•••H•••N	**a**	**b**	**c**	**σ**	**maxdev**	**N**
PBC	16.5	-0.13	3.17	1.7	3.3	10

(c) Using functional dipole moments to improve problematic cases with large deviations from the rest of the series

The use of the dipole moment has increased the accuracy of the stabilisation energy estimation. Despite of this, a closer look on the large deviations in the 2 and 3 parameter fits (see Table II in Appendix I) reveals that there are still many cases, where there was only a little, or no improvement at all on the large deviations with the inclusion of the dipole moment parameter. In a few cases the deviation has actually turned worse. In almost all of these cases a dipole molecule that has two functional groups is involved. That is to say, the moiety with the dipole moment has for example keto (=O) and enol (-OH) groups, or amine ($-NH_2$) and cyanide groups (-C≡N). For example, in the case of H_2NCN--H-$O(CH_3)_2^+$ the proton binding happens via the -C≡N functional group, while clearly the total dipole moment of the molecule is affected by the $-NH_2$ functional group as well. This brings up the question if the total dipole moment value used in these cases is reasonable.

We can try to replace the total dipole moment value with the dipole moment value of the functional group, by using the dipole moment value of the smallest corresponding moiety. For example, we can replace the total μ of 3.88 D in entry 86 at Table I (HOCHO--H-$NH_2CO^{\bullet+}$ tH-t) with a 'functional' dipole moment value of the functional group. For this we choose the smallest corresponding fragment, CH_2O, to give the functional μ value, 2.24 D. This decreases the deviation of the entry from the fitted line from 7.3 to 5.0 kcal mol^{-1}, clearly improving the situation, and it also lowers the standard deviation by 0.1 kcal mol^{-1}. Thus, we could try replacing all the other dipole moment values for moieties with two functional groups with their functional μ values.

From a careful inspection of the data presented in Table II (in Appendix I), we find other possible situations, where replacing the dipole moment of the neutral monomer by its functional group equivalent might be reasonable. We have identified in Table 6 the monomers for which we can replace μ by the functional μ (fμ).

The new parameters obtained using the functional dipole moment (fμ) are shown in Table 7. Here, we have used the CH_2O dipole moment value for HNCO and OCO cases. The use of the dipole moment of the functional groups rather than the total dipole moment values brings improvement in the standard deviation in the N•••H•••O three-

Table 6. The dipole moment of the functional groups (in bold) of the monomers are changed to their corresponding smallest monomer's dipole moment values.

Monomer	dipole moment	smallest	new dipole moment
HO**CO**$^{\bullet}$	2.99 D	HCO$^{\bullet}$	1.60 D
HN**CO**	2.21 D	CH_2O / CO†	2.24 / 0.12 D
CH_3O**CN**	4.58 D	HCN	2.94 D
HO**CH**O HHt	3.88 D	CH_2O	2.24 D
HO**CH**O HHc	1.43 D	CH_2O	2.24 D
NH_2CN	4.58 D	NH_3	1.73 D
O**CO**	0.00 D	CH_2O / CO†	2.24 / 0.12 D
NH_2**CO**$^{\bullet}$	3.61 D	CHO$^{\bullet}$	1.60 D
CH_3O**CO**$^{\bullet}$	3.53 D	CHO$^{\bullet}$	1.60 D
HO**CN**	3.94 D	HCN	2.94 D

† chosen value depends on the electron distribution study (see discussion in 3.3. (d)

Table 7. The reproduction of the three-parameter fit using Eq. (2), and results obtained for the same fit using functional dipole moments as shown in Table 6 for O•••H•••O, N•••H•••N, N•••H•••O, and C•••H•••O PBC sets. No triplet species or symmetric dimers are included.

O•••H•••O	**a**	**b**	**c**	**σ**	**maxdev**	**N**
3-param.	26.5	-0.31	1.31	1.7	4.4	61
using fμ	27.1	-0.33	1.44	1.9	5.4	"
N•••H•••N	**a**	**b**	**c**	**σ**	**maxdev**	**N**
3-param.	16.5	-0.13	3.17	1.7	3.3	10
using fμ	16.2	-0.16	3.62	1.9	3.2	"
N•••H•••O	**a**	**b**	**c**	**σ**	**maxdev**	**N**
3-param.	22.8	-0.19	1.24	3.7	8.4	31
using fμ	7.60	-0.08	7.19	2.9	6.4	"
C•••H•••O	**a**	**b**	**c**	**σ**	**maxdev**	**N**
3-param.	21.6	-0.34	3.01	1.1	2.5	9
using fμ			No changes			

parameter fit, but the O•••H•••O and N•••H•••N sets are worsened. Also noticeable now are the large *c* parameter and small *a* parameter values in the N•••H•••O set when using

the fμ. This indicates now that the importance of the dipole moment values in this set increases dramatically when using functional dipole moments. The reason for this behaviour is not clear, although it might be explained by the fact that in the N•••H•••O set consists of neutral molecules with a large dipole moment.

(d) Persistent problematic cases

A few problematic dimers with large deviations still remain, and especially the varying changes of σ between N•••H•••O, and O•••H•••O and N•••H•••N after using the functional dipole moments is puzzling. It seems that for some dimers with two functional groups, with not so large deviations, the use of functional dipole moment did not improve the linear correlation. Despite of this, the encouraging results for the N•••H•••O scheme pushed us to pursue the matter a bit further. We have selected a few most problematic cases (from Table II in Appendix I) from the O•••H•••O and N•••H•••O sets, namely entries 8, 14, 31, 40 and 65 from the O•••H•••O set, and entries 80, 101 and 103 from the N•••H•••O set, to consider more carefully what could be the reason.

The problematic HOCO-H•••OCNH$^{\bullet+}$ dimers (ctt and ttt isomers) have the proton covalently bound to the HOCO$^{\bullet}$-moiety. In these cases the introduction of the dipole moment parameter does not do much to their deviation from the linear correlation. A closer look into the arrangements of the electrons in the ctt and ttt isomers reveal that HOMOs of these complexes have π-like orbitals at the HNCO moiety, with a node at the C atom (see Figure 1). In these cases the dipole moment of the HNCO might be much smaller than indicated for the free fragment, since the electron arrangement is similar to CO_2 molecule (Figure 1). Therefore, we can expect a lot smaller dipole moment value to represent the HNCO moiety and we replace the dipole moment value of 2.21 D with μ of C≡O, that is, with 0.12 D.

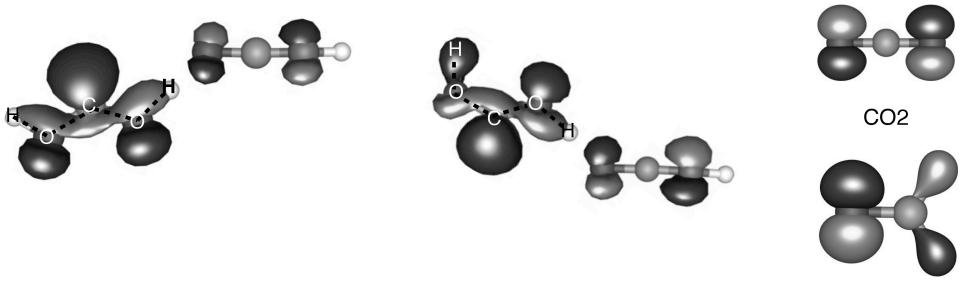

Figure 1. The HOMO orbitals of four species: HOCO-H—OCNH$^{\bullet+}$ ttt, HOCO-H--OCNH$^{\bullet+}$ ctt, CO_2, and CH_2O.

The HOMO checks on HO-H--OCO$^{\bullet+}$, CH_2OH-H-OCO$^{\bullet+}$ and H_2O-H--OCO^{+} indicate that the OCO part retains its neutral electron structure. Therefore the use of functional dipole moment of CH_2O is not justified. Instead, we will replace these with

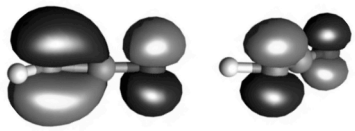

HNCO--H-NCO.+

Figure 2. The HOMO orbital of species: HNCO--H-$NCO^{\bullet+}$

the dipole moment value of CO (see Table 4). With these changes, the σ improves for the O•••H•••O PBC set from 1.9 to 1.4 kcal mol^{-1} (Table 8), thus we get an improvement compared to the original PBC extended Meot-Ner fit.

The situation could be similar for the HNCO--H-$NCO^{\bullet+}$ dimer, which also shows large deviance from the fit (3.9 kcal mol^{-1}), when using the functional dipole moment. In Figure 2 is placed the HOMO of this dimer. As we can see, the situation here is not the same. The node does not seem to lie on carbon atom, as in CO_2, and the ungerade and gerade parts of the orbitals touch the C, as in CH_2O (Figure 1). Thus, the use of CH_2O dipole moment value is justified. The problem must thus lie either in the B3LYP geometry of the dimer, or the polarization effect is strong in this molecule.

For N•••H•••O set, HOCHO-H--NH_2CN^+ ctc and HOCHO--H-NH_2CN^+ cct are also problematic in the extended Meot-Ner scheme. For the first complex, use of the functional dipole moment value of NH_3 improves the situation. Unfortunately, for the second dimer, where the proton is now covalently bound to the NH_2 group and HOCHO is the neutral part, use of the functional dipole moment does not improve the situation much. The deviation from the linear correlation improves to 5.4 kcal mol^{-1} from 6.5 kcal mol^{-1}, and shows now the largest deviation in the series. When inspecting closely the geometry, we find that the C=O of the HOCHO part is tilted to point also towards the $C^{\bullet+}$ of the $NH_2C^{\bullet+}N$ moiety, and furthermore, the H--N-C angle is only 102.1º (see Figure 3). This is smaller than in regular sp^3 orientation, indicating that there is possibly a strong dipole-quadrupole moment interaction besides the ion-dipole interaction. The functional dipole moment value used therefore is fine, and should not be changed to another one to improve the correlation.

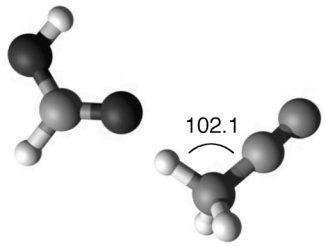

Figure 3. Geometry of HOCHO-H--NH_2CN^+

In Table 8 are shown the final values for the O•••H•••O PBC set after studying the electronic structure of the selected problematic cases. The deviations from the linear correlations for all the entries affected can be found in Table II in Appendix I. From these results we see that the use of CO dipole moment in place of CH_2O in certain cases is more appropriate. Nevertheless, this requires some more effort to study the electron distribution in the HOMO orbitals before assigning a functional μ value to certain moieties, which makes the estimations more difficult.

Table 8. The final parameters for the O•••H•••O series, obtained using the corrected functional dipole moment.

O•••H•••O	a	b	c	σ	maxdev	N
using fμ, corr	25.2	-0.30	2.49	1.4	3.4	61

3.4. The feasibility of the use of functional μ in two functional groups containing complexes

We can check the feasibility of our use of functional dipole moments also by dividing the test sets into subsets containing one and two functional group moieties for the dipole moment. There are enough points (> 4 data points) for all the subsets to do this for O•••H•••O and N•••H•••O PBC sets. The results of the one functional group and two functional groups fits are shown in Table 9.

Table 9. The one functional group (1fg), two functional groups (2fg), and two functional groups with functional μ (2fg,fμ) subset fits for O•••H•••O and N•••H•••O PBC sets.

O•••H•••O	a	b	c	σ	maxdev	N
PBC (1fg)	24.9	-0.29	2.36	1.4	3.5	35
PBC (2fg)	25.1	-0.27	1.51	1.8	3.7	26
PBC (2fg,fμ)	24.8	-0.31	3.00	1.1	3.1	26
N•••H•••O	**a**	**b**	**c**	**σ**	**maxdev**	**N**
PBC (1fg)	15.3	-0.15	4.54	1.7	3.9	20
PBC (2fg)	19.2	-0.11	1.57	5.0	7.2	11
PBC (2fg,fμ)	-6.25	0.06	12.48	3.7	7.6	11

From Table 9 it is apparent that the use of functional dipole moments does increase the accuracy of our extended Meot-Ner relation for O•••H•••O case. The decrease of **σ** in O•••H•••O subsets (PBC (2fg) value 1.8 kcal mol^{-1} to PBC (2fg,fμ) value 1.1 kcal mol^{-1} is rather pleasing, and we are reaching a rather good accuracy for our estimations with the maximum deviation only at 3.1 kcal mol^{-1}. We also note the fact that the one functional group (PBC (1fg)) and two functional groups (PBC (2fg,fμ) parameters are very close to each other, indicating that both these subsets can be handled with the common parameters.

The use of fμ improves the accuracy also for the N•••H•••O two functional groups subset, from 5.0 to 3.7 kcal mol^{-1}. Unfortunately, the maximum deviation does not go down and we still have large deviations for some of the species. Also, the parameters between the PBC (1fg) and PBC (2fg,fμ) are very different. This indicates that the use of the fμ has not been successful, or other effects besides the dipole moment should be accounted for to explain this discrepancy. Rather, the similarity between PBC (1fg) and PBC (2fg) parameters suggest that the N•••H•••O set should be treated without functional dipole moments.

4. Conclusions

It was found in our study that the hydrogen-bridged radical cations and proton-bound dimers can be handled with single parameters. The yielded parameters for O•••H•••O (after removing the triplet state species) and N•••H•••O proton-bound complex sets, viz. a = 29.6 kcal mol^{-1} and b = -0.35 for the former, and a = 26.6 kcal mol^{-1} and b = -0.23 for the latter, correspond closely to those obtained by Meot-Ner [6,7]; a = 30.4 and b = -0.30 for the O•••H•••O PBD set, and a = 28.3 and b = -0.23 for the N•••H•••O PBD set. More deviance was noticed for the N•••H•••N PBC set, with a = 27.9 kcal mol^{-1} and b = -0.26, in comparison to a = 23.2 kcal mol^{-1} and b = -0.25 from the earlier study [6a]. We also obtained novel parameters a and b for C•••H•••O two-parameter Meot-Ner scheme (not including the triplet state complex): a = 25.0 kcal mol^{-1} and b = -0.39, respectively.

The use of dipole moment as a factor in the Meot-Ner relation improved the accuracy of stabilisation energy estimation. Most of the estimations could be further improved by using 'functional' dipole moments, after considering the local electronic structure of the neutral moiety in the proton-bound complex. We recommend using parameters obtained using functional dipole moments for O•••H•••O proton-bound complexes (parameters at Table 8). For N•••H•••N and N•••H•••O PBCs the use of parameters obtained without using the functional dipole moments are suggested (parameters at Table 7). The recommended three-parameter fit values for C•••H•••O can be found in Table 7. The dimers with triplet and quintet states as their ground states were not included in the fits, since their applicability with singlet-state complexes can not be guaranteed, and the reliability of the B3LYP geometries [13] is not necessarily good. Also, the symmetric dimers were omitted, due to the uncertainty whether they should be treated as their own group. It is of course clear that the ΔPA term does not affect symmetric dimers at all, but the μ term effect is rather unclear. In any case, the source for the problematic behaviour of symmetric dimers are not likely to come from the B3LYP geometries used in CBS-QB3, since CBS-APNO results were in reasonable agreement.

The check on the parameters between one and two functional groups for the O•••H•••O and N•••H•••O sets reveal that these two groups can be processed together. For the O•••H•••O set the use of the functional dipole moment yields very promising results for the 2fg,fμ subset. Unfortunately, for the N•••H•••O this is not the case. This might be due to the fact that most of the entries in the N•••H•••O set have species with large dipole moments, and the effect of the dipole moments gets overestimated when using functional dipole moments. Alternatively, the reason could lie in polarizability of these molecules. For the most problematic cases, the inclusion of a new parameter, taking into account the polarization effect, might be a solution.

References

[1] (a) D.K. Bohme, Int. J. Mass Spec. Ion Processes 115 (1992) 95; (b) J.W. Gauld, L. Radom, J. Am. Chem. Soc. 119 (1997) 9831.

[2] N.I. Butkovskaya, A. Kukui, N. Pouvesle, G. Le Bras, Phys. Chem. A, 109(29) (2005) 6509; (b) H.J. Tobias, P.J. Ziemann, J. Phys. Chem. A, 105 (2001) 6129.

[3] (a) S. Petrie, D.K. Bohme, Mass Spec. Rev. 26 (2007) 258; (b) R. Glaser, B. Hodgen, D. Farrelly, E. Mckee, Astrobiology 7(3) (2007) 455; (c) H.K. Ervasti, K.J. Jobst, P.C. Burgers, P.J.A. Ruttink, J.K. Terlouw, Int. J. Mass Spec. 262 (2007) 88.
[4] (a) J.L. Holmes, C. Aubry, P.M. Mayer, Assigning Structures to Ions in Mass Spectrometry, CRC Press, Boca Raton, 2007; (b) D.K. Bohme, Int. J. Mass Spec. Ion Proc. 115 (1992) 95.
[5] J.W. Larson, T.B. McMahon, J. Am. Chem. Soc. 104 (1982) 6255.
[6] (a) M. Meot-Ner, J. Am. Chem. Soc. 106 (1984) 1257; (b) M. Meot-Ner, L. W. Sieck, J. Phys. Chem. 89 (1985) 5222.
[7] M. Meot-Ner, Chem. Rev. 105 (2005) 213.
[8] (a) M.A. Trikoupis, P.J.A. Ruttink, P.C. Burgers, J.K. Terlouw, Eur. J. Mass Spectrom. 10 (2004) 801; (b) P.C. Burgers, J.K. Terlouw, in: N.M.M. Nibbering (Ed.), Encyclopedia of Mass Spectrometry, vol. 4, Elsevier, Amsterdam, 2005, 173; (c) R. Lee, P.J.A. Ruttink, P.C. Burgers, J.K. Terlouw, Int. J. Mass Spec. 255–256 2006 244.
[9] (a) K. Sung, J. Chem. Soc., Perkin Trans. 2, (2002) 1658; (b) C. Laurence, M. Berthelot, Perspect. Drug Discovery Des. 18 (2000) 39.
[10] T.D. Fridgen, J. Phys. Chem. A 110 (2006) 6122.
[11] Gaussian 98 (Revision A.7), M.J. Frisch, G.W. Trucks, H.B. Schlegel, G.E. Scuseria, M.A. Robb, J.R. Cheeseman, V.G. Zakrzewski, J.A. Montgomery, Jr., R.E. Stratmann, J.C. Burant, S. Dapprich, J.M. Millam, A.D. Daniels, K.N. Kudin, M.C. Strain, O. Farkas, J. Tomasi, V. Barone, M. Cossi, R. Cammi, B. Mennucci, C. Pomelli, C. Adamo, S. Clifford, J. Ochterski, G. A. Petersson, P. Y. Ayala, Q. Cui, K. Morokuma, D.K. Malick, A.D. Rabuck, K. Raghavachari, J.B. Foresman, J. Cioslowski, J.V. Ortiz, A.G. Baboul, B.B. Stefanov, G. Liu, A. Liashenko, P. Piskorz, I. Komaromi, R. Gomperts, R.L. Martin, D.J. Fox, T. Keith, M.A. Al-Laham, C.Y. Peng, A. Nanayakkara, C. Gonzalez, M. Challacombe, P.M.W. Gill, B. Johnson, W. Chen, M.W. Wong, J.L. Andres, C. Gonzalez, M. Head-Gordon, E.S. Replogle, J.A. Pople, Gaussian, Inc., Pittsburgh PA, 1998.
[12] (a) F.C. Grozema, P.Th. Van Duijnen, J. Phys. Chem. A, 102 (1998) 7984; (b) F.C. Grozema, R. Telesca, H.T. Jonkman, L.D.A. Siebbeles, J.G. Snijders, J. Chem. Phys., 102(21) (2001) 10014.
[13] G.P.F. Wood, L. Radom, G.A. Petersson, E.C. Barnes, M.J. Frisch, J.A. Montgomery, Jr, J. Chem. Phys. 125 (2006) 094106.

APPENDIX I:

Table I. The entries of studied O•••H•••O, N•••H•••N, N•••H•••O, and C•••H•••O radical cation and cation proton-bound complexes. Included are; the difference of connecting atom distances to the proton ($\Delta d = d_1 - d_2$), heat-of-formation of the dimer ($\Delta_f H$), stabilisation energy (SE), proton affinity difference of the two dimers ($\Delta PA = PA_1 - PA_2$), and the dipole moments of the monomers. Monomer 1 is always the first monomer from the left and monomer 2 the second. All the values are obtained from CBS-QB3 calculations.

Some details of Table I need to be cleared here to help reading it. For example, for NH_2CO--H-$OCHOH^{\bullet+}$ ttt-cH dimer, one hyphen (-) means a covalent bond, while two hyphens (--) mean proton binding via ion-(induced) dipole interaction. The letter combination ttt-cH indicates, starting from the heavy atoms on the left, the *trans* (t) or *cis* (c) conformation. The first letter indicates the orientation of the first heavy atom against the fourth, the second letter the orientation of the second heavy atom against the fifth, and so on. The 'cH'-part indicates that it shows the *cis*-conformation for the last hydrogen atom, compared to the fourth heavy atom from the left. In the case of HOCHO--H-$OHCH_3^+$ tH-ct we start from the first hydrogen atom on the left, which is now *trans* to the third heavy atom from the left. The first heavy atom starts now with c, compared to the fourth from the left.

#	CBS-QB3 calculations on	**Δd**	**$\Delta_f H$**	**SE**	**ΔPA**	**μ_1**	**μ_2**
	O•••H•••O radical cations	**$d_1 - d_2$**	**dimer**		**$PA_1 - PA_2$**		
1	H_2O--H-$OCHO^{\bullet+}$ c	0.08	82.0	*30.1*	0.1	2.07	2.38
2	NH_2CO--H-$OCHOH^{\bullet+}$ ttt-cH	0.25	62.2	31.3	0.1	3.61	1.43
3	HNCO-H--$OCOH^{\bullet+}$ tct	-0.06	108.5	26.5	0.2	2.21	2.99
4	H_2O--H-$OCHO^{\bullet+}$ t	0.15	82.6	29.5	0.6	2.07	2.38
5	H_2O-H--$OCCH_3^{\bullet+}$ t	-0.15	109.5	31.6	0.8	2.07	2.42
6	NH_2CO--H-$OCH_2^{\bullet+}$ ct	0.28	134.3	30.2	0.9	3.61	2.24
7	CH_2OH-H--$OH_2^{\bullet+}$	-0.10	106.8	31.4	1.2	1.55	2.07
8	HOCO-H--$OCNH^{\bullet+}$ ctt	-0.21	110.4	24.6	2.1	1.97	2.21
9	CH_2O-H--$OCH_3^{\bullet+}$	-0.03	143.7	29.5	2.3	2.24	2.05
10	CH_3OH-H--$OCNH_2^{\bullet+}$	-0.28	102.1	32.0	2.4	1.70	3.61
11	CH_3OCO--H-$OCH_2^{\bullet+}$	0.18	97.3	29.3	2.5	3.53	2.24
12	H_3CO-H--$OH_2^{\bullet+}$	-0.15	114.8	29.9	3.2	2.05	2.07
13	H_2O-H--$OCOH^{\bullet+}$ tt	-0.21	68.9	29.5	3.6	2.07	2.99
14	HOCO-H--$OCNH^{\bullet+}$ ttt	-0.22	106.8	24.4	3.6	2.99	2.21
15	CH_2O-H--$OHCH_2^{\bullet+}$	-0.15	136.7	28.3	4.3	2.24	1.55
16	NH_2CO--H-$OCHOH^{\bullet+}$ ctt-cH	0.41	66.2	27.3	4.5	3.61	1.43
17	H_2O-H--$OCCH_3^{\bullet+}$ c	-0.23	113.5	27.6	4.9	2.07	2.42
18	H_2O-H--$OCOH^{\bullet+}$ tc	-0.23	72.4	28.0	5.1	2.07	1.97
19	CH_2CHO-H--$OHCH_3^{\bullet+}$	-0.20	105.5	29.5	5.7	2.83	1.70
20	CH_2O-H--$OCHO^{\bullet+}$ tt	-0.15	111.6	26.0	6.1	2.24	2.38

Table I, continued

#	CBS-QB3 calculations on **O•••H•••O radical cations**	**Δd** $d_1 - d_2$	**Δ_fH** **dimer**	**SE**	**ΔPA** $PA_1 - PA_2$	**μ_1**	**μ_2**
21	CH_2O-H--$OCCH_3^{\bullet+}$ tr	-0.28	138.4	28.3	6.3	2.24	2.42
22	NH_2CO--H-$OH_2^{\bullet+}$ c	0.03	105.4	28.2	6.4	3.61	2.07
23	H_2O-H--$OCOH^{\bullet+}$ ct	-0.29	*71.0*	*27.4*	7.4	2.07	2.99
24	NH_2CO--H-$OCH_2^{\bullet+}$ tc	0.07	129.4	28.6	7.4	3.61	2.24
25	CH_2O-H--$OCOH^{\bullet+}$	-0.33	97.5	26.4	9.1	2.24	2.99
26	CH_2O-H--$OCCH_3^{\bullet+}$ cis	-0.37	141.5	25.2	10.4	2.24	2.42
27	CH2O-H--$OCOH^{\bullet+}$ ttc	-0.32	101.1	24.8	10.6	2.24	1.97
28	$CH_3(CH_2)$O-H--$OH_2^{\bullet+}$	-0.31	104.6	26.8	11.7	2.14	2.07
29	CH_3OH-H--$OCH_3^{\bullet+}$	-0.29	116.8	25.0	12.1	1.70	2.05
30	NH_2CO-H--$OH_2^{\bullet+}$ t	-0.10	99.9	27.2	12.9	3.61	2.07
31	HO-H--$OCO^{\bullet+}$	-0.33	*117.1*	*20.6*	13.0	1.76	0.00
32	CH_3OH-H--$OHCH_2^{\bullet+}$	-0.31	108.3	25.3	14.1	1.70	1.55
33	CH_2CHO-H--$OCH_2^{\bullet+}$	-0.37	*131.7*	*24.8*	15.5	2.83	2.24
34	CH_3CHO-H--$OCH_3^{\bullet+}$ ct	-0.37	123.5	23.5	16.4	2.66	2.05
35	H_2O-H--$OCH^{\bullet+}$ t	-0.37	131.2	21.9	19.9	2.07	1.60
36	CH_2CHO-H--$OH_2^{\bullet+}$	-0.37	*101.4*	*24.2*	21.0	2.83	2.07
37	H_2O-H--$OH^{\bullet+}$	-0.37	131.2	21.2	22.9	2.07	1.76
38	CH_2O-H--$OCH^{\bullet+}$ t	-0.45	159.1	19.5	25.4	2.24	1.60
39	CH_3OH-H--$OCH^{\bullet+}$ t	-0.52	129.6	17.6	35.2	1.70	1.60
40	CH_2OH-H--$OCO^{\bullet+}$	-0.55	*87.0*	*13.6*	37.1	1.55	0.00
41	HO-H--$OC^{\bullet+}$	-0.54	195.0	11.7	37.6	1.76	0.12
42	CH_3CHO-H--$OCH^{\bullet+}$ tt	-0.54	135.1	16.6	39.5	2.66	1.60
43	HCO-H--$OC^{\bullet+}$ t	-0.54	194.6	9.8	40.6	1.60	0.12
44	CH_3CHO-H--$OCH^{\bullet+}$ ttc	-0.61	136.7	15.0	43.1	2.66	1.60
45	H_2NCHO-H--$OCH^{\bullet+}$ tt	-0.64	116.8	13.8	54.7	3.85	1.60
46	CH_3O-H--$OC^{\bullet+}$	-0.70	168.5	7.6	63.7	2.08	0.12
47	CH_2OH-H--$OC^{\bullet+}$	-0.69	*161.6*	8.0	61.7	1.55	0.12

#	CBS-QB3 calculations on **O•••H•••O cations**	**Δd** $d_1 - d_2$	**Δ_fH** **dimer**	**SE**	**ΔPA** $PA_1 - PA_2$	**μ_1**	**μ_2**
48	H_2O--H--OH_2^+	0.00	51.5	33.8	0.0	2.07	2.07
[a]	*H_2O--H--OH_2^+ (APNO)*	"	*50.9*		"	-	-
49	CO--H--OC^+	0.00	187.6	21.0	0.0	0.12	0.12
[a]	*CO--H--OC^+ (APNO)*	"	*187.5*		"	-	-
50	OCO--H--OCO^+	0.00	24.3	21.5	0.0	0.00	0.00
[b]	*OCO--H--OCO^+ (APNO)*	"	*26.8*		"	-	-
[a]	*OCO--H--OCO^+ (APNO)*	*0.25*	*27.2*		"	-	-

Table I, continued (2)

#	CBS-QB3 calculations on **O•••H•••O cations**	**Δd** $d_1 - d_2$	**Δ_fH** dimer	**SE**	**ΔPA** $PA_1 - PA_2$	**μ_1**	**μ_2**
51	CH_2O--H--OCH_2^+	0.00	110.0	31.7	0.0	2.24	2.24
b	*CH_2O--H--OCH_2^+ (APNO)*	"	*111.8*		"	-	-
a	*CH_2O--H--OCH_2^+ (APNO)*	*0.10*	*111.8*		"	-	-
52	O_2-H-$O_2^{\cdot+}$	0.00	247.9	22.1	0.0	0.00	0.00
53	HOCHO--H-$OHCH_3^+$ tH-ct	0.23	16.2	32.1	1.6	3.88	1.71
54	CO--H-$O_2^{\cdot+}$	0.03	217.9	16.7	2.4	0.12	0.00
55	CH_3OH-H--$OCHOH^+$ ttc	-0.15	15.5	30.3	2.5	1.71	1.43
56	CH_3CHO-H--$OCHOH^+$ tt-tH	-0.24	22.9	31.5	2.7	1.71	3.88
57	CH_2O-H--OH_2^+	-0.17	80.9	29.9	5.5	2.24	2.07
58	CH_3CHO-H--$OCHOH^+$ ttc	-0.41	22.1	28.2	6.8	1.71	1.43
59	HOCHO-H--OCH_2^+ tct	-0.16	42.6	27.3	7.3	1.43	2.24
60	HOCHO-H--OCH_2^+ ctt	-0.26	43.3	26.6	11.4	2.99	2.24
61	CH_3OH-H--OH_2^+	-0.31	52.5	26.9	15.3	1.70	2.07
62	NH_2CHO-H--$OCHOH^+$ tcc-tH	-0.46	7.7	25.6	17.9	3.85	3.88
63	NH_2CHO-H--$OCHOH^+$ ttc-tH	-0.44	6.6	26.7	17.9	3.85	3.88
64	NH_2CHO-H--$OCHOH^+$ ctc-cH	-0.63	8.4	24.1	23.3	3.85	1.43
65	H_2O-H--OCO^+	-0.50	32.7	15.0	35.9	2.07	0.00
66	H_2O-H--OC^+	-0.65	107.8	8.9	60.5	2.07	0.12
67	CH_2O-H--OC^+	-0.71	134.6	7.6	66.0	2.24	0.12

#	**N•••H•••N radical cations**	**Δd** $d_1 - d_2$	**Δ_fH** dimer	**SE**	**ΔPA** $PA_1 - PA_2$	**μ_1**	**μ_2**
68	CH_3CN--H-$NH_2^{\bullet+}$	0.38	210.4	32.1	0.2	3.88	1.96
69	$OCNH_2$-H--$NCH^{\bullet+}$	-0.58	197.5	23.3	2.7	3.61	2.94
70	CH3OCN--H-$NH_2^{\bullet+}$	0.34	191.1	29.1	4.2	4.58	1.96
71	NH_3-H--$NH_2^{\bullet+}$	-0.58	175.2	21.0	17.6	1.71	1.96
72	CH_3NH_2-H--$NH_2^{\bullet+}$	-0.67	172.6	18.5	28.3	1.70	1.96

#	CBS-QB3 calculations on **N•••H•••N cations**	**Δd** $d_1 - d_2$	**Δ_fH** dimer	**SE**	**ΔPA** $PA_1 - PA_2$	**μ_1**	**μ_2**
73	H_3N--H--NH_3^+	0.00	114.0	26.6	0.0	1.71	1.71
74	HCN--H--NCH^+	0.00	227.9	30.9	0.0	2.94	2.94
75	HCN--H-NH_2CN^+	0.46	237.1	23.0	4.4	2.94	4.58
76	CH_3NH_2-H--NH_3	-0.56	113.4	22.1	10.7	1.38	1.71
77	CH_3CN-H--NCH^+	-0.41	204.5	24.6	16.4	3.88	2.94
78	H_3N-H--$NCCH_3^+$	-0.58	141.9	27.6	17.4	1.71	3.88
79	H_3N-H--NCH^+	-0.67	161.6	21.2	33.8	1.71	2.94

Table I, continued (3)

#	**N•••H•••O radical cations**	**Δd** $d_1 - d_2$	**$\Delta_f H$** **dimer**	**SE**	**ΔPA** $PA_1 - PA_2$	**μ_1**	**μ_2**
80	HNCO--H-$NCO^{\bullet+}$	0.77	191.9	17.4	0.0	2.21	0.73
81	HCN--H-$OCNH_2^{\bullet+}$ c	0.29	194.9	28.7	0.1	2.94	3.61
82	HCN--H-$OCH_3^{\bullet+}$	0.31	202.6	28.8	3.3	2.94	2.05
83	HOCHO--H-$NH_2CO^{\bullet+}$ cH-t	0.40	75.1	18.5	3.6	1.43	3.61
84	$OCNH_2$-H--$OCH_2^{\bullet+}$	-0.49	140.7	21.0	3.7	3.61	2.24
85	HCN--H-$OHCH_2^{\bullet+}$	0.27	195.0	27.9	5.3	2.94	1.55
86	HOCHO--H-$NH_2CO^{\bullet+}$ tH-t	0.46	76.3	19.1	5.9	3.88	3.61
87	NH_2CO-H--$NCH^{\bullet+}$ t	-0.31	188.9	28.2	6.4	3.61	2.94
88	HCN-H--$OCCH_3^{\bullet+}$ c	-0.21	201.7	22.9	11.4	2.94	2.42
89	H_2N-H--$OCH_2^{\bullet+}$	-0.40	173.9	23.1	17.2	1.96	2.24
90	H_2N-H--$OH_2^{\bullet+}$	-0.37	143.2	22.8	22.7	1.96	2.07
91	H_3N-H--$OCH^{\bullet+}$ t	-0.70	148.0	12.6	60.2	1.71	1.60
92	H_3N-H--$OH^{\bullet+}$	-0.71	148.2	11.7	63.2	1.71	1.76
93	H_2N-H--$OC^{\bullet+}$	-0.80	191.8	5.6	83.2	1.96	0.12

#	**N•••H•••O cations**	**Δd** $d_1 - d_2$	**$\Delta_f H$** **dimer**	**SE**	**ΔPA** $PA_1 - PA_2$	**μ_1**	**μ_2**
94	HCN--H-OCH_2^+	0.34	169.2	30.6	1.0	2.94	2.24
95	$NCNH_2$-H--OH_2^+	-0.31	149.4	25.1	2.1	4.58	2.07
96	HOCN--H-$OHCH_3^+$	0.32	99.3	31.9	2.5	3.94	1.70
97	CH_2O--H-NH_2CN^+	0.28	179.9	22.2	3.4	2.24	4.58
98	H_2NCN--H-$O(CH_3)_2^+$	0.35	129.8	31.2	4.8	4.58	1.30
99	H_3N-H--$OCHNH_2^+$	-0.37	75.4	29.7	5.5	1.71	3.85

#	CBS-QB3 calculations on **N•••H•••O cations**	**Δd** $d_1 - d_2$	**$\Delta_f H$** **dimer**	**SE**	**ΔPA** $PA_1 - PA_2$	**μ_1**	**μ_2**
100	HCN--H-OH_2^+	0.21	139.5	29.3	6.5	2.94	2.07
101	HOCHO-H--NH_2CN^+ ctc	-0.52	112.2	18.0	10.7	1.43	4.58
102	H_2NCN-H--$OCHOH^+$ ct	-0.21	91.6	27.0	11.6	4.58	3.88
103	HOCHO--H-NH_2CN^+ cct	0.10	112.0	18.2	14.8	3.88	4.58
104	H_2NCN-H--$OCHOH^+$ tc	-0.08	90.2	24.3	15.7	4.58	1.43
105	H_2NCN-H--$OCHOH^+$ cc	-0.33	94.3	20.2	20.1	4.58	1.43
106	CH_3CN-H--OH_2^+	-0.21	114.9	24.2	22.9	3.88	2.07
107	NH_2CN-H--OH_2^+	-0.28	126.0	22.1	28.5	4.58	2.07
108	H_3N-H--OCH_2^+	-0.58	104.8	18.9	34.8	1.71	2.24
109	H_3N-H--OH_2^+	-0.53	73.1	19.7	40.3	1.71	2.07
110	CH_3NH_2-H--OH_2^+	-0.60	70.8	17.0	51.1	1.38	2.07

Table I, continued (4)

#	**C•••H•••O radical cations**	**Δd** $d_1 - d_2$	**$\Delta_f H$ dimer**	**SE**	**ΔPA** $PA_1 - PA_2$	**μ_1**	**μ_2**
111	OC--H-$OH^{\bullet+}$	0.02	185.0	21.3	0.4	0.12	1.76
112	H_2O-H--$CH_2OH^{\bullet+}$	-0.25	115.4	24.1	3.9	2.07	1.55
113	CH_3OCH_2-H--$OH_2^{\bullet+}$	-0.31	104.6	23.1	15.4	1.38	1.38
114	CH_2OH-H--$CO^{\bullet+}$	-0.66	155.9	13.7	23.7	1.55	0.12
115	CH_2O-H--$CHO^{\bullet+}$	-0.48	162.3	16.8	25.4	2.24	1.60

#	**C•••H•••O cations**	**Δd** $d_1 - d_2$	**$\Delta_f H$ dimer**	**SE**	**ΔPA** $PA_1 - PA_2$	**μ_1**	**μ_2**
116	HNC-H--OH_2^+	-0.29	148.1	20.7	20.7	3.05	2.07
117	H_2O-H--CO^+	-0.61	101.7	15.0	22.5	2.07	0.12
118	CH_2O-H--CO^+	-0.68	129.1	13.1	28.0	2.24	0.12
119	OC-H--OC^+	-0.57	162.2	8.4	38.0	0.12	0.12
120	OC-H--$O_2^{\cdot+}$	-0.58	191.0	6.5	40.4	0.12	0.00

[a] CBS-APNO results for selected (a)symmetric O•••H•••O complexes.

[b] Symmetry is forced, and the $\Delta_f H_{dimer}$ include ZPE from the asymmetric UHF calculation.

Table II. ΔPA and μ values used in the fits after removal of triplets and symmetric dimers, and announcing if the functional μ values were used. The deviations from the calculated stabilisation energies (SE), shown in Table I, from using original Meot-Ner fit (ΔSE_M), with the extended Meot-Ner fit using μ values (ΔSE_μ), using functional dipole moment values as depicted in Table 4 (($\Delta SE_{\mu,f}(1)$), where applicable, and with using functional μ values after HOMO check ($\Delta SE_{\mu,f}(2)$).

#	CBS-QB3 **O•••H•••O complexes**	**ΔPA**	**μ**	**μ(f) used?**	**ΔSE_M**	**ΔSE_μ**	**$\Delta SE_{\mu,f}(1)$**	**$\Delta SE_{\mu,f}(2)$ corrected**
1	H_2O--H-$OCHO^{\bullet+}$ c	0.1	2.07		0.0	-0.9	-0.1	0.2
2	NH_2CO--H-$OCHOH^{\bullet+}$ ttt-cH	0.1	3.61	yes	-1.2	0.0	-2.0	-2.2
3	HNCO-H--$OCOH^{\bullet+}$ tct	0.2	2.99	yes	3.6	3.9	2.8	2.6
4	H_2O--H-$OCHO^{\bullet+}$ t	0.6	2.07		0.4	-0.4	0.3	0.6
5	H_2O-H--$OCCH3^{\bullet+}$ t	0.8	2.42		-1.7	-2.1	-1.3	-0.7
6	NH_2CO--H-$OCH_2^{\bullet+}$ ct	0.9	3.61	yes	-0.4	0.8	-1.1	-1.3
7	CH_2OH-H--$OH_2^{\bullet+}$	1.2	2.07		-1.7	-2.5	-1.8	-1.4
8	HOCO-H--$OCNH^{\bullet+}$ ctt	2.1	2.21	yes	4.8	4.2	5.0	0.2
9	CH_2O-H--$OCH_3^{\bullet+}$	2.3	2.05		-0.2	-1.0	-0.3	0.1
10	CH_3OH-H--$OCNH_2^{\bullet+}$	2.4	3.61	yes	-2.7	-1.5	-2.5	-2.0
11	CH_3OCO--H-$OCH_2^{\bullet+}$	2.5	3.53	yes	-0.1	1.1	-0.8	-0.9
12	H_3CO-H--$OH_2^{\bullet+}$	3.2	2.07		-0.9	-1.6	-0.9	-0.6
13	H_2O-H--$OCOH^{\bullet+}$ tt	3.6	2.99	yes	-0.7	-0.1	-1.3	-1.4
14	HOCO-H--$OCNH^{\bullet+}$ ttt	3.6	2.21	yes	4.4	3.9	4.7	0.0
15	CH_2O-H--$OHCH_2^{\bullet+}$	4.3	1.55		0.3	-1.1	-0.4	-0.6
16	NH_2CO--H-$OCHOH^{\bullet+}$ ctt-cH	4.5	3.61	yes	1.2	2.6	0.6	0.5
17	H_2O-H--$OCCH_3^{\bullet+}$ c	4.9	2.42		0.8	0.6	1.3	2.1
18	H_2O-H--$OCOH^{\bullet+}$ tc	5.1	1.97	yes	0.3	-0.4	-0.3	-0.4
19	CH_2CHO-H--$OHCH_3^{\bullet+}$	5.7	1.70		-1.4	-2.5	-1.9	-1.8
20	CH_2O-H--$OCHO^{\bullet+}$ tt	6.1	2.38	yes	1.9	1.8	1.4	1.3
21	CH_2O-H--$OCCH_3^{\bullet+}$ tr	6.3	2.42		-0.4	-0.5	0.2	1.0
22	NH_2CO--H-$OH_2^{\bullet+}$ c	6.4	3.61	yes	-0.4	1.1	-0.9	-1.0
23	H_2O-H--$OCOH^{\bullet+}$ ct	7.4	2.99	yes	0.0	0.8	-0.5	-0.5
24	NH_2CO--H-$OCH_2^{\bullet+}$ tc	7.4	3.61	yes	-1.2	0.4	-1.7	-1.7
25	CH_2O-H--$OCOH^{\bullet+}$	9.1	2.99	yes	0.4	1.3	0.0	0.0
26	CH_2O-H--$OCCH_3^{\bullet+}$ cis	10.4	2.42		1.2	1.3	1.9	2.8
27	CH_2O-H--$OCOH^{\bullet+}$ ttc	10.6	1.97	yes	1.5	1.1	1.1	1.1
28	$CH_3(CH_2)O$-H--$OH_2^{\bullet+}$	11.7	2.07		-0.9	-1.2	-0.6	0.0
29	CH_3OH-H--$OCH_3^{\bullet+}$	12.1	2.05		0.7	0.5	1.0	1.6
30	NH_2CO-H--$OH_2^{\bullet+}$ t	12.9	2.07		-1.8	-1.9	-1.4	-0.8
31	HO-H--$OCO^{\bullet+}$	13.0	0.00	yes	4.8	1.9	5.4	0.9
32	CH_3OH-H--$OHCH_2^{\bullet+}$	14.1	1.55		-0.3	-1.1	-0.6	-0.5
33	CH_2CHO-H--$OCH_2^{\bullet+}$	15.5	2.24		-0.3	-0.1	0.4	1.3

Table II, continued

#	CBS-QB3	ΔPA	μ	μ(f)	ΔSE_M	ΔSE_μ	$\Delta SE_{\mu,f}(1)$	$\Delta SE_{\mu,f}(2)$
	O•••H•••O complexes			**used?**				**corrected**
34	CH_3CHO-H--$OCH_3^{\bullet+}$ ct	16.4	2.05		0.7	0.7	1.1	1.8
35	H_2O-H--$OCH^{\bullet+}$ t	19.9	1.60		1.0	0.6	0.9	1.2
36	CH_2CHO-H--$OH_2^{\bullet+}$	21.0	2.07		-1.7	-1.4	-1.1	-0.2
37	H_2O-H--$OH^{\bullet+}$	22.9	1.76		0.6	0.6	0.9	1.4
38	CH_2O-H--$OCH^{\bullet+}$ t	25.4	1.60		1.4	1.3	1.5	2.0
39	CH_3OH-H--$OCH^{\bullet+}$ t	35.2	1.60		-0.3	0.2	0.2	0.9
40	CH_2OH-H--$OCO^{\bullet+}$	37.1	0.00	yes	3.0	1.5	4.5	0.6
41	HO-H--$OC^{\bullet+}$	37.6	0.12		4.7	3.4	3.2	2.4
42	CH_3CHO-H--$OCH^{\bullet+}$ tt	39.5	1.60		-0.9	-0.2	-0.2	0.6
43	HCO-H--$OC^{\bullet+}$ t	40.6	0.12		5.5	4.3	4.1	3.4
44	CH_3CHO-H--$OCH^{\bullet+}$ ttc	43.1	1.60		-0.6	0.3	0.2	1.1
45	H_2NCHO-H--$OCH^{\bullet+}$ tt	54.7	1.60		-3.6	-2.1	-2.4	-1.2
46	CH_3O-H--$OC^{\bullet+}$	63.7	0.12		-0.7	-0.6	-1.2	-1.4
47	CH_2OH-H--$OC^{\bullet+}$	61.7	0.12		-0.4	-0.4	-1.0	-1.2
53	HOCHO--H-$OHCH_3^+$ tH-ct	1.6	3.88	yes	-2.5	-1.0	-2.4	-1.8
55	CH_3OH-H--$OCHOH^+$ ttc	2.5	1.43	yes	-1.1	-2.7	-0.9	-0.3
56	CH_3CHO-H--$OCHOH^+$ tt-tH	2.7	3.88	yes	-2.3	-0.7	-2.1	-1.6
57	CH_2O-H--OH_2^+	5.5	2.07		-1.8	-2.3	-1.7	-1.2
58	CH_3CHO-H--$OCHOH^+$ ttc	6.8	1.43	yes	-0.5	-1.9	-0.2	0.5
59	HOCHO-H--OCH_2^+ tct	7.3	2.24		0.2	-0.1	0.6	1.2
60	HOCHO-H--OCH_2^+ ctt	11.4	2.24		-0.6	-0.6	-0.1	0.7
61	CH_3OH-H--OH_2^+	15.3	2.07		-2.3	-2.4	-1.9	-1.2
62	NH_2CHO-H--$OCHOH^+$ tcc-tH	17.9	3.88	yes	-2.0	0.5	-1.2	-0.3
63	NH_2CHO-H--$OCHOH^+$ ttc-tH	17.9	3.88	yes	-3.1	-0.6	-2.3	-1.4
64	NH_2CHO-H--$OCHOH^+$ ctc-cH	23.3	1.43	yes	-2.5	-2.9	-1.5	-0.4
65	H_2O-H--OCO^+	35.9	0.00	yes	2.0	0.4	0.5	-0.4
66	H_2O-H--OC^+	60.5	0.12		-0.8	-0.9	-1.5	-1.7
67	CH_2O-H--OC^+	66.0	0.12		-1.5	-1.3	-2.0	-2.1

#	CBS-QB3	ΔPA	μ	μ(f)	ΔSE_M	ΔSE_μ	$\Delta SE_{\mu,f}(1)$	N/A
	N•••H•••N complexes			**used?**				
68	CH_3CN--H-$NH_2^{\bullet+}$	0.2	3.88		-4.7	-3.3	-1.8	
69	$OCNH_2$-H--$NCH^{\bullet+}$	2.7	2.94		3.5	2.2	3.2	
70	CH_3OCN--H-$NH_2^{\bullet+}$	4.2	4.58	yes	-2.7	1.4	-2.9	
71	NH_3-H--$NH_2^{\bullet+}$	17.6	1.96		2.3	-0.5	-0.5	
72	CH_3NH_2-H--$NH_2^{\bullet+}$	28.3	1.96		2.3	0.7	0.3	
75	HCN--H-NH_2CN^+	4.4	2.94		3.4	2.3	3.2	

Table II, continued (2)

#	CBS-QB3 **N•••H•••N complexes**	**ΔPA**	**μ**	**μ(f) used?**	**ΔSE_M**	**ΔSE_μ**	**$\Delta SE_{\mu,f}(1)$**	**N/A**
76	CH_3NH_2-H--NH_3	10.7	1.71		2.8	-1.5	-1.4	
77	CH_3CN-H--NCH^+	16.4	2.94		-1.0	-0.8	-0.3	
78	H_3N-H--$NCCH_3^+$	17.4	3.88		-4.2	-1.0	-0.1	
79	H_3N-H--NCH^+	33.8	2.94		-1.7	0.4	0.3	
#	**N•••H•••O complexes**	**ΔPA**	**μ**	**μ(f) used?**	**ΔSE_M**	**ΔSE_μ**	**$\Delta SE_{\mu,f}(1)$**	**N/A**
80	HNCO--H-$NCO^{\bullet+}$	0.0	2.21	yes	9.2	8.1	6.3	
81	HCN--H-$OCNH_2^{\bullet+}$ c	0.1	2.94		-2.1	-2.3	0.1	
82	HCN--H-$OCH_3^{\bullet+}$	3.3	2.94		-2.9	-3.0	-0.3	
83	HOCHO--H-$NH_2CO^{\bullet+}$ cH-t	3.6	1.43	yes	7.3	5.4	4.9	
84	$OCNH_2$-H--$OCH_2^{\bullet+}$	3.7	2.24		4.8	3.8	2.4	
85	HCN--H-$OHCH_2^{\bullet+}$	5.3	2.94		-2.5	-2.5	0.4	
86	HOCHO--H-$NH_2CO^{\bullet+}$ tH-t	5.9	3.88	yes	6.1	7.3	4.1	
87	NH2CO-H--$NCH^{\bullet+}$ t	6.4	2.94		-3.0	-3.0	0.1	
88	HCN-H--$OCCH_3^{\bullet+}$ c	11.4	2.42		1.1	0.7	1.2	
89	H_2N-H--$OCH_2^{\bullet+}$	17.2	2.24		-0.4	-0.8	-0.7	
90	H_2N-H--$OH_2^{\bullet+}$	22.7	2.07		-1.3	-1.8	-2.1	
91	H_3N-H--$OCH^{\bullet+}$ t	60.2	1.60		0.5	0.7	1.8	
92	H_3N-H--$OH^{\bullet+}$	63.2	1.76		0.7	1.2	3.6	
93	H_2N-H--$OC^{\bullet+}$	83.2	0.12		2.2	1.4	-3.7	
94	HCN--H-OCH_2^+	1.0	2.94		-4.3	-4.4	-2.0	
95	$NCNH_2$-H--OH_2^+	2.1	2.07		1.0	-0.2	-2.8	
96	HOCN--H-$OHCH_3^+$	2.5	3.94	yes	-5.8	-4.7	-3.3	
97	CH_2O--H-NH_2CN^+	3.4	2.24		3.6	2.7	1.2	
98	H_2NCN--H-$O(CH_3)_2^+$	4.8	4.58	yes	-5.7	-3.6	-2.8	
99	H_3N-H--$OCHNH_2^+$	5.5	3.85	yes	-4.3	-3.2	-6.4	
100	HCN--H-OH_2^+	6.5	2.94		-4.1	-4.1	-1.0	
101	HOCHO-H--NH_2CN^+ ctc	10.7	4.58	yes	6.2	8.4	1.1	
102	H_2NCN-H--$OCHOH^+$ ct	11.6	3.88	yes	-3.0	-1.6	-4.2	
103	HOCHO--H-NH_2CN^+ cct	14.8	3.88	yes	5.1	6.6	4.3	
104	H_2NCN-H--$OCHOH^+$ tc	15.7	1.43	yes	-1.2	-2.8	-1.8	
105	H_2NCN-H--$OCHOH^+$ cc	20.1	1.43	yes	1.9	0.5	1.9	
106	CH_3CN-H--OH_2^+	22.9	2.07		-2.8	-3.2	-3.5	
107	NH_2CN-H--OH_2^+	28.5	2.07		-2.0	-2.2	-1.9	
108	H_3N-H--OCH_2^+	34.8	2.24		-0.1	0.0	2.1	
109	H_3N-H--OH_2^+	40.3	2.07		-2.2	-2.0	-0.4	
110	CH_3NH_2-H--OH_2^+	51.1	2.07		-1.9	-1.4	1.5	

Table II, continued (3)

#	**C•••H•••O complexes**	**ΔPA**	**μ**	**μ(f) used?**	**ΔSE_M**	**ΔSE_μ**	**N/A**	**N/A**
111	$OC\text{--}H\text{-}OH^{\bullet+}$	0.4	0.12		3.6	0.6		
112	$H_2O\text{-}H\text{--}CH_2OH^{\bullet+}$	3.9	1.55		-0.6	0.9		
113	$CH_3OCH_2\text{-}H\text{--}OH_2^{\bullet+}$	15.4	1.38		-4.0	-2.5		
114	$CH_2OH\text{-}H\text{--}CO^{\bullet+}$	23.7	0.12		2.1	0.3		
115	$CH_2O\text{-}H\text{--}CHO^{\bullet+}$	25.4	1.60		-1.6	1.1		
116	$HNC\text{-}H\text{--}OH_2^{+}$	20.7	2.07		-3.7	0.2		
117	$H_2O\text{-}H\text{--}CO^{+}$	22.5	0.12		1.2	-0.7		
118	$CH_2O\text{-}H\text{--}CO^{+}$	28.0	0.12		1.1	-0.6		
119	$OC\text{-}H\text{--}OC^{+}$	38.0	0.12		1.9	0.8		

Chapter 4

Dissociation of protonated oxalic acid $[HOOC\text{-}C(OH)_2]^+$ into $H_3O^+ + CO + CO_2$: An experimental and CBS-QB3 computational study

Abstract

The predominant dissociation process observed for metastable protonated oxalic acid ions $HOOC\text{-}C(OH)_2^+$ (generated by self-protonation) leads to $H_3O^+ + CO + CO_2$. We have traced the mechanism of this intriguing reaction using the CBS-QB3 model chemistry. Our calculations show that a unique ter-body complex, $O{=}C{=}O\cdots H_3O^+\cdots CO$, plays a key role in the rearrangement process. This complex can also dissociate to the proton bound dimers $[H_2O\cdots H\cdots O{=}C{=}O]^+$ and $[H_2O\cdots H\cdots CO]^+$ which are minor processes observed in the metastable ion mass spectrum. A further minor process leads to the proton bound dimer $O{=}C{=}O\cdots H^+\cdots CO$ which is formed by water extrusion from the ter-body complex. Arguments are provided that the ter-body complex is also generated in the ion source by the collision encounter between neutral and ionized oxalic acid.

Henri K. Ervasti, Richard Lee, Peter C. Burgers, Paul J.A. Ruttink, Johan K. Terlouw, *Int. J. Mass Spec.* **249-250**, 240-251 (2006)

Henri Ervasti (2008): Computational and experimental studies on stabilities, reactions and reaction rates of cations and ion-dipole complexes

1. Introduction

The unimolecular dissociation paths of neutral oxalic acid, HOOC-COOH, have been examined previously by different experimental techniques [1a–c] and by various computational methods [1b–d]. The experimental studies have shown that ultra-violet photolysis and infrared multiphoton absorption lead to the following products: H_2O, CO, CO_2 and HCOOH, although their relative abundances vary considerably.

In an early computational study Kakumoto et al. [1b] calculated, at the Hartree-Fock (HF) level of theory and by using the 3–21G and 4–31G basis sets, the barrier heights associated with the unimolecular dissociation of oxalic acid. The lowest energy path corresponded to the formation of $H_2O + CO + CO_2$ with a relatively low barrier of 24 kcal mol^{-1}, whereas the barrier for the formation of CO_2 + HCOOH was found to be significantly higher, 67 kcal mol^{-1}. The barrier to form $C(OH)_2$, dihydroxycarbene, which could act as an intermediate for formation of HCOOH and of $H_2O + CO$, was found to be 37 kcal mol^{-1} . A more recent theoretical study [1d] confirmed the earlier finding that formation of $H_2O + CO + CO_2$ is energetically the most favorable reaction, with a barrier of 42 kcal mol^{-1}. The barrier for the formation of HCOOH + CO_2 was found to be 62 kcal mol^{-1}.

Kinetic studies by Kakumoto et al. [1b] and by Higgins et al. [1d] support the finding from theory that formation $H_2O + CO_2 + CO$ is the favored unimolecular processes although Higgins et al. [1d] propose that a bimolecular process, rather than a unimolecular process, leads to HCOOH and CO, which would be kinetically more favorable than the unimolecular process.

Experimental and theoretical studies of oxalic acid ions are scarce. Ionized oxalic acid has been used to generate ionized dihydroxycarbene, $C(OH)_2^{\bullet+}$ via loss of CO_2 [2]. A computational study has appeared [1e] dealing with oxalic acid anions and dianions, but no cations were studied. Here, we investigate the unimolecular rearrangement and dissociation pathways of protonated oxalic acid. Interestingly, we observe that its major dissociation products ($H_3O^+ + CO_2 + CO$) are analogous to those ($H_2O + CO_2 + CO$) observed for the unimolecular dissociation of oxalic acid itself; note that of these products H_2O has the highest proton affinity. Using the CBS-QB3 model chemistry, a pathway was traced where the key intermediate is the ter-body complex $O{=}C{=}O\cdots H_3O^+\cdots CO$, which could also be viewed as a hydronium bound dimer. It is proposed that this ter-body complex is also generated in a collision encounter between ionized and neutral oxalic acid.

2. Experimental and theoretical methods

The experiments were performed with the VG analytical ZAB-R mass spectrometer of BEE geometry (B, magnet; E, electric sector) [3] using an electron ionization source at an accelerating voltage of 8 kV. Metastable ion (MI) mass spectra were recorded in the second field free region (2ffr). The CID mass spectra of the 2ffr metastable peaks were obtained in the 3ffr using O_2 as collision gas (Transmittance, T = 70%). All spectra were recorded using a PC-based data system developed by Mommers Technologies Inc. (Ottawa).

Table 1. Enthalpies of formation of protonated oxalic acid and isomers derived from CBS-QB3 calculations.

Ions		E_{total} (0 K)	ZPE	$\Delta_f H^o$ (0 K)	$\Delta_f H^o$ (298 K)
$(HO)_2C\text{-}COOH^+$ [S]	**1a$_1$**	−378.16186	38.2	14.8	11.2
$(HO)_2C\text{-}COOH^+$ [W]	**1a$_2$**	−378.16176	38.3	14.8	11.3
$(HO)_2C\text{-}COOH^+$ [S]	**1a$_3$**	−378.15723	38.1	17.7	14.1
$(HO)_2C\text{-}COOH^+$ [S]	**1a$_4$**	−378.15159	37.9	21.2	17.7
$(HO)_2C\text{-}COOH^+$ [U]	**1a$_5$**	−378.14544	37.8	25.1	21.6
$(HO)_2C\text{-}COOH^+$ [U]	**1a$_6$**	−378.13285	37.3	33	29.6
TS **1a$_1$–1a$_2$**	Rotation	−378.13862	36.8	29.4	25.7
TS **1a$_1$–1a$_5$**	Rotation	−378.13048	36.5	34.4	30.9
TS **1a$_3$–1a$_5$**	Rotation	−378.12937	36.5	35.1	31.6
TS **1a$_4$–1a$_1$**	Rotation	−378.14302	36.9	26.6	23
TS **1a$_5$–1a$_6$**	Rotation	−378.12703	36.4	36.6	33.2
TS **1a$_4$–1a$_6$**	Rotation	−378.11796	36.1	42.3	39
$H_2O\text{-}C(=O)COOH^+$	**1b$_1$**	−378.12420	36.1	38.4	35.3
$H_2O\text{-}C(=O)COOH^+$	**1b$_3$**	−378.12652	35.9	37	34.2
$[O=C=O\cdots HOH(H)\cdots C=O]^+$	**1c$_1$**	−378.19180	34.1	−4.0	−5.7 [−4.7][a]
$[HO\text{-}(=O)\cdots O(H)H\cdots C=O]^+$	**1c$_2$**	−378.13396	34.4	32.2	30.3
$[O=C\cdots H\cdots O(H)\text{-}(=O)OH]^+$	**1c$_3$**	−378.14849	34.7	23.1	20.7
$[O=C=O\cdots H\cdots O(H)\text{-}H)=O]^+$	**1d$_1$**	−378.16585	34.9	12.2	10.0 [11.0][a]
$[O=C=O\cdots H\cdots O(H)\text{-}H)=O]^+$	**1d$_2$**	−378.16560	34.8	12.4	10.3
$[O=C=O\cdots H\cdots O\text{-}C(H)\text{-}H]^+$	**1d$_3$**	−378.19586	36.9	−6.6	−9.2
$[O=C=O\cdots H\text{-}C(OH)_2]^+$	**1d$_4$**	−378.19737	36.9	−7.6	−10.2
$(HO)_3C\text{-}C=O^+$	**1e**	−378.17585	36	5.9	3.7
$[O=C\cdots H\cdots O\text{-}C(OH)_2]^+$	**1f**	−378.18502	36.2	0.2	−2.5
$(HO)_2C\text{-}O\text{-}C(H)=O^+$	**1g**	−378.15797	36	17.9	14.1
$[O=C=O\cdots H\cdots O(H)\text{-}C\text{-}H]^+$	**1h**	−378.10775	34.7	48.7	46.4
TS **1b$_3$–1c$_1$** (Fig. 2)		−378.11318	34.7	45.3	42.6
TS **1a$_1$–1e** (Fig. 2)		−378.08623	35.4	62.2	58.7
TS **1c$_1$–1d$_1$** (Fig. 2)		−378.16149	32.3	15	13.4
TS **1d$_2$–1d$_3$** (Fig. 2)		−378.14591	34.7	24.7	21.7 [23.8][a]
TS **1d$_1$–1d$_2$** (Fig. 2)		−378.16086	34.6	15.4	12.9
TS **1a$_2$–1b$_3$** (Fig. 2)		−378.12456	35.2	38.1	34.5
TS **1c$_3$–1g** (Fig. 5)		−378.14653	33.8	24.3	21.2
TS **1f–1g** (Fig. 5)		−378.14563	34.9	24.9	22.1
TS **1c$_2$–1c$_3$** (Fig. 5)		−378.13306	33.7	32.8	30.4
TS **1c$_1$-1c$_2$** (Fig. 5)		−378.13502	33.8	32	29.5
TS **1a$_4$–1h**		−378.09033	34.7	59.6	56.3
TS **1a$_4$–1d$_4$**		−378.08291	35	64.3	61.4

[a] Values in square brackets refer to CBS-APNO results.

Table 2. Enthalpies of formation of dissociation products of protonated oxalic acid derived from CBS-QB3 calculations[a]

Ions		E_{total} (0 K)	ZPE	Δ_fH^o (0 K)	Δ_fH^o (298 K)
$H_3O^+ + CO + CO_2$					21
H_3O^+		−76.59652	21.4	145.2	143.6
CO		−113.18197	3.1	−27.7	−26.9
CO_2		−188.37223	7.3	−95.8	−95.9
$H\text{-}C(OH)_2^+ + CO_2$					1
$[O{=}C\cdots H\cdots OH_2]^+ + CO_2$					6
$H\text{-}C(OH)_2^+$ [b]	**2a**	−189.80656	29	99.9	97.2
$H\text{-}C(=O)OH_2^+$	**2b**	−189.77544	26.5	119.5	117.5
$[O{=}C\cdots H\cdots OH_2]^+$	**2c**	−189.80110	25.7	103.4	101.7
$[C{=}O\cdots H\cdots OH_2]^+$	**2d**	−189.79193	25.7	109.1	107.8
$HO\text{-}C\text{-}OH_2^+$	**2e**	−189.71594	26.3	156.8	154.8
Fig. 5(b)	**2a-CO**	−303.00598	33	61.3	59.2
Fig. 5(b)	**2b-CO**	−302.97500	30.8	80.8	79.2
Fig. 5(b)	**2b-CO'**	−302.97453	31	81.1	79.4
Fig. 5(b)	**2c-CO**	−303.00040	30.2	64.8	63.6
TS **2a-CO − 2b-CO**		−302.96963	30.8	84.1	81.6
TS **2b-CO − 2b-CO'**		−302.96943	30.8	84.3	82.3
TS **2b-CO' − 2c-CO**		−302.96824	28.4	85	84.1
$C(OH)_3^+ + CO$					8
$[O{=}C{=}O\cdots H\cdots OH_2]^+ + CO$					6
$C(OH)_3^+$ [b]	**3a**	−264.98695	32.2	38	34.6
$HO\text{-}C(=O)OH_2^+$	**3b**	−264.94565	30.6	63.9	61
$[O{=}C{=}O\cdots H\cdots OH_2]^+$	**3c**	−264.99197	29.6	34.8	32.7
TS **3a − 3b**		−264.90297	28.4	90.7	87.3
TS **3b − 3c**		−264.92845	29.1	71	68.3
$HO\text{-}C(=O)C{=}O^+ + H_2O$					52
$[O{=}C{=}O\cdots H\cdots C{=}O]^+ + H_2O$					29
$HO\text{-}C(=O)C{=}O^+$	**4a**	−301.76187	19.4	111.5	110.5
$[O{=}C{=}O\cdots H\cdots C{=}O]^+$	**4b**	−301.80091	17.5	87.4	87.1
H_2O		−76.33746	13.2	−57.5	−58.2
$HO\text{-}C{=}O^+$		−188.57461	13.3	142.5	141.8
$H\text{-}C{=}O^+$		−113.40509	10.2	197.6	197.5
$HO\text{-}C\text{-}OH^{\bullet+}$ (W conformer)		−189.12578	20.4	161.9	160.3
HO-C-OH (S conformer)		−189.45926	20.5	−47.4	−49.1
$HOCO^{\bullet}$		−188.87250	13	−44.5	−45.2
$(HO)_2C{=}O$ [b]		−264.69558	24.5	−144.5	−146.9

[a] E_{total} in Hartrees, all other values in kcal mol^{-1} , including the ZPE scaled by 0.99.

[b] Lowest energy conformer.

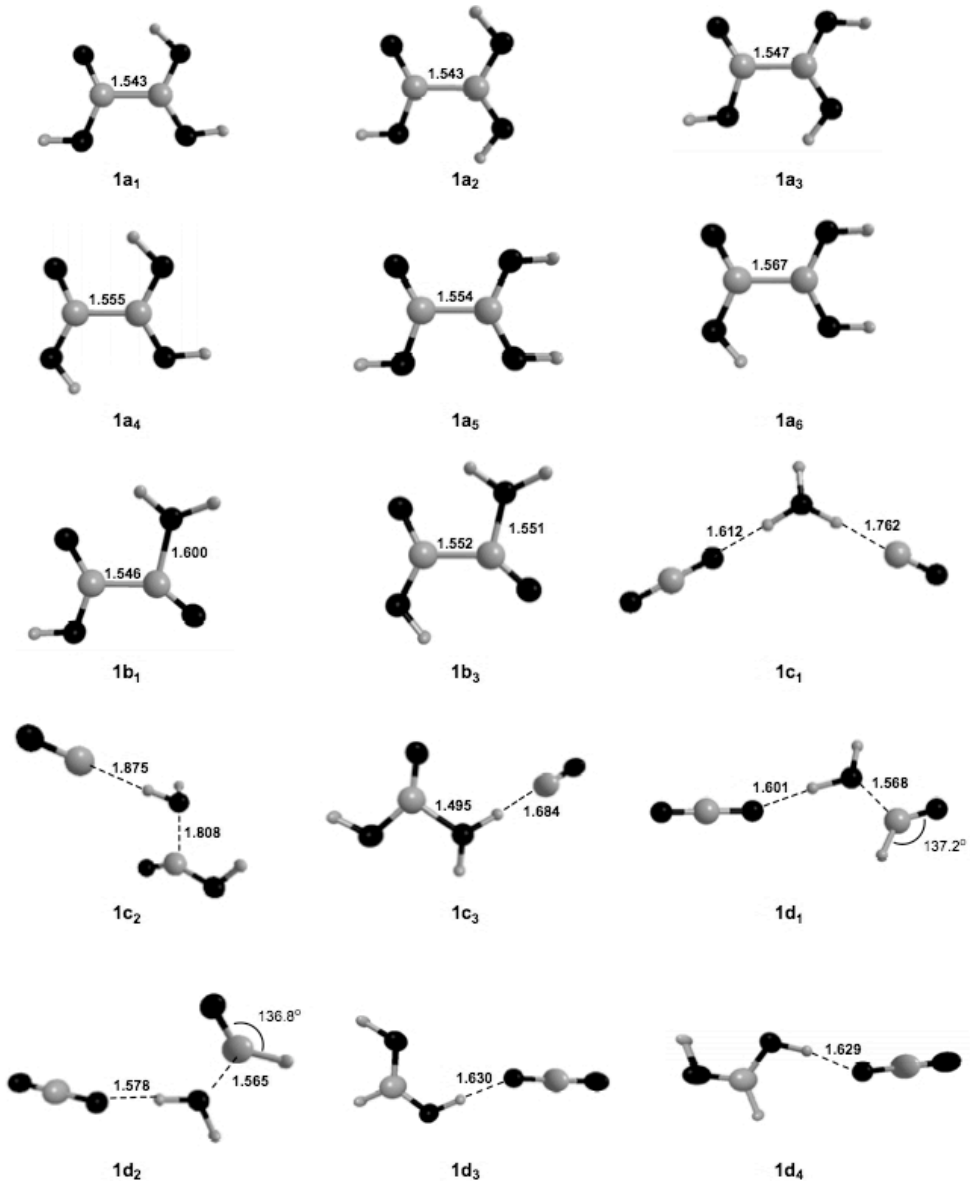

Figure 1. The CBS-QB3 optimized geometries for protonated oxalic acid isomers and selected transition states.

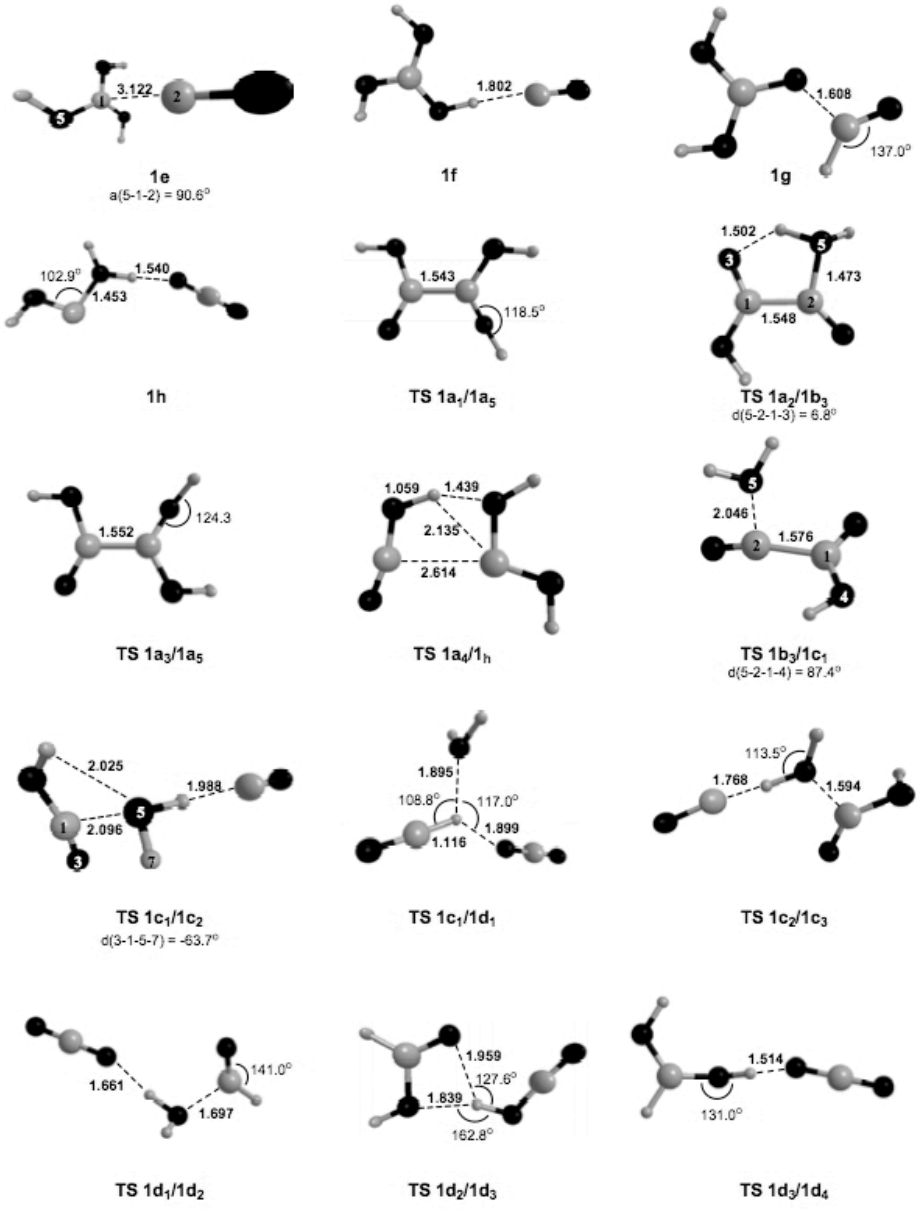

Fig. 1. *Continued*.

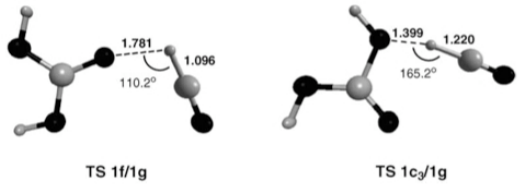

Fig. 1. *Continued(2)*.

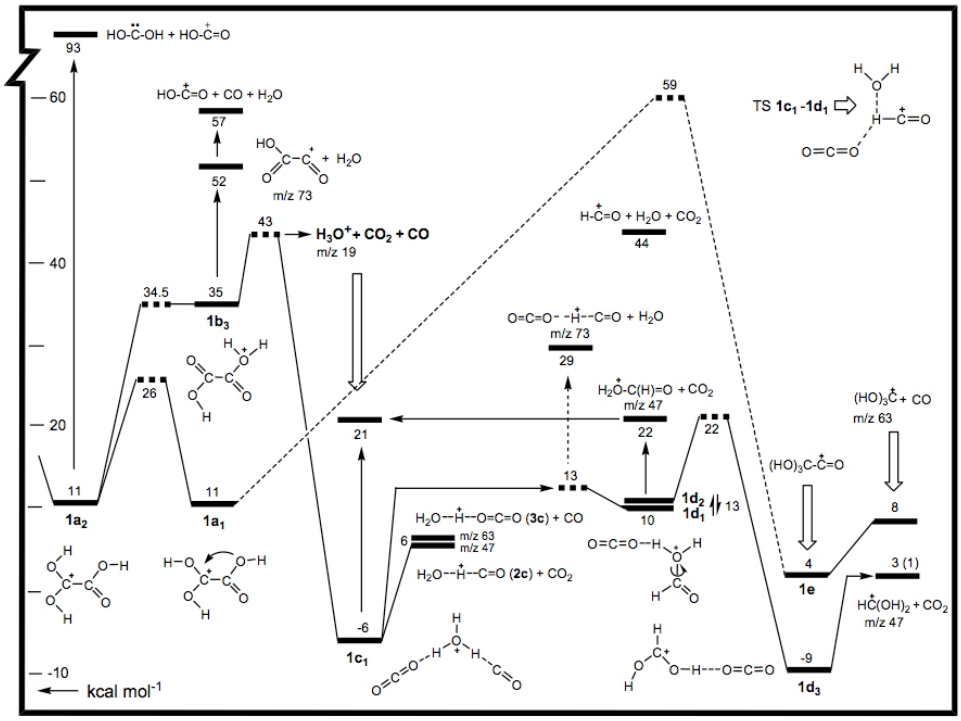

Figure 2. Potential energy diagram derived from CBS-QB3 (298K, Tables 1 and 2) calculations describing the dissociation chemistry of metastable protonated oxalic acid ions.

It is difficult to introduce oxalic acid into the ion source at controlled low pressures. When a probe tube containing anhydrous oxalic acid is introduced into the ion source, the pressure rapidly rises to $1–3\times10^{-5}$ Torr. At these pressures self-protonation is complete, i.e., there is no signal for ionized oxalic acid. We attempted to protonate oxalic acid by other means, but we could not eliminate the contribution of self-protonation (Section 3).

The computations were performed using GAMESS UK [4] and Gaussian 98 [5] program packages. Initial optimizations of the molecules were obtained at DFT/B3LYP level of theory, after which CBS-QB3 model chemistry [6] implemented in the Gaussian 98

program package was used to obtain accurate complete basis set (CBS)-extrapolated values for the energy. From these accurate energies the values of the heat of formation at room temperature for each species was calculated using Radom's temperature correction method [7]. Spin contaminations were within acceptable range. The resulting total energies and enthalpies of formation for minima and connecting transition states (TS) in the protonated oxalic acid system are presented in Tables 1 and 2. Fig. 1 displays the optimized geometries for the principal species and Fig. 2 shows our derived potential energy surface (PES) for the rearrangement/dissociation processes of protonated oxalic acid. The complete set of computational results is available from the authors upon request.

3. Results and discussion

3.1. Structure, energy and stability of protonated oxalic acid

The most favorable protonation site of gaseous organic acids, RC(=O)OH, is at the C(=O) oxygen atom to produce the carbenium ion R–$C^+(OH)_2$ [8]. In these ions the two powerful electron donating OH groups stabilize the positive charge by resonance. Depending on its nature, the substituent R may or may not lead to further stabilization.

In line with the above, our calculations show that for oxalic acid too the most favorable protonation site is at one of the carbonyl groups. Several conformers exist for the ground state, i.e., **1a$_1$–1a$_6$** in Fig. 1. The lowest conformers are found with the CBS-QB3 method to be 11.2 kcal mol^{-1} for structure **1a$_1$**, and 11.3 kcal mol^{-1} for structure **1a$_2$**. Slightly higher, at Δ_fH = 14.1 kcal mol^{-1}, is structure **1a$_3$** and clearly higher one can find structures **1a$_4$**, **1a$_5$**, and **1a$_6$**, at 17.7, 21.6, and 29.6 kcal mol^{-1}, respectively. All the stationary points of **1a$_1$–1a$_6$** can be transformed into each other over moderate barriers of ~15–21 kcal mol^{-1} (Table 1). Protonation at one of the OH groups leads to even higher energy species, **1b$_1$–1b$_3$** and so these will be inaccessible by low-energy protonation experiments. However, one of these structures, i.e., **1b$_3$**, plays a crucial role in the dissociation of **1a$_1$**.

Collision mass spectrometry based experiments lend support for structure HOOC-$C^+(OH)_2$ formed by self-protonation. The CID mass spectrum, see Fig. 3(b), shows two intense peaks at *m/z* 45 and 46. These peaks, it is proposed, arise from the simple bond cleavages, **1a$_1$** → $COOH^+$ + $C(OH)_2$ and **1a$_1$** → $COOH^\bullet$ + $C(OH)_2^{\bullet+}$. The calculated threshold energies of these processes are 93 and 115 kcal mol^{-1}, respectively, see Table 2 and so the signal at *m/z* 45 should be more abundant. From Fig. 3(b) it can be seen that the peaks at *m/z* 45 and 46 are of almost equal height, but the signal at *m/z* 45 is significantly broader making it the more abundant one. The peaks at *m/z* 29 and 19 correspond to consecutive dissociations of *m/z* 45 and 46 (part or all of *m/z* 19 may also be of metastable origin, see below). Minor peaks at *m/z* 74 and 56 can also be attributed to structure HOOC-$C^+(OH)_2$ where loss of $OH^\bullet$ may lead to ionized dihydroxycarbene, $O{=}C{=}C(OH)_2^{\bullet+}$, *m/z* 74, which then loses H_2O to produce $O{=}C{=}C{=}O^{\bullet+}$, *m/z* 56 ($O{=}C{=}C(OH)_2^{\bullet+}$ + $OH^\bullet$ lies at 126 kcal mol^{-1}, from $\Delta_fH[O{=}C{=}C(OH)_2^{\bullet+}]$ = 117 kcal mol^{-1}, CBS-QB3, this work, and $\Delta_fH[OH^\bullet]$ = 9 kcal mol^{-1} [8]) and so this process can only be observed upon collisional excitation.

The activation energy for the cleavage of lowest energy requirement is 82 kcal mol^{-1}

(see Fig. 2), which is similar in magnitude to bond dissociation energies of neutral molecules and so protonated oxalic acid would appear to be very stable. However, far below this dissociation limit, $\mathbf{1a_1}$ can undergo an intriguing rearrangement by step-wise or synchronous decarbonylation and decarboxylation.

3.2. Rearrangement and dissociation reactions of protonated oxalic acid

The MI mass spectrum of $\mathbf{1a_1}$ is shown in Fig. 3(a). The most important peak is at *m/z* 19 (H_3O^+) corresponding to the loss of CO and CO_2. Minor signals are observed at *m/z* 63 (loss of CO), *m/z* 47 (loss of CO_2) and *m/z* 73 (loss of H_2O). The signals at *m/z* 29, 45, 46 and 56 are completely of collision origin resulting from the presence of residual collision gas. In the following we discuss the metastable losses of CO, CO_2, CO + CO_2 and of H_2O.

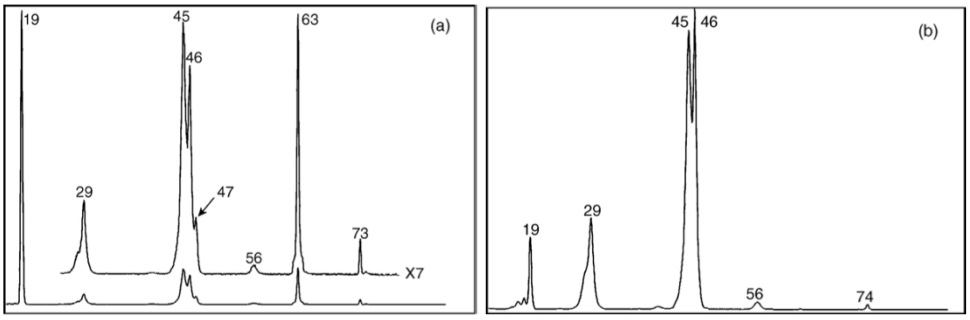

Figure 3. MI and CID mass spectra of protonated oxalic acid, item (a) and (b), respectively.

First we identify the $CH_3O_2^+$ ions at *m/z* 47 and the $CH_3O_3^+$ ions at *m/z* 63. In Fig. 4(a) and (b) are given the reference CID spectra of the *m/z* 47 $CH_3O_2^+$ ions, to wit protonated formic acid, $HC(OH)_2^+$ generated from ionized ethyl formate, and the proton bound dimer $H_2O\cdots H^+\cdots CO$ formed in a CI experiment of CO with a trace of water [**9**]. The latter CID spectrum is dominated by a narrow peak at *m/z* 19, whereas that for $HC(OH)_2^+$ gives an intense peak at *m/z* 29. The CID spectrum of the $CH_3O_2^+$ ions generated from metastable $\mathbf{1a_1}$ is shown in Fig. 4(c). Now we had already observed that in the MI mass spectrum of $\mathbf{1a_1}$ the metastable peak at *m/z* 47 is much weaker than the collision induced peak at *m/z* 46 and so the CID spectrum of *m/z* 47 will be heavily contaminated by contributions from $C(OH)_2^{\bullet+}$. This species gives signals at *m/z* 29, 28, 18, 17 and 12 in a ratio of 100:40:14:13:2 and so we can only use the narrow peak at *m/z* 19 to identify the $CH_3O_2^+$ ions. Such a signal is compatible with the structure $H_2O\cdots H^+\cdots CO$, where the proton will be more closely associated with the water molecule because the proton affinity (PA) of water is larger than that of CO [8]. However, we cannot exclude the possibility that some $HC(OH)_2^+$ ions are co-generated. We have tried to separate the *m/z* 47 peak from the intense signal at *m/z* 46 by examining the MI spectrum of the fully D labeled ions DOOC-$C(OD)_2^+$, where *m/z* 50 is separated from *m/z* 48. However, in this experiment we find that *m/z* 50 is now contaminated by DO-C-$^{18}OD^{\bullet+}$ generated by losses of CO_2 from the oxalic acid-OD_2, ^{18}O molecular ions.

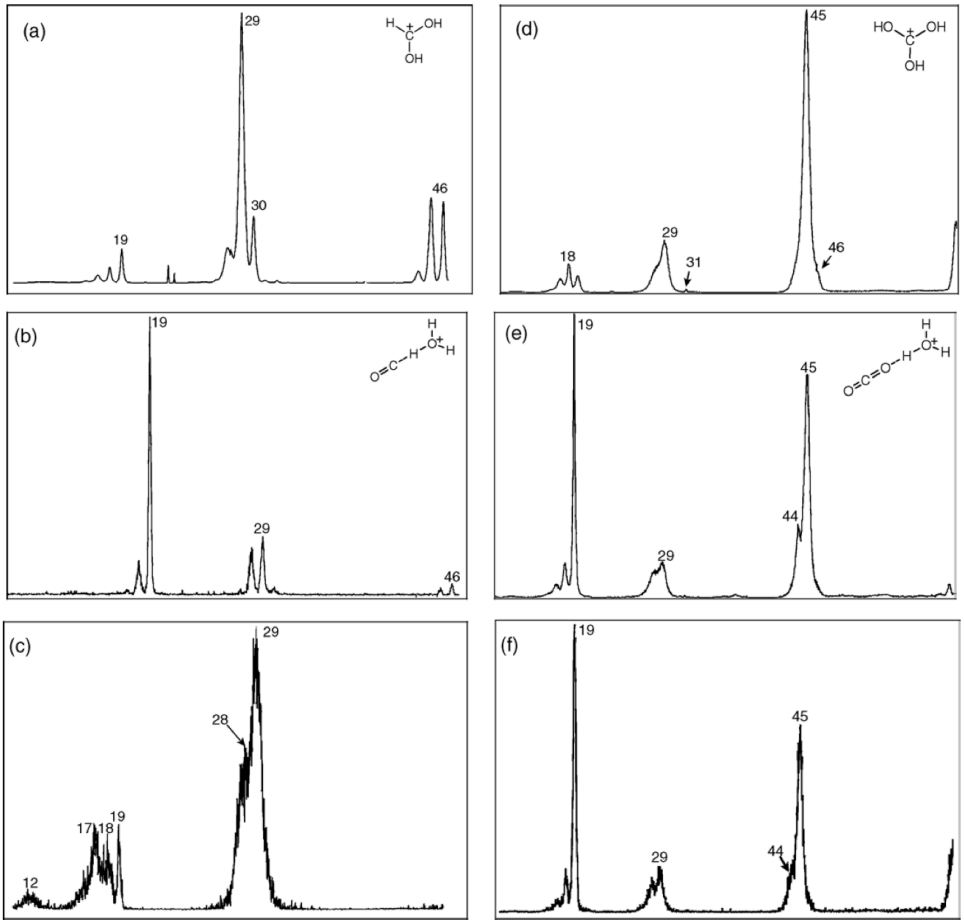

Figure 4. CID mass spectra of *m/z* 47 $CH_3O_2^+$ ions (items a–c) and *m/z* 63 $CH_3O_3^+$ ions (items d–f): (a) protonated formic acid $HC(OH)_2^+$; (b) proton-bound dimer $[H2O–H–CO]^+$; (c) *m/z* 47 $CH_3O_2^+$ ions generated from the unimolecular decomposition of protonated oxalic acid ions; (d) $C(OH)_3^+$; (e) proton bound dimer $[H_2O–H–OCO]^+$; (f) *m/z* 63 $CH_3O_2^+$ ions generated from the unimolecular decomposition of protonated oxalic acid ions.

In Fig. 4(d) and (e) are given the reference CID spectra of *m/z* 63 $CH_3O_3^+$, namely protonated carbonic acid, $C(OH)_3^+$, formed from ionized diethyl carbonate [10], and the proton bound dimer $H_2O\cdots H^+\cdots O=C=O$ generated by the dissociative ionization of dihydroxyfumaric acid [10]. The latter spectrum is characterized by a narrow peak at *m/z* 19, H_3O^+, as was also the case for $H_2O\cdots H^+\cdots CO$, see above. The CID spectrum of the $CH_3O_3^+$ ions generated from metastable $\mathbf{1a_1}$ ions is given in Fig. 4(f) and it can be seen that these ions are $H_2O\cdots H^+\cdots O=C=O$ to the exclusion of $C(OH)_3^+$.

Thus, the following dissociations have been established:

$$HOOC\text{-}C^{+}(OH)_2 \rightarrow H_2O\cdots H^{+}\cdots O{=}C{=}O + CO \quad (1)$$
$$HOOC\text{-}C^{+}(OH)_2 \rightarrow H_2O\cdots H^{+}\cdots CO + CO_2 \quad (2)$$
$$HOOC\text{-}C^{+}(OH)_2 \rightarrow H_3O^{+} + CO + CO_2 \quad (3)$$

According to our calculations the conformer **1a$_2$** (Δ_fH = 11.3 kcal mol^{-1}) can rearrange without a barrier to the hydroxyl protonated form HOOC-C(=O)OH$_2^+$, **1b$_3$**, which lies 35 kcal mol^{-1} above **1a$_2$**; alternatively, see Table 1 and Fig. 2, we can start from **1a$_1$** (Δ_fH = 11.2 kcal mol^{-1}) which can then, via a barrier at 26 kcal mol^{-1}, rearrange to **1a$_2$**. The associated transition state (TS **1a$_2$–1b$_3$**) as well as **1b$_3$** are essentially planar. Next the H_2O moiety rotates to such an extent (TS **1b$_3$–1c$_1$**) that the carboxyl hydrogen can be transferred to the H_2O ionic part. This leads to collapse to the ter-body [11] complex O=C=O···H_3O^+···C=O (**1c$_1$**) which in fact is a double hydrogen bridged species and which can also be viewed as a hydronium bound dimer. Thus, after the second hydrogen shift, the C-C bond stretches and the incipient H_3O^+ ion inserts itself into this elongated C-C bond forming H-bonds with CO and CO_2. This ter-body complex serves as the reacting configuration (RC) for reactions (1)–(3). It can be seen from Table 2 and Fig. 2 that the dissociation energies to produce H_3O^+ from $H_2O\cdots H^+\cdots O{=}C{=}O$ and $H_2O\cdots H^+\cdots C{=}O$ are the same, 15 kcal mol^{-1}. This means that CO and CO_2 have the same hydronium ion affinity. Thus, energetically it makes no difference whether we associate H_3O^+ with CO or CO_2 and as a consequence association with a second CO or CO_2 molecule, too, makes no difference. As can be seen from Fig. 2, a single complexation leads to a stabilization of 15 kcal mol^{-1} and the second one to a further stabilization of 12 kcal mol^{-1}.

We note here that the barrier for formation of $H_3O^+ + CO + CO_2$ is 32 kcal mol^{-1}, which is similar to the barrier found for formation of $H_2O + CO + CO_2$ for neutral oxalic acid, 24 [1b] or 42 kcal mol^{-1} [1d] although the respective mechanisms are very different. Hence, protonation does not appear to accelerate decomposition of oxalic acid.

The ter-body complex **1c$_1$** may also lead to the loss of H_2O to produce the proton bound dimer O=C=O···H^+···CO (*m/z* 73). According to our calculations the O-H···C hydrogen in **1c$_1$** may move towards the C atom of CO and the H_2O molecule is then "extracted" from the complex to produce the TS (**1c1–1d1**) which can be considered as the proton bound dimer O=C=O···H^+···CO with an additional water molecule associated with the proton. This TS may generate the proton bound dimer O=C=O···H^+···O(H)-CH=O, **1d$_1$**, or it may shed H_2O to produce O=C=O···H^+···C=O, *m/z* 73. This ion could fragment further to $HCO^+ + CO_2$ (+ H_2O) and this process has a threshold energy of 44 kcal mol^{-1}. Since the intensity ratio *m/z* 29:*m/z* 45 is the same in Fig. 3(a) and (b) we conclude that most of *m/z* 29 in the MI spectrum (Fig. 3(a)) is of collision induced origin. This leads to an important conclusion: the internal energy of metastable protonated oxalic acid cannot be much larger than 44 kcal mol^{-1} which imposes an upper energy limit upon our theoretical calculations. Thus, certain mechanistic alternatives, how attractive they may be, can now be ruled out. For example, the barrier for a least-motion extrusion of CO from conformer **1a$_1$** to produce $C(OH)_3^+$ from **1e** lies at 59 kcal mol^{-1} (see Fig. 2) and so this process can be ruled out.

In the same vein, direct formation of $HC(OH)_2^+$ by loss of CO_2 is also energetically prohibited: the transition state associated with the 1,3-H shift in the reaction sequence **1a$_4$**

→ **1d$_4$** → $HC(OH)_2^+$ + CO_2 lies at 61 kcal mol^{-1} (Table 2). Alternatively, a 1,4-H shift with a concomitant C-C cleavage in **1a$_4$** would yield ion **1h**, O=C=O···H-O$^+$(H)-C-OH. This ion could rearrange into **1d$_4$**, O=C=O···H-C$^+$$(OH)_2$, by proton transport catalysis, and then lose CO_2. However, the transition state for **1a$_4$** → **1h** lies at 56 kcal mol^{-1}, see Table 1, and so this process can also be ruled out.

Summarizing, our CBS-QB3 calculations can rationalize the formation of the dissociation products (H_3O^+, $H_2O{\cdots}H^+{\cdots}C{=}O$, $H_2O{\cdots}H^+{\cdots}O{=}C{=}O$ and $O{=}C{=}O{\cdots}H^+{\cdots}C{=}O$) of protonated oxalic acid in terms of the intermediary of the ter-body complex $O{=}C{=}O{\cdots}H_3O^+{\cdots}C{=}O$. However, some disconcerting questions remain, to wit:

1. We can rationalize the formation of the proton bound dimers $H_2O{\cdots}H^+{\cdots}C{=}O$ and $H_2O{\cdots}H^+{\cdots}O{=}C{=}O$; we can also rationalize that the conventional species $HC(OH)_2^+$ and $C(OH)_3^+$ are not formed directly from **1a**. However, can we also rule out the formation of $HC(OH)_2^+$ and $C(OH)_3^+$ via other pathways, for example, via further isomerization of the molecular ion or of the product ions?
2. The products $H_2O{\cdots}H^+{\cdots}C{=}O$ and $H_2O{\cdots}H^+{\cdots}O{=}C{=}O$ are formed with a large amount of excess energy (37 kcal mol^{-1}, see Fig. 2) and so the question arises as to why these proton bound dimers (or at least part of them) remain intact. Also, what is the reason that two iso-energetic products (formation of *m/z* 47 and 63) give markedly different ion yields in the MI spectrum? And lastly, formation of *m/z* 73 needs 23 kcal mol^{-1} more energy than generation of *m/z* 47, so why are the two corresponding metastable peaks of nearly equal intensity?

3.3. Transformation of $O{=}C{=}O{\cdots}H_3O^+{\cdots}C{=}O$ into $O{=}C{=}O{\cdots}H\text{-}O\text{-}CHOH^+$

With respect to the first question, we have already established that the ter-body complex **1c$_1$** can rearrange into $O{=}C{=}O{\cdots}H^+{\cdots}O(H)\text{-}CH{=}O$, **1d$_1$**, see Fig. 2. This species can rearrange via a low barrier to its conformer **1d$_2$**. In this species the CO_2 molecule can accept the proton and after passing TS (**1d$_2$–1d$_3$**) at 22 kcal mol^{-1}, the proton is donated back to the carbonyl oxygen atom of the incipient HO-CH=O molecule to produce the very stable complex $HC(OH)_2^+{\cdots}O{=}C{=}O$ (**1d$_3$**) which can then shed CO_2 to produce $HC(OH)_2^+$. This constitutes an example of proton-transport catalysis (PTC [12]), by now a well-established process. In a recent publication [13] on the isomerization/dissociation reactions of metastable $HC(OH)_2^+$ ions, **2a**, it was concluded that these ions can rearrange via a 1,3-H shift to the ion–dipole complex H-C$^+$(=O)···OH_2, **2b**, which is a transient species only and which collapses to the complex $O{=}C{\cdots}H^+{\cdots}OH_2$, **2c**. For the reverse reaction **2b** → **2a** the barrier was found to be 30 kcal mol^{-1}. When we complex **2a** with CO_2 as in **1d$_2$** the barrier is reduced to 12 kcal mol^{-1}, see Fig. 2 (TS **1d$_2$–1d$_3$**) and so CO_2 does catalyze the reaction to some extent by PTC. This barrier lies far beneath the energy for formation of **1d$_2$** from protonated oxalic acid, so that energetically PTC may well occur. However, as discussed above, we cannot conclude from our experimental data whether or not this process actually occurs to some extent. The reason that the CO_2 assisted isomerization (**2b** → **2a**) still has a sizeable barrier lies in the low PA of CO_2 (129 kcal mol^{-1}) compared to the PAs of H-C(=O)-OH at =O (179 kcal mol^{-1} [8]) and at -OH (159 kcal mol^{-1}, from Table 2). Indeed, when we complex **2b** with a species having a higher PA, e.g., CO (PA = 142 kcal mol^{-1}, i.e., more in line with Radom's PA criterion [14]) we calculate that the barrier is

reduced to a mere 2 kcal mol^{-1}.

3.4. Transformation of $O=C=O\cdots H_3O^+\cdots C=O$ in to $O=C\cdots H\text{-}O\text{-}C(OH)_2^+$

Experimentally, the situation is much clearer for the loss of CO, where the sole product is $H_2O\cdots H^+\cdots O=C=O$, **3c**, to the exclusion of $C(OH)_3^+$, $\mathbf{3a_1}$. We have traced a low energy pathway where CO catalyzes the transformation $\mathbf{3c} \rightarrow \mathbf{3a_1}$ and the results of our calculations are shown in Fig. 5. In Fig. 5(a) is shown the potential energy surface (PES) for rearrangement/dissociation processes of the solitary ions $H_2O\cdots H^+\cdots O=C=O$ and $C(OH)_3^+$. Starting from $\mathbf{3a_1}$, a 1,3-H shift requires 52 kcal mol^{-1} to produce the ion–dipole complex $HOC^+(=O)\cdots OH_2$, **3b**, which can either lose water as indicated, or it can shift the proton from $HOCO^+$ to H_2O to produce **3c** which can then dissociate. However, when we start from low energy ions **3c** isomerization into $\mathbf{3a_1}$ will not take effect because the barrier (52 kcal mol^{-1}) is much larger than the threshold for dissociation into $H_3O^+ + CO_2$. It is also clear that even ions **3c** having internal energies of 37–39 kcal mol^{-1}, i.e., those formed from protonated oxalic acid as depicted in Fig. 2 cannot isomerize into $\mathbf{3a_1}$.

How does the situation change when the proton bound dimer **3c** is complexated with CO, as in $\mathbf{1c_1}$? Here, see Fig. 5(b), we find that isomerization of $\mathbf{1c_1}$ into $\mathbf{1c_3}$, the CO complexed analog of **3b**, requires about as much energy as rearrangement for the isolated ion. However, the next steps leading to **1f**, the analogue of **3a**, require substantially less energy when the ion is associated with CO. In this rearrangement of $\mathbf{1c_3} \rightarrow \mathbf{1f}$ the CO molecule attracts the proton, and then the C atom of the incipient HCO radical forms a covalent bond with the keto oxygen atom (as indicated by the arrow) to form the carbenium ion **1g**. The next step is analogous to decarbonylation of ionized methyl formate [15]: the O-C bond stretches and the proton is inserted into this stretched bond to from the complex **1f** that could then dissociate. The reaction $\mathbf{1c_3} \rightarrow \mathbf{1f}$ could be called proton-transport catalysis, but it proceeds via a covalently bonded carbenium ion. The activation energy for the rearrangement $\mathbf{1c_1} \rightarrow \mathbf{1f}$ is 36 kcal mol^{-1}, compared to 54 kcal mol^{-1} for the solitary ions and considering that ions $\mathbf{1c_1}$ have an internal energy of 49–51 kcal mol^{-1}, formation of $C(OH)_3^+$ is energetically feasible. In Fig. 2, the barrier for the above CO assisted reaction lies at 30 kcal mol^{-1}, at the energy level for formation of *m/z* 73. Experimentally it is found that *m/z* 73 is formed whereas $C(OH)_3^+$ is not. We propose that kinetic factors rule against the formation of $C(OH)_3^+$: the internal energy available to $\mathbf{1c_1}$ is so large that the ion will preferentially undergo simple cleavage reactions rather than complicated rearrangement processes.

3.5. Formation of $O=C=O\cdots H_3O^+\cdots C=O$ from the oxalic acid dimer radical cation

The second problem concerns the observation that at least part of the **2c** and **3c** ions having large internal energies (37–39 kcal mol^{-1}) remain intact. The excess energy is 22–24 kcal mol^{-1}, which should be more than sufficient to completely dissociate these complexes within the metastable time frame. The origin of the problem may lie in the method of ion preparation. As mentioned in Section 2 protonated oxalic acid was produced by self-protonation, putatively by the following reaction:

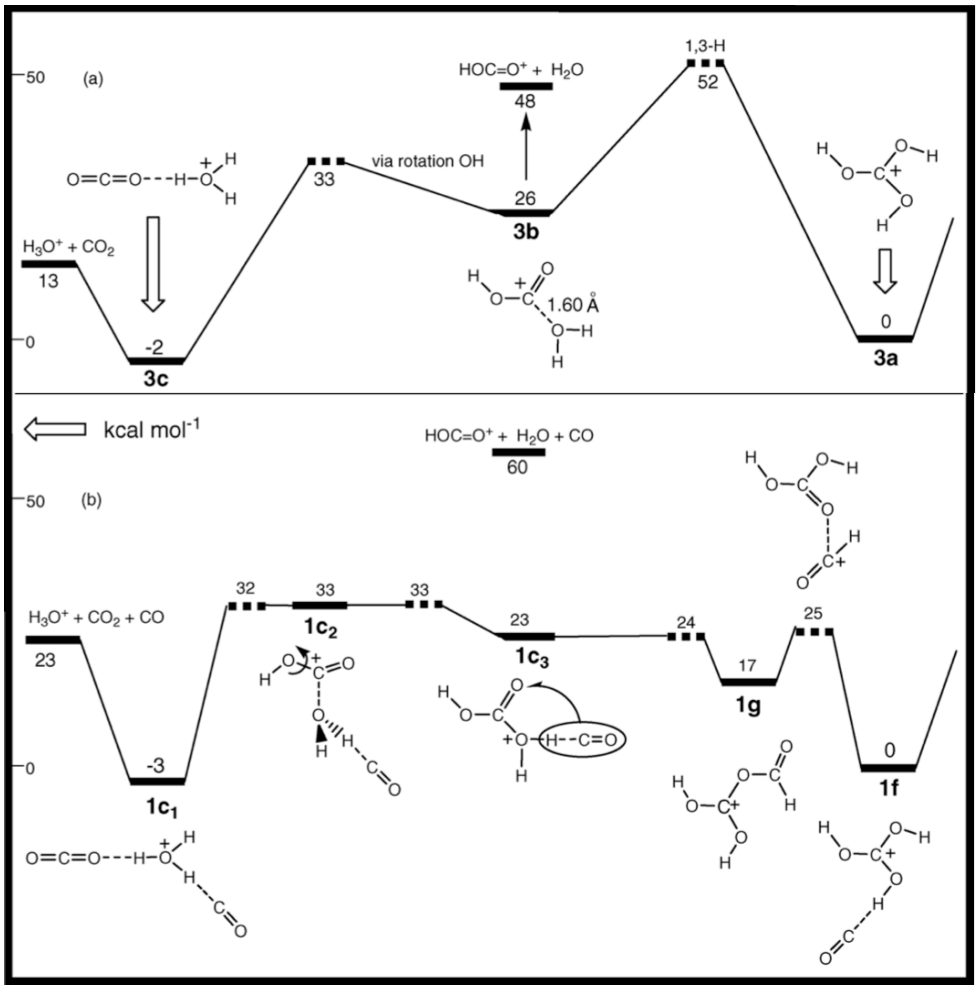

Figure 5. Potential energy diagrams derived from CBS-QB3 calculations describing the isomerization and dissociation reactions of protonated carbonic acid isomers: (a) represents the case of solitary ions; (b) shows the effect of complexation with CO.

$$HOOC\text{-}COOH + HOOC\text{-}COOH^{\bullet+} \rightarrow HOOC\text{-}C(OH)_2^{+} + {}^{\bullet}OOC\text{-}COOH \qquad (4)$$

According to our ab initio calculations the PAs of oxalic acid and of the radical ${}^{\bullet}OOC\text{-}COOH$ are similar and so the proton can easily shift from the radical cation to the neutral molecule. Next an interesting phenomenon may occur: our calculations indicate that the C-C bond in the radical ${}^{\bullet}OOC\text{-}COOH$ is very weak so that the radical may dissociate exothermically to $HOCO^{\bullet} + CO_2$. That is to say the initial hydrogen bridged radical cation

HOOC-C(=O)-O$^{\bullet}$···H^{+}···O-C(OH)-COOH, see also Fig. 6, loses COOH$^{\bullet}$ to produce protonated oxalic acid complexated with CO_2 . Next, the ter-body complex **1c$_1$** is generated by the same mechanism as shown in Fig. 2 for solitary protonated oxalic acid but now with CO_2 as a spectator molecule. That CO_2 is no more than a spectator follows from the observation that the activation energies for the isolated reaction and for reaction with CO_2 are equal (32 kcal mol^{-1}).

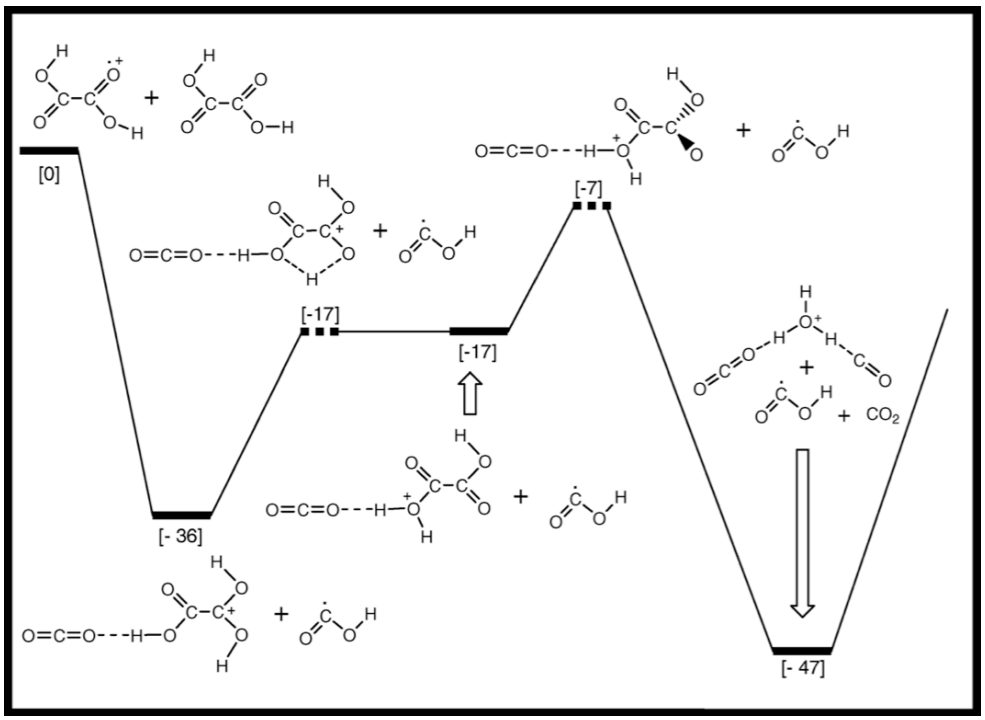

Fig. 6. Potential energy diagram derived from B3LYP/CBSB7 calculations describing the formation of the ter-body complex O=C=O···H_3O^{+}···C=O from the collision encounter between neutral and ionized oxalic acid. The relative energies are in kcal mol^{-1}.

The overall reaction depicted in Fig. 6 is exothermic by 41.5 kcal mol^{-1} and so the ter-body complex thus formed is expected to dissociate. However, this ion-molecule reaction takes place in the source under chemical ionization conditions where the ter-body complex can be collisionally stabilized. Hence, it is entirely possible that in the ion source ions **1c$_1$** are already present in admixture with solitary protonated oxalic acid ions. Such **1c$_1$** ions we argue are the precursors for formation of *m/z* 47 and 63 as observed in the MI mass spectrum, whereas protonated oxalic acid would dissociate only to H_3O^{+}. Can we prove this hypothesis? We could for example try to protonate oxalic acid by other means than by self-protonation. However, as mentioned in Section 2, it proved very hard to reduce the amount of self-protonation in favour of protonation by another agent (e.g., H_2O). Another attempt

would be to purify the *m/z* 91-ion beam by a neutralization-reionization experiment followed by MI analysis of the survivors. The idea behind this approach is that upon neutralization the ter-body complexes will undoubtedly fall apart while the radicals HOOC-$^{\bullet}$C(OH)$_2$ could well survive neutralization: our calculations indicate that their dissociation into HOOC-COOH + H$^{\bullet}$ requires 29 kcal mol^{-1}. Thus, following reionization and subsequent mass selection, the MI mass spectrum of pure **1a** ions was to be recorded. Unfortunately, the yield of the survivor signal was very low; in addition the MI spectrum of *m/z* 91 is very weak and these two effects combined precluded a successful experiment.

We have also measured the kinetic energy releases ($T_{0.5}$ values) for the processes leading to *m/z* 19 (55 meV) and *m/z* 63 (35 meV). Now formation of *m/z* 63 has a larger reverse term than generation of *m/z* 19 (37 versus 22 kcal mol^{-1}, see Fig. 2) and so the $T_{0.5}$ value for formation of *m/z* 63 should be larger than that for *m/z* 19 [16,17], the opposite of what is observed. In addition, the fraction of kinetic energy released in the formation of *m/z* 63, relative to the reverse term, is only 2%, an unprecedentedly low value. We therefore, propose that in the ion source a mixture of ions **1a$_1$** (or **1a$_2$**) and **1c$_1$** are produced. The former rearranges into energy rich **1c$_1$** which rapidly dissociates to H_3O^+ with a relatively large kinetic energy release and to *m/z* 73, O=C=O···H$^+$···C=O. Any *m/z* 47 ions (H$_2$O···H$^+$···C=O) and *m/z* 63 ions (H$_2$O···H$^+$···O=C=O) formed from **1a$_1$** via **1c$_1$** will dissociate completely to H_3O^+. By contrast, low energy **1c$_1$** ions generated in the ion source produce only *m/z* 47 and 63 by direct bond cleavage with relatively small kinetic energy releases. Thus, the formation in the ion source of **1c$_1$** in admixture with **1a$_1$** provides a rationale for the questions raised at the end of Section 3.2.

4. Summary

Protonation of oxalic acid leads to the carbenium ion HOOC-C$^+$(OH)$_2$. Mass spectrometry based experiments reveal that this species dissociates for the major part to H_3O^+ + CO + CO_2, products that do not reveal the original connectivity. The mechanism of this intriguing reaction has been elucidated using the CBS-QB3 model chemistry. Key intermediate and also the reacting configuration in this rearrangement is the ter-body complex O=C=O···H$_3$O$^+$···C=O, **1c$_1$**, which can also be viewed as a hydronium bound dimer. The observed dissociation parallels that observed for neutral oxalic acid which dissociates into H_2O + CO + CO_2. Minor processes involve the formation of H$_2$O···H$^+$···C=O, H$_2$O···H$^+$···O=C=O and O=C=O···H$^+$···C=O, the proton bound analogue of the ter-body complex.

Acknowledgements

JKT thanks the Natural Sciences and Engineering Research Council of Canada (NSERC) for continuing financial support. PJAR and HKE thank the Netherlands Organization for Scientific Research for making available the TERAS supercomputer of SARA in Amsterdam.

References

[1] (a) S. Yamamoto, R.A. Back, J. Phys. Chem. 89 (1985) 622; (b) T. Kakumoto, K. Saito, A. Imamura, J. Phys. Chem. 91 (1987) 2366; (c) J. Nieminen, M. Räsänen, J. Murto, J. Phys. Chem. 96 (1992) 5303; (d) J. Higgins, X. Zhou, R. Liu, T.T.-S. Huang, J. Phys. Chem. A 101 (1997) 2702; (e) C. Chen, S.-F. Shyu, Int. J. Quantum Chem. 76 (2000) 541.

[2] P.C. Burgers, A.A. Mommers, J.L. Holmes, J. Am. Chem. Soc. 105 (1983) 5976.

[3] H.F. van Garderen, P.J.A. Ruttink, P.C. Burgers, G.A. McGibbon, J.K. Terlouw, Int. J. Mass Spectrom. Ion Proc. 121 (1992) 159.

[4] GAMESS-UK is a package of ab initio programs written by M.F. Guest, J.H. van Lenthe, J. Kendrick, K. Schoffel, P. Sherwood, with contributions from R.D. Amos, R.J. Buenker, H.J.J. van Dam, M. Dupuis, N.C. Handy, I.H. Hillier, P.J. Knowles, V. Bonacic-Koutecky, W. von Niessen, R.J. Harrison, V.R. Saunders, A.J. Stone, D.J. Tozer, and A.H. de Vries. The package is derived from the original GAMESS code due to M. Dupuis, D. Spangler, and J. Wendolowski, NRCC Software Catalogue 1, vol. 1, Program no. QG01 (GAMESS) (1980).

[5] Gaussian 98, Revision A.9, M.J. Frisch, G.W. Trucks, H.B. Schlegel, G.E. Scuseria, M.A. Robb, J.R. Cheeseman, V.G. Zarzewski, J.A. Montgomery Jr, R.E. Stratman, J.C. Burant, S. Dapprich, J.M. Millam, A.D. Daniels, K.N. Kudin, M.C. Strain, O. Farkas, J. Tomasi, V. Barone, M. Cossi, R. Cammi, B. Mennucci, C. Pomelli, C. Adamo, S. Clifford, J. Ochterski, G.A. Petersson, P.Y. Ayala, Q. Cui, K. Morokuma, D.K. Malick, A.D. Rabuck, K. Raghavachari, J.B. Foresman, J. Ciolowski, J.V. Ortiz, A.G. Baboul, B.B. Stefanov, G. Liu, A. Liashenko, P. Piskorz, I. Komaromi, R. Gomperts, R.L. Martin, D.J. Fox, T. Keith, M.A. Al-Laham, C.Y. Peng, A. Nanayakkara, G. Gonzalez, M. Head-Gordon, E.S. Repogle, J.A. Pople, Gaussian Inc., Pittsburgh PA, 1998.

[6] (a) J.A. Montgomery Jr., M.J. Frisch, J.W. Ochterski, G.A. Petersson, J. Chem. Phys. 110 (1999) 2822; (b) J.A. Montgomery Jr., M.J. Frisch, J.W. Ochterski, G.A. Petersson, J. Chem. Phys. 112 (2000) 6532.

[7] A. Nicolaides, A. Rauk, M.N. Glukhovtsev, L. Radom, J. Phys. Chem. 100 (1996) 17460.

[8] S. Lias, J.E. Bartmess, J.F. Liebman, J.L. Holmes, R.D. Levin, W.G. Mallard, J. Phys. Chem. Ref. Data 17 (Suppl. 1) (1988).

[9] See also: C. Schalley, D. Schröder, H. Schwarz, Int. J. Mass Spectrom. Ion Proc. 153 (1996) 173.

[10] J. Hrusak, G.A. McGibbon, H. Schwarz, J.K. Terlouw, Int. J. Mass Spectrom. Ion Proc. 160 (1997) 117.

[11] (a) G.v.d. Rest, J. Chamot-Rooke, P. Mourgues, T.B. McMahon, H.E. Audier, J. Am. Soc. Mass Spectrom. 12 (2001) 938; (b) G.v.d. Rest, L.B. Jensen, A. Azeim, P. Mourgues, H.E. Audier, J. Am. Soc. Mass Spectrom. 15 (2004) 966.

[12] (a) D.K. Bohme, Int. J. Mass Spectrom. Ion Process. 115 (1992) 95; (b) C.Y. Wong, P.J.A. Ruttink, P.C. Burgers, J.K. Terlouw, Chem. Phys. Lett. 387 (2004) 204; (c) C.Y. Wong, P.J.A. Ruttink, P.C. Burgers, J.K. Terlouw, Chem. Phys. Lett. 390 (2004) 176, and references cited therein.

[13] R. Srikanth, K. Bhanuprakash, R. Srinivas, C.Y. Wong, J.K. Terlouw, J. Mass Spectrom. 39 (2004) 303.
[14] J.W. Gauld, L. Radom, J. Am. Chem. Soc. 119 (1997) 9831.
[15] N. Heinrich, T. Drewello, P.C. Burgers, J.C. Charles, J. Schmidt, W. Kulik, J.K. Terlouw, H. Schwarz, J. Am. Chem. Soc. 114 (1992) 3776.
[16] J.L. Holmes, K. Cartledge, A.D. Osborne, Int. J. Mass Spectrom. Ion Phys. 29 (1979) 171.
[17] C.J. Proctor, B. Kralj, A.G. Brenton, J.H. Beynon, Org. Mass Spectrom. 15 (1980) 619.

Chapter 5

The acrylonitrile dimer ion: A study of its dissociation via self-catalysis, self-protonation and cyclization into the pyrimidine radical cation

Abstract

Large energy barriers prohibit the rearrangement of solitary acrylonitrile ions, CH_2=CHC≡$N^{\bullet+}$, into their more stable hydrogen-shift isomers CH_2=C=C=$NH^{\bullet+}$ or CH=CH-C=$NH^{\bullet+}$. This prompted us to examine if these isomerizations occur by self-catalysis in acrylonitrile dimer ions. Such ions, generated by chemical ionization experiments of acrylonitrile with an excess of carbon dioxide, undergo five dissociations in the s time frame, as witnessed by peaks at *m/z* 53, 54, 79, 80 and 105 in their metastable ion mass spectrum. Collision experiments on these product ions, deuterium labeling, and a detailed computational analysis using the CBS-QB3 model chemistry lead to the following conclusions: (i) the *m/z* 54 ions are ions CH_2=CHC=NH^+ generated by self-protonation in ion–dipole stabilized hydrogen-bridged dimer ions [CH_2=CHC≡N···H-C(C≡N)CH_2]$^{\bullet+}$ and [CH_2=CHC≡N···H-C(H)C(H)C≡N]$^{\bullet+}$; the proton shifts in these ions are associated with a small reverse barrier; (ii) dissociation of the H-bridged ions into CH_2=C=C=$NH^{\bullet+}$ or CH=CH–C=$NH^{\bullet+}$ by self-catalysis is energetically feasible but kinetically improbable: experiment shows that the *m/z* 53 ions are CH_2=CHC≡$N^{\bullet+}$ ions, generated by back dissociation; (iii) the peaks at *m/z* 79, 80 and 105 correspond with the losses of HCN, C_2H_2 and $H^{\bullet}$, respectively. The calculations indicate that these ions are generated from dimer ions that have adopted the (much more stable) covalently bound "head-to-tail" structure [CH_2=CHC=N–C(H_2)C(H)C≡N]$^{\bullet+}$; experiments indicate that the *m/z* 79 (C_5H_5N) and *m/z* 105 ($C_6H_6N_2$) ions have linear structures but the *m/z* 80 ($C_4H_4N_2$) ions consist of ionized pyrimidine in admixture with its stable pyrimidine-2-ylidene isomer. Acrylonitrile is a confirmed species in interstellar space and our study provides experimental and computational evidence that its dimer radical cation yields the ionized prebiotic pyrimidine molecule.

Henri K. Ervasti, Karl J. Jobst, Peter C. Burgers, Paul J.A. Ruttink, Johan K. Terlouw
Int. J. Mass Spec. **262**(1-2), 88–100 (2007)

Henri Ervasti (2008): Computational and experimental studies on stabilities, reactions and reaction rates of cations and ion-dipole complexes

1. Introduction

In the context of our experimental and theoretical studies on self-catalysis in dimer radical cations [1] by proton-transport catalysis (PTC) and related mechanisms [2], we observed that dimer ions of acrylonitrile are readily generated in chemical ionization experiments of the monomer in the presence of a large excess of CO_2. The low-energy (metastable) dimer ions primarily dissociate into *m/z* 54 ions by self-protonation but *m/z* 53 monomer ions are also generated, either by back dissociation or self-catalysis. Surprisingly, the dimer ions undergo three more competing dissociations. Of these the loss of C_2H_2 aroused our interest because a collision experiment indicated that the resulting *m/z* 80 ions may well be pyrimidine ions [3]. Acrylonitrile is a confirmed species in astrochemistry [4] - it was first detected in the Sgr B2 cloud [5a] and since then also in the cold cloud TMC-1 [5b] and the atmosphere of Saturn's moon Titan [5c,d] - and a further study of a potential route to the formation of the prebiotic pyrimidine molecule via the above ion-molecule reaction seemed worthwhile.

Ion–molecule interactions have been shown to play a role in the production of larger molecular species in astrochemistry [6] and mass spectrometry has long been an indispensable tool in their study [7]. Ion–molecule reactions are advantageous over neutral–neutral reactions without activation energy because their rate coefficients may be higher by as much as a factor of 10^4 if the molecule is polar [4]. This is the case with acrylonitrile that has a large dipole moment.

We further note that the search for prebiotic molecular species in the interstellar medium is a subject of considerable interest. The driving force behind this quest lies in the role these molecules may have played in the formation of life on Earth [8]. So far, as many as 130 molecular species have been identified, largely in the dense regions of dust clouds. Nevertheless, only a handful of biologically important molecules have yet been confirmed [4,9]. An early search for pyrimidine was unsuccessful [10a] but recently this integral DNA component was tentatively identified in the Sgr B2, Orion KL and W51 interstellar clouds [10b,c]. A route to its formation has not been established but it has been suggested that it could be formed by the aggregation of HCN and acrylonitrile either in the gas-phase or on the surface of dust grains [10a].

In this study, we report the results of a detailed experimental and computational analysis of the rich and complex chemistry of the acrylonitrile dimer radical cation. It will be shown that interaction of an acrylonitrile ion with its neutral counterpart leads to hydrogen-bridged radical cations. These may undergo self-protonation or isomerize into the very stable distonic ion $[CH_2{=}CH{-}C{=}N{-}CH_2{-}CH{-}C{\equiv}N]^{\bullet+}$ which can be viewed as a head-to-tail dimer and which acts as precursor for the observed losses of $H^{\bullet}$, HCN and C_2H_2. The latter process proceeds via cyclization and produces ionized pyrimidine in admixture with its 2-ylide isomer. Self-catalysis, although energetically quite possible, is not observed: this process requires considerable reorientation making it kinetically unfavourable.

2. Experimental and computational details

2.1. Experimental procedures

The experiments were performed with the VG Analytical ZAB-R mass spectrometer of BEE geometry (B, magnet; E, electric sector) [11] equipped with a standard chemical ionization source operating at 120 ºC. The repeller voltage was held close to 0 V and the primary ionization was accomplished with 100 eV electrons. Gaseous acrylonitrile and CO_2 in a ca. 1:10 molar ratio were admitted to the ion source via separate inlet systems at a total indicated pressure (monitored by a remote ionization gauge) of (7–10) × 10^{-5} Torr.

Metastable ion (MI) mass spectra were recorded in the second field free region (2ffr); collision-induced dissociation (CID) mass spectra were recorded in the 2 and 3ffr using oxygen as collision gas (transmittance, T = 70%). The CID mass spectra of the 2ffr metastable peaks were obtained in the 3ffr using O_2 as collision gas. For these experiments the maximum available accelerating voltage, 10 kV, was used. CID spectra of reference ions having a translational energy close to that of the product ions resulting from (MI or CID) dissociations in the 2ffr, were also obtained in the 3ffr. All spectra were recorded using a PC-based data system developed by Mommers Technologies Inc. (Ottawa).

Acrylonitrile, 2-chloroacrylonitrile and carbon dioxide were of research grade (Aldrich) and used without further purification. The deuterium labeled nitriles CD2=CDC≡N (99.4 at.% D) and CH_2=CDC≡N (99.4 at.% D) were purchased from CDN Isotopes Canada.

2.2. Computational aspects

The calculations were performed with the CBS-QB3 model chemistry [12] using Gaussian 98 [13a] and 03, Rev C.02 [13b] and (for selected transition state searches) GAMESS-UK [14]. In this model chemistry the geometries of minima and connecting transition states are obtained from B3LYP density functional theory in combination with the 6-311G(2d,d,p) basis set (also denoted as the CBSB7 basis set). The resulting total energies and enthalpies of formation for minima and connecting transition states (TS) in the acrylonitrile dimer system of ions are presented in Table 1. Computational and experimental enthalpies for the monomer ion and various dissociation products from the dimer ions are presented in Table 2. Fig. 3 displays the optimized geometries for the principal species. The correct identity of transition states was verified (where not trivially evident) by means of intrinsic reaction coordinate (IRC) calculations. The complete set of computational results is available from the authors upon request.

A previous detailed CBS-QB3 study of a system of ions of comparable size and complexity [15] argues that a conservative estimate of the error in energies derived from the method is ±2 kcal mol^{-1} for local minima and ±4 kcal mol^{-1} for transition states. However, most of the open shell species in the present study have spin-contaminations that exceed the "acceptable" range (0.75–0.79) in the CCSD(T), MP2 and MP4 components of the method. For example, the acrylonitrile ion **AN**, the pyrimidine ion **PY**1, the vinylpyrimidine ion **VP**1 and the dimer ion **D**1 of Scheme 7 have $<S^2>$ values of 0.99, 1.29, 1.47 and 0.97, respectively. It is difficult to assess the effect of strong spin-

Table 1. Energetic data[a] derived from CBS-QB3 calculations pertinent to the ion chemistry of acrylonitrile and 2-chloroacrylonitrile described in Schemes 1 and 8.

	CBS-QB3		QB3		Expt.
Ionic/neutral species	E(total) [0 K]	ZPE	$\Delta_fH^o_0$	$\Delta_fH^o_{298}$	$\Delta_fH^o_{298}$
CH_2=CHC≡N ANN	−170.53848	31.5	48	46	44[b]
CH_2=CHC≡$N^{\bullet+}$ ^{2}A´´ **AN**	−170.13793	30.4	299	298	296[b]
^{2}A´ **AN**	−170.08412	29.6	333	332	–
CH_2=C=C=$NH^{\bullet+}$ ^{2}A´ **AN**1	−170.16624	28.4	282	281	–
CH=CH–C=$NH^{\bullet+}$ ^{2}A´ **AN**2	−170.15296	29.5	290	289	–
CH_2=C–CH=$N^{\bullet+}$ ^{2}A´ **AN**3	−170.08760	27.9	331	330	–
HC≡C–C≡NH^+	−169.58533	23.5	277	277	–
TS **AN** → **AN**1 (Scheme 1)	−169.99871	25.6	387	385	–
TS **AN** → **AN**3 (Scheme 1)	−170.06537	26.2	345	344	–
TS **AN**3 → **AN**1 (Scheme 1)	−170.06355	25.8	346	345	–
CH_2=CH–C=NH^+ ^{1}A´ **ANP**	−170.83610	38.2	226	224	223[c]
$CH_3CHC{\equiv}N^+$ ^{1}A´	−170.76564	36.7	271	269	–
H_2C=C–C≡$N^{\bullet}$ **AN**R1	−169.87318	22.2	100	100	–
HC=CH–C≡$N^{\bullet}$ **AN**R2	−169.86085	22.7	108	107	–
TS ANR1 → **AN**R2	−169.78975	18.7	153	152	–
H_2C=CClC≡N	−629.69426	25.8	42.6	42.5	–
H_2C=CClC≡$N^{\bullet+}$ (Scheme 8)	−629.30609	25.1	286	286	287[d]
H_2C=CClC=NH^+	−629.98240	32.5	227	226	–
HC=CCl–C≡$N^{\bullet}$	−629.01464	17.3	104	105	–
D1(Cl) (Scheme 8)	−801.07231	59.4	(290)	(288)	–[e]
D4(Cl)	−801.06640	58.8	(293)	(291)	–[e]
TS **D**1(CI) → **D**4(CI) (Scheme 8)	−801.00057	55.9	(332)	(330)	–[e]
$C_5H_5N^{\bullet+}$ (m/z 79) (Scheme 7)	−247.41820	49.6	297	295	–[f]
PY1 (m/z 80) (Scheme 7)	−263.53204	46.8	264	260	260[b]
PY2 (m/z 80) (Scheme 7)	−263.52851	48.1	266	263	–[f]
TS **PY**1 → **PY**2	−263.42505	42.9	331	328	–
$C_6H_5N_2^+$ (m/z 105) (Scheme 7)	−340.19954	58.7	281	278	–[f]
TS **D**4 → $C_6H_5N_2^+$ + $H^{\bullet}$ (Scheme 7)	−340.69641	59.3	335	331	–

[a] E (total) (in Hartrees, all other components, including the ZPE scaled by 0.99, are in kcal mol^{-1}.

[b] From Ref. [17e].

[c] From PA = 187.5 kcal mol−1 [17b].

[d] From IE = 10.58 eV [17c] and using the calculated enthalpy of the neutral.

[e] E(total) refers to B3LYP/CBSB7 energies; the enthalpies were calculated using the CBS-QB3 values of **AN**Cl + **AN**N as the anchor.

[f] The dissociation levels for the loss of $H^{\bullet}$, HCN and C_2H_2 in Scheme 7 were obtained from the calculated ionic enthalpies of this table and CBS-QB3 298 K values for $H^{\bullet}$, C_2H_2 and HCN of 52.1, 55.2 and 31.7 kcal mol^{-1}, respectively.

contamination on the errors in the CBS-QB3 derived energies but the incorporation of a spin-correction factor and the use of DFT derived geometries are expected to mitigate adverse effects [16]. In this context we note, see Table 1, that the available experimental Δ_fH_{298} values for AN and PY1, 296 and 260 kcal mol^{-1}, are gratifyingly close to the calculated values, 298 and 260 kcal mol^{-1}, respectively. In the same vein, the Δ_fH_0 value of 100 kcal mol^{-1} for the severely spin-contaminated radical CH_2=C$^{\bullet}$–C≡N (**AN**R1 in Table 1, $<S^2>$ = 1.33) is virtually the same as the benchmark value, 100.2 kcal mol^{-1}, obtained in the elaborate theoretical study of spin-contaminated radicals by Mayer et al. [16]. Finally we note that our mechanistic proposals of Scheme 7 remain essentially the same if the energy diagram were based upon the (relative) energies of the CBSB7 component of the method where spin-contamination is not an issue.

However, one anomalous result warrants further discussion. It concerns the hydrogen-bridged radical cations **HBRC**-1 and **HBRC**-2 which, unlike **HBRC**-3 and **HBRC**-4, show a very large difference in the stabilization energy (SE) derived from the B3LYP/CBSB7 and CBS-QB3 calculations. The DFT calculation yields an SE of 24 kcal mol^{-1} for both ions whereas the full CBS-QB3 method predicts much lower values: 17 kcal mol^{-1} for **HBRC**-1 and 15 kcal mol^{-1} for **HBRC**-2. An explanation for this unusually large discrepancy may involve the following. For the related complex HCN···H-C(CN)=$CH_2^{\bullet+}$, in which HCN (μ = 3.0 D) [17a] replaces the acrylonitrile (μ = 3.9 D) [17a] component, the DFT and CBS-QB3 methods yield the same stabilization energy of 15 kcal mol^{-1}. The same value was obtained with the more sophisticated CBS-APNO method. This suggests that the DFT calculation overestimates the stabilization energies for **HBRC**-1/2. The DFT calculation also yields a much more delocalized charge distribution than expected for an ion–dipole complex, probably because the two components of **HBRC**-1/2 are identical. In contrast, the DFT charge distribution of the HCN–acrylonitrile complex is as expected: the charge is largely localized on the acrylonitrile moiety. Thus the unrealistic charge distributions and stabilization energies of **HBRC**-1/2 may well be connected to the "sameness" of their components [18]. We further note that a poor DFT result for the geometries of these complexes may adversely affect the CBS-QB3 derived stabilization energies. As discussed in Section 3.2, **HBRC**-1/2 are key intermediates in the dissociation chemistry of the dimer ions but precise knowledge of their stabilities is not required.

3. Results and discussion

3.1. The self-protonation of acrylonitrile in the dimer ions and the occurrence of proton-transport catalysis

The base peak at *m/z* 54 in the MI spectrum of the acrylonitrile dimer ion at *m/z* 106, see Fig. 1 corresponds to the generation of protonated acrylonitrile ions. Since the proton affinity (PA) of acrylonitrile, 187.5 kcal mol^{-1} [17b], is typical of a nitrile rather than an alkene, these ions undoubtedly have the structure CH_2=CHC≡NH^+ (**AN**P) and not $CH_3CHC{\equiv}N^+$. Indeed, it follows from the results of Table 1 that the self-protonation CH_2=CHC≡$N^{\bullet+}$ (**AN**) + CH_2=CHC≡N → $CH_3CHC{\equiv}N^+$ + CH_2=C$^{\bullet}$–C≡N is endothermic, by 25 kcal mol^{-1}, whereas formation of **AN**P with either CH_2=C$^{\bullet}$–C≡N (**AN**R1) or

Table 2. Energy data[a] derived from CBS-QB3 calculations pertinent to the dissociation chemistry of acrylonitrile dimer ions as described in Schemes 2–7.

	B3LYP/CBSB7	CBS-QB3		QB3	
Ionic/neutral species	E(total)	E(total) [0 K]	ZPE	$\Delta_f H^o_0$	$\Delta_f H^o_{298}$
HBRC-1 (Scheme 2)	−341.41042	−340.70404	62.5	330	327
HBRC-2 (Scheme 2)	−341.41065	−340.70269	62.5	331	329
HBRC-3 (Scheme 3)	−341.44531	[b]	59.7	(314)	(311)
HBRC-4 (Scheme 3)	−341.43001	−340.74531	60.4	304	301
D1 (Scheme 2)	−341.45639	−340.76886	64.7	289	286
D2 (Scheme 2)	−341.42145	−340.73700	63.6	309	306
D3 (Scheme 2)	−341.42048	−340.73037	64.5	313	310
TS HBRC-1 → D1	−341.41026	−340.70490	62.6	330	327
TS HBRC-2 → D1	−341.41043	−340.70290	62.4	331	328
TS HBRC-1 → HBRC-3	−341.39392	−340.70212	58.9	331	328
TS HBRC-2 → HBRC-4	−341.38607	−340.69777	58.8	334	331
D4 (Scheme 7)	−341.46192	−340.77004	64.5	289	285
D5 (Scheme 7)	−341.43638	−340.74755	64.8	303	298
D6 (Scheme 4)	−341.43667	−340.74303	65.5	306	302
D7 (Scheme 5)	−341.44061	−340.74904	64.8	302	298
D8 (Scheme 7)	−341.42623	−340.73286	62.7	312	308
TS D1 → D4	−341.39405	−340.70471	61.8	330	326
TS D1 → D6	−341.35331	−340.66747	59.8	353	349
TS D4 → D7	−341.37789	−340.68846	60.9	340	336
TS D7 → VP1	−341.43441	−340.74342	64.7	305	301
TS D4 → D5	−341.43278	−340.74516	64.1	304	300
TS D5 → VP1	−341.39167	−340.70135	63.9	332	327
TS D5 → D8	−341.42123	−340.73015	63.2	314	309
VP1 (Scheme 7)	−341.49269	−340.79467	67.1	273	268
VP1b (Scheme 7) (text)	−341.43299	−340.72866	65.8	315	310
VP1a (Scheme 7) (text)	−341.48804	−340.79785	67.7	271	266
VP2 (Scheme 7)	−341.46800	−340.77584	67.8	285	280
VP2a (Scheme 7) (text)	−341.46520	−340.77672	67.1	284	280
TS VP1 → VP2	−341.41261	−340.72597	66.0	316	311
TS VP1 → VP1a	−341.44621	−340.76169	63.5	294	289
TS VP2 → VP2a	−341.42553	−340.74089	64.4	307	302
TS VP1 → VP1b	−341.41280	−340.72419	64.6	318	313

[a] E(total) in Hartrees, all other components, including the ZPE scaled by 0.99, are in kcal mol^{-1}.

[b] Estimate from a B3LYP/CBSB7 calculation using HBRC-4 as the anchor; the CCSD(T) component in the CBS-QB3 calculation did not converge.

$^{\bullet}$CH=C(H)C≡N (**AN**R2) is exothermic, by 20 and 13 kcal mol^{-1}, respectively. One would therefore expect that in encounter complexes of ionized acrylonitrile with its neutral counterpart, protonation at the cyano group readily occurs and that, when energized, these complexes dissociate into **AN**P (*m/z* 54) rather than **AN** (*m/z* 53). Yet, in the s time frame

metastable dimer ions show four other competing dissociations including loss of acrylonitrile. One explanation for the presence of the substantial *m/z* 53 peak in the MI spectrum is that the protonation process leading to *m/z* 54 involves a significant reverse energy barrier. This would make dissociation of the dimer into its ionic and neutral acrylonitrile components more competitive with the protonation. Alternatively, the *m/z* 53 ions in the MI spectrum of Fig. 1 do not represent ions **AN** but rather ions $CH_2=C=C=NH^+$ (**AN**1), which are more stable by 17 kcal mol^{-1}, see Table 1.

Solitary ions **AN** cannot isomerize into **AN**1: the calculated energy requirement (CBS-QB3 data Table 1) for this isomerization – a 1,3-H shift at 87 kcal mol^{-1} or, more economically, two consecutive 1,2-H shifts at 46–47 kcal mol^{-1} – is quite high and well above that for dissociation of the incipient ions **AN**1 by $H^\bullet$ loss into the N-protonated cyanoacetylene ion [3], see Scheme 1.

However, the high barrier for the one-step isomerization via a 1,3-H shift in the solitary ion may vanish in the encounter complex if the neutral component catalyses the transformation. Criteria for successful proton-transport catalysis have been developed by Bohme [2d], and Radom and co-workers [19]. The most important criterion predicts that a smooth isomerization **AN** → **AN**1 would occur if the PA of the base (B) (acrylonitrile) lies between the PA of $CH_2=C^\bullet–C\equiv N$ at C and at N. If PA(B) is too low, proton abstraction will not take place. If PA(B) is too high, the incipient ion BH^+ will not release the proton: dissociation to $CH_2=C^\bullet\text{-}C\equiv N + BH^+$ ($CH_2=CHC\equiv NH^+$ (**AN**P)) will ensue instead. From the CBS-QB3 results in Table 1 we derive values of 168, 185 and 188 kcal mol^{-1} for PA($CH_2=C^\bullet–C\equiv N$ at C), PA($CH_2=C^\bullet–C\equiv N$ at N) and PA(B), respectively; the latter value is in excellent agreement with the experimental value. Thus the PA of the base is too high, but only marginally so, which implies that PTC cannot *a priori* be ruled out.

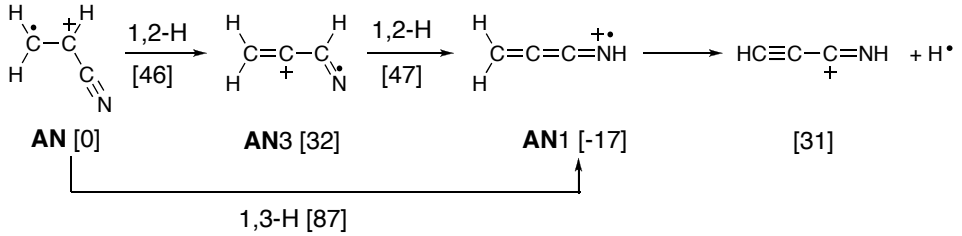

Scheme 1. Isomerization of the acrylonitrile radical cation, **AN**, into its isomer **AN**1; the values in square brackets are relative energies in kcal mol^{-1} derived from CBS-QB3 (298 K) calculations.

Various ion–dipole complexes may be formed in the reaction of acrylonitrile with its ionic counterpart which, because of the large dipole moment of the nitrile (μ = 3.9 D), are expected to have stabilization energies in the 10–20 kcal mol^{-1} range. Among these, two hydrogen-bridged dimer ions may be envisaged, viz. **HBRC**-1 and **HBRC**-2 as depicted in Scheme 2. These C–H–N hydrogen-bridged radical cations [20] are calculated to have stabilization energies of 15–17 kcal mol^{-1} at the CBS-QB3 level of theory. They both lie in a very shallow potential well with small barriers for rearrangement into ion–dipole

complexes that are not hydrogen-bridged. More importantly, these HBRCs can also rearrange with a negligible barrier into the covalently bound isomer **D**1 that has a much larger stabilization energy, 58 kcal mol^{-1}. Two more covalently bound isomers were identified as stable minima viz. ions **D**2 and **D**3 in Scheme 2. The latter ion has been proposed as the dimer ion core in an infrared photodissociation study of acrylonitrile cluster ions $(CH2{=}CHC{\equiv}N)_n^{\bullet+}$ (n = 3–10) [21]. Both isomers are considerably less stable than **D**1 and play no obvious role in the dissociation chemistry of the dimer ions. In contrast, as we shall see in the next section, ion D1 may act as the reacting configuration for a 1,2-H shift that initiates the observed losses of $H^{\bullet}$, HCN and C_2H_2 from the low-energy dimer ions.

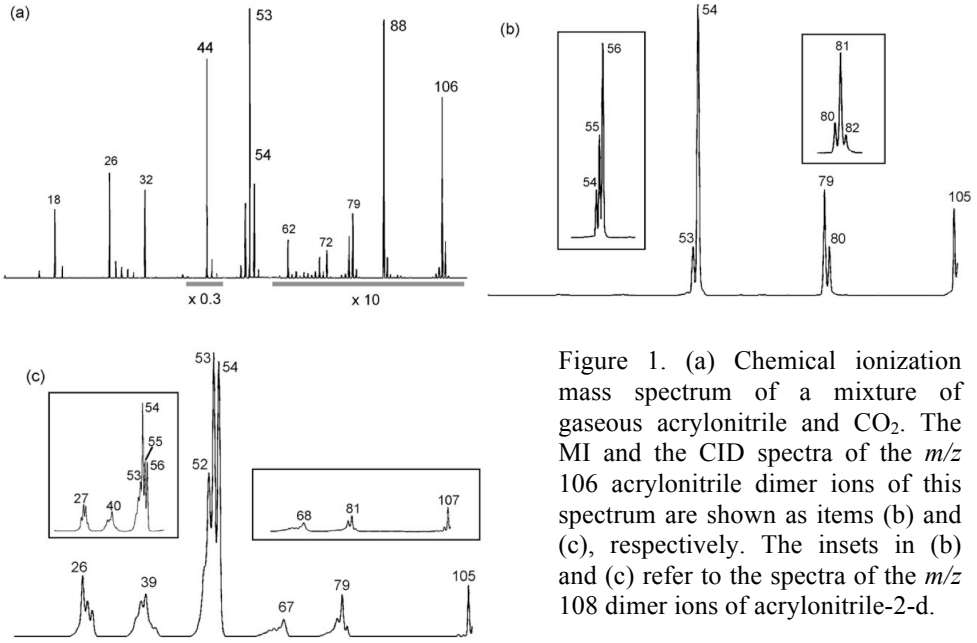

Figure 1. (a) Chemical ionization mass spectrum of a mixture of gaseous acrylonitrile and CO_2. The MI and the CID spectra of the *m/z* 106 acrylonitrile dimer ions of this spectrum are shown as items (b) and (c), respectively. The insets in (b) and (c) refer to the spectra of the *m/z* 108 dimer ions of acrylonitrile-2-d.

The self-protonation leading to *m/z* 54 – and also the formation of *m/z* 53 if proton-transport catalysis plays a role – most likely involves **HBRC**-1 and **HBRC**-2. That the self-protonation reaction in these ions does not proceed spontaneously follows from a consideration of the symmetries of the corresponding electronic wave functions. Radical cation AN as well as the radicals **AN**R1 and **AN**R2 are planar. The **AN** ground state (Δ_fH_{298} = 298 kcal mol^{-1}) has $^2A''$ symmetry; the lowest $^2A'$ state lies 34 kcal mol^{-1} higher in energy. The ground states of the radicals **AN**R1 and **AN**R2, however, have $^2A'$ symmetry. The lowest $^2A''$ states for these radicals correspond to excitation energies of 52 and 53 kcal mol^{-1}, respectively. Since these excitation energies are much larger than the stabilization energies of **HBRC**-1 and **HBRC**-2, the reaction cannot proceed through any of the excited states. As a consequence, the symmetry of the wave function has to change during the proton transfer for the reaction to proceed at energies below the threshold for disproportionation into an acrylonitrile ion and neutral (344 kcal mol^{-1}). Thus, assuming

that the complex is planar, we have to deal with the intersection between the two PESs corresponding to the $^2A'$ and $^2A''$ states of the complex. However, the two states can be connected by lowering the symmetry of the nuclear framework of the CH_2=$CHC{\equiv}N^{\bullet+}$ moiety. This leads to a TS by distorting the nuclear framework of this moiety such that the CH_2=CH π-bond is partially broken. The transition states for the self-protonation reactions depicted in Scheme 3a and b were found to lie just above the corresponding hydrogen-bridged complexes **HBRC**-1/2. The barrier for formation of **AN**R1 is lower than that for **AN**R2, by 3 kcal mol^{-1}, leading to the expectation that **AN**R1 is preferentially formed. Note that the two radicals cannot freely interconvert because of a prohibitively high barrier of 52 kcal mol^{-1}, see Table 1.

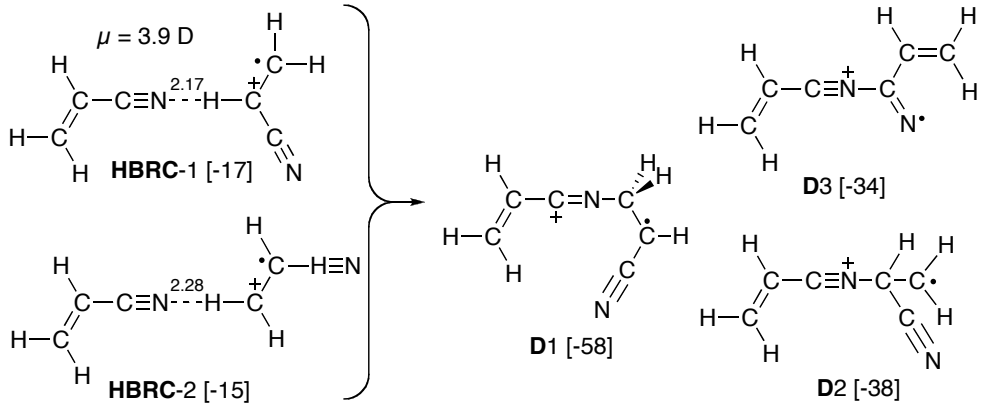

Scheme 2. Structures of stable acrylonitrile dimer ions and their stabilization energies (kcal mol^{-1}) relative to the dissociation level CH_2=$CHCN^{\bullet+}$ (AN) + CH_2=CHCN; the values in square brackets refer to CBS-QB3 (298 K) calculations.

Our chemical ionization experiments involving acrylonitrile-2-d, CH_2=$CDC{\equiv}N$, are in qualitative agreement with the scenario depicted in Scheme 3. The deuterated dimer ions dissociate into both CH_2=$CDC{\equiv}ND^+$ (*m/z* 56) + CH_2=$C^{\bullet}$–C≡N (**AN**R1) and CH_2=$CDC{\equiv}NH^+$ (*m/z* 55) + $^{\bullet}$CH=C(D)C≡N (**AN**R2). This is seen from the inset in the MI spectrum of Fig. 1b, where the *m/z* 56 peak is about twice as intense as the *m/z* 55 peak. Thus both **AN**R1 and **AN**R2 radicals are formed with a relative abundance of 2:1, and note that **AN**R1 is thermodynamically the more stable radical. The peak intensity ratio (*m/z* 56 + *m/z* 55)/*m/z* 54 equals the *m/z* 54/*m/z* 53 peak intensity ratio (6.0) in the spectrum of the unlabelled dimer indicating that there is no isotope effect associated with the reactions.

We further note that after passing the transition state, **AN**P may be formed directly or via N–H–N bridged complexes with **AN**R1 or **AN**R2, *viz*. **HBRC**-3 and **HBRC**-4 in Scheme 3. (We note that the stabilization energies calculated for these HBRCs, ca. 30 kcal mol^{-1}, is close to that obtained by experiment for the N–H–N bridged proton bound dimer of acrylonitrile, 30.7 kcal mol^{-1} [22]). However, these HBRCs may also accommodate back-donation of the abstracted proton which would lead to the isomerization of the **AN** ion into either of its more stable isomers CH_2=C=C=$NH^{\bullet+}$ (**AN**1) or CH=CH=C=$NH^{\bullet+}$ (**AN**2).

These ions both turn out to have $^2A'$ ground states, enabling the corresponding proton transfers to take place spontaneously, provided these processes are exothermic. Using the CBS-QB3 derived Δ_fH_{298} values of the components in Table 1, we obtain the following energies for the dissociation products: Δ_fH_{298}(**AN**1 + **AN**N) = 327 kcal mol^{-1} and Δ_fH_{298}(**AN**2 + **AN**N) = 335 kcal mol^{-1}. These energies are only slightly higher than those for the products of the self-protonations: Δ_fH_{298}(**AN**P + **AN**R1) = 324 kcal mol^{-1} and Δ_fH_{298}(**AN**P + **AN**R2) = 331 kcal mol^{-1}. This implies that the PTC processes cannot be ruled out on energetic grounds because the energy available in the dimer ions is sufficiently high for either dissociation route. On the other hand, both reactions are exothermic for ions that pass either of the transition states where their configuration is such that formation of **AN**P involves a mere bond cleavage whereas the formation of the PTC ions **AN**1 or **AN**2 requires a significant rearrangement. This makes it unlikely that the PTC processes can effectively compete with the self-protonations. In this context it is important to note that both self-protonation reactions occur and that the self-protonation of Scheme 3b lies 4 kcal mol^{-1} higher in energy than the PTC process of Scheme 3a. Yet, only self-protonation is observed.

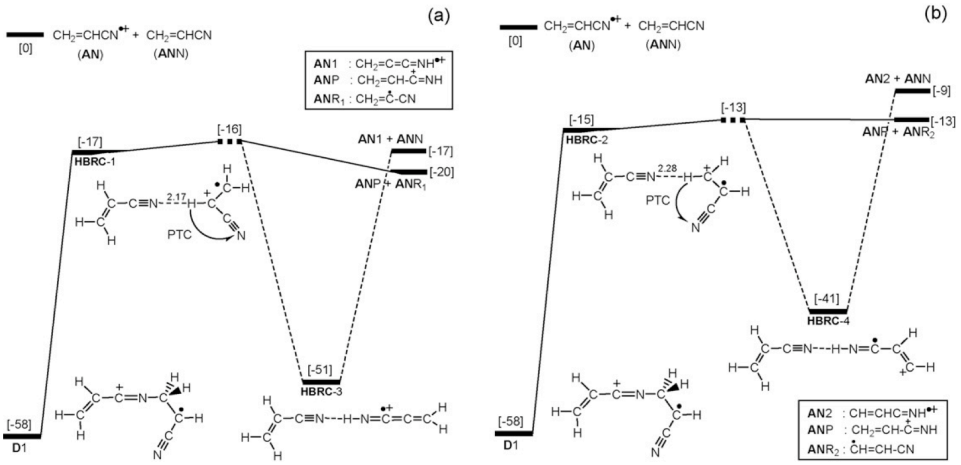

Scheme 3. (a and b) Potential energy diagrams (CBS-QB3 calculations) describing the self-protonation reaction and the occurrence of proton-transport catalysis in acrylonitrile dimer ions. The relative energies are in kcal mol^{-1}.

Evidence that PTC does not play a significant role comes from an experiment in which we probed the structure of the *m/z* 53 ions in the MI spectrum of Fig. 1 by obtaining their CID mass spectrum. This spectrum is shown in Fig. 2a: it is virtually identical with that of acrylonitrile ions generated by electron impact and characteristically different from that of ions **AN**1 and **AN**2 discussed in a previous study [3].

*3.2. Back-dissociation versus self-protonation in the acrylonitrile dimer ions **HBRC**-1/2*

In the previous section we have established that the *m/z* 53 ions in the MI spectrum do not result from proton-transport catalysis but rather are ions **AN** resulting from a back-dissociation. It follows from the energy diagram of Scheme 3, that dimer ions dissociating back into **AN** + **AN**N can only do so at energies largely in excess of that required for self-protonation. Prima facie, therefore, the observed competition in the s time frame of the back-dissociation with the self-protonation is surprising. However, the following considerations may rationalize why dissociation by self-protonation requires a sizable excess energy. First, the majority of the reacting configurations do not correspond to **HBRC**-1/2, which lie in very shallow wells, but to the much more stable ion **D**1 (at 286 kcal mol^{-1}). According to RRKM theory [23], this implies that a relatively large excess energy is needed. The same argument applies to the dissociations of the very stable ions **HBRC**-3/4.

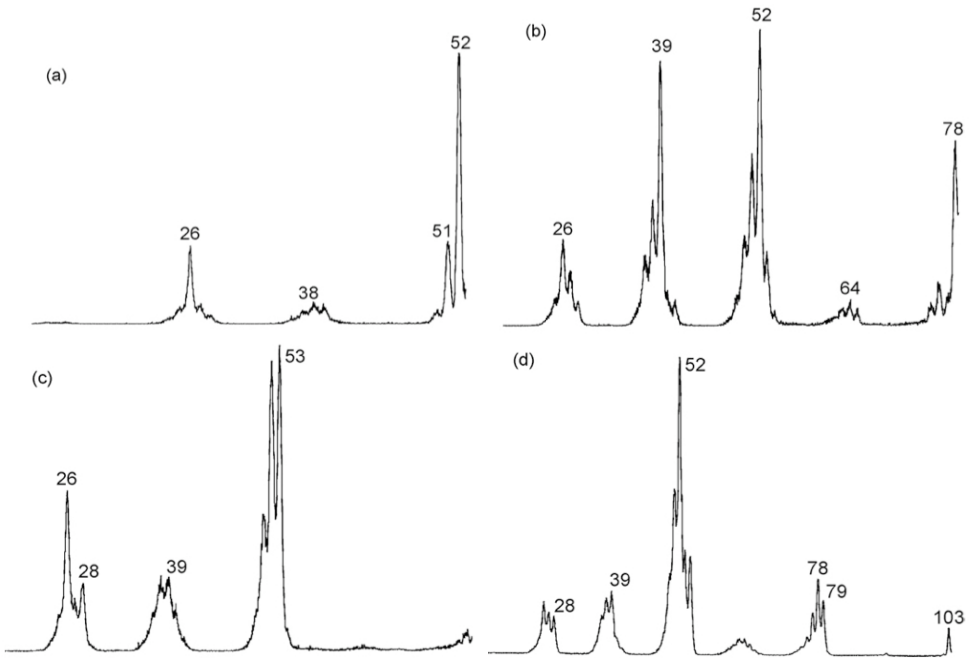

Fig. 2. CID mass spectra of product ions generated from metastable acrylonitrile dimer ions: (a) *m/z* 53 ions (loss of acrylonitrile); (b) *m/z* 79 ions (loss of HCN); (c) *m/z* 80 ions (loss of CH); (d) *m/z* 105 ions (loss of H$^{\bullet}$).

Second, the large dipole moment of acrylonitrile (μ = 3.9 D) and also of the radicals **AN**R1/2 (μ = 3.8 and 3.2 D, respectively; calculated values) probably leads to a dramatic decrease, by some orders of magnitude, of the dissociation rate constants, as compared to

an RRKM (variational transition state theory) estimate. It has been argued that such dissociations do not behave statistically, as classical trajectory calculations have shown that the trajectories leading to dissociation are quasi-periodical instead of chaotic because of the large ion–dipole stabilization [24]. We suggest that the non-planarity of the transition states connecting **HBRC**-1 to **HBRC**-3 and **HBRC**-2 to **HBRC**-4 also contributes to a non-statistical behaviour. Our calculations show that the distortions in the CH_2=CHC≡$N^{\bullet+}$ moiety lead to transition states that are 10–13 kcal mol^{-1} lower in energy than the corresponding (planar) minimum energy crossing points. The self-protonation will then only be effective if the internal rotation of the CH_2 -group in the CH2=CHC≡$N^{\bullet+}$ moiety is excited and the CH_2=CHC≡N moiety approaches the ion from the right direction. Because of the large ion–dipole stabilization for all other orientations, the reaction may be substantially slowed down by non-statistical behaviour.

Experimental evidence that the self-protonation is relatively slow comes from a comparison of the MI and CID spectra of the dimer ions presented in Fig. 1: self-protonation dominates the MI spectrum, but in the CID spectrum the *m/z* 54 peak is diminished with respect to the *m/z* 53 back-dissociation.

*3.3. Self-protonation via the covalently bound acrylonitrile dimer ions **D**1?*

We have also entertained the possibility that protonated acrylonitrile product ions are generated via a hydrogen shift in covalently bound dimer ions. An obvious route for ions **D**1 is the one shown in Scheme 4, where the second step is a simple bond cleavage.

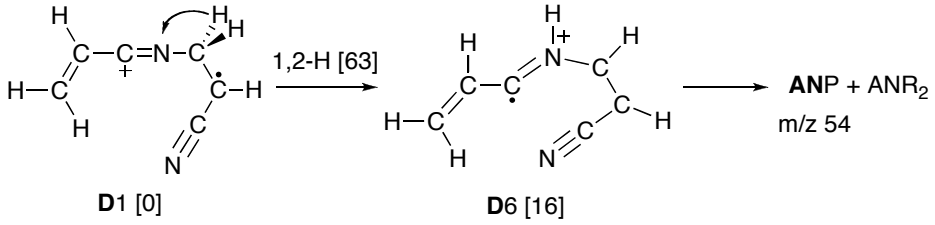

Scheme 4

This route is not feasible: the 1,2-H shift for the isomerization **D**1 → **D**6 is calculated to be more energy demanding than the formation of **AN**P (*m/z* 54) via the HBRCs and also, see Scheme 6, the formation of *m/z* 105 ions by loss of $H^{\bullet}$ from **D**1. Another possibility is that ions **D**6 are generated from ion **D**7, by a 1,4-H shift. The formation of **D**7 from **D**1, see Scheme 5 below, was considered because our calculations indicate that **D**7 readily cyclizes into the vinyl pyrimidine type ions **VP**1/2 of Scheme 7. Ion **D**7 could thus account for the observed loss of C_2H_2 from the acrylo nitrile dimer ions and the formation of *m/z* 80 pyrimidine type product ions. This scenario is not a viable option either: the barrier for the isomerization **D**1 → **D**7 via two consecutive 1,2-H shifts, see Scheme 5, is so high that it is unl ikely that ions **D**7 play a role in the dissociation chemistry of the acrylonitrile dimer ions. Thus it seems likely that the formation of *m/z* 54 in the MI spectrum of the dimer ions occurs via **HBRC**-1/2. However, these HBRCs and the related non-hydrogen bridged ion–

dipole complexes cannot account for the competing loss of $H^{\bullet}$ and also that of HCN and C_2H_2, which may well involve a cyclic precursor ion. As we shall see in the next section rearrangement reactions starting from the covalently bound dimer ions **D**1 can account for all three losses.

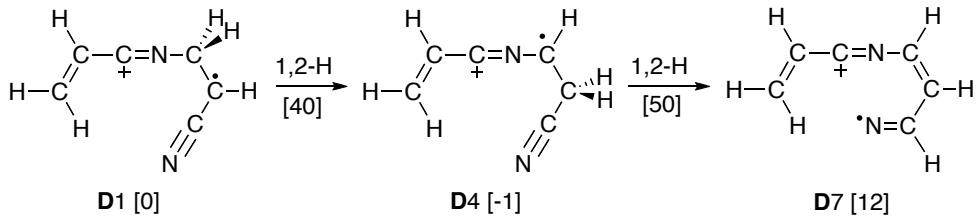

Scheme 5. Isomerization pathways of acrylonitrile dimer ions **D**1 into ions **D**7. The relative energies in square brackets are in kcal mol^{-1} and were obtained from CBS-QB3 calculations (Table 2).

*3.4. The dissociation of the acrylonitrile dimer ion **D**1: generation of ionized pyrimidine and its isomer ionized pyrimidine-2-ylidine*

The mechanistic proposal for the dissociation of the dimer ions **D**1 by loss of HCN, C_2H_2 and $H^{\bullet}$ is presented in Scheme 7. Its analysis will await the evaluation of the experimental evidence for the proposed product ion structures. That the neutrals lost from **D**1 are HCN rather than $C_2H_3^{\bullet}$ and also C_2H_2 rather than $CN^{\bullet}$ is confirmed by the MI spectrum of the fully deuterated dimer ion (*m/z* 112) which displays a single peak at *m/z* 84 in the *m/z* 80 region.

The CID spectrum of the *m/z* 79 C_5H_5N ions generated by loss of HCN from the metastable dimer ions is shown in Fig. 2b. The major peaks at *m/z* 52 (loss of HCN and/or $C_2H_3^{\bullet}$), *m/z* 39 ($C_3H_3^{+}$) and *m/z* 26 ($C_2H_2^{\bullet+}$) are compatible with the proposed linear $C_5H_5N^{\bullet+}$ isomer of Scheme 7. Reference CID mass spectra of non-cyclic $C_5H_5N^{\bullet+}$ isomers are not available so that this structure assignment must remain tentative. We further note that the CID spectrum of Fig. 2b is incompatible with that of ionized pyridine or its distonic analogues. These very stable cyclic $C_5H_5N^{\bullet+}$ isomers all display CID spectra that are dominated by a peak at *m/z* 52 (loss of HCN) [25].

A different scenario obtains for the structure assignment of the *m/z* 80 ions. Here the overall appearance of the CID mass spectrum of the metastably generated ions is that of a cyclic $C_4H_4N_2^{\bullet+}$ ion, viz. ionized pyrimidine (**PY**1) and/or one of its ylide counterparts **PY**2–**PY**5 shown in Scheme 6 (relative energies in kcal mol^{-1} from Ref. [3]).

We have previously studied the above system of $C_4H_4N_2^{\bullet+}$ ions in detail, by both theory and experiment [3]. The calculations of this study predict that the five stable pyrimidine isomers have comparable energies but also high interconversion barriers. In spite of this, ions **PY**1–**PY**4 (**PY**5 was not experimentally accessible) display similar CID mass spectra. However, the isomers can be differentiated on the basis of the intensity ratios of the *m/z* 26 ($C_2H_2^{\bullet+}$) and *m/z* 28 ($HCNH^{+}$) peaks, which result from high-energy CID

dissociations. A comparison of the CID mass spectrum of Fig. 2c with the CID mass spectra of **PY**1–**PY**4 of our previous study [3] indicates that the loss of C_2H_2 from **D**1 yields ionized pyrimidine in admixture with its ylide isomer PY2 in a 1:1 ratio. The analysis of the CID spectra allows the possibility that the co-generated distonic ion is **PY**3 rather than **PY**2 but in our quest of mechanistic proposals for the C_2H_2 loss we have not been able to find a plausible pathway for its generation.

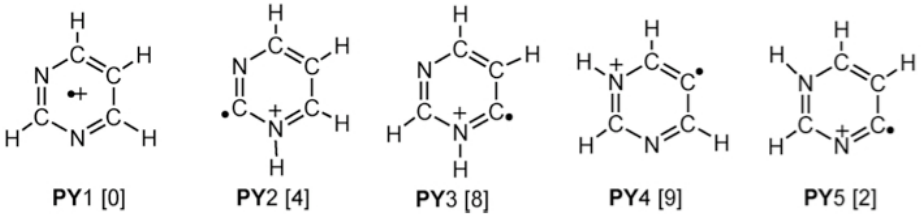

Scheme 6.

The CID mass spectrum of the *m/z* 105 ions generated by loss of $H^{\bullet}$ is presented in Fig. 2d. Reference spectra are not available for this system of ions. However, the base peak in the spectrum at *m/z* 52 can readily be rationalized in terms of the structure proposed in Scheme 7, viz. by invoking a simple bond cleavage into $CH{=}CHC{\equiv}N^{+}$ (*m/z* 52) + $CH_2{=}CHC{\equiv}N$. Further support for the structure assignment comes from exploratory calculations which confirm that the least energy demanding $H^{\bullet}$ loss from **D**1 is that of a methylene hydrogen and the discussion of the mixed dimer ions D1(Cl) at the end of this section. We now turn to a discussion of our mechanistic proposals using the energy diagram of Scheme 7 as a guide.

Formation of pyrimidine via loss of C_2H_2

As discussed above, see Scheme 2, the reaction between two acrylonitrile monomers can lead to a variety of possible dimers. The most stable direct chemically bonded dimer was found to be **D**1 which has a stabilization energy of 58 kcal mol^{-1} relative to **AN** + **AN**N. A six member ring with the N–C–N connectivity of pyrimidine may be envisaged to occur by ring closure of **D**1 but such a species is not a minimum on the potential energy surface. In contrast, ions **D**4 generated from a 1,2-H shift in **D**1, can readily lead to the desired ring closure. The fairly energy demanding 1,2-H shift for the transformation **D**1 → **D**4 (40 kcal mol^{-1}) allows the incipient ions **D**4 to cyclize into **D**5. This ion can further rearrange by a 1,2-H shift into the 2-vinylpyrimidine radical cation, **VP**1, which may serve as the immediate precursor for the loss of C_2H_2, see Scheme 7. Another route to the formation of **VP**1 involves the facile ring closure of ions **D**7 in Scheme 5. However, the minimum energy requirement for the transformation **D**1 → **D**7, lies at 336 kcal mol^{-1}, some 10 kcal mol^{-1} above the transformation **D**1 → **D**4. Considering the energy requirements for the competing losses of $H^{\bullet}$ and HCN, see Scheme 7, we see that this transformation is not a viable option.

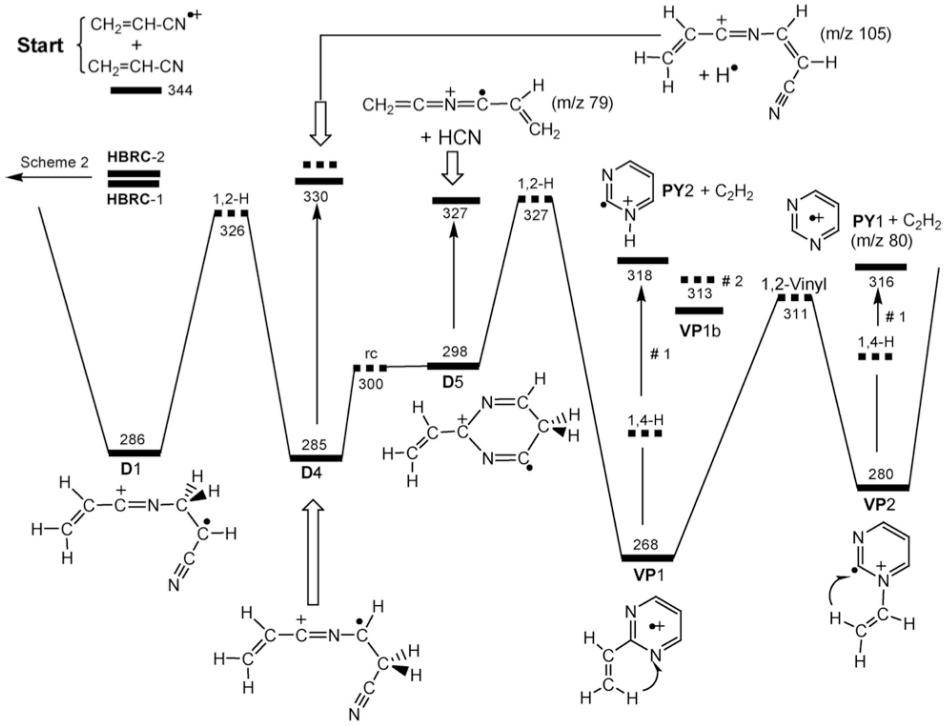

Scheme 7. Energy diagram derived from CBS-QB3 298 K calculations (kcal mol^{-1}) describing the losses of C_2H_2, HCN and H from metastable acrylonitrile dimer ions **D**1. Note #1: dissociation from VP1a and VP2a, see text; Note #2: exchange vinyl H atoms via **VP**1b, see text.

Ion **VP**1 can readily lose C_2H_2 through a simple 1,4-H shift to **VP**1a to generate the distonic pyrimidine isomer **PY**2 whose energy level lies at 318 kcal mol^{-1}. To generate the slightly more stable pyrimidine ion **PY**1, the 2-vinylpyrimidine ion **VP**1 may first go through a 1,2 vinyl-shift at 311 kcal mol^{-1} (TS **VP**1–**VP**2 in Scheme 7). The resulting stable distonic isomer **VP**2 may then dissociate into **PY**1 + C_2H_2 via a low-lying 1,4-H shift analogous to the **VP**1–**VP**1a shift. Thus, the formation of both **PY**1 and **PY**2 is energetically possible since the activation energy for the 1,2-vinylidene shift turns out to be relatively small (43 kcal mol^{-1}). Our collision experiments show that the peak at *m/z* 80 in Fig. 1b indeed represents a mixture of isomers **PY**1 and **PY**2. Note that the interconversion of **PY**2 and **PY**1 via a 1,2-H shift is not feasible: the activation energy for this isomerization is prohibitively high, 65 kcal mol^{-1}, as has been previously calculated by Lavorato et al. [3].

One further point deserves comment: following the proposal of Scheme 7, the deuterated dimer ions generated from acrylonitrile-2-d, CH_2=CDC≡N, are expected to lose C_2HD. The *m/z* 81 peak in the inset of Fig. 1b, part of which originates from the loss HCN,

shows that this is indeed the case. However, loss of C_2H_2 (*m/z* 82) is also observed, indicating that the vinyl hydrogens in ion **VP**1 undergo exchange. Our calculations rationalize such an exchange via recurrent 1,2-H shifts between **VP**1 and **VP**1b (see Scheme 7 and Fig. 3), with a TS at 313 kcal mol^{-1}.

Loss of H• and loss of HCN

Our computational analysis indicates that the loss of H• proceeds from **D**1 to **D**4, yielding the *m/z* 105 ion structure depicted in Scheme 7. The thermochemical threshold for these dissociation products lies at 330 kcal mol^{-1} but this reaction was calculated to have a small reverse activation energy of 2 kcal mol^{-1}. Note that the TS **D**5 → **VP**1 at 327 kcal mol^{-1} was found to be about 5 kcal mol^{-1} lower in energy than the TS for this dissociation.

The energetically most favourable path for the HCN loss involves ring opening of **D**5 (TS at 309 kcal mol^{-1}) to generate ion **D**8 (structure shown in Fig. 3) at 308 kcal mol^{-1}. This ion can lose HCN without a reverse barrier yielding the linear *m/z* 79 ion depicted in Scheme 7. The energy requirement of this reaction is the same as that for the pyrimidine formation.

The mixed dimer ion of acrylonitrile and 2-chloroacrylonitrile

Further support for the mechanistic proposal of Scheme 7 comes from a brief analysis of the dissociation behaviour of the dimer ion of acrylonitrile and 2-chloroacrylonitrile. The ionization energy of the chloro compound is lower than that of the parent nitrile (11.58 eV versus 11.91 eV [17c]. Therefore, the chloro analogue of ion **D**1 depicted in the scheme below, **D**1(Cl), is expected to be the principal species in this system of ions. The metastable dimer ions show only two reactions: (i) formation of $C_6H_5N_2^+$ ions (*m/z* 105) by loss of Cl• and (ii) formation of 2-chloroacrylonitrile ions (*m/z* 87) by loss of acrylonitrile.

Loss of Cl• dominates the MI spectrum: the *m/z* 105: *m/z* 87 peak intensity ratio is 4:1. However, this ratio reverses to 1:4 in the CID spectrum of the dimer ions and *m/z* 87 is now the base peak. To probe the structure of the *m/z* 105 product ions we obtained their CID mass spectrum and found it to be identical with that of the *m/z* 105 ions generated by loss of H• from ions **D**1 in Scheme 7. These observations indicate that the Cl• loss is not a direct bond cleavage but rather occurs upon a 1,2-H shift in ions **D**1(Cl), as depicted in Scheme 8.

The product enthalpies for the two dissociation reactions presented in the scheme (CBS-QB3 results Table 1) indicate that the two reactions can only compete if the 1,2-H shift barrier preceding the Cl• loss is sufficiently high. This is indeed the case: our B3LYP/CBSB7 calculations predict the barrier to lie at 330 kcal mol^{-1}, which allows the two processes to compete. However, once ions **D**1(Cl) have undergone the 1,2-H shift, immediate dissociation by loss of Cl• ensues because the reaction is strongly exothermic. This is not the case for the loss of H• from **D**1, which is slightly endothermic, see Scheme 7. This would explain why ions **D**1(Cl) do not further rearrange to lose HCN and C_2H_2 whereas ions **D**1 do.

Finally, we note that metastable ions **D**1(Cl) do not dissociate, via the chloro analogue of **HBRC**-1, into CH_2=CHC≡NH^+ + •CH=C(C1)C≡N although the energy requirement for this reaction, 329 kcal mol^{-1}, is 3 kcal mol^{-1} lower than that for the back dissociation (Table 1). This is not really surprising considering that in this system too the self-protonation reaction is expected to involve reverse activation energy.

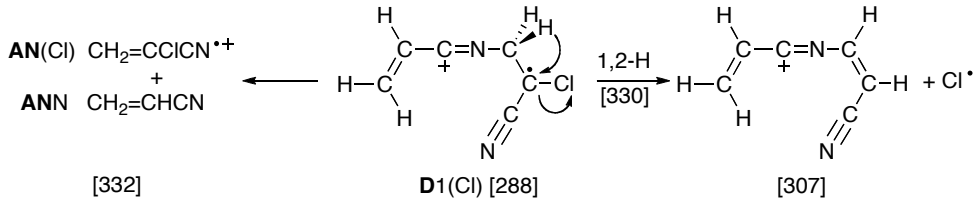

Scheme 8.

4. Summary

Our combined computational and experimental study shows that the interaction of an acrylonitrile ion with its neutral counterpart leads to hydrogen-bridged ion–dipole complexes which may undergo self-protonation (but not self-catalysis) or else isomerize into the very stable covalently bound species **D**1 of Scheme 7. **D**1 ions act as the starting point configuration for the reactions that lead to the losses of $H^{\bullet}$, HCN and C_2H_2.

The latter process involves a crucial cyclization step that ultimately yields ionized pyrimidine in admixture with its 2-ylide isomer. This process may be relevant in the context of the quest for the prebiotic pyrimidine molecule in astrochemistry. Neutralization of the isomeric ions by charge exchange with molecular targets in the keV translational energy regime yields pyrimidine and its 2-ylide as stable neutral species [3]. The 2-ylide does not convert into the more stable pyrimidine by an intramolecular 1,2-H shift [3] but this isomerization may readily occur by intermolecular interaction, e.g., with H_3O^+ on an icy surface. Such a surface could also promote electron-ion recombination followed by isomerization as has been proposed for the formation of acetic acid in space in a recent SIFT study [7b,26].

Finally we note that a detailed analysis [27] of the ion–molecule reaction of acrylonitrile with HCN indicates that ionized pyrimidine could be generated via an analogous mechanism.

Acknowledgements

JKT thanks the Natural Sciences and Engineering Research Council of Canada (NSERC) for continuing financial support and Dr M.A. Trikoupis (OME Toronto) and Richard Lee for valuable discussions. PJAR and HKE thank the Netherlands Organization for Scientific research (NWO) for making available the SGI TERAS computer of SARA (Amsterdam).

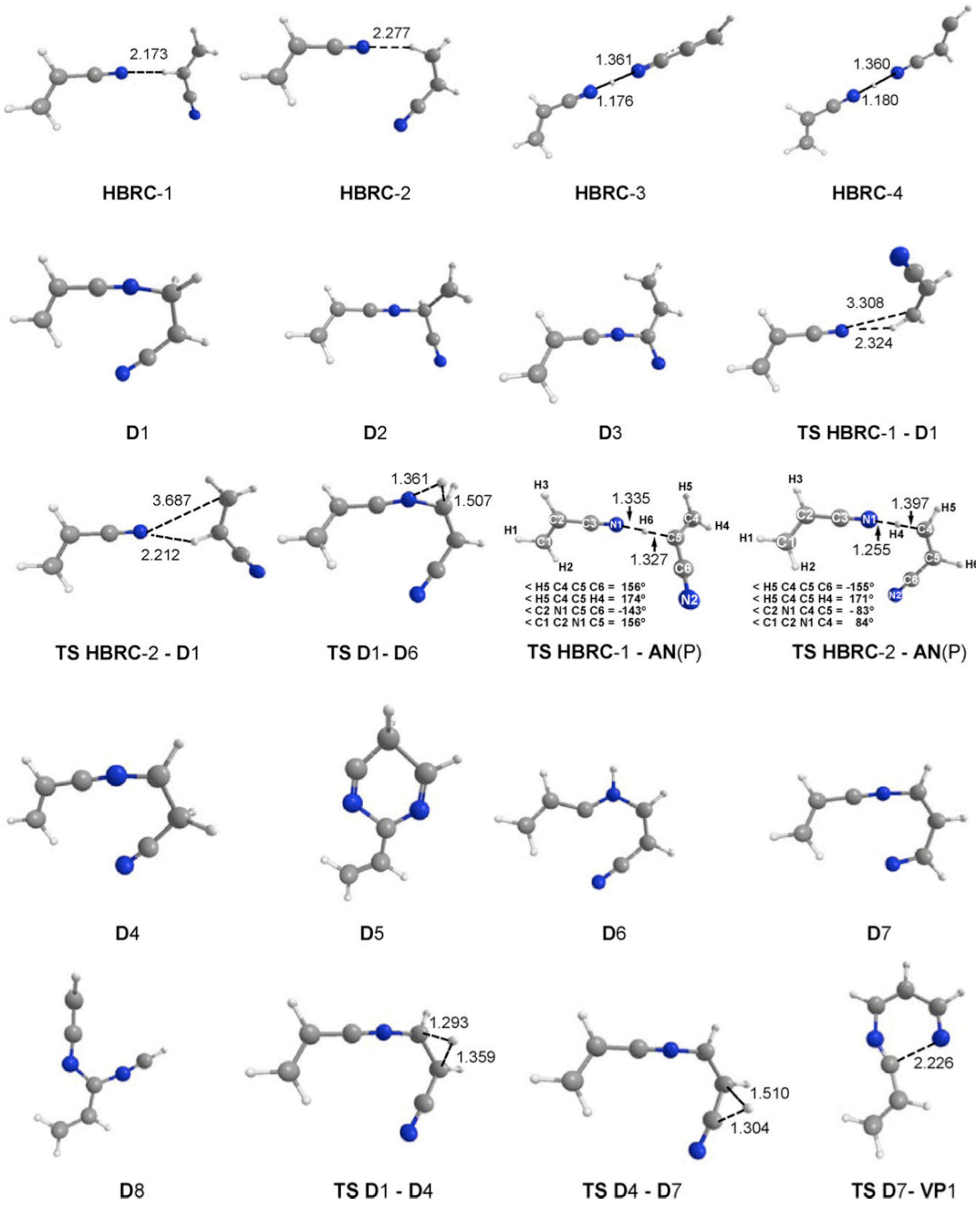

Figure 3. Selected optimized geometries (CBSB7 basis set) for stable intermediates and transition states involved in the dissociation chemistry of low energy acrylonitrile dimer radical cations.

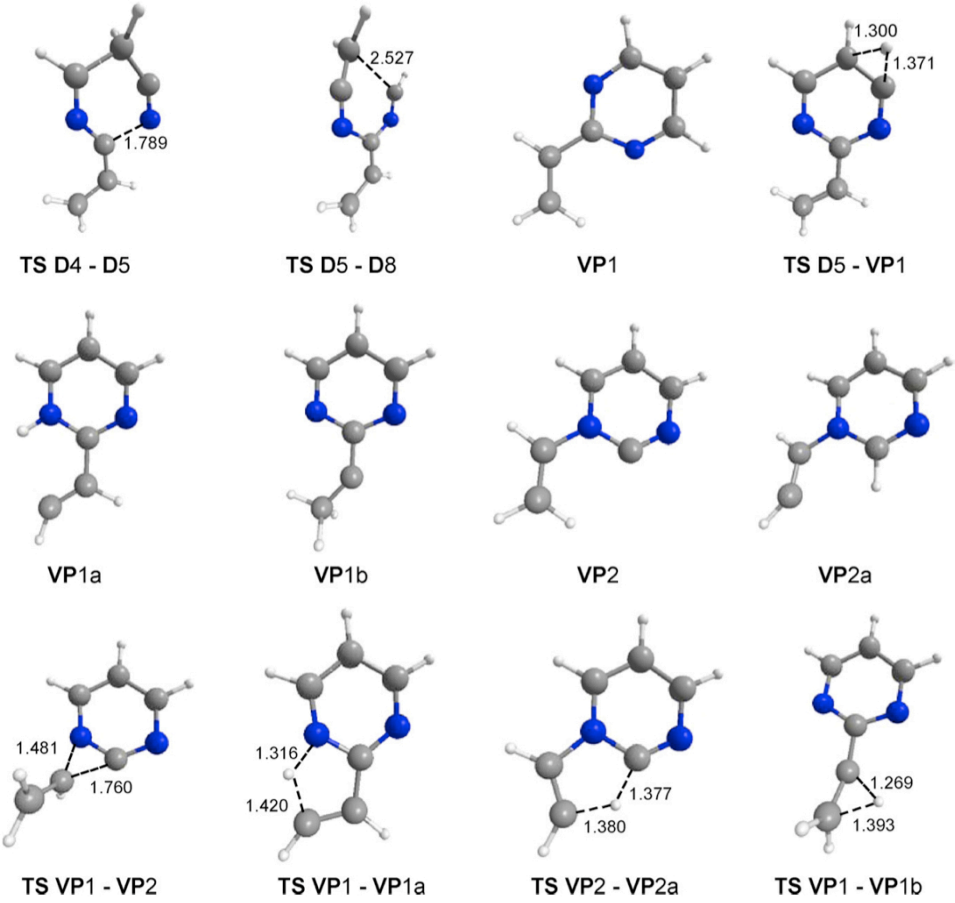

Figure 3. (*Continued*)

References

[1] (a) M.A. Trikoupis, P.J.A. Ruttink, P.C. Burgers, J.K. Terlouw, Int. J. Mass Spectrom. 217 (2002) 97; (b) M.A. Trikoupis, P.J.A. Ruttink, P.C. Burgers, J.K. Terlouw, Eur. J. Mass Spectrom. 10 (2004) 801.

[2] (a) For selected recent references see: G. van der Rest, P. Mourgues, H.E. Audier, Int. J. Mass Spectrom. 231 (2004) 83; (b) C.Y. Wong, P.J.A. Ruttink, P.C. Burgers, J.K. Terlouw, Chem. Phys. Lett. 390 (2004) 176; C.Y. Wong, P.J.A. Ruttink, P.C. Burgers, J.K. Terlouw, Chem. Phys. Lett. 387 (2004) 204; (c) X. Wang, J.L. Holmes, Can. J. Chem. 83 (2005) 1903; (d) P.C. Burgers, P.J.A. Ruttink, Int. J. Mass Spectrom. 242 (2005) 49; (e) For an early review see: D.K. Bohme, Int. J. Mass Spectrom. 115 (1992) 95.

[3] D.J. Lavorato, T.K. Dargel, W. Koch, G.A. McGibbon, H. Schwarz, J.K. Terlouw, Int. J. Mass Spectrom. 210–211 (2001) 43.
[4] E. Herbst, Chem. Soc. Rev. 30 (2001) 168.
[5] (a) F.F. Gardner, G. Winnewisser, Astrophys. J. 195 (1975) L127; (b) H.E. Matthews, T.J. Sears, Astrophys. J. 272 (1983) 149; (c) F. Raulin, Adv. Space Res. 7 (1987) 71; (d) M.C. Pietrogrande, P. Coll, R. Sternberg, C. Szopa, R. Navarro-Gonzales, C. Vidal-Madjar, F. Dondi, J. Chromatogr. A 939 (2001) 69.
[6] P.M. Woods, T.J. Millar, A.A. Zijlstra, E. Herbst, Astrophys. J. 574 (2002) L167.
[7] (a) S. Petrie, D.K. Bohme, Top. Curr. Chem. 225 (2003) 37; (b) S. Petrie, D.K. Bohme, Mass Spectrom. Rev., in press.
[8] C.F. Chyba, P.J. Thomas, L. Brookshaw, C. Sagan, Science 249 (1990) 366.
[9] Y.-J. Kuan, S.B. Charnley, H.-C. Huang, Z. Kisiel, P. Ehrenfreund, W.-L. Tseng, C.-H. Yan, Adv. Space Res. 33 (2004) 31.
[10] (a) M.N. Simon, M. Simon, Astrophys. J. 184 (1973) 757; (b) Y.-J. Kuan, C.-H. Yan, S.B. Charnley, Z. Kisiel, P. Ehrenfreund, H.-C. Huang, Royal Astro. Soc. 345 (2003) 650; (c) Z. Peeters, O. Botta, S.B. Charnley, Z. Kisiel, Y.-J. Kuan, P. Ehrenfreund, Astron. Astrophys. 433 (2005) 583.
[11] H.F. van Garderen, P.J.A. Ruttink, P.C. Burgers, G.A. McGibbon, J.K. Terlouw, Int. J. Mass Spectrom. Ion Proc. 121 (1992) 159.
[12] (a) J.W. Ochterski, G.A. Petersson, J.A. Montgomery Jr., J. Chem. Phys. 104 (1996) 2598; (b) J.A. Montgomery Jr., M.J. Frisch, J.W. Ochterski, G.A. Petersson, J. Chem. Phys. 112 (2000) 6532.
[13] (a) M.J. Frisch, G.W. Trucks, H.B. Schlegel, G.E. Scuseria, M.A. Robb, J.R. Cheeseman, V.G. Zakrzewski, J.A. Montgomery Jr., R.E. Stratmann, J.C. Burant, S. Dapprich, J.M. Millam, A.D. Daniels, K.N. Kudin, M.C. Strain, O. Farkas, J. Tomasi, V. Barone, M. Cossi, R. Cammi, B. Mennucci, C. Pomelli, C. Adamo, S. Clifford, J. Ochterski, G.A. Petersson, P.Y. Ayala, Q. Cui, K. Morokuma, N. Rega, P. Salvador, J.J. Dannenberg, D.K. Malick, A.D. Rabuck, K. Raghavachari, J.B. Foresman, J. Cioslowski, J.V. Ortiz, A.G. Baboul, B.B. Stefanov, G. Liu, A. Liashenko, P. Piskorz, I. Komaromi, R. Gomperts, R.L. Martin, D.J. Fox, T. Keith, M.A. Al-Laham, C.Y. Peng, A. Nanayakkara, M. Challacombe, P.M.W. Gill, B. Johnson, W. Chen, M.W. Wong, J.L. Andres, C. Gonzalez, M. Head-Gordon, E.S. Replogle, J.A. Pople, Gaussian 98 Revision A.11, Gaussian Inc., Pittsburg, PA, 1998; (b) M.J. Frisch, G.W. Trucks, H.B. Schlegel, G.E. Scuseria, M.A. Robb, J.R. Cheeseman, J.A. Montgomery Jr., T. Vreven, K.N. Kudin, J.C. Burant, J.M. Millam, S.S. Iyengar, J. Tomasi, V. Barone, B. Mennucci, M. Cossi, G. Scalmani, N. Rega, G.A. Petersson, H. Nakatsuji, M. Hada, M. Ehara, K. Toyota, R. Fukuda, J. Hasegawa, M. Ishida, T. Nakajima, Y. Honda, O. Kitao, H. Nakai, M. Klene, X. Li, J.E. Knox, H.P. Hratchian, J.B. Cross, V. Bakken, C. Adamo, J. Jaramillo, R. Gomperts, R.E. Stratmann, O. Yazyev, A.J. Austin, R. Cammi, C. Pomelli, J.W. Ochterski, P.Y. Ayala, K. Morokuma, G.A. Voth, P. Salvador, J.J. Dannenberg, V.G. Zakrzewski, S. Dapprich, A.D. Daniels, M.C. Strain, O. Farkas, D.K. Malick, A.D. Rabuck, K. Raghavachari, J.B. Foresman, J.V. Ortiz, Q. Cui, A.G. Baboul, S. Clifford, J. Cioslowski, B.B. Stefanov, G. Liu, A. Liashenko, P. Piskorz, I. Komaromi, R.L. Martin, D.J. Fox, T. Keith, M.A. Al-Laham, C.Y. Peng, A. Nanayakkara, M. Challacombe, P.M.W. Gill, B. Johnson, W. Chen,

M.W. Wong, C. Gonzalez, J.A. Pople, Gaussian 03 (Revision C.02), Gaussian, Inc., Wallingford, CT, 2004.
[14] GAMESS-UK is a package of ab initio programs written by M.F. Guest, J.H. van Lenthe, J. Kendrick, K. Schoffel, P. Sherwood, with contributions from R.D. Amos, R.J. Buenker, H.J.J. van Dam, M. Dupuis, N.C. Handy, I.H. Hillier, P.J. Knowles, V. Bonacic-Koutecky, W. von Niessen, R.J. Harrison, A.P. Rendell, V.R. Saunders, A.J. Stone, D.J. Tozer, A.H. de Vries. The package is derived from the original GAMES S code due to M. Dupuis, D. Spangler, J. Wendolowski, NRCC Software Catalogue 1, vol. 1, Program No. QG01 (GAMESS), 1980.
[15] L.N. Heydorn, Y. Ling, G. de Oliveria, J.M.L. Martin, Ch. Lifshitz, J.K. Terlouw, Zeitschrift f ür Physikalische Chemie 215 (2001) 141.
[16] P.M. Mayer, C.J. Parkinson, D.M. Smith, L. Radom, J. Chem. Phys. 108 (1998) 604.
[17] (a) D.R. Lide (Ed.), Handbook of Chemistry and Physics, 87th ed., CRC Press, Boca Raton, 2006; (b) E.P.L. Hunter, S.G. Lias, J. Phys. Chem. Ref. Data 27 (1998) 3; (c) NIST Chemistry WebBook, July 2006. National Institute of Standards and Technology, Gaithersburg, MD, 20899 (http://webbook.nist.gov); (d) Y.-R. Luo, Handbook of Dissociation Energies in Organic Compounds, CRC Press, Boca Raton, 2003; (e) S.G. Lias, J.E. Bartmess, J.F. Liebman, J.L. Holmes, R.O. Levin, W.G. Maillard, J. Phys. Chem. Ref. Data 17 (Suppl. 1) (1988).
[18] T. Bally, G.N. Sastry, J. Phys. Chem. A 101 (1997) 7923.
[19] J.W. Gauld, L. Radom, J. Am. Chem. Soc. 119 (1997) 9831.
[20] P.C. Burgers, J.K. Terlouw, in: N.M.M. Nibbering (Ed.), Encyclopedia of Mass Spectrometry, vol. 4, Elsevier, Amsterdam, 2005, p. 173.
[21] M. Ichihashi, Y. Sadanaga, T. Kondow, J. Chem. Phys. A 102 (1998) 8287.
[22] M. Meot-Ner, L.W. Sieck, J. Am. Chem. Soc. 113 (1991) 4448.
[23] T. Baer, W.L. Hase, Unimolecular Reaction Dynamics, Theory and Experiments, Oxford University Press, New York, 1996.
[24] T. Baer, J.A. Booze, in: W.L. Hase (Ed.), Advances in Classical Trajectory Methods, vol. 2, JAI Press Inc., Hampton Hill, 1994, p. 1.
[25] D.J. Lavorato, J.K. Terlouw, G.A. McGibbon, T.K. Dargel, W. Koch, H. Schwarz, Int. J. Mass Spectrom. 179–180 (1998) 7.
[26] G. Orlova, V. Blagojevic, D.K. Bohme, J. Phys. Chem. A 110 (2006) 8266.
[27] H.K. Ervasti, K.J. Jobst, P.C. Burgers, P.J.A. Ruttink, J.K. Terlouw, in preparation.

Chapter 6

A computational study of the pyrimidine radical cation: Its dissociation by loss of HC≡N and its generation by association of HC≡N with ionized acrylonitrile

Abstract

The CBS-QB3 computational method was used to probe mechanisms for the prominent loss of HCN that dominates the dissociation of metastable pyrimidine ions. This model chemistry was also used to explore the possibility that the pyrimidine ion is generated in the ion-molecule reaction of ionized acrylonitrile with HCN, a reaction of potential interest in interstellar chemistry.

Our calculations indicate that the HCN loss from low-energy pyrimidine ions yields the distonic $C_3H_3N^{\bullet+}$ ion $HC{=}CHC{=}NH^{\bullet+}$, rather than ionized acrylonitrile, $CH_2{=}CHC{\equiv}N^{\bullet+}$, or its more stable diene-imine isomer $CH_2{=}C{=}C{=}NH^{\bullet+}$, as proposed previously.

Our computational analysis of the ion-molecule reaction of $CH_2{=}CHC{\equiv}N^{\bullet+}$ and HCN indicates that generation of ionized pyrimidine is energetically feasible, *via* a multistep rearrangement from the covalently bound adduct ion $[HC{\equiv}N{-}C(H_2)C(H)C{\equiv}N]^{\bullet+}$.

Nevertheless, RRKM calculations predict that this reaction cannot effectively compete with Proton Transport Catalysis (PTC) in $CH_2{=}CHC{\equiv}N^{\bullet+}$/HCN encounter complexes which converts the acrylonitrile ion mainly into its more stable (and unreactive) isomer $CH_2{=}C{=}C{=}NH^{\bullet+}$. In these (hydrogen-bridged) encounter complexes a proton transfer reaction which leads to $HC{\equiv}N{-}H^+ + CH_2{=}C^{\bullet}{-}C{\equiv}N$ may also take place.

Henri K. Ervasti, Karl J. Jobst, Peter C. Burgers, Paul J.A. Ruttink, Johan K. Terlouw, manuscript for publication in preparation

Henri Ervasti (2008): Computational and experimental studies on stabilities, reactions and reaction rates of cations and ion-dipole complexes

1. Introduction

Ion-molecule interactions in the rarefied gas-phase have proven to be a good way to rationalise various reactions of relevance to astrochemistry that are not possible between neutral molecules [1]. Such interactions can lead to protonation and de-protonation, isomerisation by Proton-Transport Catalysis (PTC) [2], and the formation of new product molecules via various covalently bonded (metastable) reaction intermediates and their (possible) consecutive dissociations [2,3].

A case in point is the study of Chapter 5 on the ion-molecule reaction of the acrylonitrile ion with its neutral counterpart [4]. The resulting dimer radical cation does not only dissociate by self-protonation, it can also rearrange to yield the pyrimidine ion by loss of C_2H_2. Ion-molecule reaction studies using Selected Ion Flow Tube (SIFT) experiments by Petrie et al. [5] indicate that the dimer formation takes place at close to the collision rate. This observation was later confirmed with flowing afterglow selected-ion flow drift tube (FA/SIFDT) experiments [6], which show a 30% yield of the complex, the major reaction (70%) being self-protonation. These observations make it reasonable to assume that the above pyrimidine ion formation also plays a role in astrochemistry, as acrylonitrile [7a] is a confirmed species in interstellar dust clouds. The prebiotic pyrimidine molecule could also be formed in interstellar clouds by the reaction of neutral acrylonitrile and HCN (also a confirmed species in interstellar dust clouds [7b]) but so far there is no experimental or computational support for this suggestion [8].

An a priori more attractive possibility for the gas-phase synthesis of (ionized) pyrimidine involves the reaction of *ionized* acrylonitrile with HCN. This ion-molecule reaction has also been the topic of a SIFT study by Petrie et al. [5]. This study shows that the reaction results mainly in adduct formation with varying degrees of H loss. The reaction is evidently exothermic in view of the number of product channels, yet it occurs at only 6% of the collision rate. The authors argue that such a behaviour indicates that "the adduct $C_4H_4N_2^{\bullet+}$ does not correspond to a deep well in the CH_2=CHC≡$N^{\bullet+}$/HCN potential energy surface, a deduction which would remove the aromatic cations of pyrazine, pyridazine and *pyrimidine* from contention as possible product ions." However, it should be noted that this "deduction" only refers to the probability that the ion-molecule reaction CH_2=CHC≡$N^{\bullet+}$ + HCN plays a role in astrochemistry. This is because the observed low total bimolecular rate coefficient indicates that efficient radiative stabilization of the complex ion is unlikely. In other words, there is no reason (nor experimental evidence) to assume that ionized pyrimidine is not generated by the ion-molecule reaction under SIFT conditions where the complex is stabilized by collisions. Another intriguing question concerns the contention that the $C_4H_4N_2^{\bullet+}$ adduct ion does not occupy a deep potential well: on the basis of simple ion-dipole (molecule) interactions it is difficult to see why CH_2=CHC≡$N^{\bullet+}$/HCN complexes would behave differently from the CH_2=CHC≡$N^{\bullet+}$/CH_2=CHC≡N complexes discussed in Chapter 5.

These considerations prompted us to use computational chemistry to probe the structure(s) and the dissociation chemistry of CH_2=CHC≡$N^{\bullet+}$/HCN complexes generated by the ion-molecule reaction of the $C_3H_3N^{\bullet+}$ isomer CH_2=CHC≡$N^{\bullet+}$ with HCN, with the emphasis on the potential generation of the pyrimidine radical cation.

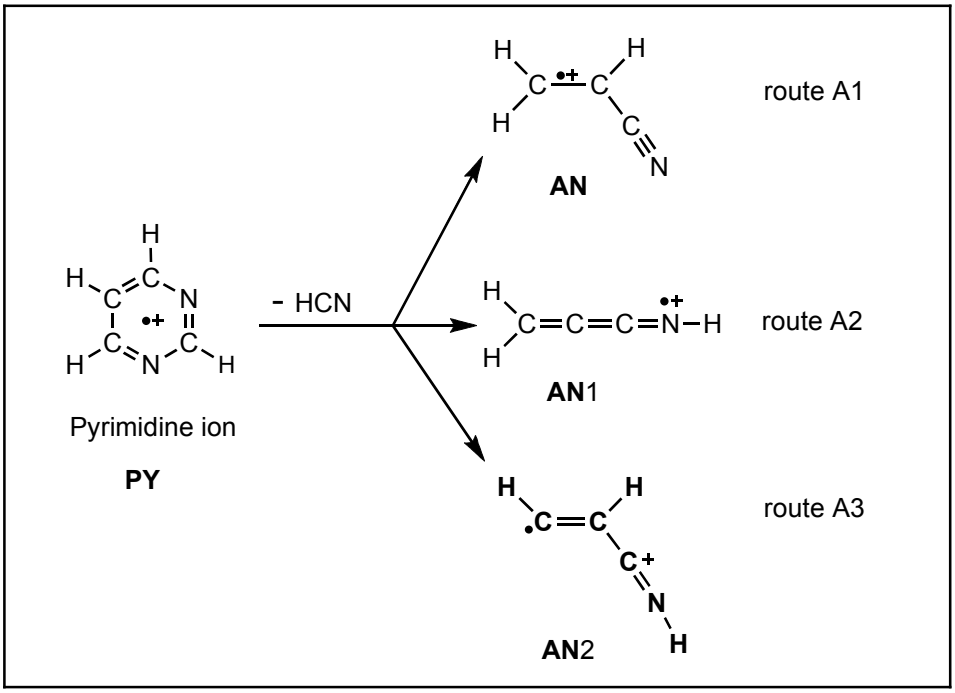

Scheme 1.

First, we will present a computational analysis of the dissociation chemistry of the pyrimidine radical cation. This because detailed experimental studies [9,10] show that pyrimidine ions predominantly dissociate by loss of HCN into $C_3H_3N^{\bullet+}$ ions.

The photoelectron-photoion coincidence (PEPICO) study by Buff and Dannacher [9] shows that this process represents the dissociation reaction of lowest energy requirement and that it has a critical energy of ~63 kcal mol^{-1}. This implies that the energy level for $C_3H_3N^{\bullet+}$ + HCN lies at 323 ± 2 kcal mol^{-1} and that the heat of formation of the $C_3H_3N^{\bullet+}$ product ion is ≤ 293 kcal mol^{-1}. Buff and Dannacher further proposed that the reaction takes place via route A1 of Scheme 1, to yield ionized acrylonitrile, CH_2=CHC≡$N^{\bullet+}$ (**AN**), as the $C_3H_3N^{\bullet+}$ product ion. The combined tandem mass spectrometric and theoretical study of ionized pyrimidine and its 1,2-H shift isomers [10] concludes that this is clearly not the case: the CID mass spectrum of **AN** is entirely different from that of the $C_3H_3N^{\bullet+}$ ions generated from metastable and/or collis ionally energized pyrimidine ions. Instead, this study proposes that the reaction follows route A2 of Scheme 1, yielding the remarkably stable ionic acrylonitrile isomer CH_2=C=C=$NH^{\bullet+}$ (**AN**1). However, a very recent experimental and theoretical study of ionized acrylonitrile and its principal isomers [11] provides strong evidence that the CID mass spectrum of ref. 9 is not that of **AN**1 but rather that of the distonic ion **AN**2 depicted as the product ion of route A3 in Scheme 1. The calculated $\Delta_fH^o_{298}$ values for **AN**, **AN**1 and **AN**2 are 297, 281 and 287 kcal mol^{-1}

respectively [11], from CBS-APNO calculations. Thus, metastable pyrimidine ions do not lose HCN to yield ionized acrylonitrile, but rather yield a more stable isomer. Our computational analysis presented in Section 3.1. provides an attractive mechanistic rationale for route A3 which satisfies the tentative identification of the structure of the product ion, **AN**2. As mentioned above, the main objective of the present study is to examine whether a gas-phase synthesis of the pyrimidine ion may be expected to occur in encounter complexes of ionized acrylonitrile and HCN, that is, the reverse of route A1 in Scheme 1.

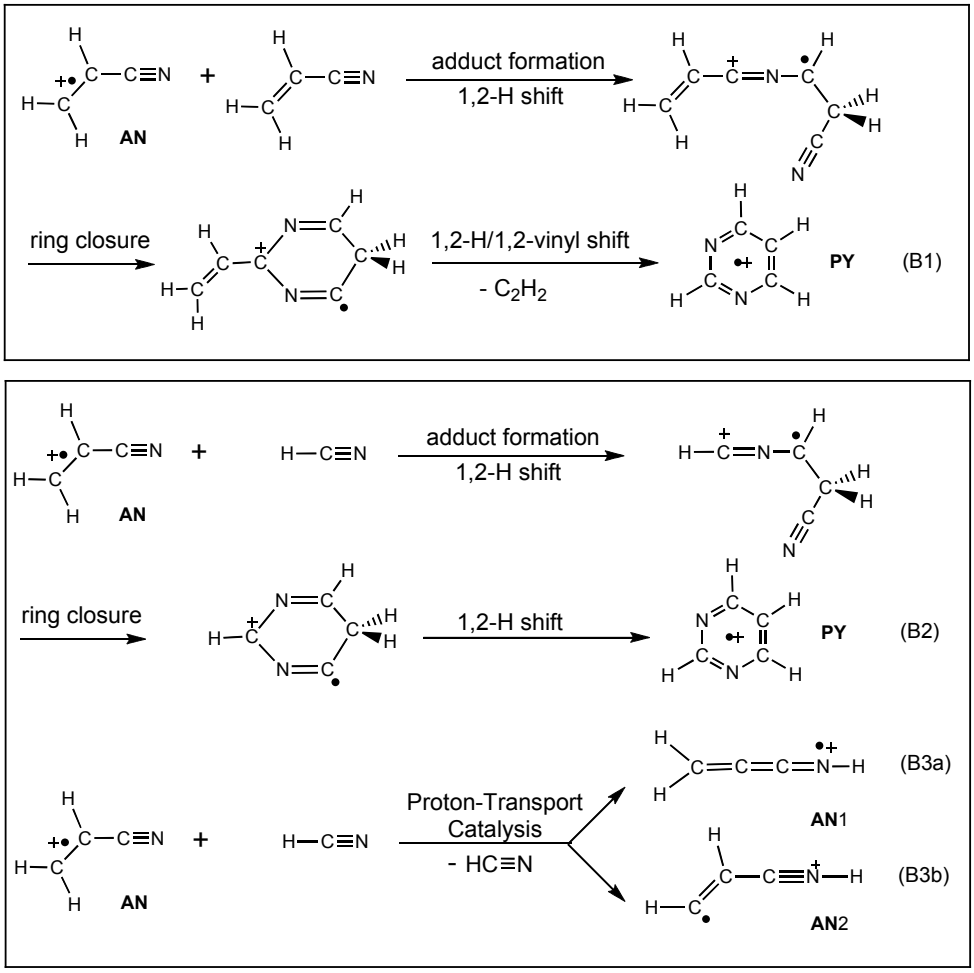

Scheme 2.

One possibility would be that it occurs by route B2 of Scheme 2, that is, analogously to the mechanism reported in Chapter 5 for the reaction of **AN** with its neutral counterpart.

AN forms a covalently bound head-to-tail dimer with its neutral counterpart and then proceeds to ring closure and C_2H_2 elimination to form pyrimidine, as shown in reaction B1 of Scheme 2 (some steps omitted, see Chapter 5 for the full description). We have also examined potentially competing reaction paths, *viz*. protonation of HCN by **AN**, and the HCN catalysed isomerization of **AN** into **AN**1 or **AN**2, shown as reactions B3(a) and B3(b) of Scheme 2.

It will be shown in Section 3.2. that from an energetic point of view, reactions B2 and B3(a,b), as well as the protonation – deprotonation reaction that leads to $HC{\equiv}N{-}H^+$ + $CH_2{=}C^{\bullet}{-}C{\equiv}N$ are all feasible.

The isomerisation of **AN** into **AN**1 by proton transport catalysis is the route of lowest energy requirement and RRKM-based reaction-rate constant calculations predict that the pyrimidine ion formation cannot effectively compete with the PTC and protonation – deprotonation reactions.

2.Theoretical methods

The calculations were performed with the CBS-QB3 model chemistry [12] using Gaussian 98 and Gaussian 03 [13] and for selected transition state searches GAMESS-UK [14] was used. In this model chemistry, the geometries of minima and transition states are obtained using the B3LYP density functional theory functional, as they are implemented in the respective programs, in combination with the 6-311G(2d,d,p) basis set (also denoted as the CBSB7 basis set). All the computational results are found in Table 1. These include the energies in Hartree, zero-point energies (ZPE) in kcal mol^{-1}, and heats of formation at 0K and 298K in kcal mol^{-1}, which are calculated using Radom's method [15]. The resulting energy level diagrams are shown in Schemes 3 and 4, and molecular structures in Figure 1. The correctness of transition states was verified (where not trivially evident) by means of Intrinsic Reaction Coordinate (IRC) calculations.

Several of the calculations showed spin contamination beyond the accepted values (0.75-0.79). The largest $<S^2>$ value was found to be 1.50 for TS **D**4-**PY** (see Table 1). It is not expected (see Chapter 5) that this will greatly affect the estimated accuracy of the energies of the minima and the transition states. For example, CBS-APNO calculations on **AN**R1 ($<S^2>$ = 1.39) and TS **D**4-**PY** yield 100 and 299 kcal mol^{-1}, almost equal to the CBS-QB3 results (Table 1).

The geometry optimization of TS **HB**1–**HB**2 is complicated by the change of symmetry going from **HB**1 (^{2}A") to **HB**2 (^{2}A'). Keeping the nuclear framework planar would result in a crossing geometry, where the energies of the two possible wave functions are equal. The Minimal Energy Crossing Point [16] does not correspond to a stationary point on either PES. However, a TS with a lower energy should exist for a non-planar geometry, where the wave functions of the two symmetries are mixed. This TS was foundusing a number of partial optimizations, where in each optimization the reaction coordinate is kept fixed (Opt=ModRedundant in Gaussian). The value of the reaction coordinate is changed by small steps going from one optimization to the next one. The final geometry from the optimization with the highest energy is taken as the starting geometry

Table 1. Collected S^2 values from the last step of the CBS-QB3 calculation, CBS-QB3 0K energies in Hartree, scaled zero-point energies (ZPE), heats of formation at 0K and 298K, and proton affinities (PA) of selected molecules in kcal mol^{-1}.

Species	S^2	$E_{CBS-QB3}$ (0 K)	ZPE	$\Delta_f H$ (0 K)	$\Delta_f H$ (298 K)	PA
CN^-	1.13	-92.587532	3.0	106	107	118
HCN	-	-93.287505	10.2	32	32	171
$HCNH^+$	-	-93.558307	16.3	227	226	
ANR1 (CH_2CCN^-)	1.39	-169.87318	22.2	100	100	[a]167/184
ANR2 ($CHCHCN^-$)	1.14	-169.86085	22.7	108	107	[b]175/192
ANP (CH_2CHCNH^+)	-	-170.83608	38.2	227	224	
AN ($CH_2CHCN^{\cdot+}$)	0.99	-170.13793	30.4	299	298	
AN1 ($CH_2CCNH^{\cdot+}$)	1.19	-170.16622	28.4	282	281	
AN2 ($CHCHCNH^{\cdot+}$)	0.99	-170.15456	29.5	289	288	
AN3 ($CH_2CNCH^{\cdot+}$)	1.40	-170.13919	28.4	299	297	
HB1	0.99	-263.44906	41.2	316	315	
HB1a	0.99	-264.44810	41.3	317	316	
HB2	1.25	-263.49064	39.7	290	289	
HB3	1.02	-263.47936	40.4	297	296	
TS **HB1-D1**	0.99	-263.44788	41.1	317	315	
TS **HB1-HB2**	1.32	-263.43521	37.9	325	323	
TS **HB1a-HB3**	1.21	-263.42936	38.7	329	327	
D1	0.97	-263.49108	43.5	290	288	
D2	0.92	-263.48996	43.0	291	288	
D3	1.10	-263.47297	44.0	301	298	
D4	1.46	-263.47266	43.6	302	299	
D5	0.96	-263.49249	43.1	289	287	
Db1	1.13	-263.46756	42.1	305	303	
D1 [– H^-]	-	-262.92228	37.6	282	280	
PY	1.28	-263.53204	46.8	264	260	
PY1	0.95	-263.52314	47.6	270	266	
TS **D**1-**D**2	1.06	-263.42636	40.5	331	328	
TS **D**2-**D**3	0.98	-263.47093	43.0	303	299	
TS **D**2-**D**4	1.23	-263.41275	39.8	339	336	

Table 1, continued

TS **D**3-**PY**	0.92	-263.43094	43.4	328	324
TS **D**4-**PY**	1.50	-263.46953	43.6	304	300
TS **PY**-**PY**1	1.00	-263.43340	42.5	326	323
TS **PY**1-**D**5	1.33	-263.46678	43.1	305	302

[a] PA at C_2/N
[b] PA at C_1/N

for the final TS geometry optimization. Since we expect the TS to be non-planar, it is important to start the first partial optimization with a slightly non-planar geometry.

For selected transition states, an RRKM [17] study was performed to estimate the reaction rates in the various reaction paths. The reaction rates were calculated with and without rotational constants, using the Beyer-Swinehart [18] direct-count algorithm. The results yield an upper bound to the actual reaction rates and these rates allow a comparison between the reaction rates of selected reaction paths and product yields.

3. Results and discussion

3.1 The HCN loss from low-energy pyrimidine ions

In the PEPICO study [9] mentioned above, the appearance energy for the loss of HCN from pyrimidine was found to lie at 323 ± 2 kcal mol^{-1}. This value will serve as the "dissociation limit" for our reaction path calculations. We anticipate from the experimental results of Lavorato *et al*. [10] that dissociation into **AN**1 + HCN, or **AN**2 + HCN will be the prevailing reaction.

The potential energy diagram of Scheme 3 shows that starting from the pyrimidine radical cation, **PY**, a simple dissociation pathway into **AN**2 + HCN is available. From **PY** we reach the experimentally characterized [10] pyrimidine-2-ylidene, **PY**1**,** via a 1,2 H-shift, whose TS lies at 323 kcal mol^{-1}, that is, at the experimentally determined dissociation limit. A consecutive ring opening via a relatively low TS **PY**1-**D**5 at 302 kcal mol^{-1} leads to **D**5, which can then dissociate into **AN**2 + HCN. The combined heat of formation of **AN**2 + HCN is 320 kcal mol^{-1} (see Table 1), making it a favourable dissociation product. The formation of the more stable **AN**1 isomer (via the PTC reaction path of Scheme 4) can be ruled out, as it requires passing TS **D1-D2**, which lies too high in energy.

Other possible reactions starting from **PY** include a 1,2-H shift from the carbon between the two nitrogens to the adjacent nitrogen atom. The TS for this reaction has been reported [10] to lay circa 5 kcal mol^{-1} higher in energy (**TS 1**$^{\bullet+}$/**3**$^{\bullet+}$ in ref. 10) than the already proposed 1,2 H-shift (**TS 1**$^{\bullet+}$/**2**$^{\bullet+}$ in ref. 10), and thus this isomerization can be ruled out.

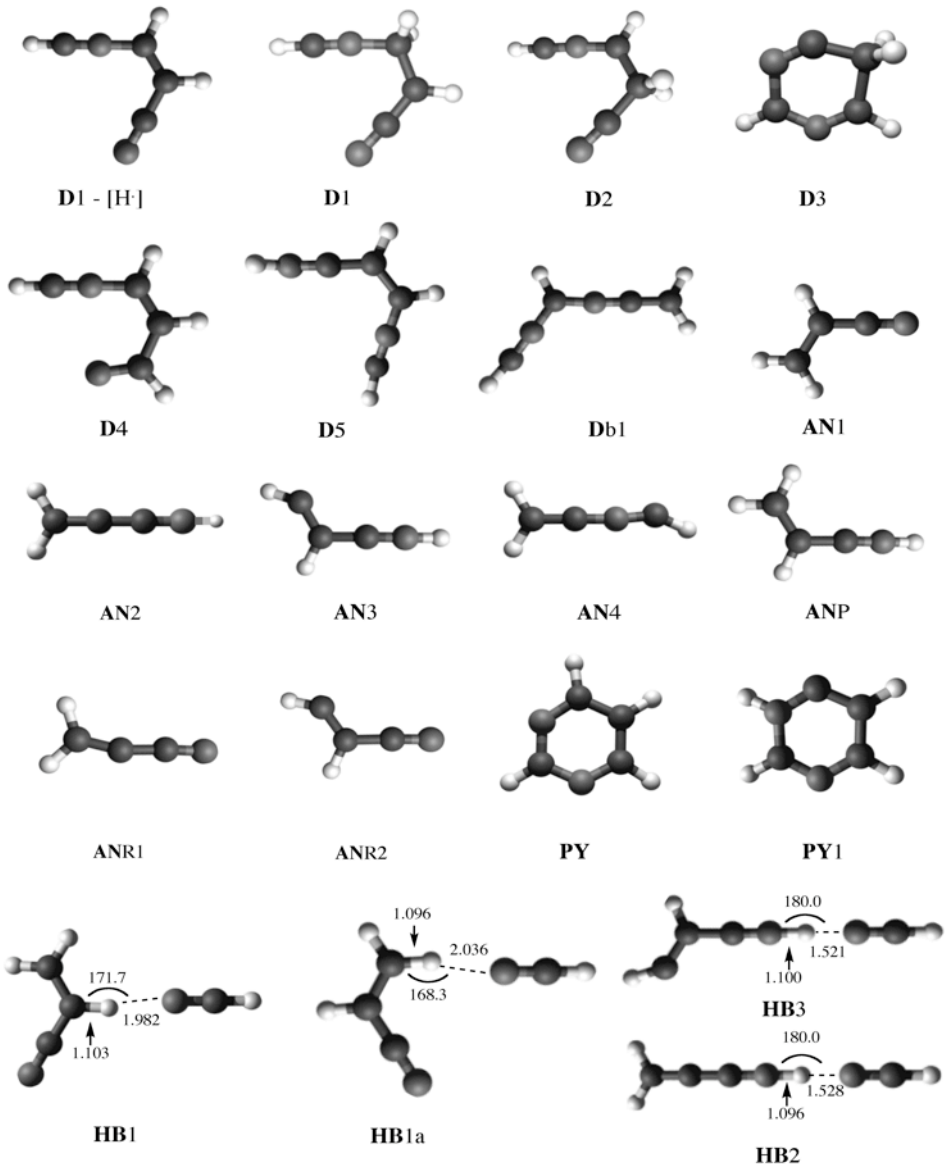

Figure 1: Geometries and structural information of the ground and transition state structures.

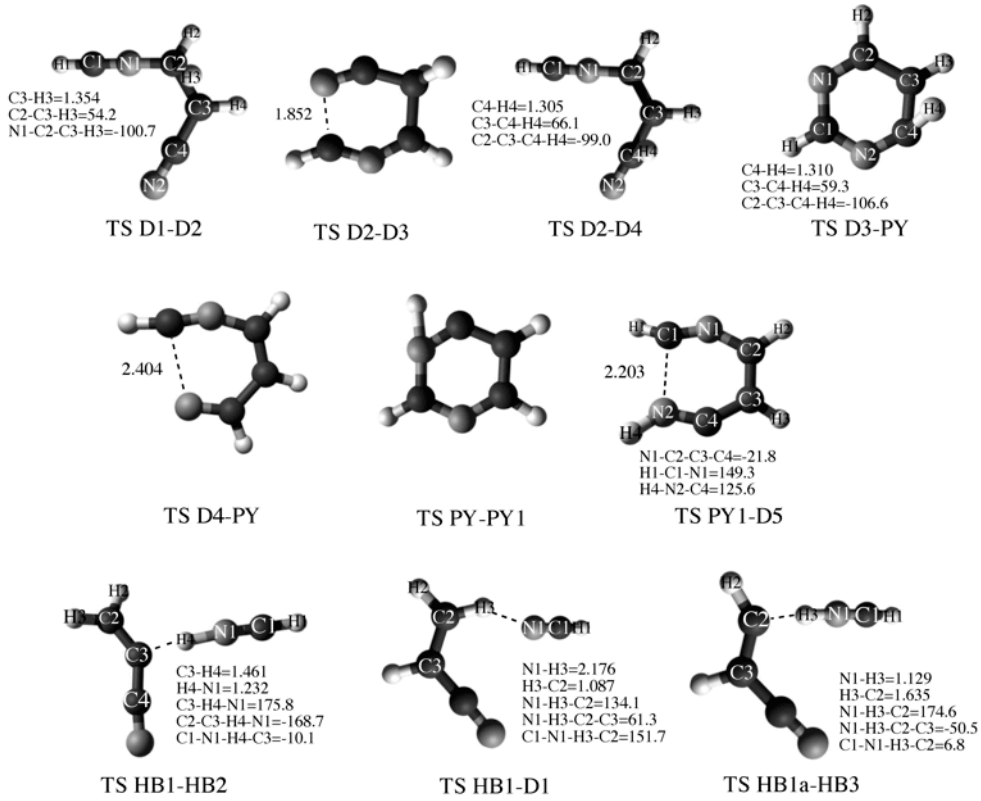

Figure 1, continued.

Yet another 1,2 H-shift can be envisaged: the transformation **PY** to **D**3 whose TS lies at 324 kcal mol^{-1}, slightly above the experimental dissociation limit. This route can also be ruled out since it is too energy demanding: it leads either to **AN**3 + HCN at 329 kcal mol^{-1}, or to **AN** + HCN at 330 kcal mol^{-1}. Other 1,2 H-shifts in **PY** are conceivable, but these are energetically even more unfavourable [10].

A ring opening between the nitrogen-sandwiched C(H) and either of the nitrogens has a TS of only 300 kcal mol^{-1} to form ion **D**4 whose structure is shown in Scheme 3. This ion could lose HCN by direct bond cleavage to yield two different $C_3H_3N^{\bullet+}$ isomers whose enthalpies [11] are higher than that of **AN**. Scheme 3 further shows that further rearrangements of ion **D**4 are too energy demanding.

Thus we propose that the loss of HCN from low-energy pyrimidine ions leads to the acrylonitrile isomer **AN**2 via a 1,2 H-shift and a consecutive ring opening as discussed above and presented in Scheme 3. Further support for this proposal comes from the observation that the kinetic energy release ($T_{0.5}$ value) for the loss of HCN from **PY** (32 meV) is slightly higher than that for the loss of HCN from **PY**1 (13 meV) [10].

3.2. The AN + HCN ion-molecule reaction

Pyrimidine formation

For the reaction involving **AN** and HCN, we now have the dissociation limit at 330 kcal mol^{-1}, as can be seen from Scheme 4. The covalently bound dimer ion, **D**1, formed from the association of the two monomers, has a stabilization energy of 42 kcal mol^{-1} against back-dissociation.

This ion can rearrange by a 1,2 H-shift to **D**2 with the TS lying at 328 kcal mol^{-1} (Scheme 3), just below the dissociation limit. The transformation of this ion into **D**4 is unfavourable: TS **D**2-**D**4 lies at 336 kcal mol^{-1}, 6 kcal mol^{-1} above the dissociation limit. Ion **D**2 could also lose H$^{\bullet}$, but the energy level for this dissociation lies fairly high in energy, at 332 kcal mol^{-1} (from the data in Table 1).

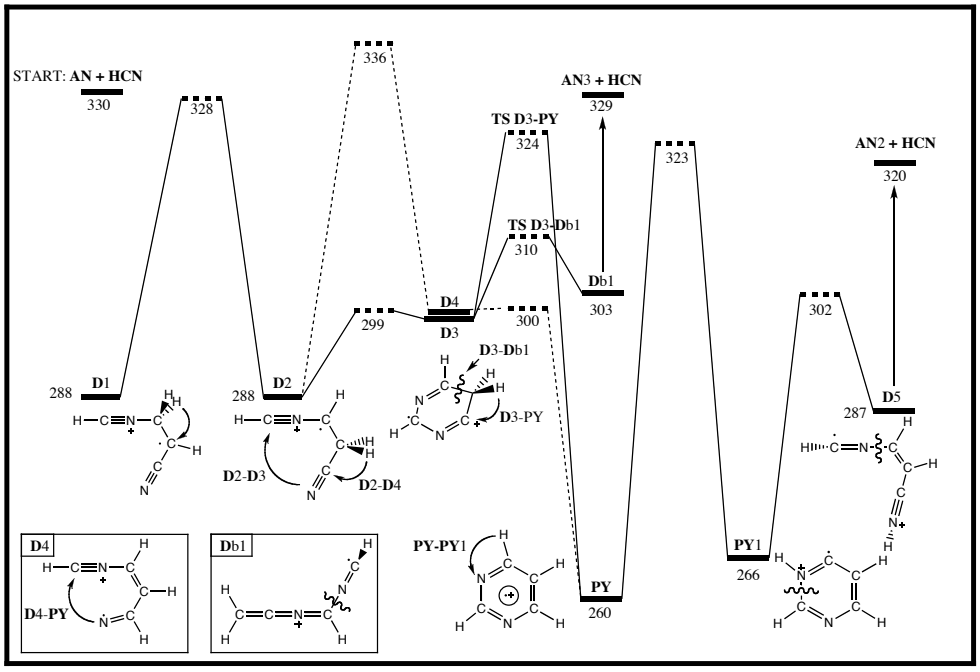

Scheme 3. Energy level diagram for the ion-molecule reaction **AN** + HCN leading to the formation of the pyrimidine ion (**PY**) and the loss of HCN. The dashed line indicates an alternative route between **D**2 and **PY** of higher energy requirement. All energies are in kcal mol^{-1}.

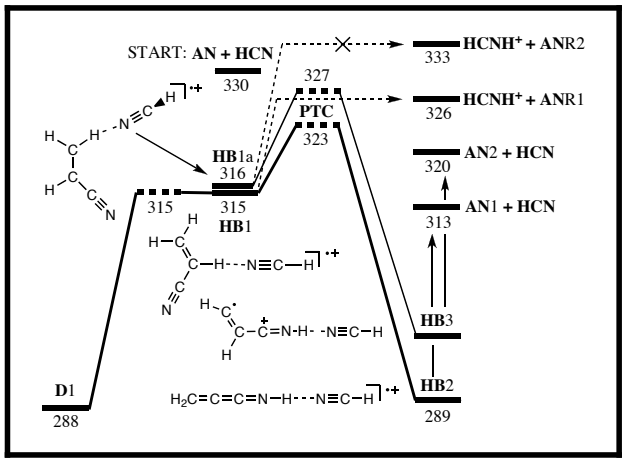

Scheme 4. An energy level diagram for the ion-molecule reactions of association of **AN** + HCN. The solid lines indicate proton transport catalysis (PTC) reaction paths. Dashed lines are for the proton transfer reactions. Note that **D**1 is the same as in Scheme 3.

Instead, ion **D**2 may undergo a facile ring closure (TS at 299 kcal mol^{-1}), forming pyrimidine's 1,2 H-shift isomer **D**3 at 298 kcal mol^{-1}. A second energy demanding 1,2 H-shift, whose TS lies at 324 kcal mol^{-1}, would complete the transformation of **D**2 into **PY**. Scheme 3 shows how the pyrimidine radical cation occupies a deep potential well relative to continued or reverse reactions. **PY** can nevertheless isomerise into **PY**1 and finally dissociate to products **AN**2 and HCN at 320 kcal mol^{-1}, via TS **PY**1-**D**5 at 302 kcal mol^{-1}, and **D**5 at 287 kcal mol^{-1} (Scheme 3).

Protonation reactions

In the system studied, there are possibilities to form two hydrogen-bridged complexes, such as [HC≡N•••H–C(=CH_2)C≡N^+] (**HB**1) and [HC≡N•••H–C(H)=C(H)C≡N^+] (**HB**1a). The first complex goes through a proton transfer reaction and the Δ_fH_{298K} of the products ($HCNH^+$ + **AN**R1**)** is at 326 kcal mol^{-1} (from Table 1), 4 kcal mol^{-1} under the starting energy. The second complex suggests the possibility for proton abstraction from the methylene group, leading to the formation of $HCNH^+$ and **AN**R2. The Δ_fH_{298K} sum for this reaction's products equals 333 kcal mol^{-1} (Table 1), making it unlikely as it is above our energy limit.

Clearly, of the two reactions mentioned above, the first is energetically more favourable. Since the proton affinity of HCN is higher than that of C_2 in **AN**R1 (171 versus 167 kcal mol^{-1}, see Table 1), protonation of HCN takes place. A similar reaction to form **AN**R2 + $HCNH^+$ is not likely, because the PA at C_1 (Table 1) is 4 kcal mol^{-1} larger than that of HCN.

Proton Transport Catalysis (PTC) reactions

The fact that the proton affinity of HCN (171 kcal mol^{-1}) is in between the PA of **AN**R1 at C (167 kcal mol^{-1}), and the PA of **AN**R1 at N (185 kcal mol^{-1}), indicates the possibility of a PTC reaction.

Initially, a hydrogen bridged radical cation, **HB**1, is formed from the reactants **AN** + HCN (Scheme 4). The catalyst, HCN, moves the proton connected to the middle C atom in the **AN** moiety to the N atom to form **AN**1. Scheme 4 shows that this leads to the formation

of **HB**1, which then through the TS **HB**1-**HB**2 at 323 kcal mol^{-1} yields **HB**2. This TS is 5 kcal mol^{-1} below the TS **D**1-**D**2 in the pyrimidine formation and 3 kcal mol^{-1} below the products of the protonation reaction, $HCNH^+$ + **AN**R1. Ion **HB**2 then dissociates into **AN**1 + HCN with a combined $\sum\Delta_fH_{298K}$ of 313 kcal mol^{-1} (Table 1). This means we would get isomer **AN**1 as the main product from the reactants **AN** and HCN.

The geometry for TS **HB**1-**HB**2 was found as described in Section 2. The bridging N—H distance was taken as the reaction coordinate. The non-planarity of the TS reveals itself in the internal rotation of the CH_2 group. That this rotation is necessary to enable the transition explains that the activation barrier (8 kcal mol^{-1}) is much higher than one would expect on the basis of the relevant PAs (167, 171 and 184 kcal mol^{-1} for CH_2=C$^\bullet$-CN at C$^\bullet$, HCN and CH_2=C$^\bullet$-CN at N respectively).

A similar reaction with **AN**R2 might be possible, leading from **HB**1a, HCN•••HC(H)=CH-$CN^{\bullet+}$ to **HB**3, HC$^\bullet$=CH-CNH^+•••NCH. Here too the transition is accompanied by a change of the wave function symmetry. The matching TS **HB**1a–**HB**3 was found in the same way as TS **HB**1–**HB**2 and appears to lie at 327 kcal mol^{-1}, 3 kcal mol^{-1} below the starting energy (**AN** + HCN at 330 kcal mol^{-1}**)**. Therefore this reaction also plays a role in our system. Note that the activation barrier with respect to **HB**1a (11 kcal mol^{-1}) is higher than in the previous case (8 kcal mol^{-1}), which may be explained by the higher PA of **AN**R2 at the terminal C (175 kcal mol^{-1}) compared to the PA of HCN (171 kcal mol^{-1}).

RRKM studies

Even though the PTC reaction is on energetic terms the most favoured reaction, other reactions might also occur due to kinetic aspects in non-statistical behaviour incited by the ion-dipole interactions of the ion-molecule complex, similarly to the acrylonitrile dimer system [4].

The competing reaction paths for the **AN** + HCN reaction are the pyrimidine formation and its dissociation into **AN**2 + HCN, and the PTC reactions to form **AN**1 + HCN or **AN**2 + HCN. These correspond to reactions B2 + A3, B3(a), and B3(b) in Schemes 1 and 2, respectively. The covalently bound dimer ion **D**1 and TS **D**1-**D**2 are used in the rate determination of the first reaction and **HB**1 with TS **HB**1-**HB**2 for the second reaction. Δ_fH_{298K} energy of 330 kcal mol^{-1}, the starting energy, and 335 kcal mol^{-1} was applied in the RRKM calculations.

From the two competing PTC-reactions with the rearrangement of **AN** to **AN**1 or **AN**2, the B3(a) reaction to produce **AN**1 (Scheme 4) is slightly over 100 times faster than B3(b) for a total energy of 330 kcal mol^{-1} (see Table 2). An increase in the total energy of the system to 335 kcal mol^{-1} lowers this ratio to 25:1, implying that at higher energies **AN**2 formation might become a competing process.

The RRKM results indicate that rearrangement via the PTC-reaction B3(a) is over eight orders of magnitude faster than the B2 + A3 reaction. Addition of more internal energy to the system does not change this situation much. At a total energy of 335 kcal mol^{-1}, see Table 2, the reaction rate of reaction B2 + A3 increases by almost a factor of a thousand, while the rate of reaction B3(a) increases by only a factor of five. The difference is still nevertheless too large for any pyrimidine formation in the system and much more excess energy would be needed for pyrimidine formation to become competitive.

Therefore, using the RRKM results we argue that the formation of the pyrimidine ion does not occur to any meaningful extent in the association reaction studied, even though the process was found to be *energetically* possible.

Table 2. The RRKM reaction rates from selected ground and transition states, in s^{-1}. Total energy (E_{TOT}), activation energy (E_{ACT}) and excess energy (E_{XS}) in kcal mol^{-1}.

Ground state	Transition state	E_{TOT}	E_{ACT}	E_{XS}	k (s^{-1})
D1	TS **D**1-**D**2	330	40	2	8.64E+00
		335	40	7	3.60E+03
HB1	TS **HB**1-**HB**2	330	8	7	1.00E+09
		335	8	12	5.19E+09
HB1a	TS **HB**1a-**HB**3	330	11	3	8.88E+06
		335	11	8	2.07E+08

4. Conclusions

With our calculations we have shown that the loss of HCN from low-energy pyrimidine ions exclusively yields the **AN**2 isomer as the complementary dissociation product. Both the formation of **AN** and **AN**1 ions include energy-demanding steps which are above the experimentally determined dissociation limit, 323 kcal mol^{-1}, and thus their formation is not expected.

The reaction relevant to interstellar chemistry, **AN** + HCN, has been suggested [5] to result into various degrees of H dissociation and adduct formation. The possibility of pyrimidine formation was considered unlikely as it was thought that pyrimidine has only a shallow potential well against the reactants. In contrast, our computations leave no doubt that a deep potential well (70 kcal mol^{-1} compared to the starting energy of 330 kcal mol^{-1}) is apparent for pyrimidine, making it reasonable to assume, due to collisional stabilisation, that it could contribute to the observed $C_4H_4N_2^+$ peak in the experiments by Petrie at al. [5]. The pyrimidine ion would, however, eventually dissociate into **AN**2 + HCN as this reaction is energetically feasible.

The main reaction in the association of **AN** + HCN is a Proton Transport Catalysis reaction, which leads to the isomerization of **AN** into **AN**1. The highest point in the energy level diagram is at only 323 kcal mol^{-1}. Also feasible is an isomerization leading to isomer **AN**2 through a PTC reaction, although this reaction is estimated to be a 100 times slower than the **AN**1 formation. For the pyrimidine ion formation the rate-determining TS lies at 328 kcal mol^{-1}. According to our RRKM analysis, this reaction is about eight orders of magnitude slower than the PTC reaction. Formation of protonated HCN and **AN**R1 was also found to be energetically feasible, although this would also be a minor process in low-energy reactions.

References

[1] S. Petrie, D.K. Böhme, Mass Spectrom. Rev. 26(2) (2007) 258.
[2] For selected recent references see : (a) G. van der Rest, P. Mourgues, H.E. Audier, Int. J. Mass Spectrom. 231 (2004) 83; (b) C.Y. Wong, P.J.A. Ruttink, P.C. Burgers, J.K.Terlouw, Chem. Phys. Lett. 390, (2004) 176; (ibid) 387 (2004) 204: (c) X. Wang, J.L. Holmes, Can. J. Chem. 83 (2005) 1903 ; (d) P.C. Burgers, P.J.A. Ruttink, Int. J. Mass Spectrom. 242 (2005) 49; (d) For an early review see : D.K. Böhme, Int. J. Mass Spectrom. 115 (1992) 95.
[3] E. Uggerud, Mass Spectrometry Reviews 11 (1992) 389.
[4] H. K. Ervasti, K. J. Jobst, P. C. Burgers, P. J. A. Ruttink, and J. K. Terlouw, Int. J. Mass Spectrom. 262 (2007) 88.
[5] S. Petrie, T. J. Chirnside, C. G. Freeman, M. J. McEwan, Int. J. Mass Spectrom. Ion Processes 107 (1991) 319.
[6] D. B. Milligan, P.F. Wilson, M. J. McEwan, V. G. Anicich, Int. J. Mass Spectrom. 185/7 (1999) 663.
[7] (a) F.F. Gardner, G. Winnewisser, Astrophys. J. 195 (1975) L127; (b) L.E. Snyder and D Buhl, Astrophys J. 163 (1971) L47.
[8] (a) M.N. Simon, M. Simon, Astrophys. J. 184 (1973) 757 ; (b) Y.-J. Kuan, C.-H. Yan, S.B. Charnley, Z. Kisiel, P. Ehrenfreund, H.-C. Huang, Royal Astro. Soc. 345 (2003) 650; (c) Z. Peeters, O. Botta, S.B. Charnley, Z. Kisiel, Y.-J. Kuan, P. Ehrenfreund, Astron. Astrophys. 433 (2005) 583.
[9] R. Buff, J. Dannacher, Int. J. Mass Spectrom. Ion Processes 62 (1984) 1.
[10] D. J. Lavorato, T.K. Dargel, W. Koch, G.A. McGibbon, H. Schwarz, J.K. Terlouw, Int. J. Mass Spec. 210/211 (2001) 43.
[11] K.J. Jobst, S.A. Hasan, J.K.Terlouw, Chem. Phys. Lett. 450(4-6) (2008) 243.
[12] J.A. Montgomery, Jr, M.J. Frisch, J.W. Ochterski, G.A. Petersson, J. Chem. Phys. 110 (1999) 2822; ibid. 112 (2000) 6532.
[13] Gaussian 98 (Revision A.7), M. J. Frisch, G. W. Trucks, H. B. Schlegel, G. E. Scuseria, M. A. Robb, J. R. Cheeseman, V. G. Zakrzewski, J. A. Montgomery, Jr., R. E. Stratmann, J. C. Burant, S. Dapprich, J. M. Millam, A. D. Daniels, K. N. Kudin, M. C. Strain, O. Farkas, J. Tomasi, V. Barone, M. Cossi, R. Cammi, B. Mennucci, C. Pomelli, C. Adamo, S. Clifford, J. Ochterski, G. A. Petersson, P. Y. Ayala, Q. Cui, K. Morokuma, D. K. Malick, A. D. Rabuck, K. Raghavachari, J. B. Foresman, J. Cioslowski, J. V. Ortiz, A. G. Baboul, B. B. Stefanov, G. Liu, A. Liashenko, P. Piskorz, I. Komaromi, R. Gomperts, R. L. Martin, D. J. Fox, T. Keith, M. A. Al-Laham, C. Y. Peng, A. Nanayakkara, C. Gonzalez, M. Challacombe, P. M. W. Gill, B. Johnson, W. Chen, M. W. Wong, J. L. Andres, C. Gonzalez, M. Head-Gordon, E. S. Replogle, and J. A. Pople, Gaussian, Inc., Pittsburgh PA, 1998.
[14] M.F. Guest, I.J. Bush, H.J.J. Van Dam, P. Sherwood, J.M.H. Thomas, J.H. Van Lenthe, R.W.A. Havenith and J. Kendrick, Molecular Physics 103 (2005) 719.
[15] A. Nicolaides, A. Rauk, M.N. Glukhovtsev, L. Radom, J. Phys. Chem. 100 (1996) 17460.
[16] M. Haranczyk, P. C. Burgers, P. J. A. Ruttink, Int. J. Mass Spectrom. 220 (2002) 53.
[17] (a) R.G. Gilbert and S.C. Smith in : "Theory of Unimolecular and Recombination Reactions", Blackwell Scientific Publications, London, 1990; (b) T. Baer and W.L.

Hase in : Unimolecular Reaction Dynamics, Theory and Experiments, Oxford University Press, New York, 1996.

[18] T. Beyer, D.F. Swinehart, ACM Commun. 16 (1973) 379.

Chapter 7

Qualitative estimate of the ion-dipole interaction effect on the dissociative channels in the H_2O^+-CH_2-$^{\bullet}CO \rightarrow H_2O + CH_2CO^{\bullet+}$ reaction using semi-classical trajectory calculations

Abstract

Reaction rates in reactions, where an ion-dipole interaction is present, are sometimes considerably slower than what expected from RRKM calculations. More precise reaction rates can be achieved using semi-classical trajectory calculations instead of the RRKM method, but these are time-consuming. We have created a scheme to cut down the number of trajectories needed to create an ensemble to estimate the ion-dipole effect on the reaction rate. The scheme uses the interpolation of "basic" trajectories, which are trajectories including only the reaction coordinate and one normal mode, to appraise the results for various mixtures of excess energy over the vibrations. As an example system, we have studied the dissociation reaction H_2O^+-CH_2-$^{\bullet}CO \rightarrow H_2O + CH_2CO^{\bullet+}$ to give an estimate how much the reaction rate is slowed down by the attractive forces between the ion and the dipole, compared to the RRKM estimate. In comparison, a neutral system with dissociation reaction $^{\bullet}CH_2$-CH_2-$CH_3 \rightarrow CH_2$=$CH_2 + CH_3^{\bullet}$ with an activation energy similar to the depth of the potential well is also studied. We find that the reaction rate is slowed down by the ion-dipole interaction at small excess energies ($\approx$ 2.7 kcal mol^{-1}) to 5% of the RRKM estimate while at larger excess energies ($\approx$ 9.4 kcal mol^{-1}) the reaction proceeds already at nearly 50% of the rate of an RRKM estimate. The neutral system done in comparison confirms that the RRKM estimates are in reasonable agreement with trajectory calculations in this case, as all of the trajectories lead to dissociation.

1. Introduction

In mass spectrometry, many ions make a dimer with a neutral counterpart or isomerise into hydrogen bridged radical cations, which can then dissociate. Very often, the formed complex has the charge localized in one part of the complex, while the other part tends to keep in close vicinity, especially if it has a large dipole moment to form a strong ion-dipole interaction. This situation may be modelled as:

$$M^{\bullet+} \rightarrow TS \rightarrow D\text{—}I^{\bullet+} \rightarrow D + I^{\bullet+} \quad , \qquad (1)$$

where $D\text{—}I^{\bullet+}$ is the ion-dipole complex (with or without a hydrogen bond). If the transition state (TS) energy is much lower than the dissociation limit the overall rate will be determined by the energy of the products. If the TS energy is much higher, the passing of the TS is the rate-determining step. If they are close together, the two processes are in competition.

The calculation of reaction rates can be done using various methods [1-3]. Experimentally it is difficult to study ion-dipole dissociations as an isolated process. The usual starting point for an experiment is a monomer, which is then ionized. In the usual experimental methods it is not possible to see whether the ionized monomer has rearranged or formed a complex with a neutral monomer to estimate the reaction rate for its dissociation. At best, one can get a number of dissociations and for these dissociation ratios, and only the total reaction rate coefficient is known [4].

In the Rice-Ramsberger-Kassel-Markus (RRKM) model a dividing surface is chosen for the transition state, so that any trajectory started from the reactants pass this surface only once, reaching the product region. It is possible to choose this dividing surface to lie at the rate-determining TS of the reaction path, but this does not necessarily guarantee the satisfaction of the condition of trajectories passing the dividing surface only once. Thus, the dividing surface can also be placed deeper in the product valley in order to minimize the reaction rate. Nevertheless, the reaction rate achieved will be an upper bound to the actual reaction rate [1].

However, problems arise with ion-dipole dissociations, since there is no tight (static) transition state. A loose TS may be defined, governed by centrifugal barriers connected to the overall rotation of the complex. The height of the barrier has a $1/R^2$ dependence (where R is the distance between the centres-of-mass of ion and dipole). The ion-dipole interaction also shows a $1/R^2$ dependence [2]. Moreover, the interaction depends on the orientation of the dipole, i.e. on the amount of energy available in the internal rotation of the dipole.

In the RRKM method it is difficult to take into account ion-dipole interactions together with the conservation of the total angular momentum. There are indications from a trajectory study, which used a very simple model for the PES [5], that the system will be trapped in the well associated with the ion-dipole attraction even if the total energy is well above the dissociation limit, slowing down the reaction considerably. Therefore we decided to try semi-classical trajectory calculations. Our calculations are aimed to make an estimate of the *change* in the reaction rate due to the presence of the ion-dipole well.

Model systems for studying ion-dipole effect

We have studied process (1) by the semi-classical trajectory method for the following model system:

$$H_2O^+\text{-}CH_2\text{-}^{\bullet}CO \rightarrow TS \rightarrow H_2O\text{---}CH_2CO^{\bullet+} \rightarrow H_2O + CH_2CO^{\bullet+} \qquad (2)$$

According to RHF/4-31G calculations [6], the activation energy for the first step in reaction (2) is small (see Table 1 and Figure 1), and almost no excess energy is needed for this step to proceed in the microsecond time frame. In the second step, the reaction coordinate (the normal mode associated with the imaginary frequency) does not coincide with the dissociation coordinate and therefore the excess energy at the TS geometry will not be completely available to the dissociation, if there would be no coupling between the various degrees of freedom. Actually, the coupling between the normal modes appears to be strong in the neighbourhood of the TS geometry. In many cases, the trajectories appear not to dissociate directly [6], and are semi-periodic. In these cases the distance between the centres-of-mass of the dissociation products (R) reaches a maximum and then decreases again. This is the turning point. These trajectories show chaotic behaviour in the sense that their long-term behaviour cannot be related to their starting conditions in a consistent way. It is also not possible to get reliable information about the time needed for dissociation from the semi-periodic trajectories, apart from the fact that they need much more time than a trajectory, which dissociates directly.

In order to enable us to compare the ion-dipole dissociation with a standard dissociation, we have also run some trajectories for the following process:

$$^{\bullet}CH_2\text{-}CH_2\text{-}CH_3 \rightarrow TS \rightarrow CH_2{=}CH_2 + CH_3^{\bullet} \qquad (3)$$

Here the well separating the TS and the dissociation products is very shallow [6] according to the RHF/4-31G relative energies (see Table 2 and Figure 2). Therefore all trajectories for (3) starting at the TS are expected to dissociate. The activation energy E_A for this reaction is comparable in magnitude to that of the potential well in process (2), and the reverse activation energy is also similar.

Interpolation methods

We want to calculate the number of open channels, which do dissociate directly (n_{diss}) related to the total number of open channels (n_{open}) available at the TS geometry. The dissociation percentage [$(n_{diss}/n_{open})\cdot 100\%$] will be studied as a function of excess energy (E_{exc}). In metastable dissociations, where the excess energy is small, there are not that many open channels. Nevertheless the number of open channels turned out to be too large for calculating all the associated trajectories explicitly for process (2). Instead we use an interpolation technique, explained in Section 2.3, in order to obtain results for situations where the excess energy is distributed over more than one vibration.

To shorten the time needed for calculating the trajectories, we have tried to find a reliable criterion for a certain cut-off distance of the separating fragments to decide upon the outcome of a trajectory at large distances. Note that it is not enough to find out whether

the trajectory dissociates directly or not, we also need a quantitative measure from the cut-off point to use in the interpolation method.

Table 1: Energies (Hartree) and energy levels (ΔE) for the $H_2OCH_2CO^{\bullet+}$

Species	Energy	ΔE (kcal mol^{-1})
$H_2OCH_2CO^{\bullet+}$	-227.08994	-5.4
TS	-227.08126	0
H_2O---$CH_2CO^{\bullet+}$	-227.12795	-30.4
$H_2O + CH_2CO^{\bullet+}$	-227.08959	-5.2

Table 2: Energies (Hartree) and energy levels (ΔE) for the $CH_3CH_2CH_2^{\bullet}$

Species	Energy	ΔE (kcal mol^{-1})
$CH_3CH_2CH_2^{\bullet}$	-117.46358	-31.6
TS	-117.41325	0
$CH_3^{\bullet}$---C_2H_4	-117.42775	-9.1
$CH_3^{\bullet} + C_2H_4$	-117.42713	-8.7

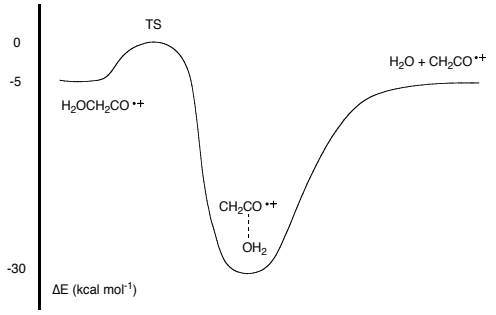

Figure 1. The RHF/4-31G PES for process (2).

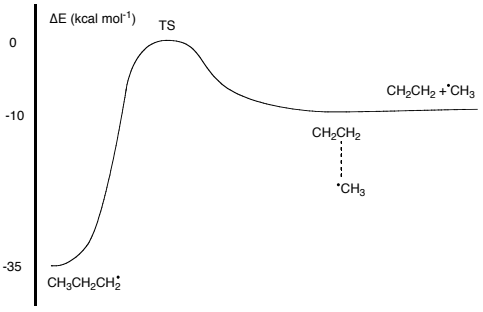

Figure 2. The RHF/4-31G PES for process (3).

2. Method of calculation

2.1. General

Since most trajectories contain many steps due to the long-range character of the ion-dipole interaction we have used the simple RHF/4-31G method for doing the ab initio calculations. See Figure 3 for the geometries for process (2). All trajectories were started at the TS geometry and for each step in the trajectory the properties of the system (gradients, potential energy) are evaluated by an ab initio calculation. For the dynamics classical mechanics was used.

To achieve a (large enough) ensemble of trajectories to make estimations of the reactions rate, the excess energy must be distributed over the reaction coordinate and the vibrations in all possible ways, according to:

$$E_{exc} = \sum_{i=0} T_i \qquad (4)$$

where T_0 is kinetic energy in the reaction coordinate ("vibration" 0) and T_i is kinetic energy in the i-th vibration, where $T_i = n\ \varepsilon_i$ with n = integer, and ε_i = i-th frequency for the TS ($1 \leq i \leq 17$). No account was taken of the zero-point vibrational energies. The frequencies and the properties of the normal modes of the TSs of processes (2) and (3) are given in Table 3 and 4, respectively.

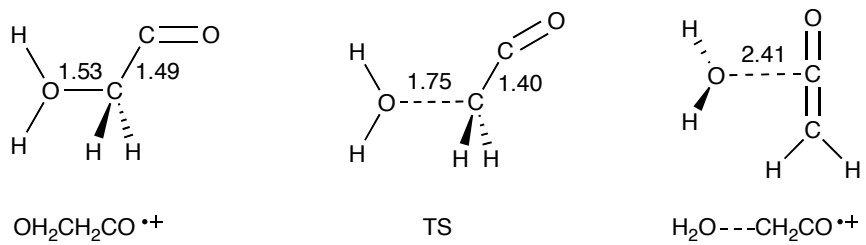

Figure 3: Structures for the $H_2OCH_2CO^{\bullet+}$ system. Left: H_2O^+-CH_2-$^{\bullet}CO$, middle: TS, and right: H_2O---$CH_2CO^{\bullet+}$, for process (2).

As the number of trajectories needed to describe the excess energy distribution in "all possible ways" will be very large, we have considered an alternative approach. In this approach we need first a number of "basic" trajectories, where E_{exc} is divided between the reaction coordinate and one of the vibrations (T_0 and T_i, respectively) with varying amounts. These "basic" trajectories are then combined into "general" trajectories to estimate the behaviour of a trajectory with distribution of E_{exc} over T_0 and several T_i, as in Eq. (4)).

2.2 Basic trajectories

Basic trajectories are trajectories with $E_{exc} = T_0 + T_i$ ($1 \leq i \leq 17$). The maximum value for the excess energy considered was taken as $E_{exc}^{\max}$ = 16 mHartree = 10.0 kcal mol^{-1} ≈ 3500 cm^{-1}. As a consequence only the vibrations 1-15 of the TS have to be considered for process (2) (see Table 1a). For both T_0 and T_i a grid spacing of 2.5 mHartree = 1.57 kcal mol^{-1} = 550 cm^{-1} was chosen. For all trajectories it was considered necessary to have $T_0 > 0$ at the TS geometry in order to enable the system to move in the direction of the dissociation at all. We take T_0 = 0.3, 1.0, 3.5, 6.0, 8.5, 11.0, and 13.5 mHartree. T_i was given values of 1.0, 2.5, 5.0, 7.5, 10.0, 12.5, and 15.0 mHartree. Since the results appear to be rather sensitive to T_0 for small values of T_0, the grid point T_0 = 0 was replaced by T_0 = 0.3. The results for the trajectories are obtained at either the turning point for the semi-periodic trajectories, or at a cut-off distance R_{max}. We have chosen R_{max} = 20 a.u., and the choice for R_{max} was checked by running some trajectories with much larger R_{max}.

The results for the trajectories are divided into three groups according to their final energies (E_f, which equals the sum of the kinetic and potential energies, $T_{zz}(R) + V_{zz}(R)$. The subscript 'zz' means we are talking about the relative energies between the separating fragments) at the cut-off distance, or at the turning point:

(i) $E_f > 0.5$ mH: dissociative;
(ii) -0.5 mH $< E_f < 0.5$ mH: undecided;
(iii) $E_f < -0.5$ mH: semi-periodic.

Thus all trajectories (and the interpolated results) with $E_f > 0.5$ mHartree (group (i)) will be counted as dissociative, and those with $E_f < -0.5$ mHartree (group (iii)) semi-periodic. For group (ii) the outcome is not very clear. First, the result may be affected by the fluctuating

Table 3. Properties of the normal modes of the TS for the process (2).

vib.	freq (cm^{-1})	components[a]	symmetry
0	-617	13 / 12 / 124 / 137	σ
1	143	7312 / 8312	π
2	281	13 / 213	σ
3	355	7312 / 8312 / 124	π
4	515	7315 / 8315 / 7316 / 8316	π
5	567	13 / 124	σ
6	815	137 / 138	σ
7	973	12 / 312 / 137 / 138	σ
8	1034	215 / 216 / 5132 / 6132 / 3124	π
9	1107	5124 / 6124	π
10	1364	5124 / 6124	σ
11	1576	516	σ
12	1788	738	σ
13	2245	12 / 24	σ
14	3311	15 / 16	σ
15	3424	15 / 16	π
16	3833	37 / 38	σ
17	3977	37 / 38	π

[a] for the geometry

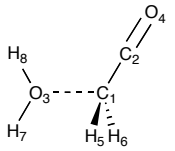

Table 4. Properties of the normal modes of the TS for the process (3).

vib.	freq (cm^{-1})	Components[a]	symmetry
0	-473	23	σ
1	111	8321 / 9321 / 10321	π
2	256	123	σ
3	400	413 / 513 / 623 / 723	π
4	610	832	σ
5	620	932 / 1032	π
6	847	4127 / 5126	σ
7	888	412 / 512 / 621 / 721	π
8	932	832 / 932 / 1032	σ
9	1027	413 / 513 / 623 / 723	π
10	1072	623 / 723 / 832 / 932	σ
11	1300	12	σ
12	1364	412 / 512 / 621 / 721	π
13	1579	839 / 8310	π
14	1583	9310	σ
15	1619	412 / 512 / 621 / 721	σ
16	1678	412 / 512 / 621 / 721	σ
17	3240	38 / 39 / 310	σ
18	3298	415 / 512 / 621 / 721	σ
19	3310	415 / 512 / 621 / 721	σ
20	3375	415 / 512 / 621 / 721	π
21	3389	38 / 39 / 310	σ
22	3399	38 / 39 / 310	π
23	3406	415 / 512 / 621 / 721	π

[a] for the geometry

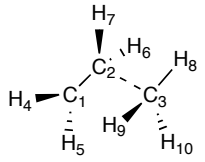

potential energy caused by oscillating dipole moment. Second, trajectories with a very small positive E_f will take a very long time to dissociate, causing them to fall outside the time frame of the dissociative trajectories. For this reason we will count them as semi-periodic.

2.3. Interpolations

For basic trajectories

We can interpolate E_f for the basic vibrations with arbitrary T_0, and T_i from using results in the surroundings of our value of interest. We can consider the explicitly calculated results as a grid of E_f in the directions x and y. In this case we look for the nearest final energies (E_f) obtained around the point, $E_f(x_p,y_p)$, we are interested in. The nearest grid points yield $E_f(x_0,y_0)$, $E_f(x_1,y_0)$, $E_f(x_0,y_1)$ and $E_f(x_1,y_1)$ (Figure 4). The interpolation is then carried out using equation

$$E_f(x_p,y_p) = E_f(x_0,y_0) + xa + yb + xy(c-a-b)\,, \qquad (5)$$

where

$$x = \frac{(x_p - x_0)}{(x_1 - x_0)}, \quad y = \frac{(y_p - y_0)}{(y_1 - y_0)}$$

and

$$a = E_f(x_1,y_0) - E_f(x_0,y_0)$$
$$b = E_f(x_0,y_1) - E_f(x_0,y_0)$$
$$c = E_f(x_1,y_1) - E_f(x_0,y_0)\,.$$

Here it is assumed that E_f is known for 4 points surrounding the point $E_f(x_p,y_p)$ wanted (see Figure 4). If these are in the same plane, we have $c = a + b$, i.e. $E_f(x,y) = E_f(x_0,y_0) + xa + yb$. We have used the above interpolation method in order to compensate for the non-planarity of the surface defined by the 4 grid points. If the 4th point $E_f(x_1,y_1)$ lies outside the range of basic trajectories, we have assumed $c = a + b$, ignoring the entry for the 4th point.

For the interpolation a maximum E_{exc} of 9.35 kcal mol^{-1} (= 14.9 mHartree) was chosen. The chosen E_{exc} must be smaller than the largest E_{exc} used for the basic trajectories, so that we will have enough points surrounding the interpolation point.

The RRKM program was used to characterize the number of open channels for passing the TS, using the frequencies given in Table 3. At maximum excess energy, 9.35 kcal mol^{-1} (which equals 3300 cm^{-1}, thus we have to take into account only vibrations 1-13 now), this corresponds to ~7500 open channels.

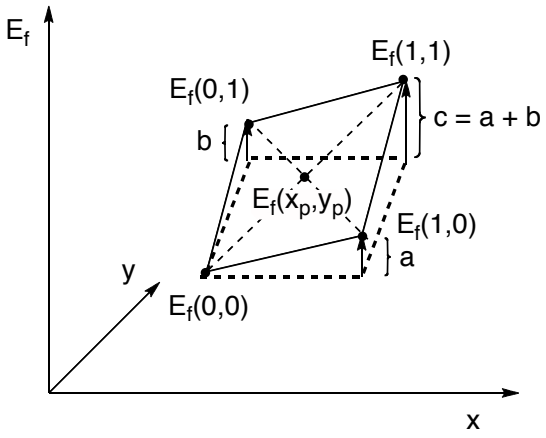

Figure 4. The value for wanted point $E_f(x_p,y_p)$ can be interpolated from the values of the four surrounding grid points.

For general trajectories

The energy is distributed according to Eq. 4. The result for this trajectory is estimated by second interpolation using weighted averages of the results of the basic trajectories (or, of the interpolated values between the grid points). Our test calculations show that the final energy of a mixture of vibrations does not change linearly according to the amount of energy located in the vibrations (see Figure 5 for an example). To get the final energy E_f for a mixture of vibrations, we use:

$$E_f = \frac{\sum_i w_i E_i(T_0,T_v)}{\sum_i w_i} \tag{6}$$

where $E_i(T_0,T_v)$ is a (interpolated) final energy contribution associated with the i-th vibration, using the energy available in all vibrations T_v (= $E_{exc} - T_0$), and w_i is a weight factor

$$w_i = \frac{T_i}{T_v} \cdot \tag{7}$$

The weighted averages are calculated separately for trajectories resulting at positive and negative E_f, and these averages are used in the second interpolation, See Appendix I for more details.

We have tested a number of non-linear models for the interpolation scheme (see Appendix II for the tested models). The interpolation model chosen for the second interpolation is based on an exponential fitting (Model 2 in Appendix II). We will explain it more in detail here. It is defined as follows:

$$y = A\, e^{(-\alpha x)} + B \tag{8}$$

To define the coefficients A, B and α for the exponential function, we have to use three points for the x (admixture ratio of two or more vibrations contributing to the T_v) with corresponding values of y (= E_f), see Figure 5. In Figure 5, x_1 stands at 0% admixture (only a dissociative trajectory, or a weighted average of dissociative trajectories, is present), x_2 at a mixture of two or more vibrations with dissociative and semi-periodic results (we use 50/50% admixture), and x_3 at 100% admixture (only a semi-periodic trajectory, or a weighted average of semi-periodic trajectories, is present). For x_1 and x_3 we have obtained y_1 and y_3 from trajectory calculations, or from the weighted averages (Eq. (6)) of the interpolations for the positive and negative E_f. We still need the value y_2 for the exponential fitting. We can find y_2, located at the 50/50% admixture of two vibrations (position x_2 in Figure 5), using:

$$x_2, \quad y_2 = \tfrac{1}{2}\left(y_1 + y_3\right) + \Delta y_2 \quad with \quad \Delta y_2 = \tfrac{1}{2}F\left(y_1 - y_3\right) . \tag{9}$$

Here, the parameter F determines the deviation from the linear E_f change along the mixing of the vibrations, which in case of no deviation correspond to taking $F = 0$. The parameter is used to adjust the height and curvature of the curve. Note, however, that F has to be taken such that the fitted curve does not have a maximum (which will happen if F is too large). The value of parameter F will be chosen according to test cases.

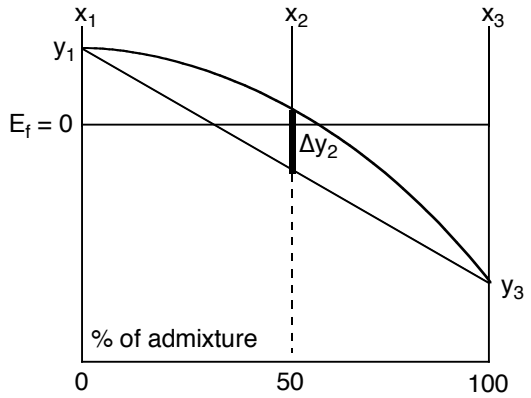

Figure 5. The linear interpolation (straight line) and the actual change (curved line) of E_f corresponding to making a mixture of two (or the weighted averages of) dissociative and semi-periodic trajectories.

After obtaining y_2, the coefficients A and B, and the exponential coefficient α can then be obtained from equations:

$$A = \frac{\Delta_1 \Delta_2}{\Delta_1 - \Delta_2},$$

$$B = y_2 - \frac{\Delta_1 \Delta_2}{\Delta_1 - \Delta_2}, \; and$$

$$\alpha = \tfrac{1}{2}\ln\frac{y_1 - B}{y_3 - B}, \; where$$

$$\Delta_1 = y_1 - y_2$$
$$\Delta_2 = y_2 - y_3 \quad .$$

The above interpolation method works in situations, where we are mixing two or more vibrations, with the same total E_{exc} and T_0 for the system. For example, we might want to mix trajectories of vibrations i and $i+1$, which both have T_0 of 5 mHartree and E_{exc} is 16 mHartree (thus $T_i = T_{i+1} = 11$ mHartree). In position x_1 we have the respective E_f obtained from the trajectory with $E_{exc} = T_0 + T_i$, and in position x_3 we have the respective E_f obtained from the trajectory with $E_{exc} = T_0 + T_{i+1}$. As the E_{exc} and T_0 stay the same during the mixing, values for T_i and T_{i+1} must change. Thus in the case of 50/50% admixture we have $T_i = T_{i+1}$ = 5.5 mHartree.

It should be noted that the interpolations including semi-periodic results might use results obtained at shorter distances than the chosen cut-off value (20 a.u). This can have an effect on the accuracy of the interpolations since we use (weighted averages of) final energies, which are obtained at varying distances.

2.4. Choice of the sign for the initial velocities

In the neighbourhood of the TS the coupling between the reaction coordinate and most vibrations turns out to be large. As a consequence the behaviour of many trajectories depends heavily on the sign of the initial velocity in the vibrational mode (the velocity in the reaction coordinate is always taken to be positive, i.e. the system is moving towards dissociation). Because of the generally strong coupling between the reaction coordinate and the vibrations, all trajectories have been run with positive and negative initial vibrational velocities.

For the interpolation of the general trajectories, all possible combinations of choosing the signs for the vibrations involved must be taken into account. If n vibrations contribute to the open channel, this amounts to 2^n calculations of E_f. The contribution to the count of dissociative channels (C_{diss}) is then given by

$$C_{diss} = \frac{n_{diss}}{2^n}, \quad (0 \le C_{diss} \le 1) \,, \tag{10}$$

where n_{diss} is the number of times E_f is found to be positive. Note that while each choice for the velocity signs is handled independently, in the final count each open channel is given the same weight.

3. Results

In this section we will go through the results obtained for the processes (2) and (3), see how the choice of the sign of the initial velocity affects the trajectories and use the interpolation method to predict the behaviour in more general situations, where the excess energy is divided over various vibrational states. The interpolation method, using exponential fitting, will give us a qualitative view on how much the reaction rate of process (2) is slowed down due to the ion-dipole interactions.

3.1. Results from the basic trajectories and the effect of the choice of sign of the initial velocities

The transition state turns out to be almost planar. Therefore the vibrations show predominant σ (A') or π (A") character (see Table 3). The reaction coordinate has σ-character. As expected, the vibrations with π-character do not couple significantly with the σ-type vibrations and for these vibrations the results do not depend on the sign of the initial velocity. So, we have only the vibrations 2, 5-7, and 10-14 (remember that we do not consider vibrations with $v > 3500$ cm^{-1}) with σ-character, and for these normal modes the choice of the sign of the initial velocity is expected to have an effect.

A series of basic trajectories were calculated for various excess energies, as described in Section 2.2, and with positive and negative initial velocity for all the relevant normal modes. The results from these trajectories can be seen in Table I in Appendix III.

3.2. Using the interpolation scheme in calculating the amount of dissociative channels

The grid points used for the estimation of arbitrary $E_f(T_0,T_i)$ are in Table I in Appendix III. The energy levels studied start from 930 cm^{-1} (= 2.66 kcal mol^{-1}), having 180 cm^{-1} steps until reaching 3270 cm^{-1} (= 9.35 kcal mol^{-1}). It was not possible to obtain quantitatively reliable results for all cases. However, for our purpose only the sign of the result is needed in order to decide whether a trajectory is dissociative or not.

We have placed some example interpolations using linear model and exponential model with three different values for F in Table 5. The effect of choosing only positive or negative initial velocities for the normal modes is shown in Figure 6. The choice of F and the initial velocity effect will be discussed in the next section.

We have collected the results of our interpolations in Table 6. The first energy level in Table 6 (E_{exc} = 930 cm^{-1}) corresponds to 38 open channels at the TS geometry. For this we find $n_{diss} / n_{open} = 0.03$ for the linear model, and $n_{diss} / n_{open} = 0.05$ for the exponential model. Here, the reaction is slowed down more than an order of magnitude. The percentage of the open channels leading to dissociation increases with the increasing E_{exc}, giving at the largest E_{exc} = 3270 cm^{-1} $n_{diss} / n_{open} = 0.29$ for the linear model, and $n_{diss} / n_{open} = 0.51$ for the exponential model with $F = 0.5$.

Our reference system, the $^{\bullet}CH_2$-CH_2-CH_3 dissociation (process (3)), shows us that in the case of no ion-dipole interaction all the trajectories with $3.5 < E_{exc} < 15.0$ mHartree lead to dissociation with $E_f > 0.5$ mHartree.

4. Discussion

First we will discuss the choice of the sign of the initial velocity, which seems to have a marked effect to the results in cases where the vibrations are closely coupled with the reaction coordinate. Then we will discuss the interpolation method, which yields qualitative results about the percentage of dissociative channels. Here, we have compared two models,

the linear and the exponential model. The obtained results for processes (2) and (3) are compared.

The results obtained at the cut-off distance for the dissociative trajectories, or at the turning point for the semi-periodic trajectories might not be always accurate. For example, the effect of oscillating dipole is not taken into account for trajectories with $R_{final} < R_{max}$, which will cause fluctuations in the potential energy. In addition, the varying turning point distances for some E_f obtained for the semi-periodic trajectories is a potential problem. We will discuss some possible methods to overcome these problems and we will also consider an alternative approach to the interpolation method to make the method quantitative.

Table 5. Some examples of the mixed vibrational mode results, obtained with linear model (model 0), exponential model (model 2) with F = 0.4, 0.5, and 0.6, and trajectory calculations.

T_0	**T_i (mHartree)**			**model:**	**0**	**2**	**2**	**2**	**Calc.**
mHartree	i = 1	2				F = 0.4	F = 0.5	F = 0.6	
3.9	7.0	0.0			-3.9	-3.9	-3.9	-3.9	-3.9
"	5.7	1.3			-1.9	-0.2	0.3	0.9	1.2
"	4.5	2.5			0.2	2.5	3.1	3.8	2.5
"	3.2	3.8			2.3	4.5	5.0	5.5	3.6
"	1.9	5.1			4.3	5.9	6.3	6.6	4.9
"	0.6	6.4			6.4	7.0	7.1	7.2	6.4
"	0.0	7.0			7.5	7.5	7.5	7.5	7.5
	i = 1	2	3						
2.9	5.1	1.3	1.6		-2.7	-1.2	-0.7	-0.1	0.4
"	3.8	2.6	"		-0.9	1.4	2.0	2.7	1.8
"	2.6	3.8	"		1.0	3.3	4.0	4.6	2.9
"	1.3	5.1	"		2.8	4.8	5.3	5.7	4.2
	i = 1	2	8						
1.1	5.1	0	4.7		-5.4	-5.4	-5.4	-5.4	-5.9
"	3.8	1.3	"		-4.0	-2.7	-2.2	-1.7	-3.1
"	2.6	2.6	"		-2.6	-0.5	0.2	0.9	-1.1
"	1.3	3.8	"		-1.2	1.3	2.0	2.7	0.1
"	0.0	5.10	"		0.2	2.7	3.3	4.0	0.5

Choice of the initial velocity

From the results for the basic trajectories in Table I (Appendix III) it can be seen that the dissociation is stimulated by certain vibrations with certain sign of the initial velocity, while others might be inhibited. Stimulation holds particularly for vib 2p (p is to indicate a positive initial velocity for the vibration) and for vib 5n (n indicates negative initial velocity). For both vibrations the sign of the initial velocity is essential: vib 2n and vib 5p in turn lead to semi-periodic trajectories, unless T_0 is very large (Table I). The coupling between the reaction coordinate and the normal mode thus greatly affects the behaviour of the trajectory. Note that the mentioned vibrations contain the $(H_2)O—C(H_2)$ distance, i.e. the dissociation coordinate, and therefore they will couple with the reaction coordinate. On

the other hand, as expected, the trajectories which do not contain the reaction coordinate result in similar kind of trajectories depending on T_0. Also, the choice of the initial velocity has almost no effect in these cases.

The interpolation method

We have found in our test calculations that Δy_2 is always positive. Thus, the linear model is underestimating the E_f values in the interpolation. This can also be seen from the examples in Table 5: The linear model gives underestimated E_f for the interpolation of vibrations of opposite character, i.e. where the signs of the E_i are different, compared to the calculated trajectories. For the exponential model the results depend on the chosen F. In some cases, the $F = 0.6$ works better, meanwhile in some other cases the $F = 0.5$ or 0.4 is better. However, as the important area of more accurate results is around the $0 < E_f < 1$ mHartree region to decide if the trajectory belongs to dissociative or semi-periodic group, we have focused on which F gives the best accordance with the small values. For this area we decided that $F = 0.5$ gives the most reasonable compromise.

From the results using only positive or negative initial velocities and model 2 (Figure 6), it can be seen that changing the signs of the initial velocities has a marked effect on the number of dissociative trajectories. With increasing excess energy, the dissociation percent reaches 70 at 9.35 kcal mol^{-1} when all the initial velocities point in the positive direction. On the other hand, taking into account only negative initial velocities, we just surpass 25% of dissociation. Clearly, using only one initial velocity will lead into large error. Therefore we must consider only the average of the two extremes.

From Table 6 we see again that the linear model gives far lower dissociation percentage than is expected from the exponential model. From the results obtained using the exponential interpolation, in Table 6, we see that the choice of F seems to come more important at higher excess energies. The reaction rates (using $F = 0.5$) will be slower than a statistical estimate by one order of magnitude at small excess energies, while at excess energy of 9.35 kcal mol^{-1} the reaction rate is still slowed by about one half.

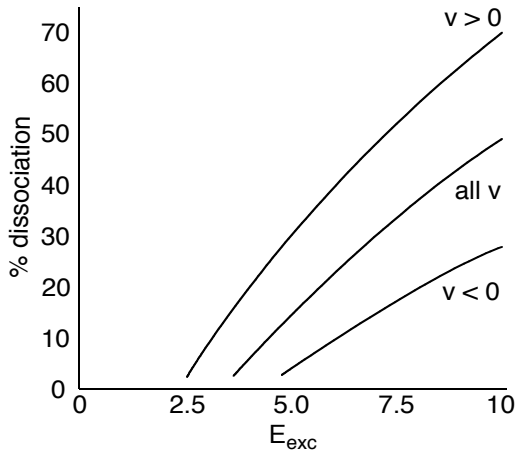

Figure 6. The effect of choosing only positive (v > 0) or negative (v < 0) initial velocities in the trajectory calculations (using model 2). As we need to take in consideration all possible combinations, have to use the average of the two cases (all v).

Table 6. The percentage of open channels leading directly to dissociation obtained using interpolated general trajectories for the linear model (model 0) and the exponential model (model 2) with three different *F* values. The number of points (n_{points}) considered is larger than the number of open channels (n_{open}) due to taking into account positive and negative initial velocities and their mixtures in the interpolation.

E_{exc}	n_{open}	n_{points}		**Dissociation percent**			
kcal mol^{-1}, cm^{-1}			model:	0	2 F = 0.4	2 F = 0.5	2 F = 0.6
2.66, 930	38	124		3	3	5	5
3.17, 1110	65	250		3	6	6	8
3.69, 1290	112	488		5	10	10	12
4.20, 1470	175	868		6	11	12	14
4.72, 1650	276	1556		8	13	15	17
5.23, 1830	426	2684		10	16	19	22
5.75, 2010	637	4422		13	21	24	28
6.26, 2190	930	7234		15	25	28	34
6.78, 2370	1362	11640		17	28	33	38
7.29, 2550	1956	18266		19	32	37	42
7.80, 2730	2754	28288		22	36	41	46
8.32, 2910	3845	43212		24	40	45	50
8.83, 3090	5335	65040		26	43	48	53
9.35, 3270	7275	96350		29	46	51	56

Comparison of the ion-dipole and neutral dissociation processes

We found that all of the trajectories calculated for process (3) are dissociative and can be categorized into category (i). This also confirms that the semi-periodic behaviour is indeed caused by the ion-dipole interaction, and not by some other effect.

Improving the interpolation

The interpolation method uses the results obtained directly from the trajectory calculations, either from the chosen cut-off distance, or from the semi-periodic turning point. This brings in problems in cases where the trajectory shows strong potential energy fluctuations due to the dipole moment oscillation. The problem is, in which point of the oscillation the final value is obtained, and this can cause a large error: Our test trajectories show that the dipole moment effect works even over long distances and at the cut-off distance the amplitude of the oscillation can be several mHartree. To overcome this, we can use a simple averaging scheme. We can average the potential energy over a number of points, which should correspond to about one oscillation. As the wavelength seems to increase with the distance, we have to choose a value that works best around the cut-off distance.

In cases where the trajectory is semi-periodic and reaches a turning point, an extrapolation method could be used so that these trajectories can be included in the interpolation at any wanted distance. The extrapolations will result in unphysical negative kinetic energies beyond the turning point. This situation can be nevertheless justified by noting that a mixture of semi-periodic and dissociative vibrations will result at least to a turning point with larger distance, or to dissociation. If we want to estimate the outcome of such a trajectory more quantitatively, we need the extrapolated values beyond the turning point of the semi-periodic trajectory.

To reach towards quantitative estimations, we would like to be able to estimate the Δy_2 value at different distances x accurately for each case. Instead of using some parameter F to account for Δy_2 at some admixture of weighted averages of dissociative and semi-periodic trajectories, we might rather approach the problem from another perspective: First, the potential and kinetic energies of the basis trajectories should be mathematically fitted for all the grid points. The best type of fit seems to involve inverse square dependence on the distance, since both the kinetic and potential energies vary like R^{-2}. The fits yield a number of parameters: For kinetic energy we should get two parameters $a_{i,v}$ and $b_{i,v}$ for vibration i and amount of energy placed in the vibration, v. The $b_{i,v}$ from the extrapolations may also be used for Kinetic Energy Release (KER) estimations, since they will represent the total energy at $R = \infty$. A negative $b_{i,v}$ indicates a semi-periodic trajectory without KER. For the potential energy we will have only one parameter $c_{i,v}$ since potential energy goes to zero at $R = \infty$. Then, weighted averages of the potential and kinetic energy fits will enable us to estimate the outcome of a trajectory, which mixes two (and possibly more) trajectories together in a quantitative way. Unfortunately, the parameters $a_{i,v}$, $b_{i,v}$ and $c_{i,v}$ are different for all the basic trajectories, and different also if different amount of T_i is used in the vibration. If quantitative estimations are needed in larger range of total energies, the number of parameters might become unnecessarily large. Reducing the number of grid points can reduce the number of parameters, and it might be possible that they are simply scalable according to their total energies, simplifying the problem.

5. Conclusions

Trajectory calculations on a model system (2) have shown that the passing of the TS slightly higher than the dissociation limit does not constitute the rate-determining step if there is a deep well separating the TS and the dissociation. Even if enough internal energy is available for the dissociation, the system is trapped in the well in many cases. However, for higher values of the excess energy the probability of getting trapped decreases significantly. As an overall conclusion for our model system we find that the rate constant for the metastable time window is decreased by about one order of magnitude in the excess energy range of 2.5-10 kcal mol^{-1}. This result may be expected to depend crucially on the TS energy with respect to the dissociation limit.

The choice of the initial velocity direction also has a marked effect. The reaction rates were nearly twice as large when choosing positive initial velocities exclusively for the normal modes, compared to choosing exclusively negative sign for the initial velocities. The average of these two extremes gives the final result, since all the possible combinations of positive and negative initial velocities have to be taken into account.

The calculations on the comparison process (3) reveal that for a neutral system with similar activation energy, as was the depth of the ion-dipole well for process (2), the trajectories lead almost certainly to dissociation. Thus, the effect on the semi-periodic behaviour in the ion-dipole system comes from the ion-dipole interaction, which also accounts for the slower reaction rates than the RRKM estimate.

5. Future Work

The proposed method using inverse square fitting and making weighted averages of the fits to use in the interpolations should be done to see how well the qualitative estimations compare to the quantitative estimations. The quantitative analysis might be necessary to do with less grid points to avoid having a large set of parameters. This can affect its accuracy. Finally, a comparison to experimentally obtained results from an ion-dipole dissociation is also needed to validate the method. For this, a system that has a deep potential well caused by the ion-dipole interactions and that has been studied experimentally should be chosen. In addition, the kinetic energy release estimation from combining the $b_{i,v}$ parameters from the fits should be done and compared to experimentally obtained results.

References

[1] T. Baer and W.L. Hase, Unimolecular Reaction Dynamics: Theory and Experiments, 1996, Oxford University Press, Oxford, UK.
[2] T. Baer and J.A. Booze in: W.L. Hase (ed.), Advances in Classical Trajectory Methods, Vol 2, JAI Press Inc., Hampton Hill, UK, 1994.
[3] R.D. Levine, Molecular Reaction Dynamics, Cambridge University Press, Cambridge, UK, 2005.
[4] D.B. Milligan, P.F. Wilson, M.J. McEwan, V.G. Anicich, Int. J. Mass Spectrom. 185/186/187 (1999) 663.
[5] (a) J.A. Nummela, B.K. Carpenter, J. Am. Chem. Soc. 124 (2002) 8512; (b) B. K. Carpenter, J. Phys. Org Chem. 16 (2003) 858.
[6] Our work.

Appendix I

For the interpolation of more than one dissociative and one semi-periodic trajectory, we assemble weighted averages of the final energies for the dissociative and semi-periodic trajectories separately. For dissociative trajectories we use:

$$\text{at} \quad x_1, \quad y_1 = \frac{\sum_i w_i^+ E_i(T_0, T_v)}{\sum_i w_i^+} \tag{A}$$

where w_i^+ is the weight for a dissociative trajectory ($E_f > 0$). Similarly, for semi-periodic trajectories we use:

$$\text{at} \quad x_3, \quad y_3 = \frac{\sum_i w_i^- E_i(T_0, T_v)}{\sum_i w_i^-} \tag{B}$$

where w_i^- is the weight for a semi-periodic trajectory ($E_f \leq 0$). The weights must satisfy the condition

$$\sum_i w_i^- + \sum_i w_i^+ = 1 \quad . \tag{C}$$

We can also adjust the position x_2 for interpolation to calculate y_2 at different admixtures:

$$x_2 = \sum_i w_i^- - \sum_i w_i^+ . \tag{D}$$

Appendix II

Model 1: quadratic fit

$$y = Ax^2 + Bx + C$$

$$A = (y_1 + y_3)/2 - y_2$$
$$B = (y_3 - y_1)/2$$
$$C = y_2$$

Model 2: Exponential fit

$$y = A\ \exp(-ax) + B$$

$$\Delta_1 = y_1 - y_2$$
$$\Delta_2 = y_2 - y_3$$

$$B = y_2 - \frac{\Delta_1\Delta_2}{\Delta_1 - \Delta_2}$$

$$A = y_2 - B = \frac{\Delta_1\Delta_2}{\Delta_1 - \Delta_2}$$

$$a = \frac{1}{2}\ln\frac{y_1 - B}{y_3 - B}$$

Model 3: Inverse fit

$$y = \frac{A}{x - x_0} + B$$

$$y_1 - y_2 = \frac{A}{x_0(x_0 + 1)}$$
$$y_2 - y_3 = \frac{A}{x_0(x_0 - 1)}$$

$$\frac{y_1 - y_2}{y_2 - y_3} = \frac{x_0 - 1}{x_0 + 1}$$

$$x_0 = \frac{y_3 - y_1}{y_1 - 2y_2 + y_3}$$

$$y_3 - y_1 = \frac{2A}{1 - x_0^2}$$

$$A = (y_1 - y_3)(x_0^2 - 1)/2$$

$$B = y_2 - \frac{A}{x_0}$$

Model 4: Quadratic inverse fit

$$y = \frac{A}{(x - x_0)^2} + B$$

$$Y = \frac{y_2 - y_1}{y_3 - y_2} = \frac{2x_0^3 - 3x_0^2 + 1}{2x_0^3 + 3x_0^2 - 1} = \frac{T_0}{N_0}$$

Iterative:

i) :

$$x_0 = x_{00} + \Delta$$

ii):

$$Y = \frac{y_2 - y_1}{y_3 - y_2} = \frac{2(x_{00} + \Delta)^3 - 3(x_{00} + \Delta)^3 + 1}{2(x_{00} + \Delta)^3 + 3(x_{00} + \Delta)^3 - 1} \approx$$

$$\frac{(2x_{00}^3 - 3x_{00}^2 + 1) + 6x_{00}\Delta(x_{00} - 1)}{(2x_{00}^3 - 3x_{00}^2 + 1) + 6x_{00}\Delta(x_{00} + 1)} = \frac{T_{00} + 6x_{00}\Delta(x_{00} - 1)}{N_{00} + 6x_{00}\Delta(x_{00} + 1)} = Y$$

iii): Solve for Δ:

$$x_0 = x_{00} + \frac{T_{00} - N_{00}Y}{6x_{00}((x_{00} + 1)Y - (x_{00} - 1))}$$

iv): $x_{00} = x_0$, back to i) etc. until convergence.

$$y_3 - y_1 = \frac{4Ax_0}{(1 - x_0^2)^2}$$

$$A = \frac{(y_3 - y_1)(1 - x_0^2)^2}{4x_0}$$

$$B = y_2 - \frac{A}{x_0^2}$$

.

Appendix III

Table I. The final energies E_f obtained from the trajectory calculations. These results are also used as the grid points for the interpolations. Letter 'p' after the vibration number denotes positive initial velocity, and letter 'n' negative initial velocity.

vib 1p

$T_0 \setminus T_i$	0.0	1.0	2.5	5.0	7.5	10.0	12.5	15.0
0.3		-5.9	-6.0	-5.8	-5.9	-5.5	-3.6	-3.1
1	-5.3	-5.4	-5.6	-5.7	-5.8	-4.3	-3.5	-4.4
3.5	-3.5	-4.8	-5.0	-4.9	-4.1	-2.8	-2.0	
6	-1.8	-2.7	-2.1	-2.2	-1.6	-0.2		
8.5	-0.1	-0.8	-1.0	-0.4	0.4			
11	1.2	0.6	0.6	1.2				
13.5	2.5	2.0	1.7					

vib 1n

$T_0 \setminus T_i$	0.0	1.0	2.5	5.0	7.5	10.0	12.5	15.0
0.3		-5.9	-6.0	-5.8	-5.9	-5.5	-3.6	-3.1
1	-5.3	-5.4	-5.6	-5.7	-5.8	-4.3	-3.5	-4.4
3.5	-3.5	-4.8	-5.0	-4.9	-4.1	-2.8	-2.0	
6	-1.8	-2.7	-2.1	-2.2	-1.6	-0.2		
8.5	-0.1	-0.8	-1.0	-0.4	0.4			
11	1.2	0.6	0.6	1.2				
13.5	2.5	2.0	1.7					

vib 2p

$T_0 \setminus T_i$	0.0	1.0	2.5	5.0	7.5	10.0	12.5	15.0
0.3		-3.9	-3.1	-2.7	-3.0	-3.9	-5.4	-5.7
1	-5.3	-1.3	0.6	2.6	4.4	5.8	7.4	8.9
3.5	-3.5	0.7	2.8	5.4	7.6	9.6	11.5	
6	-1.8	2.1	4.3	7.2	9.5	11.9		
8.5	-0.1	3.5	5.7	8.7	11.5			
11	1.2	4.7	7.2	10.3				
13.5	2.5	6.2	8.7					

vib 2n

$T_0 \setminus T_i$	0.0	1.0	2.5	5.0	7.5	10.0	12.5	15.0
0.3		-7.0	-7.8	-10.0	-10.6	-11.2	-11.1	-10.7
1	-5.3	-7.1	-8.2	-9.7	-10.2	-11.3	-11.5	-11.2
3.5	-3.5	-6.8	-7.9	-9.0	-10.1	-10.9	-11.4	
6	-1.8	-6.2	-7.8	-9.3	-9.4	-9.9		
8.5	-0.1	-3.0	-5.9	-8.4	-9.3			
11	1.2	-2.3	-3.0	-4.0				
13.5	2.5	-0.8	-1.7					

Table 1, continued

vib 3p										
$T_0 \setminus T_i$	**0.0**	**1.0**	**2.5**	**5.0**	**7.5**	**10.0**	**12.5**	**15.0**
0.3		-5.8	-5.8	-6.2	-6.8	-6.8	-8.1	-8.0
1	-5.3	-5.6	-5.5	-5.8	-6.1	-6.0	-6.1	-6.8
3.5	-3.5	-3.8	-4.0	-4.4	-4.9	-5.1	-5.2	
6	-1.8	-1.9	-2.1	-2.4	-2.7	-2.3		
8.5	-0.1	-0.3	-0.5	-0.7	-1.1			
11	1.2	1.2	0.9	0.5				
13.5	2.5	2.4	2.1					

vib 3n										
$T_0 \setminus T_i$	**0.0**	**1.0**	**2.5**	**5.0**	**7.5**	**10.0**	**12.5**	**15.0**
0.3		-5.8	-5.8	-6.2	-6.8	-6.8	-8.1	-8.0
1	-5.3	-5.6	-5.5	-5.8	-6.1	-6.0	-6.1	-6.8
3.5	-3.5	-3.8	-4.0	-4.4	-4.9	-5.1	-5.2	
6	-1.8	-1.9	-2.1	-2.4	-2.7	-2.3		
8.5	-0.1	-0.3	-0.5	-0.7	-1.1			
11	1.2	1.2	0.9	0.5				
13.5	2.5	2.4	2.1					

vib 4p										
$T_0 \setminus T_i$	**0.0**	**1.0**	**2.5**	**5.0**	**7.5**	**10.0**	**12.5**	**15.0**
0.3		-5.4	-4.4	-1.8	0.3	2.0	3.3	5.0
1	-5.3	-4.9	-3.4	-1.2	0.7	2.2	3.8	4.9
3.5	-3.5	-2.8	-1.4	0.5	2.2	3.6	5.2	
6	-1.8	-1.0	0.2	1.8	3.2	5.0		
8.5	-0.1	0.5	1.5	3.0	4.7			
11	1.2	1.7	2.6	4.3				
13.5	2.5	3.1	4.0					

vib 4n										
$T_0 \setminus T_i$	**0.0**	**1.0**	**2.5**	**5.0**	**7.5**	**10.0**	**12.5**	**15.0**
0.3		-5.4	-4.4	-1.8	0.3	2.0	3.3	5.0
1	-5.3	-4.9	-3.4	-1.2	0.7	2.2	3.8	4.9
3.5	-3.5	-2.8	-1.4	0.5	2.2	3.6	5.2	
6	-1.8	-1.0	0.2	1.8	3.2	5.0		
8.5	-0.1	0.5	1.5	3.0	4.7			
11	1.2	1.7	2.6	4.3				
13.5	2.5	3.1	4.0					

vib 5p										
$T_0 \setminus T_i$	**0.0**	**1.0**	**2.5**	**5.0**	**7.5**	**10.0**	**12.5**	**15.0**
0.3		-5.9	-6.4	-6.7	-6.9	-6.9	-6.8	-6.8
1	-5.3	-5.7	-6.3	-7.6	-9.0	-8.7	-9.7	-10.2
3.5	-3.5	-4.9	-4.7	-4.7	-5.5	-5.9	-6.0	
6	-1.8	-2.8	-3.3	-3.7	-3.5	-3.6		
8.5	-0.1	-0.6	-1.2	-1.1	-1.5			
11	1.2	1.0	0.9	0.6				
13.5	2.5	2.5	2.3					

vib 5n										
$T_0 \setminus T_i$	**0.0**	**1.0**	**2.5**	**5.0**	**7.5**	**10.0**	**12.5**	**15.0**
0.3		-3.5	-1.9	0.0	1.2	2.4	3.0	3.6
1	-5.3	-3.0	-1.9	-0.4	0.7	1.5	2.0	2.4
3.5	-3.5	-2.1	-1.3	-0.4	0.2	0.7	1.1	
6	-1.8	-0.8	-0.3	0.3	0.6	0.8		
8.5	-0.1	0.5	0.8	1.1	1.1			
11	1.2	1.7	1.9	1.9				
13.5	2.5	2.8	2.7					

Table 1, continued(2)

vib 6p

$T_0 \setminus T_i$	0.0	1.0	2.5	5.0	7.5	10.0	12.5	15.0
0.3		-4.2	-2.2	0.3	2.1	3.9	5.4	7.6
1	-5.3	-3.1	-1.0	1.3	3.3	5.0	7.1	8.6
3.5	-3.5	-0.8	0.9	3.2	5.2	7.1	9.2	
6	-1.8	0.7	2.4	4.7	6.7	8.9		
8.5	-0.1	2.1	3.6	5.9	8.3			
11	1.2	3.4	5.0	7.4				
13.5	2.5	4.6	6.4					

vib 6n

$T_0 \setminus T_i$	0.0	1.0	2.5	5.0	7.5	10.0	12.5	15.0
0.3		-5.8	-5.8	-5.8	-5.7	-6.1	-6.3	-7.3
1	-5.3	-5.9	-6.0	-5.9	-6.3	-6.4	-6.8	-6.7
3.5	-3.5	-5.6	-6.3	-6.7	-6.6	-7.4	-6.0	
6	-1.8	-3.4	-3.9	-3.4	-3.4	-3.0		
8.5	-0.1	-1.9	-2.0	-2.4	-2.2			
11	1.2	-0.2	-1.1	-0.9				
13.5	2.5	1.1	0.5					

vib 7p

$T_0 \setminus T_i$	0.0	1.0	2.5	5.0	7.5	10.0	12.5	15.0
0.3		-5.5	-5.5	-4.5	-4.3	-5.8		
1	-5.3	-5.3	-5.4	-5.3	-5.1	-5.1	-5.0	-3.8
3.5	-3.5	-4.8	-4.7	-4.7	-4.6	-5.5	-5.2	
6	-1.8	-2.7	-3.1	-3.9	-4.0	-4.1		
8.5	-0.1	-0.5	-0.7	-0.9	-1.5			
11	1.2	1.1	1.1	0.8				
13.5	2.5	2.7	1.6					

vib 7n

$T_0 \setminus T_i$	0.0	1.0	2.5	5.0	7.5	10.0	12.5	15.0
0.3		-5.8	-5.8	-5.5	-4.8	-4.4	-3.8	-3.3
1	-5.3	-4.8	-3.9	-2.4	-2.5	-1.7	-1.6	-0.8
3.5	-3.5	-2.6	-1.8	-1.2	-0.6	-0.3	0.1	
6	-1.8	-1.0	-0.6	-0.4	0.3	0.3		
8.5	-0.1	0.2	0.2	0.8	0.7			
11	1.2	1.4	1.5	1.4				
13.5	2.5	2.5	2.3					

vib 8p

$T_0 \setminus T_i$	0.0	1.0	2.5	5.0	7.5	10.0	12.5	15.0
0.3		-5.7	-5.8	-6.0	-6.3	-6.4	-6.2	-6.7
1	-5.3	-5.4	-5.5	-5.8	-6.0	-6.6	-6.5	-7.1
3.5	-3.5	-3.9	-4.1	-4.6	-5.2	-5.4	-5.7	
6	-1.8	-1.9	-2.2	-2.5	-2.8	-2.5		
8.5	-0.1	-0.2	-0.4	-0.6	-1.2			
11	1.2	1.2	1.0	0.4				
13.5	2.5	2.4	2.1					

vib 8n

$T_0 \setminus T_i$	0.0	1.0	2.5	5.0	7.5	10.0	12.5	15.0
0.3		-5.7	-5.8	-6.0	-6.3	-6.4	-6.2	-6.7
1	-5.3	-5.4	-5.5	-5.8	-6.0	-6.6	-6.5	-7.1
3.5	-3.5	-3.9	-4.1	-4.6	-5.2	-5.4	-5.7	
6	-1.8	-1.9	-2.2	-2.5	-2.8	-2.5		
8.5	-0.1	-0.2	-0.4	-0.6	-1.2			
11	1.2	1.2	1.0	0.4				
13.5	2.5	2.4	2.1					

Table 1, continued(3)

vib 9p

$T_0 \setminus T_i$	0.0	1.0	2.5	5.0	7.5	10.0	12.5	15.0
0.3		-5.5	-5.4	-4.8	-2.7	-0.7	1.6	3.8
1	-5.3	-5.2	-3.9	-1.7	0.2	1.6	2.8	3.8
3.5	-3.5	-3.4	-2.6	-1.1	0.3	1.4	2.1	
6	-1.8	-1.8	-1.2	0.0	1.1	1.6		
8.5	-0.1	-0.3	0.2	1.2	1.9			
11	1.2	1.1	1.5	2.3				
13.5	2.5	2.4	2.7					

vib 9n

$T_0 \setminus T_i$	0.0	1.0	2.5	5.0	7.5	10.0	12.5	15.0
0.3		-5.5	-5.4	-4.8	-2.7	-0.7	1.6	3.8
1	-5.3	-5.2	-3.9	-1.7	0.2	1.6	2.8	3.8
3.5	-3.5	-3.4	-2.6	-1.1	0.3	1.4	2.1	
6	-1.8	-1.8	-1.2	0.0	1.1	1.6		
8.5	-0.1	-0.3	0.2	1.2	1.9			
11	1.2	1.1	1.5	2.3				
13.5	2.5	2.4	2.7					

vib 10p

$T_0 \setminus T_i$	0.0	1.0	2.5	5.0	7.5	10.0	12.5	15.0
0.3		-5.8	-5.3	-3.2	-2.0	-0.5	0.8	2.2
1	-5.3	-4.6	-3.2	-1.7	-0.2	1.3	2.4	3.3
3.5	-3.5	-2.1	-0.9	0.6	1.9	3.1	3.9	
6	-1.8	-0.5	0.5	1.8	2.8	3.6		
8.5	-0.1	0.8	1.6	2.8	3.5			
11	1.2	2.0	2.7	3.4				
13.5	2.5	3.1	3.4					

vib 10n

$T_0 \setminus T_i$	0.0	1.0	2.5	5.0	7.5	10.0	12.5	15.0
0.3		-5.4	-5.3	-5.2	-5.1	-5.0	-4.5	-3.8
1	-5.3	-5.3	-5.1	-4.6	-3.5	-2.4	-1.7	-1.3
3.5	-3.5	-4.5	-4.8	-4.7	-4.8	-4.3	-4.4	
6	-1.8	-2.6	-2.7	-2.2	-2.0	-1.6		
8.5	-0.1	-0.6	-0.7	-0.1	0.1			
11	1.2	1.1	1.3	1.5				
13.5	2.5	2.6	2.7					

vib 11p

$T_0 \setminus T_i$	0.0	1.0	2.5	5.0	7.5	10.0	12.5	15.0
0.3		-5.3	-5.3	-5.1	-5.0	-4.9	-5.1	-5.0
1	-5.3	-5.0	-4.3	-3.8	-3.5	-3.3	-3.0	-2.5
3.5	-3.5	-2.7	-2.0	-1.3	-0.8	-0.5	-0.5	
6	-1.8	-0.8	-0.3	0.3	0.7	0.8		
8.5	-0.1	0.7	1.1	1.5	1.7			
11	1.2	1.9	1.4	2.7				
13.5	2.5	3.2	3.4					

vib 11n

$T_0 \setminus T_i$	0.0	1.0	2.5	5.0	7.5	10.0	12.5	15.0
0.3		-5.8	-6.1	-6.3	-6.2	-6.3	-6.4	-6.4
1	-5.3	-5.8	-5.8	-6.2	-6.2	-6.5	-7.0	-6.4
3.5	-3.5	-4.8	-5.4	-5.5	-6.0	-6.1	-6.0	
6	-1.8	-2.8	-3.3	-3.5	-4.4	-4.8		
8.5	-0.1	-0.9	-1.4	-1.9	-2.0			
11	1.2	0.7	0.3	-0.4				
13.5	2.5	2.0	1.5					

Table 1, continued(4)

vib 12p

$T_0 \setminus T_i$	0.0	1.0	2.5	5.0	7.5	10.0	12.5	15.0
0.3		-5.3	-5.3	-4.7	-5.1	-4.9	-4.4	-3.8
1	-5.3	-5.3	-4.9	-4.5	-3.8	-3.4	-2.9	-2.3
3.5	-3.5	-2.9	-2.2	-1.2	-0.5	0.2	0.4	
6	-1.8	-0.6	0.1	1.0	1.7	2.2		
8.5	-0.1	1.0	1.7	2.9	3.5			
11	1.2	2.5	3.5	4.4				
13.5	2.5	4.0	4.9					

vib 12n

$T_0 \setminus T_i$	0.0	1.0	2.5	5.0	7.5	10.0	12.5	15.0
0.3		-5.8	-6.1	-6.3	-6.2	-6.3	-6.4	-6.6
1	-5.3	-5.3	-5.3	-6.0	-6.2	-6.5	-7.0	-6.4
3.5	-3.5	-4.0	-3.8	-3.5	-2.5	-2.6	-2.0	
6	-1.8	-2.7	-2.8	-2.1	-2.6	-2.0		
8.5	-0.1	-1.1	-1.5	-1.8	-1.8			
11	1.2	0.2	-0.4	-0.9				
13.5	2.5	1.4	0.5					

vib 13p

$T_0 \setminus T_i$	0.0	1.0	2.5	5.0	7.5	10.0	12.5	15.0
0.3		-5.7	-5.7	-5.7	-5.4	-5.5	-5.5	-5.6
1	-5.3	-5.4	-5.4	-5.5	-5.3	-5.2	-5.3	-5.6
3.5	-3.5	-3.6	-3.6	-3.6	-3.6	-3.7	-4.0	
6	-1.8	-1.7	-1.7	-1.7	-1.7	-1.8		
8.5	-0.1	-0.1	-0.1	-0.2	-0.6			
11	1.2	1.2	1.2	0.8				
13.5	2.5	2.4	2.2					

vib 13n

$T_0 \setminus T_i$	0.0	1.0	2.5	5.0	7.5	10.0	12.5	15.0
0.3		-5.6	-5.6	-5.5	-5.5	-5.6	-5.7	-5.6
1	-5.3	-5.5	-5.5	-5.5	-5.2	-5.3	-5.2	-5.3
3.5	-3.5	-3.8	-3.7	-3.8	-3.8	-3.9	-4.1	
6	-1.8	-1.8	-1.9	-1.9	-1.8	-1.9		
8.5	-0.1	-0.1	-0.5	-0.1	-0.5			
11	1.2	1.2	1.4	1.1				
13.5	2.5	2.7	2.6					

Henri Ervasti (2008): Computational and experimental studies on stabilities, reactions and reaction rates of cations and ion-dipole complexes

Summary in English

Usually a neutral molecule is more passive to react than its ionised counterpart. Therefore ionization is used to reduce stability and increase reactivity of molecules. An ionised and a neutral molecule can form a complex, if there exists an attractive electrostatic interaction, such as ion-dipole interaction. The ion and the neutral can also form a proton-bound complex. The proton-bound complex can initiate proton exchange, isomerisation, or covalently bound adduct formation. For isomerisation the important mechanisms are the proton-transport catalysis and the so-called 'Quid-pro-Quo' (give-to-gain) mechanisms.

Positively charged ionised molecules are considered to take part in certain chemical reactions happening in interstellar space and upper layers of atmosphere. It is possible to study these reactions using for example mass spectrometry and molecular modelling. Mass spectrometry is used in studying ionised molecules and their fragmentation in μs (microsecond) timeframe. Ionised molecules dissociate into smaller fragments, which can then be detected and used to wit the reactions of the sample molecular ion. Often the precise reaction mechanism remains nevertheless unsolved. With computations, the precise reaction mechanisms occurring in the reactions can be explained from the calculated energy levels of different stages of the reactions. It is also possible to predict the reaction rates of these reactions either using statistical methods or trajectory calculations.

In **Chapter 2** the effect of functional group substitution on neutral and ionised ketene are studied. The effects include proton affinity and the relative stability of the neutral ketene, and the relative stability of the ion against dissociation of carbon monoxide from it. We find that electron-donating substituents show stabilising positive induction effects, while electron acceptor substituents destabilise the ketene ion, showing negative induction effect. The stabilising effect on the ketene ion might not, though, necessarily lead into more demand of energy for carbon monoxide dissociation. This is due to the resonance stabilisation of the product ion, caused by electron donation from the substituent to the product ion. This makes the dissociation more favourable, and in some cases it is so strong that the existence of a covalently bound substituted ketene ion is not possible.

Protonation in other positions than the most probable one, and ketene reactions with an ammonium ion are also discussed. Moreover, the chapter includes a discussion on the heat-of-formation estimations for some of the substituted ketenes.

The stabilisation effects on proton-bound complexes are studied in **Chapter 3**. It has been pointed out that there is a linear correlation between the complex stability, and the proton affinity difference of the monomers at the connecting atoms of the proton binding. This correlation can be used to estimate stabilities of ion-dipole complexes. However, in some cases the correlation does not hold. It has been suggested that in these cases there might be a strong ion-dipole interaction, which contributes to the stability of the complex. By extending the existing linear correlation method with inclusion of a dipole moment factor, we improve the correlation method and get more accurate stability estimates. In addition, we solve some of the problematic cases where the original method fails.

Chapter 4 focuses on the dissociation reaction of protonated oxalic acid. It is found from computations that the lowest-energy reaction proceeds to the dissociation into protonated water, carbon monoxide, and carbon dioxide. This happens via a unique ter-body complex. This ter-body complex is also argumented to be the reason for the main

peak in a metastable ion mass spectrum of protonated oxalic acid. Reaction paths of the minor dissociation products were also solved.

The possibility of pyrimidine formation in interstellar dust clouds from an acrylonitrile radical cation dimer is discussed in **Chapter 5**. Metastable ion mass spectrometric experiments on acrylonitrile exhibit a small amount of pyrimidine formation, which results from a covalently bound neutral acrylonitrile – ionized acrylonitrile adduct cation. The covalently bound cation cyclizes and undergoes isomerisation steps and ethene dissociation to yield a pyrimidine radical cation. This is nevertheless only a minor product, while the major product is formed in reactions involving proton-bound complexes. Self-protonation is deemed the main reaction. Self-catalysis is also deemed energetically possible, but kinetically improbable.

A related reaction of acrylonitrile with hydrogen cyanide is studied in **Chapter 6** using solely computations. Similarly to the previous system, hydrogen cyanide can form covalently bound adducts, as well as proton-bound complexes, with acrylonitrile. From our computational results we see that, in terms of energy, the adduct formation and cyclization step are possible, but these can also lead to a continued isomerisation reaction. Pyrimidine is found to lie in a deep potential well, which might increase its lifetime against the reverse dissociation and continued isomerisation reactions. Kinetic studies, however, show the adduct formation to be very slow in comparison to proton-transport catalysis of acrylonitrile isomerisation reactions. These reactions are identified as the most favourable reactions. Protonated hydrogen cyanide formation also lies under the dissociation energy limit, although this is a minor process as well.

Chapter 7 is focused on qualitative studies using semi-classical trajectory calculations on the dissociation rate of an ion-dipole complex, which has a deep potential well preceding the dissociation. As this kind of study is time-consuming, we have developed an interpolation method to predict the behaviour of 'general' trajectories in cases where many vibrational modes will be excited. This is done by mixing the results obtained for a number of 'basic' trajectories. Here, the amount of trajectory calculations needed decreases dramatically. For the moment, this method is to be used only for qualitative estimations.

It is shown that, on average, only one-tenth of the channels open to dissociation lead directly to dissociation products for moderate excess energies ($\leq$ 10 kcal mol^{-1}). The rest of the open channels lead either to a very slowly progressing dissociation (which means it will be out of the μs time frame we are interested in), or to semi-periodic behaviour of the trajectory. This means that the dissociation stops and the fragments oscillate back and forth for unknown amount of time. Therefore, for our model system the non-parameterised statistical estimate should be scaled down by about one order of magnitude.

Henri Ervasti (2008): Computational and experimental studies on stabilities, reactions and reaction rates of cations and ion-dipole complexes

Samenvatting in het nederlands

Gewoonlijk is een neutraal molecule minder reactief dan zijn geioniseerde tegenhanger. Ionisatie wordt daarom gebruikt om de stabiliteit te verminderen en de reactiviteit van moleculen te verhogen. Een ion en een neutraal molecule kunnen een complex vormen, als er een aantrekkende elektrostatische interactie bestaan, bijvoorbeeld een ion-dipool interactie. Het ion en het neutrale molecule kunnen ook een proton-gebonden complex vormen. Proton-gebonden complexen kunnen proton overdracht, isomerisatie, of het vormen van een covalente binding van het ion en het neutrale molecule initialiseren. Voor isomerisatie de belangrijkste mechanismen zijn proton-transpoort katalyse en het zogenoemde 'Quid-pro-Quo' (uitwisselings) mechanisme.

Positief geladen moleculen worden geacht een rol te spelen in bepaalde chemische reacties die in de interstellaire ruimte en in de hogere niveaus van de atmosfeer plaats vinden. Het is mogelijk om deze reacties te bestuderen door gebruik te maken van bijvoorbeeld massaspektrometrie en moleculaire modellen. Massaspektrometrie wordt gebruikt om geioniseerde moleculen en hun fragmentaties op een tijdschaal van mikrosekonden (μs) te bestuderen. De geioniseerde moleculen worden in kleinere fragmenten opgesplitst, die geïdentificeerd worden en die gebruikt worden om de reacties van het originele moleculaire ion te weten te komen. Niettemin blijft het precieze reactiemechanisme vaak onbekend. Met berekeningen kunnen de gedetailleerde reactiemechanismen die in de reacties optreden, uitgelegd worden, met behulp van de berekende energieniveaus en voor de dynamica statistische methoden of baanberekeningnen.

In **Hoofdstuk 2** wordt het effect van substitutie van funktionele groepen op de proton affiniteit en de relatieve stabiliteit van neutrale ketenen, en de relatieve stabiliteit van geioniseerde ketenen tegen de afsplitsing van koolmonoxide uit het ion, bestudeerd. We hebben gevonden dat substituenten die elektronen doneren, een stabiliserend (positief) induktie-effect vertonen, terwijl de substituenten die elektronen opnemen het keteen ion destabiliseren door een negatief inductie-effect. Het stabiliserende effect op het keteen-ion leidt echter niet tot een energetisch ongunstigere afscheiding van koolmonoxide. Dit komt door de resonantiestabilisatie van het production, veroorzaakt door elektrondonatie van de substituent naar het produktion. Dit maakt de afsplitsing energetisch gunstiger en in sommige gevallen is dit effect zo sterk dat een covalent gebonden gesubstitueerd keteen ion niet stabiel is.

Protonering in andere posities dan de meest waarschijnlijke en een reactie van keteen met het ammoniak ion worden ook besproken. Het hoofdstuk bevat ook een discussie over het schatten van de vormingswarmte van sommige gesubstitueerde ketenen.

Het stabiliserende effect van proton-gebonden complexen wordt in **Hoofdstuk 3** bestudeerd. Uit de literatuur is bekend dat er een lineaire correlatie bestaat tussen het verschil in proton affiniteit van de moleculen op de atomen in de proton binding en de stabiliteit van het complex. Nochtans werkt deze correlatie in sommige gevallen niet. Er is gesuggereerd dat er in deze gevallen ook een sterke ion-dipool interactie kan zijn die aan de stabiliteit van het complex bijdraagt. Door aan de oorspronkelijke lineaire correlatie methode een dipoolmoment-factor toe te voegen kunnen we de nauwkeurigheid van de

stabilisatieschatting verbeteren en een aantal problematische gevallen waarvoor de originele methode niet werkt, in het systeem inpassen.

Hoofdstuk 4 is gewijd aan de dissociatiereakties van geprotoneerd oxaalzuur. Berekeningen tonen aan dat de energetisch gunstigste reaktie doorgaat tot de afsplitsing van geprotoneerd water, koolmonoxide en kooldioxide via een speciaal drie-deeltjes complex – een hydronium (geprotoneerd water) gebonden dimeer. Dit drie-deeltjes complex is ook aangewezen als de veroorzaker van de hoofdpiek in een metastabiel-ion massaspektrum van geprotoneerd oxaalzuur. De reaktiepaden die een aantal minder belangrijke dissociatieprodukten opleveren zijn ook gevonden.

De mogelijkheid van pyrimidine vorming binnen interstellaire stofwolken van een acrylonitril dimeer radikaal kation wordt in **Hoofdstuk 5** besproken. De massaspektrometrische experimenten aan metastabiele ionen van acrylonitril geven enige pyrimidine vorming aan die komt van een covalent gebonden dimeer van neutraal acrylonitril en geioniseerd acrylonitril. Het covalent gebonden kation gaat over in een ringstructuur en levert via isomerisatiestappen en afsplitsing van acetyleen een pyrimidine radikaal kation. Dit is evenwel slechts een bijproduct; het hoofdprodukt wordt gevormd in reacties van proton-gebonden complexen, waarbij zelf-protonering de hoofdrol speelt. Ook zelf-katalyse is energetisch mogelijk, maar niet waarschijnlijk in kinetische opzicht.

Een gerelateerde reactie van acrylonitril met waterstofcyanide is in **Hoofdstuk 6** alleen met berekeningen bestudeerd. Waterstofcyanide kan zowel covalent gebonden adducten als proton gebonden complexen met acrylonitril vormen, analoog aan het vorige systeem. Aan de resultaten van onze berekeningen kunnen we zien dat de vorming van adducten en ringvorming mogelijk zijn, maar dit kan ook tot een isomerisatie leiden. Pyrimidine blijkt in en diepe potentiaal kuil te liggen, wat de overlevingstijd van pyrimidine ten opzichte van teruggaande dissociatie en voortgaande isomerisatie zal verhogen. Kinetische studies echter tonen aan dat de pyrimidinevorming heel langzaam is in vergelijking met proton-transport katalyse van de acrylonitril isomerisatie reacties, die geïdentificeerd worden als de energetisch gunstigste reacties. De vorming van geprotoneerd waterstofcyanide verloopt ook onder de dissociatiegrens, maar dit is ook een minder belangrijk proces.

Hoofdstuk 7 is een kwalitatieve studie van de dissociatiesnelheid van een ion-dipool complex met een diepe potentiaal kuil, die de dissociatie voorkomt, met gebruik van semi-klassieke baanberekeningen. Aangezien een dergelijke studie zeer rekenintensief is, hebben we een interpolatie methode ontwikkeld om het gedrag van 'algemene' trajectories te voorspellen door het combineren van de resultaten verkregen voor een aantal 'basis' trajectories, in gevallen waarin veel vibraties een rol spelen. Daardoor neemt het aantal benodigde baanberekeningen drastisch af. Op het ogenblik is deze methode alleen bedoeld om gebruikt te worden voor kwalitatieve schattingen.

Aangetoond wordt dat gemiddeld slechts een tiende van de open kanalen tot direkte dissociatie leidt voor excess energieën $\leq$ 10 kcal mol^{-1}. De andere open kanalen leiden ofwel tot een heel langzame voortgaande dissociatie (wat betekent dat dit niet binnen de µs tijdschaal waarin we geinteresserd zijn verloopt), of tot een semi-periodiek gedrag van de trajectory, wat betekent dat de dissociatie stopt, waarna de fragmenten voor onbepaalde tijd gaan oscilleren. Daarom zou de niet-geparametriseerde statistische schatting voor ons modelsysteem met ongeveer een orde van grootte teruggeschaald moeten worden.

Henri Ervasti (2008): Computational and experimental studies on stabilities, reactions and reaction rates of cations and ion-dipole complexes

Suomenkielinen yhteenveto

Tavallisesti neutraali molekyyli on hitaampi reagoimaan kuin vastaava ionisoitu molekyyli. Näin ollen ionisaatiota käytetään stabiilisuuden vähentämiseen ja molekyylien reaktiivisudeen kasvattamiseen. Ionisoitu ja neutraali molekyyli voivat muodostaa kompleksin, jos niiden välillä on puoleensavetävä elektrostaattinen vuorovaikutus, kuten esimerkiksi ioni-dipoli vuorovaikutus. Ioni ja neutraali voivat muodostaa myös protonisidoksisen kompleksin. Protonisidoksiset kompleksit voivat taasen käynnistää protonivaihdon, isomerisaation, tai kovalenttisesti sidotun yhdistymän muodostumisen. Tärkeät mekanismit isomerisaatiossa ovat protoninkuljetuskatalyysi ja niinkutsuttu 'Quid-pro-Quo' (eli vaihto) mekanismi.

Positiivisesti ladatuttujen ionisoitujen molekyylien oletetaan ottavan osaa tiettyihin yläilmakehässä ja tähtienvälisessä avaruudessa tapahtuviin kemiallisiin reaktioihin. Näitten reaktioiden tutkiminen on mahdollista käyttäen esimerkiksi massaspektrometriaa ja molekyylimallinnusta. Massaspektrometriaa käytetään ionisoitujen molekyylien ja niiden mikrosekunnin aikavälillä tapahtuvan pilkkoutumisen tutkimiseen. Usein kuitenkin täsmälliset reaktiomekanismit jäävät selvittämättä. Tällöin voidaan käyttää molekyylimallinnusta eri reaktiovaiheiden tutkimiseen laskemalla niiden vaatimat energiamäärät. On myös mahdollista ennustaa näiden reaktioiden reaktionopeuksia käyttäen statistisia menetelmiä tai liikeratalaskentaa.

Kappaleessa 2 tutkitaan funktionaalisen ryhmän vaihdon vaikutusta neutraaliessa ja ionisoiduissa keteeneissä. Tutkittavat vaikutukset sisältävät neutraalin keteenin protoniaffiniteetin ja verrannollisen stabiilisuuden, sekä keteeni-ionin ja sen hiilimonoksidia tuottavan hajoamisprosessin verrannollisen stabiilisuuden. Huomaamme että elektroneja luotaantyöntävät substituentit aiheuttavat vakauttavia positiivisia induktiovaikutuksia, kun taas elektroneja vastaanottavat substituentit epävakauttavat keteeni-ionia, aiheuttaen negatiivisen induktiovaikutuksen. Vakauttava vaikutus keteeni-ioniin ei välttämättä johda lisääntyneeseen energiatarpeeseen hiilimonoksidin poistamiseksi. Tämä johtuu tuoteionin resonanssivakautumisesta, jonka aiheuttaa tuoteioniin elektroneja luotaantyöntävä substituentti. Tämä tekee hajoamisen mielekkäämmäksi ja joissain tapauksissa tämä vaikutus on niin vahva että kovalenttisesti sidottu substituoitu keteeni ei pysty pysymään koossa.

Kappaleessa keskustellaan myös protonoitumisen tapahtumisesta muihin kuin todennäköisimpään paikkaan, ja keteenin reaktioihin ammoniumionin kanssa. Lisäksi keskustellaan joittenkin substituoitujen keteenien muodostumislämpöjen arvioinnista.

Kappaleen 3 aiheena on stabilisaatiovaikutukset protonisidoksisiin komplekseihin. Aikaisemmin on osoitettu että kompleksien vakauden ja monomeerien protonisidokseen yhdistävien atomien protoniaffiniteettien eron välillä on lineaarinen korrelaatio. Kuitenkin joissain tapauksissa korrelaatio ei pidä paikkaansa. On ehdotettu, että näissä tapauksissa voimakkaat ioni-dipolivuorovaikutukset voivat ottaa osaa kompleksin vakauteen. Lisäämällä dipolimomenttitekijän olemassaolevaan lineaarikorrelaatiomenetelmään, parannamme vakausarvioiden tarkkuutta. Lisäksi selvitämme syyn joihinkin alkuperäisessä menetelmässä olleisiin vaikeisiin tapauksiin.

Kappale 4 keskittyy protonoidun oksaalihapon hajoamisreaktioon. Tietokonelaskelmista havaitaan että matalimman energian hajoamisreaktio etenee

protonoidun veden, hiilimonoksidin ja hiilidioksidin muodostumiseen. Tämä tapahtuu ainutlaatuisen kolmirunkokompleksin kautta. Tämän kolmirunkokompleksin väitämme myös olevan syynä oksaalihapon metastabiilin massaspektrin pääpiikkiin. Myöskin vähäisempien hajoamistuotteiden reaktioreitit selvitettiin.

Pyrimidiinin akrylonitriiliradikaalikationidimeeristä muodostumisen mahdollisuutta tähtienvälisissä pölypilvissä on tutkittu **Kappaleessa 5**. Metastabiili-ioni massapekstrometriset kokeet akrylonitriilille paljastavat pienen määrän pyrimidiinin muodostumista, mikä tulee kovalenttisesti sidotusta neutraalin ja ionisoidun akrylonitriilin yhdistymäkationista. Kovalenttisesti sitoutunut kationi muodostaa renkaan ja käy läpi isomerisaatioaskeleita ja eteenin dissosiaation tuottaakseen pyrimidiiniradikaalikationin. Tämä kuitenkin on vain vähemmistötuote, kun tääs päätuote muodostuu protonisidoksisten kompleksien reaktioissa. Pääreaktio on (itse)protonaatio. (Itse)katalyysi on myös mahdollinen energialaskelmien perusteella, mutta kineettisesti epätodennäköinen.

Edelliseen reaktioon läheisesti liittyvää akrylonitriilin reaktiota vetysyanidin kanssa on tutkittu **Kappaleessa 6** käyttäen pelkästään laskentaa. Kuten edellisessä systeemissä, vetysyanidi voi muodostaa kovalenttisesti sidottuja yhdistymiä, kuten myös protonisidokseisia komplekseja, akrylonitriilin kanssa. Laskelmiemme tuloksista näemme, energeettisin perustein, että yhdistymän ja renkaan muodostuminen ovat mahdollisia, mutta nämä voivat myös johtaa pidemmälle jatkavaan isomerisaatioreaktioon. Pyrimidiinin havaitaan sijaitsevan syvässä potentiaalikuopassa, mikä voi kasvattaa sen elinaikaa takaisinhajoamis- ja eteenpäin jatkuvia isomerisaatioreaktioita vastaan. Kineettiset tarkastelut kuitenkin osoittavat yhdistymän muodostumisen olevan erittäin hidasta verrattuna akrylonitriilin isomerisaatioiden protoninkuljetuskatalyysiin. Juuri nämä reaktiot tunnistetaan olevan mielekkäimmät reaktiot. Protonoidun vetysyanidin muodostuminen on myös hajoamisenergiarajan alapuolella, vaikkakin tämä prosessi tapahtuu myöskin vain vähemmistössä.

Viimeinen kappale, **Kappale 7**, keskittyy kvalitatiivisiin tutkimuksiin ioni-dipolikompleksin, jolla on hajoamista edeltävä syvä potentiaalikuoppa, hajoamisnopeuteen käyttäen semiklassista liikeratalaskentaa. Koska tämän tyyppinen tutkimus on aikaavievää, olemme kehittäneet interpolaatiomenetelmän ennustaaksemme 'yleisten' liikeratojen käytöstä tapauksissa, joissa useat värähtelytaajudet tulevat olemaan jännitettyinä. Tämä tehdään sekoittamalla tuloksia, jotka on saatu tietylle määrälle 'perus'liikeratoja. Tällöin liikeratalaskujen määrän tarve laskee voimakkaasti. Tällä hetkellä tämä menetelmä soveltuu kuitenkin vain kvalitatiivisiin määritelmiin.

Tulokset osoittavat että keskimäärin vain yksi kymmenestä avoimesta dissosiaatiokanavasta johtaa suoraan hajoamistuotteisiin vaatimattomilla ylimääräenergioilla ($\leq$ 10 kcal mol^{-1}). Loput avoimet kanavat johtavat joko hyvin hitaisiin hajoamisiin (mikä tarkoittaa että ne eivät ole meitä kiinostavassa mikrosekunnin aikaluokassa), tai semi-periodiseen liikeradan käyttäytymiseen. Tämä taas tarkoittaa että hajoaminen keskeytyy ja osaset poukkoilevat edestakaisin tuntemattoman ajan verran. Täten meidän mallisysteemille annettua ei-parametrisoitua statistista reaktionpeusarviota pitää leikata noin yhdellä kymmenyksellä.

List of publications

"Energy and stability of protonated ketenes: inductive and resonance effects"
Henri K. Ervasti, Peter C. Burgers, and Paul J.A. Ruttink, Eur. J. Mass Spectrom. 10, 791-799 (2004).

"Dissociation of protonated oxalic acid [HOOC-C(OH)2]+ into H3O+ + CO + CO2 : an experimental and CBS-QB3 computational study"
Henri K. Ervasti, Richard Lee, Peter C. Burgers, Paul J.A. Ruttink, and Johan K. Terlouw, Int. J. Mass Spectrom. 249-250, 240-251 (2006).

"The acrylonitrile dimer ion: A study of its dissociation via self-catalysis, self-protonation and cyclization into the pyrimidine radical cation"
Henri K. Ervasti, Karl J. Jobst, Peter C. Burgers, Paul J.A. Ruttink and Johan K. Terlouw, Int. J. Mass Spectrom. 262(1-2), 88-100 (2007).

Acknowledgements

Life is about action and re-action. All the things interact. This holds true also for a theoretical chemist, working in his 'cave' for his thesis. During the past four years I have worked on my thesis, I have interacted with many, many people. And for many of them I am grateful for being there to interact with, and many I need to thank for their invaluable presence at this time.

First of all, my gratitude goes towards my Ph.D. supervisor, Dr. Paul Ruttink. I am indebted to him for his guidance and teachings over this period of time. Especially I thank him for always having the time for me, if needed help with something. I wish I had used that possibility even more to pull out more information from his superb knowledge in the field of quantum chemistry! Second, I would like to thank our group leader Dr. Joop van Lenthe for his help in many occasions during these years, and reading and correcting some of the Chapters of my thesis. In addition, I would like to thank him for amusing me often with the real sarcastic humour that only a Dutchman can provide.

The next person I definitely owe my gratitude to, is Prof. Dr. Hans Terlouw. He has shown a perfect role model of a profound and meticulous scientist who can produce excellent results on intriguing projects. I especially thank him for the opportunity to go and visit his group in McMaster University, Canada, twice, to accustom me in the field of mass spectrometry and to see how the actual experimental work is done. These trips were always fruitful and I gained very much from them! I would also like to thank Dr. Peter Burgers who has been the person connecting between theoretical and experimental work in many of my projects. Especially, I am indebted to him for involving me in the ketene project, which turned in my first article. I would also like to thank Prof. Dr. Leo Jenneskens for kindly promoting my thesis.

It is not of course without the other people I have been interacting with in and around my work I could have reached so far. I would like to thank Prof. Dr. Frans van Duijneveldt, Dr. Onno Gijzeman, Dr. Remco Havenith, Dr. Joost van Lingen, Petar Todorov, Jeroen Engelberts, Henk Eshuis, Tine Blankenstein and for briefer period of time, Dr. Walter Andriessen and Claire Samson, for useful discussions, for making me feel welcome to the group and also helping out with getting used to the dutch way of life. Petar deserves extra thanks for his friendship and being an outstanding flatmate during this time. Marcin Zielinski deserves also many thanks for working together in the problem classes and other projects, and as a flatmate of mine. I also thank Zahid Rashid for a brief encounter with an interesting person from a more exotic (at least for me!) location and I wish you all good for your studies. I would also like to thank my other colleagues from various groups in the chemistry and physics for keeping me a good company and stimulating discussions during many winter schools, conferences, DO!-days, 'borrels' and other activities. I won't forget you!

So many people to thank for and many important people are still not mentioned. I would like to thank my ex-flatmates Davide and Arhodoula (not forgetting Petar and Marcin here) for their presence in the W. A. Vultostraat and for making a great atmosphere

for all those fantastic dinners and parties (and dinner-parties!). I also remember well my time at Kanaalstraat student house in my first year, where I met so many interesting and fantastic people. Thank you, Kanaalstraat posse! Many thanks go to the ING group for the Wednesday borrels, where I met many people who have become important links in my interactions, and also for the excursions to various parts of the Netherlands. I would like to thank Steve and Dab for their introduction into the dutch cafés and bars and for organizing me my first DJing gigs here, and I would like to send my greetings also to the Casca Dura Capoeira group and contra-mestre Picapau for the good and hard training! I would also like to send my greeetings to all the guys who came to play (more or less regularly) football over the past two or so years. It has been a great way to relax at the end of the week(…end).

Birgit, Pierre, Teemu, Elena, Kostas, Paolo, Ina, Jakob, Emil, Kaisa, Kees and especially Angiu, (and many more people I met here in Utrecht I forgot to mention by name here) deserve many thanks for their support, friendship and good times. Without you the life in Utrecht would have not been half as fun as it has been! Karl and Richard from McMaster University; thanks for the co-working and help with the projects and warm hospitality in Canada. Many thanks go also for Alice for the spark to go abroad, and for the friendship over these years. Haluaisin myös muistaa suomalaisia ystäviäni: Lasse (Lars), Janne (Kepa), Jukka K., Jukka H., Mikko, Tommi, Silja, Sauli, Matti (Masa), Harri ja Joose (Kangaroose). Kiitos että olette jaksaneet pitää yhteyttä koko tämän urakan ajan!

Lopuksi haluaisin kiittää erityisesti perhettäni, isääni Aimoa, äitiäni Pirkkoa, ja siskoani Katjaa (sisältäen myös Katjan perheen eli Neilin ja Ellan) tuesta ja ymmärtämyksestä tämän koettelevan ajanjakson ajan. Aina en ehkä ole ollut yhteyksissä niin paljon kuin olisi pitänyt. Toivottavasti tässä saadaan vielä hieman parannusta aikaan! Monet kiitokset teille!

Curriculum Vitae

Henri Kristian Ervasti was born on the 23rd of November 1978 in Kuusamo, a small town situated at the northeast of Finland. In 1997, he graduated from Kuusamo's College as a student of advanced mathematics and chemistry class.

Having spent eight months in the Finnish army at Kainuun Prikaati in Kajaani, he started chemistry studies at the University of Oulu, Finland, from which he graduated in 2003. In October 2003 he was awarded a Masters degree in Physical Chemistry with a thesis entitled "Car-Parrinello molecular dynamics and molecular mechanics studies of aqueous hydrogen peroxide". In the thesis Lennart-Jones parameters for liquid phase hydrogen peroxide were developed to use in molecular mechanics simulations. Further, the solvation free energy and other physical properties of the liquid and aqueous hydrogen peroxide were studied using classical mechanics and Car-Parrinello molecular dynamics.

In February 2004, he began to study for a Ph.D. at the theoretical chemistry group of Utrecht University, The Netherlands, under the supervision of Dr. Paul Ruttink. The work involved projects with cations and their stabilities, theoretical studies on mass spectrometric experiments, and ion-dipole complexes and their stabilities and reactivity. The results of his studies are presented in this thesis and part of the work has also been published in international scientific journals. During the Ph.D. studies he attended various national and international conferences and schools.